



This work is protected by copyright and other intellectual property rights and duplication or sale of all or part is not permitted, except that material may be duplicated by you for research, private study, criticism/review or educational purposes. Electronic or print copies are for your own personal, non-commercial use and shall not be passed to any other individual. No quotation may be published without proper acknowledgement. For any other use, or to quote extensively from the work, permission must be obtained from the copyright holder/s.



Mechanical loading of bioengineered skeletal muscle *in-vitro* to mimic the transcriptional and epigenetic regulation of skeletal muscle *in-vivo*

Daniel Colin Turner

A thesis submitted in partial fulfilment of the requirements of

Keele University

for the degree of

Doctor of Philosophy (Ph.D)

June 2020

Publications

Seaborne, R. A., Hughes, D. C., **Turner, D. C.***, Owens, D. J., Sharples, A. P. *et al.*, (2019). UBR5 is a Novel E3 Ubiquitin Ligase involved in Skeletal Muscle Hypertrophy and Recovery from Atrophy. *The Journal of Physiology*, 597 (14), 3727-3749. doi: 10.1113/JP278073.

Turner, D. C.*, Seaborne, R. A. & Sharples, A. P. (2019). Comparative Transcriptome and Methylome Analysis in Human Skeletal Muscle Anabolism, Hypertrophy and Epigenetic Memory. *Scientific Reports*, 9(1), 4251. doi: 10.1038/s41598-019-40787-0.

Turner, D. C.*, Kasper A. M., Seaborne R. A., Brown, A. D., Close, G. L., Murphy, M., Stewart, C. E., Martin, N. R. W. & Sharples A. P. (2019). Exercising Bioengineered Skeletal Muscle In Vitro: Biopsy to Bioreactor. *In Methods in Molecular Biology*. 1889, 55-79. doi: 10.1007/978-1-4939-8897-6_5.

Kasper, A. M., **Turner, D. C.**, Martin, N. R. W. & Sharples, A. P. (2017). Mimicking Exercise in Three-Dimensional Bioengineered Skeletal Muscle to Investigate Cellular and Molecular Mechanisms of Physiological Adaptation. *Journal of Cellular Physiology*. 233(3),1985-1998. doi: 10.1002/jcp.25840.

Pre-Prints

Turner, D. C.*, Gorski P. P., Maasar, M. F., Seaborne, R. A., Drust, B., Sharples A. P. *et al.*, (2019). DNA methylation across the genome in aged human skeletal muscle tissue and muscle stem cells: The role of HOX genes and physical activity. *Biorxiv*. doi: <https://doi.org/10.1101/2019.12.27.886135>.

Conference Abstracts

Turner, D. C*, Seaborne, R. A., Sharples, A. P. *et al.*, (2018). Mechanical loading of murine bioengineered skeletal muscle mimics the transcriptional & epigenetic response of human skeletal muscle after exercise. *ecmjournal*.

*** Indicates primary & co-primary authorship.**

Table of Contents

CHAPTER 1 Introduction.....	1
1 General Introduction.....	2
1.1 Skeletal Muscle Embryonic Development.....	2
1.2 Postnatal Growth and Regeneration.....	5
1.2.1 The Roles of Satellite Cells in Skeletal Muscle Growth, Repair and Regeneration	5
1.3 Skeletal Muscle Structure	8
1.3.1 Gross Structure of Skeletal Muscle.....	8
1.3.2 Ultra-Structure of Skeletal Muscle	10
1.4 Skeletal Muscle Function	12
1.4.1 Skeletal Muscle Contraction.....	12
1.5 Key Regulatory Signalling Pathways Associated with Skeletal Muscle Hypertrophy and Atrophy	13
1.5.1 Positive Regulators of Skeletal Muscle Mass	13
1.5.2 Negative Regulators of Skeletal Muscle Mass.....	16
1.6 Epigenetics in Skeletal Muscle.....	17
1.6.1 Chromatin, Histones and DNA.....	17
1.6.2 DNA Methylation.....	19
1.6.3 DNA Methylation and Exercise	22
1.7 Introduction to Monolayer Cell Culture Mode.....	24
1.8 Introduction to Skeletal Muscle Bioengineering.....	27
1.8.1 Collagen	27
1.8.2 Laminin.....	28
1.8.3 Fibrin	29
1.9 Thesis Aims and Objectives	31
CHAPTER 2 Materials and Methods.....	33
2.1 Cell Culture	34
2.2 Conventional Monolayer Cell Culture.....	34
2.2.1 The C₂C₁₂ Cell Line	34
2.2.2 Human Skeletal Muscle Derived Cells (HMDCs).....	36
2.2.3 Cell Counting	40

2.2.4	Cell Cryopreservation and Resuscitation	42
2.2.5	Differentiation of C ₂ C ₁₂ Cells in Monolayer Culture	42
2.2.6	Differentiation of Human Skeletal Muscle Derived Cells	43
2.3	Dosing of UBR5 siRNA in Human Myotubes	43
2.3.1	Principle	43
2.3.2	Procedure.....	45
2.4	Bioengineered Fibrin Skeletal Muscle Constructs.....	47
2.4.1	Preparation of Reagents.....	47
2.4.2	Preparation of Culture Dishes	48
2.5	Mechanical Loading of Fibrin Skeletal Muscle Constructs.....	51
2.5.1	The TC-3 Bioreactor System	51
2.5.2	Procedure.....	52
2.6	Mechanical Loading of Human Myotubes	55
2.6.1	The Flexcell® FX-5000™ Tension System.....	55
2.6.2	Differentiation of Human Myotubes on BioFlex® Culture Plates	56
2.6.3	Mechanical Loading of Human Myotubes Using the Flexcell® FX-5000™ Tension System.....	56
2.7	Immunochemistry and Microscopy	58
2.7.1	Principle.....	58
2.7.2	Immunostaining Human Skeletal Muscle Derived Cells.....	59
2.7.3	Immunostaining Bioengineered Skeletal Muscle.....	60
2.7.4	Microscopy and Image Analysis.....	61
2.8	Lysing and Homogenising Bioengineered Skeletal Muscle Tissue for RNA and DNA.....	63
2.8.1	Lysing Human Myotubes for RNA	63
2.9	RNA Extraction and Quantitative Real-Time Polymerase Chain Reaction (qRT- PCR).....	64
2.9.1	RNA Extraction Using the AllPrep RNA/DNA Mini Kit.....	64
2.9.2	RNA Extraction Using TRIzol.....	64
2.9.3	Assessment of RNA Concentration and Purity	65
2.9.4	Principle.....	66
2.9.5	Procedure.....	68
2.9.6	Quantification of Relative Gene Expression	68
2.9.7	Primer Design.....	70

2.10 Loci-Specific Pyrosequencing	74
2.10.1 Principle.....	74
2.10.2 Procedure.....	74
2.11 Targeted Next Generation Bisulfite Sequencing.....	75
2.11.1 Principle.....	75
2.11.2 Procedure.....	76
2.12 Lysing for Protein and Puromycin Incorporation for Global Protein Synthesis	77
2.12.1 Principle.....	77
2.12.2 Procedure.....	78
2.13 Quantification of Protein Concentration Using the Bicinchoninic Acid (BCA) Protein Assay.....	78
2.13.1 Principle.....	78
2.13.2 Procedure.....	79
2.14 Acetone Protein Precipitation.....	79
2.15 SDS-PAGE and Western Blot.....	80
2.15.1 Sample Preparation	80
2.15.2 Procedure.....	80
2.16 Statistical Analysis	81
 CHAPTER 3 Characterisation of a Novel Bioreactor System for Mechanically Loading Fibrin Bioengineered Skeletal Muscle	 82
3.1 Introduction.....	83
3.1.1 Models for Investigating the Mechanisms of Mechanical Loading <i>In-Vivo</i>	83
3.1.2 Monolayer Culture Models for Investigating the Mechanisms of Mechanical Loading <i>In-Vitro</i>	85
3.1.3 Mechanical Loading of Bioengineered SkM <i>In-Vitro</i>	86
3.1.4 Aims and Objectives	91
3.2 Methods	91
3.2.1 Cell Culture	91
3.2.2 Fabrication of Fibrin Skeletal Muscle Constructs.....	92
3.2.3 Mechanical Stimulation of Fibrin Skeletal Muscle Constructs.....	92
3.2.4 Immunohistochemistry (IHC)	93

3.2.5	RNA Extraction and Quantitative Real-Time Polymerase Chain Reaction (qRT-PCR)	94
3.2.6	Statistical Analysis	96
3.3	Results	96
3.3.1	Myosin Heavy Chain (MHC) mRNA Expression After Mechanical Loading	96
3.3.2	IGF-1, IGF-IEa and MGF mRNA Expression After Mechanical Loading	98
3.3.3	IGFBP-2 and IGFBP-5 mRNA Expression After Mechanical Loading	100
3.3.4	MMP-2 and MMP-9 mRNA Expression After Mechanical Loading	102
3.3.5	MyoD and Myogenin mRNA Expression After Mechanical Loading	103
3.3.6	MuRF-1 and MAFbx mRNA Expression After Mechanical Loading	105
3.4	Discussion	106
3.4.1	Myosin Heavy Chain (MHC)-1, 2, 4 and 7 mRNA Expression After Loading	107
3.4.2	IGF-IEa and MGF mRNA Expression Significantly Increased After Loading	108
3.4.3	IGFBP-2 and IGFBP-5 mRNA Expression After Loading.....	109
3.4.4	mRNA Expression of the Matrix Remodelling Gene, MMP-9 Significantly Increased After Loading	111
3.4.5	mRNA Expression of the Myogenic Regulatory Factors, MyoD and Myogenin After Loading.....	112
3.4.6	Expression of E3 Ubiquitin Ligases, MuRF-1 and MAFbx After Loading	114
3.5	Conclusion	115
CHAPTER 4 Transcriptomic and Epigenomic Analysis of Acute Resistance Exercise in Human Skeletal Muscle		117
4.1	Introduction.....	118
4.1.1	Aims and Hypothesis	120
4.2	Methods.....	121
4.2.1	Identification of Transcriptomic Studies.....	121
4.2.2	Bioinformatic Pooled Transcriptome Analysis	125
4.2.3	Overlapping the Pooled Transcriptome with the DNA Methylome.....	126
4.2.4	Pathway Analysis	126

4.3 Results	129
4.3.1 Pooled Transcriptome Analysis Overlapped with the Methylome in Human Skeletal Muscle After Acute Resistance Exercise	129
4.3.2 Genes Associated with Cancer Pathways are Enriched in Both the Transcriptome and Methylome Data Sets in Human Skeletal Muscle After Acute Resistance Exercise	130
4.4 Discussion	137
4.4.1 Enriched Upregulated and Hypomethylated Cancer Genes Involved in ECM/Actin Structure/Remodelling and Mechano-Transduction in Human Skeletal Muscle After Acute Resistance Exercise	138
4.4.2 Enriched Upregulated and Hypomethylated Cancer Genes Involved in Protein Synthesis and TGF-β, Calcium, Retinoic and IL-6 Signalling in Human Skeletal Muscle After Acute Resistance Exercise	143
4.4.3 Enriched Downregulated and Hypermethylated Cancer Genes Identified in Human Skeletal Muscle After Acute Resistance Exercise	146
4.5 Limitations	149
4.6 Conclusion	150

CHAPTER 5 The Transcriptional and Epigenetic Regulation of Murine Fibrin Bioengineered Skeletal Muscle in Response to Mechanical Loading
..... **151**

5.1 Introduction	152
5.1.1 Aims and Objectives	154
5.2 Methods	155
5.2.1 Cell Culture	155
5.2.2 Fabrication of Fibrin Skeletal Muscle Constructs	155
5.2.3 Mechanical Loading of Fibrin Skeletal Muscle Constructs	155
5.2.4 Chronic High-Frequency Electrical Stimulation in Rats	157
5.2.5 Acute and Chronic Resistance Exercise in Humans	157
5.2.6 Immunohistochemistry (IHC)	158
5.2.7 RNA Extraction and Quantitative Real-Time Polymerase Chain Reaction (qRT-PCR)	158
5.2.8 DNA Isolation, Bisulfite Conversion and Targeted DNA Methylation ..	159
5.2.9 Statistical Analysis	160
5.3 Results	161

5.3.1	mRNA Expression of Genes that are Upregulated/Hypomethylated After Resistance Exercise in Human Skeletal Muscle were Assessed After Loading in Bioengineered Muscle.....	161
5.3.2	Epigenetic Regulation of Upregulated/Hypomethylated Genes were Assessed After Loading in Bioengineered Skeletal Muscle.....	178
5.3.3	mRNA Expression of Genes that are Downregulated/Hypermethylated after Exercise in Human Skeletal Muscle were Assessed After Loading in Bioengineered Muscle.....	183
5.3.4	Epigenetic Regulation of Downregulated/Hypermethylated Genes After Loading in Bioengineered Skeletal Muscle.....	195
5.3.5	mRNA Expression of Genes that are Significantly Altered After Acute and Chronic Resistance Exercise in Human Skeletal Muscle were Assessed After Mechanical Loading in Bioengineered Muscle	197
5.3.6	DNA Methylation of Upregulated/Hypomethylated Genes in Bioengineered and Human Skeletal Muscle were Assessed After Loading <i>In-Vitro</i>	200
5.3.7	mRNA Expression and DNA Methylation of the Most Significantly Upregulated Gene Across All Models of Loading.....	204
5.4	Discussion	207
5.4.1	mRNA Expression of Upregulated/Hypomethylated Genes After Acute Resistance Exercise in Humans were Assessed Following Mechanical Loading in Bioengineered Skeletal Muscle	208
5.4.2	DNA Methylation of Upregulated/Hypomethylated Genes After Acute Resistance Exercise in Humans were Assessed Following Mechanical Loading in Bioengineered Skeletal Muscle	210
5.4.3	mRNA Expression of Downregulated/Hypermethylated Genes After Acute Resistance Exercise in Humans were Assessed Following Mechanical Loading in Bioengineered Skeletal Muscle	211
5.4.4	DNA Methylation of Downregulated/Hypermethylated Genes After Acute Resistance Exercise in Humans were Assessed Following Mechanical Loading in Bioengineered Skeletal Muscle	212
5.4.5	mRNA Expression of Genes that are Significantly Altered After Acute and Chronic Resistance Exercise in Humans were Assessed After Mechanical Loading in Bioengineered Muscle.....	213
5.4.6	DNA methylation of Upregulated/Hypomethylated Genes in Bioengineered and Human Skeletal Muscle were Assessed After Loading <i>In-Vitro</i>	216

5.4.7	mRNA Expression and DNA Methylation of the Most Significantly Upregulated Gene Across All Models of Loading	219
5.5	Limitations.....	220
5.6	Conclusion	221
CHAPTER 6 The Mechanistic Role of UBR5 in Response to Mechanical Loading in Human Myotubes..... 222		
6.1	Introduction.....	223
6.1.1	Aims and Objectives	224
6.2	Materials and Methods.....	224
6.2.1	Cell Culture	224
6.2.2	Dosing of Human Myotubes	225
6.2.3	Mechanical Loading of Human Myotubes	226
6.2.4	RNA Extraction and Quantitative Real-Time Polymerase Chain Reaction (qRT-PCR)	228
6.2.5	Puromycin Incorporation and SDS-PAGE	229
6.2.6	Statistical Analysis	230
6.3	Results.....	231
6.3.1	UBR5 mRNA Expression After Mechanical Loading in Non-Treated Myotubes	231
6.3.2	UBR5 mRNA Expression in Loaded and Non-Loaded Myotubes After siUBR5 Treatment.....	234
6.3.3	UBR5 mRNA Expression when All Samples were Relativised to Non-Treated Myotubes at 0 hrs	234
6.3.4	Global Muscle Protein Synthesis After Mechanical Loading in Human Myotubes	235
6.4	Discussion	237
6.4.1	Transfection of Human Myotubes Induces Sufficient UBR5-Specific Knockdown at 3 hrs Post-Loading.....	237
6.4.2	UBR5 mRNA Expression After Mechanical Loading in Non-Treated Human Myotubes.....	239
6.4.3	Mechanical Loading of Human Myotubes Post-Transfection Partially Rescues UBR5 mRNA Expression	240
6.4.4	The Reduction in UBR5 mRNA Expression Post-Treatment is Negated Following Mechanical Loading	242

6.5	Limitations.....	242
6.6	Conclusion	244
CHAPTER 7	Thesis Conclusion	245
7.1	Summary of Thesis Aims and Main Findings	246
7.2	Thesis Conclusion	248
CHAPTER 8	References.....	249
CHAPTER 9	Thesis Appendices	283

List of Figures

Figure 1.1. Embryonic SkM development.....	4
Figure 1.2. SkM repair and regeneration	7
Figure 1.3. SkM gross anatomical structure	9
Figure 1.4. SkM sarcomere structure.....	11
Figure 1.5. SkM contraction	13
Figure 1.6. mTORC1 signalling pathway	15
Figure 1.7. Myostatin/Smad signalling pathway	17
Figure 1.8. Chromatin, histones and DNA structure	19
Figure 1.9. Mechanisms of DNA methylation.....	21
Figure 1.10. Myotube morphology in monolayer versus bioengineered SkM models	26
Figure 2.1. C ₂ C ₁₂ myoblasts differentiation in monolayer.....	35
Figure 2.2. Differentiation of HMDCs in monolayer	39
Figure 2.3. Cell counting using a Haemocytometer	41
Figure 2.4. Mechanisms of siRNA silencing.....	44
Figure 2.5. UBR5 siRNA target sequence locations	46
Figure 2.6. Fabrication of fibrin bioengineered SkM	48
Figure 2.7. Differentiation of C ₂ C ₁₂ 's in fibrin bioengineered SkM	50
Figure 2.8. Example of the TC-3 bioreactor.....	52
Figure 2.9. Mechanical loading of fibrin bioengineered SkM.....	53
Figure 2.10. Velocity and frequency mode settings	54
Figure 2.11. Equibiaxial loading of cells in monolayer.....	55
Figure 2.12. Mechanical loading of human myotubes	57
Figure 2.13. Immunostaining fibrin bioengineered SkM	61
Figure 2.14. Immunostaining of HMDCs for determining myogenic population.....	62
Figure 2.15. Analysis of raw C _T values for gene expression.....	69
Figure 2.16. Melt curve analysis to determine specific target amplification.....	70
Figure 2.17. Mechanisms of pyrosequencing for DNA methylation.....	73
Figure 2.18. Mechanisms of tNGBS for DNA methylation	76
Figure 3.1. Different bioreactors for loading cells and bioengineered tissues	89
Figure 3.2. Immunostained fibrin bioengineered SkM.....	94
Figure 3.3. MHC mRNA expression after mechanical loading.....	98
Figure 3.4. IGF-I, IGF-IEa and MGF mRNA expression after mechanical loading.....	100
Figure 3.5. IGFB-2 and IGFBP-5 mRNA expression after mechanical loading.....	101
Figure 3.6. MMP-2 and MMP-9 mRNA expression after mechanical loading.....	103
Figure 3.7. MyoD and myogenin mRNA expression after mechanical loading	104

Figure 3.8. MuRF-1 and MAFbx mRNA expression after mechanical loading.....	106
Figure 4.1. QC/QA, Venn diagram and PCA analysis	128
Figure 4.2. Analysis of upregulated/hypomethylated and downregulated/hypermethylated genes after acute RE in human SkM.....	130
Figure 4.3. ‘Pathways- and proteoglycans in cancer’ were significantly enriched pathways across the human transcriptome and methylome after acute RE	135
Figure 4.4. Upregulated/hypomethylated and downregulated/hypermethylated enriched in cancer genes after acute RE in humans	136
Figure 5.1. Mechanical loading and immunostaining of fibrin bioengineered SkM.....	156
Figure 5.2. Heat map representation of temporal mRNA expression after loading bioengineered SkM	156
Figure 5.3. mRNA expression of actin/ECM structure and remodelling related genes after loading in bioengineered SkM.....	166
Figure 5.4. mRNA expression of genes associated with mechano-transduction, MPS and TGF- β /calcium/IL-6/retinoic acid signalling after loading in bioengineered SkM.....	171
Figure 5.5. mRNA expression of upregulated/hypomethylated genes associated with DNA methylation, angiogenesis and tumour suppression after loading in bioengineered SkM.....	174
Figure 5.6. Upregulated/hypomethylated genes after loading/RE in bioengineered, rodent and human SkM.....	177
Figure 5.7. mRNA expression and DNA methylation of upregulated/hypomethylated genes following loading in bioengineered SkM alone.....	182
Figure 5.8. Temporal mRNA expression of downregulated/hypermethylated genes after loading in bioengineered SkM only	190
Figure 5.9. Comparison of downregulated/hypermethylated genes after loading/RE in bioengineered, rodent and human SkM	194
Figure 5.10. mRNA expression and DNA methylation of downregulated/hypermethylated genes following after loading in bioengineered SkM.....	196
Figure 5.11. Comparison of mRNA expression for genes identified in Seaborne <i>et al.</i> , (2018a) after loading/RE in bioengineered, rodent and human SkM	199
Figure 5.12. mRNA expression and DNA methylation of regulated genes after RE in human SkM were assessed after loading in bioengineered SkM	203
Figure 5.13. Temporal UBR5 mRNA and DNA methylation patterns after loading in bioengineered SkM	206
Figure 5.14. CpG-specific DNA methylation of UBR5 after loading in bioengineered SkM.....	207
Figure 6.1. Schematic representation of siUBR5 experimental procedures	227

Figure 6.2. UBR5 mRNA expression following mechanical loading in non-treated human myotubes.....	231
Figure 6.3. UBR5 mRNA expression in human myotubes after loading and gene silencing	233
Figure 6.4. Puromycin western blots for assessment of total muscle protein synthesis	236

List of Tables

Table 2.1. SkM biopsy characteristics	38
Table 2.2. UBR5/EDD1 siRNA target sequences	46
Table 2.3. Quantifying mRNA expression using the $\Delta\Delta C_T$ method	70
Table 2.4. Primer design guidelines.....	72
Table 3.1. Mouse primers for assessing mechano-responsive genes after loading in bioengineered SkM	95
Table 4.1. Transcriptome-wide acute RE studies pooled for comparative analysis	122
Table 5.1. Mouse primer sequences for genes that are significantly regulated across the human transcriptome and methylome after acute RE in humans	284
Table 5.2. Rat primer sequences for genes that are significantly regulated across the human transcriptome and methylome after acute RE in humans	291
Table 5.3. Human primer sequences for regulated genes across the human methylome after acute and chronic RE in humans.....	295
Table 5.4. Mouse primer sequences for regulated genes across the human methylome after acute and chronic RE in humans.....	299
Table 5.5. Rat primer sequences for regulated genes across the human methylome after acute and chronic RE in humans	303
Table 6.1. Human primer sequences for genes analysed	229

Abbreviations

Δ	Change
3-D	3-Dimensional
5hmC	5-hydroxy-methyl-cytosine
5mC	5-methyl-cytosine
5' UTR	5' untranslated region
ADCY3	Adenylate cyclase 3
Ach	Acetylcholine
AchR	Acetylcholine receptor
ADP	Adenosine diphosphate
ATP	Adenosine triphosphate
AFF3	AF4/FMR2 family member 3
AGTR1	Angiotensin II receptor type 1
Akt	Protein kinase B
ANK3	Ankyrin 3
ATM	ATM serine/threonine kinase
AXIN1	Axin 1
bHLH	Basic helix-loop-helix
B2M	Beta-2-microglobulin
BICC1	BicC family RNA binding protein 1
Bp	Base pairs
Ca ²⁺	Calcium
CD63	CD63 molecule
cDNA	Complementary DNA
COL4A1	Collagen type IV alpha 1 chain
CRK	CRK proto-oncogene
CSA	Cross-sectional area
CTTN	Cortactin
DNA	Deoxyribonucleic acid
DNMT1	DNA methyltransferase 1
DNMT3a	De-novo methyltransferase 3a
DNMT3b	De-novo methyltransferase 3b
DOT1L	DOT1 like histone lysine methyltransferase
DROSHA	Drosha ribonuclease III
EDL	Extensor Digitorum Longus
ESR1	Estrogen receptor 1

eIF-3B	Eukaryotic translation initiation factor 3 subunit B
ERK	Extracellular signal-regulated kinases
F2LR3	F2R like thrombin or trypsin receptor 3
FLNB	Filamin B
FOS	Fos proto-oncogene
Foxo	Forkhead box O
FoxO3	Forkhead box O3
GADD45G	Growth arrest and DNA damage inducible gamma
GRIK2	Glutamate receptor, ionotropic kainate 2
GSK3 β	Glycogen synthase kinase 3 beta
HEG1	Heart development protein with EGF like domains 1
HMDCs	Human skeletal muscle derived cells
HU	Hindlimb unloading
Hz	Hertz
IGF-1	Insulin growth factor 1
IGFBP	Insulin like growth factor binding protein
IL	Interleukin
ITGB3	Integrin subunit beta 3
ITPR3	Inositol 1,4,5-trisphosphate receptor type 3
JNK	Jun amino terminal kinases
KDR	Kinase insert domain receptor
KLHDC1	Kelch domain containing
LAMA3	Laminin subunit alpha 3
LAMA5	Laminin subunit alpha 5
MAFbx/Fbxo 32	F-box only protein 32
MBD	Methyl binding domain
MeCP	Methyl CpG binding protein
MEF2	Myocyte enhancer factor 2
MPB	Muscle protein breakdown
MPC	Muscle precursor cells
MPS	Muscle protein synthesis
mRNA	messenger RNA
MSN	Moesin
mTOR	Mammalian target of rapamycin
mTORC	Mammalian target of rapamycin complex
MuRF1/Trim63	Muscle RING finger protein-1

Myf5	Myogenic factor 5
Myf6	Myogenic factor 6
MYHC	Myosin heavy chain
MyoD	Myogenic differentiation 1
MyoG	Myogenin
NANOG	Nanog homeobox
NOS2	Nitric oxide synthase 2
ODF2	Outer dense fibre of sperm tails 2
P38 MAPK	P38 mitogen activated protein kinase
P70S6K	P70-S6 Kinase-1
Pax	Paired box protein
PGC1- α	Peroxisome proliferator activated receptor gamma co-activator 1-alpha
PI3K	Phosphoinositide 3-kinase
PLA2G16	Phospholipase A2 group XVI
POLR2a	DNA-directed RNA polymerase II subunit RPB1
qRT-PCR	Quantitative reverse transcription polymerase chain reaction
RARA	Retinoic acid receptor alpha
RASSF5	Ras association domain family member 5
RNA	Ribonucleic acid
RP-II β	RNA polymerase II subunit B
RPL13a	Ribosomal protein L13a
RPL35a	Ribosomal protein L35a
RSU1	Ras suppressor protein 1
rt-qRT PCR	Real-time quantitative reverse transcription polymerase chain reaction
RUNX1	Runt related transcription factor 1
SAH	S-adenosyl homocysteine
SAM	S-adenosyl methionine
SD	Standard deviation
SEM	Standard error of the mean
SETD3	SET domain containing 3
SkM	Skeletal muscle
SMAD	Smad family member
STAG1	Cohesin subunit SA-1
STAT3	Signal transducer and activator of transcription 3
T2D	Type II diabetes
TA	Tibialis anterior

TET	Ten-eleven translocation methylcytosine dioxygenase
THBS1	Thrombospondin 1
TIMP3	Tissue inhibitor of metalloproteinases
TNF- α	Tumour necrosis factor alpha
TOR	Target of rapamycin
TRAF1	TNF receptor associated factor 1
Trim63	Tripartite motif containing 63
TSS	Transcriptional start site
TTX	Tetrodotoxin
UBR5	Ubiquitin protein ligase E3 component N-recognin 5
WNT9a	WNT family member 9a
ZFP2	Zinc finger protein 2

Acknowledgements

First and foremost, I would like to give a special thanks to my lead supervisors, Dr. Adam Sharples and Professor Nicholas Forsyth, for their guidance and support throughout my Ph.D. Adam, your passion and knowledge is something I have always truly admired ever since we started working together. Your continued support, even during the move is truly appreciated. Nick, I appreciate all of your help, particularly since Adam's departure. I therefore thank you both. I would also like to say a special thanks to Professor Claire Stewart for your invaluable insights, and to Dr. Dan Owens who is a fantastic researcher and has become a great mentor and friend of mine throughout the last 6 months of my Ph.D. You are a great role model to the next generation of ECRs and someone I certainly look up to.

I would also like to say a special thanks to all of the administration/PGR staff (particularly Louise Coyne, LJMU and Zara Richards, Keele) and the research technicians at both LJMU (George Savage and Nicola Browning) and Keele (Katy Cressy and John Misra) for all of their support over the past 3 years. Despite not including our recent aging skeletal muscle epigenetics research within this thesis, I would also like to share my gratitude to the research nursing team led by Racquel Carpio for all of their hard work and also to orthopaedic surgeon, Ian Dos Remedios, for obtaining muscle tissue samples.

To all of my friends at LJMU and Keele (there are too many to single out), you have all significantly contributed to the best 3 years of my life. To all the lads back home who have been there for me from an early age, you know who you are and how much you mean to me. I would certainly like to share my gratitude (in no particular order) to Jordan, Imran and Tomo. All of you are more like brothers than friends and were instrumental in helping me get through in one piece.

I would also like to share my love and respect for my granddad, David Massey. Granddad, if I am half the man you are, I would consider myself a true gentleman with 'a heart of gold'. Also, a special thanks to my father, Darren Turner and stepfather, Mark Abbotts for all of their support over the years.

To my 3 sisters, Jodie, Ellie and Beau, I hope you are as proud of me as I am of all of you and understand that anything is achievable. Finally, to my mother, Sally Massey. Mom, your love and support throughout my entire life means more to me than you or anyone else can ever imagine. You have believed in me more than I have believed in myself on many occasions and for that I am forever grateful. All of the tough and difficult times we have encountered, however, we always came out of top and that's thanks to you. I love you forever and always and hope that I have made you proud. I dedicate this thesis to you.

Thesis Abstract

Skeletal muscle (SkM) is an extremely abundant and mechano-sensitive tissue, demonstrating increases in mass and function following mechanical loading/resistance exercise (RE). Over the past 3 decades, there has been considerable progress in the development of bioengineered SkM models for elucidating the cellular and molecular mechanisms underpinning load-induced SkM adaptation *in-vitro*. However, the majority of studies often employ loading regimes which lack resemblance of intermittent eccentric-lengthening contraction experienced during RE *in-vivo*. As the field of SkM epigenetics has only more recently begun to emerge, there is a paucity of data surrounding the epigenetic regulation of mechanical loading in bioengineered SkM. The work conducted herein therefore intermittently loaded bioengineered fibrin SkM *in-vitro* to determine whether mechanical loading alone recapitulates both the transcriptional and epigenetic responses in SkM following loading/RE *in-vivo*. The initial experiments (chapter 3) first characterised the use of a novel bioreactor system (i.e. which has never previously been used to bioengineered SkM) for loading bioengineered SkM which demonstrated a comparable mechano-transcriptional response of candidate genes that were differentially regulated after loading in previous well-characterised bioreactors. In order to identify appropriate genes to analyse in response to loading in bioengineered SkM, the most frequently regulated genes across both the human transcriptome and methylome after acute RE *in-vivo* were determined in chapter 4. Indeed, extensive bioinformatics analysis revealed a number of transcriptionally and epigenetically regulated genes in human SkM that were subsequently analysed at the mRNA and DNA methylation level following acute mechanical loading in fibrin engineered SkM (chapter 5). Despite few changes observed in DNA methylation, mechanical loading alone induced similar changes in gene expression compared to loading/RE in human and rodent SkM *in-vivo*. Amongst the array of genes analysed, UBR5 demonstrated the largest increase in mRNA expression across all models of loading. Therefore, the final experimental chapter of this thesis (chapter 6) wished to elucidate the mechanistic role of UBR5 after mechanical loading in human myotubes. Most interestingly, mechanical loading was able to rescue the

siRNA-induced reduction in UBR5 gene expression, further suggesting a pivotal role in load-induced adaptation.

Overall, the present thesis suggests that mechanical loading of C₂C₁₂ bioengineered fibrin muscle is a useful *in-vitro* model for investigating the transcriptional response to loading *in-vivo*. Therefore, providing a representative model for investigating the molecular mechanisms underpinning load-induced SkM adaptation. However, the application of repeated/chronic loading, with or without electrical stimulation may be necessary to evoke epigenetic alterations that are comparable to those observed following loading/RE *in-vivo*.

CHAPTER 1

Introduction

1 General Introduction

The experiments undertaken within this thesis were conducted using a self-assembling fibrin bioengineered skeletal muscle (SkM) model to investigate whether acute mechanical loading alone (i.e. in isolation of a neural input and systemic factors) *in-vitro* mimics the transcriptional and epigenetic responses to resistance exercise (RE) *in-vivo*. In an attempt to recapitulate the morphological and functional characteristics of SkM *in-vivo*, existing knowledge of native SkM development, structure and post-natal growth and regeneration must first be acknowledged as myotube formation during cell culture *in-vitro* somewhat resembles SkM development and regeneration *in-vivo*. Given the main aim of this thesis was to determine the acute molecular responses to mechanical loading alone, it is therefore important to also consider the key molecular pathways that regulate SkM adaptation following RE *in-vivo* and the common techniques used to explore these mechanisms. Therefore, an introduction into the development, structure, and molecular mechanisms of SkM adaptation (i.e. muscle mass and function) are described in the introduction of this thesis. However, common methods and techniques used for investigating the mechanisms of mechanical loading *in-vivo* and *in-vitro* are described in the introduction section of chapter 3. Furthermore, the continually evolving field of SkM epigenetics and bioengineering will be introduced with a specific focus on DNA methylation and the techniques and biomaterials frequently used within SkM bioengineering research.

1.1 Skeletal Muscle Embryonic Development

Since the 1960's, scientists have attempted to unravel the molecular mechanisms underpinning embryonic skeletal muscle (SkM) development to complete formation and regeneration of adult muscle (termed myogenesis) with the aim of improving treatment strategies for muscular disorders (both neuromuscular and musculoskeletal disorders characterised by disease of the motor neurons and muscle membrane or supporting proteins, affecting muscle regeneration) or

myopathies (i.e. muscle diseases which directly affect the muscle fibre/contractile apparatus, resulting in muscle weakness; Cardamone *et al.*, 2008; Chal & Pourquié, 2017).

Within the embryo of vertebrates, SkM arises from the paraxial mesoderm which separates into somites on either side of the neural tube and notochord (Buckingham *et al.*, 2003). Somites are further divided into the epaxial and hypaxial dermomyotome which gives rise to the musculature of the back and limbs, respectively. Myogenesis within the embryo is regulated via a number of key growth and transcription factors (see Figure 1.1). Specifically, delamination and migration of myogenic precursor cells (MPCs) from the dermomyotome are determined by the expression of the paired box transcription factor, Pax3 and tyrosine kinase receptor, c-Met, where genetic deletion of both of these genes in mice prevents delamination of cells and subsequent formation of limb musculature (Bladt *et al.*, 1995; Tajbakhsh *et al.*, 1997). Once cells migrate to the limb bud, expression of the basic helix-loop-helix (bHLH) transcription factors, Myf5 and MyoD are upregulated to direct the myogenic lineage whereas myogenic regulatory factors (MRFs), myogenin and MRF4, alongside Mef2 determine terminal differentiation of myoblasts to myocytes (Buckingham *et al.*, 2003; see Figure 1.1).

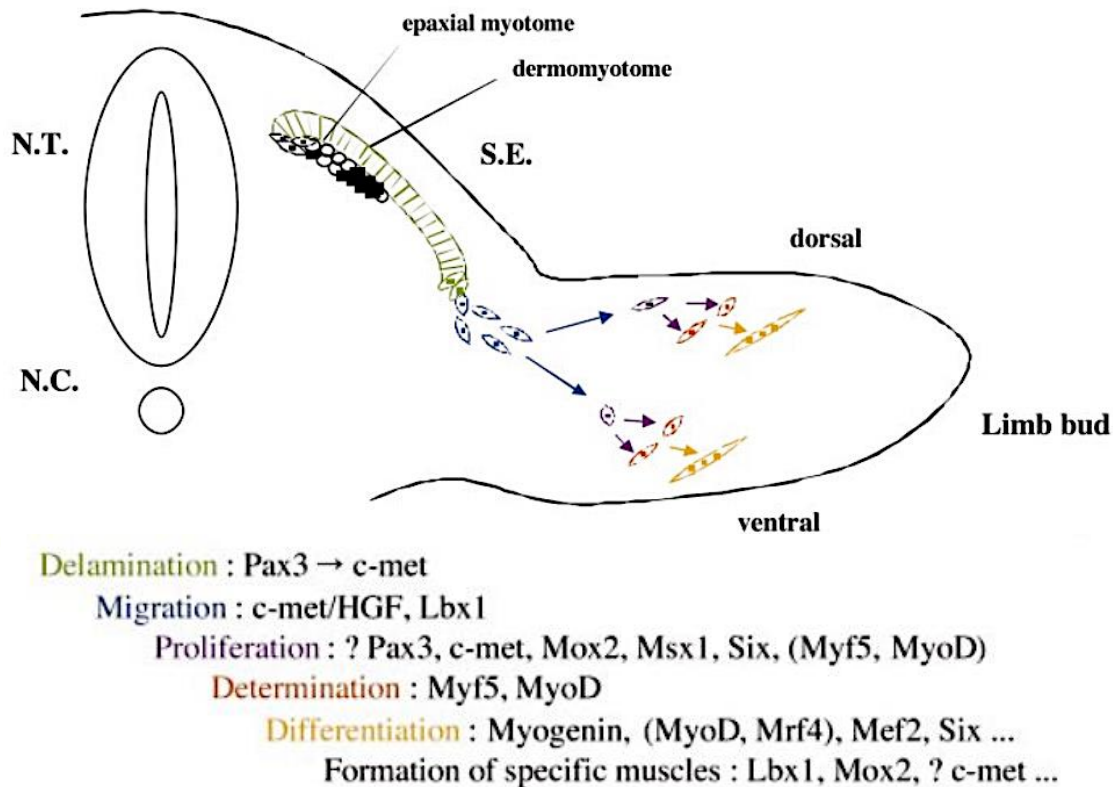


Figure 1.1. Embryonic SkM development

(NT = neural tube; NC = notochord; SE = surface ectoderm). Taken from Buckingham *et al.*, (2003).

After the transition of myoblasts to myocytes, primary myofibres/myotubes are then formed from Pax3⁺ cells at around embryonic day (E) 10.5-12.5 which express various myosin proteins (slow MHC and MLC1; Chal and Pourquié, 2017). The primary fibres act as a scaffold for the production of secondary myofibres which occurs at around E14.5-17.5 and is influenced via innervation/neural input of the fibres. Here, Pax7⁺ cells fuse to the primary fibres and begin to express fast MHC isoforms (Van Horn & Crow, 1989). A number of these Pax7 expressing cells form the population of resident stem cells (termed satellite cells) which are critical for postnatal growth and regeneration (see section 1.3).

1.2 Postnatal Growth and Regeneration

1.2.1 The Roles of Satellite Cells in Skeletal Muscle Growth, Repair and Regeneration

SkM fibres contain large quantities of myonuclei, ranging between 44 and 116 myonuclei/mm of muscle fibre (Tseng *et al.*, 1994). Interestingly, myofibre number is predetermined during gestation and therefore, hyperplasia (new fibre formation) is not thought to increase postnatally under physiological conditions (i.e. after exercise). Furthermore, myofibres are terminally differentiated as the myonuclei once incorporated into the fibre can no longer undergo mitosis. Therefore, maintenance and regeneration of adult muscle is dependent on muscle-specific stem cells, termed satellite cells which contribute to approximately ~2.5-6% of total nuclei (Zammit *et al.*, 2002). These resident muscle stem cells were first identified under electron microscopy in frog tibialis anticus muscle and were coined 'satellite cells' based on their peripheral location, as they resided between the plasma membrane and basal lamina of the muscle fibre (Mauro, 1961). Since this discovery, a plethora of research has attempted to demonstrate the importance of satellite cells during postnatal growth and regeneration and to unravel the mechanisms which govern these fundamental biological processes.

Despite early research suggesting that muscle regeneration may primarily be attributable to the presence of bone marrow-derived mesenchymal stem cells in mice SkM (Ferrari *et al.*, 1998), others have shown this was not the case (Sherwood *et al.* 2004) and that satellite cells are indeed the major contributors towards the regeneration of injured SkM (Collins *et al.*, 2005). Indeed, Collins and colleagues demonstrated that transplantation of single myofibres (derived from TA, EDL and soleus rodent muscles) containing just ~7 satellite cells regenerated >100 myofibres in injured mouse muscle (Collins *et al.*, 2005). In response to muscle injury, satellite cells undergo a series of events which underpin the repair and regeneration process. Indeed, upon damage, satellite cells are first activated (termed myoblasts) where they then migrate to the site of injury in order to differentiate and fuse to the damaged portion of the existing muscle fibre

(Schiaffino, Pierobon Bormioli and Aloisi, 1972, 1976; see Figure 1.2A). Furthermore, a subset of these activated satellite cells return to the fibre and quiesce in a process called self-renewal. This then maintains the satellite cell pool ready for future incorporation in response to muscle damage or for routine turnover of myonuclei. The activation of satellite cells is governed by the activity of key myogenic regulatory factors (MRF), Myf5 and MyoD (Tajbakhsh *et al.*, 1996) whereas migration and differentiation of satellite cells is dependent on the MRFs, Myogenin and Myf6 (otherwise known as Mrf4; Brack and Rando, 2012; see Figure 1.2B). Upon activation, satellite cells undergo asymmetric division whereby cells adopt distinct fates to enable simultaneous activation, proliferation and differentiation of myoblasts or they undertake the self-renewal program (Zammit *et al.*, 2004). Asymmetric cell division has been shown to be regulated via signalling of the P38 mitogen-activated protein kinase (MAPK) pathway (Troy *et al.*, 2012). Cells committing to differentiation have been shown to coexpress Pax7 and MyoD whereas those returning to quiescence to enable self-renewal demonstrate downregulation of MyoD. Albeit, Pax7 is still upregulated (Zammit *et al.*, 2004).

The role of satellite cells for inducing SkM muscle hypertrophy in response to mechanical loading has however been debated. Work by Rosenblatt and Parry first demonstrated that mechanical/functional overload-induced hypertrophy was completely ablated when satellite cells of the mouse EDL were lost after exposure to γ -irradiation (Rosenblatt & Parry, 1992). Despite the effects of γ -irradiation in blocking DNA synthesis, this technique lacks cellular specificity and therefore the reduced hypertrophic response cannot necessarily be extrapolated to the loss of just satellite cells. Others therefore used a Pax7⁻ depleted mouse model treated with tamoxifen to investigate whether satellite cells are indeed key players for inducing SkM hypertrophy (Mccarthy *et al.*, 2011; Fry *et al.*, 2014; Egner *et al.*, 2016). Interestingly, mechanical overload of the plantaris mouse muscle induced a similar hypertrophic response (~2-fold) in Pax7⁻ versus wild-type mice (Mccarthy *et al.*, 2011) whilst others failed to recapitulate such findings using a similar model as hypertrophy was blunted in Pax7⁻ null mice

(Egner *et al.*, 2016). Conversely however, the same group later demonstrated that the hypertrophic response to mechanical overload could not be maintained after 8 weeks of loading whereby muscle growth was blunted in Pax7⁻ mice (Fry *et al.*, 2014). Taken together, research to date therefore suggests that satellite cells may not be the key determinant of initial muscle growth following mechanical loading/RE, albeit may be integral for maintenance of SkM

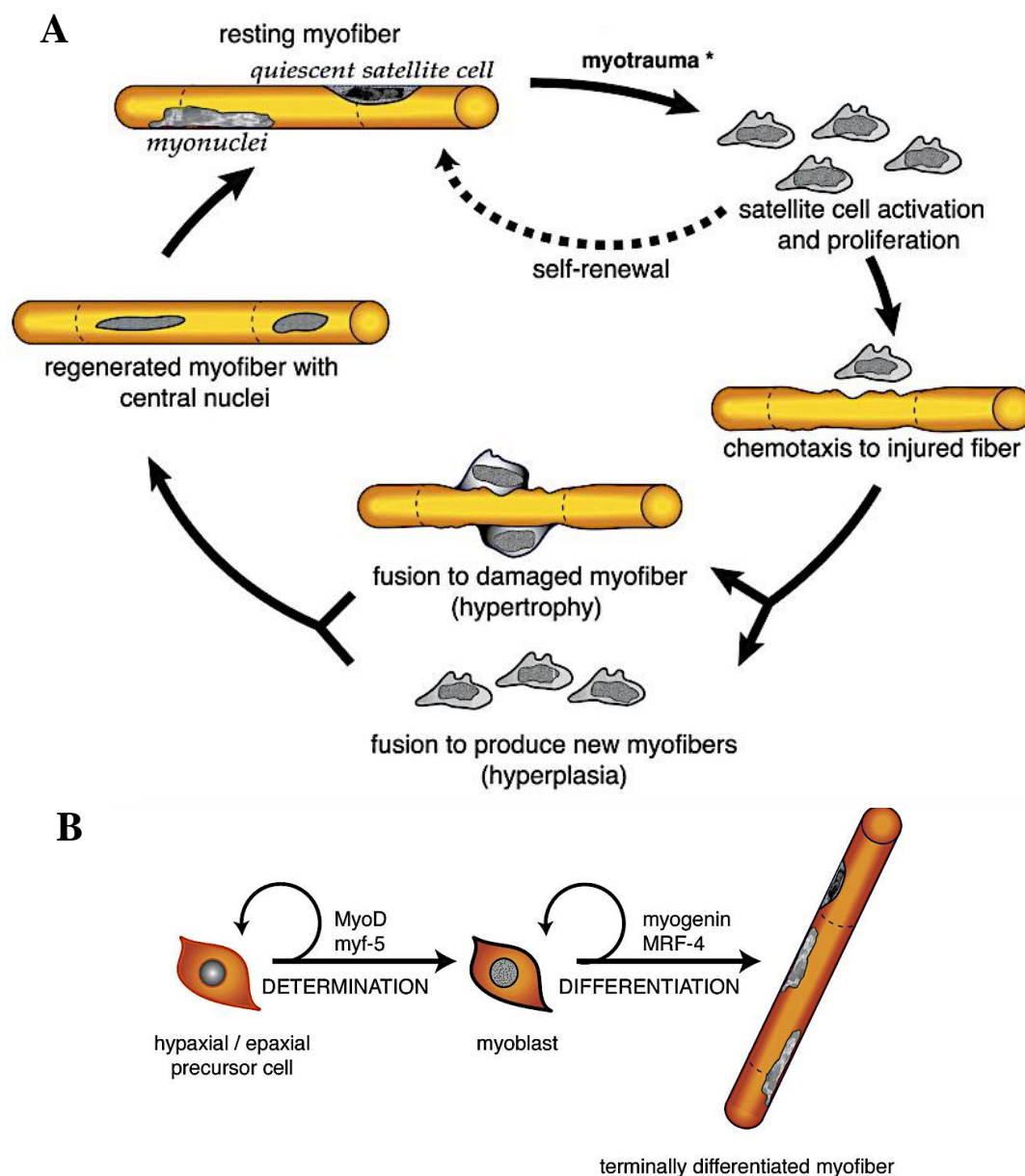


Figure 1.2. SkM repair and regeneration

Schematic representation of the cascade of events underpinning SkM repair and regeneration via the regulation of satellite cells. Taken from Hawke and Garry (2001).

1.3 Skeletal Muscle Structure

1.3.1 Gross Structure of Skeletal Muscle

Skeletal muscle (SkM) is the most abundant tissue in the human body with >600 muscles making up approximately ~30-40% of total body mass, depending on gender status, with males typically possessing larger quantities (Janssen *et al.*, 2000). Typically, SkM is composed of ~70% water (700 ml/kg SkM) and ~30% solids (300 g/kg SkM), the majority of which is protein (~70%; Wackerhage, 2014). The most abundant proteins in SkM are the key myofibrillar contractile proteins, the 480 kDa thick myosin (~20-40%) and 42 kDa thin actin (~15%) filaments (Carroll *et al.*, 2004). Given SkM is fundamental for movement, thermoregulation, posture, metabolism and is the major site for glucose utilisation and disposal (~80%; Egan and Zierath, 2012), its detailed structure and function is of paramount importance for improvements and maintenance of musculoskeletal health and performance.

SkM connects to bone via connective tissue such as tendons which attaches to either end of the muscle, termed the myotendinous junction (MTJ). SkM itself is also surrounded by sheets of connective tissue, namely (from the outer to inner layers) the epimysium, perimysium and endomysium. The epimysium encloses the entire SkM tissue, whereas the perimysium encompasses fascicles which contain bundles of several (~10-100) myofibres (MacLaren and Morton, 2011; see Figure 1.3). Finally, the endomysium separates individual myofibres which can be ~10-120 μm in diameter and ~20 cm (specifically for the large sartorius muscle; Heron and Richmond, 1993). The myofibres comprise the protein dense myofibrils/sarcomeres which contain the myosin thick and actin thin filaments, the essential units for muscle contraction (see section 1.3.2).

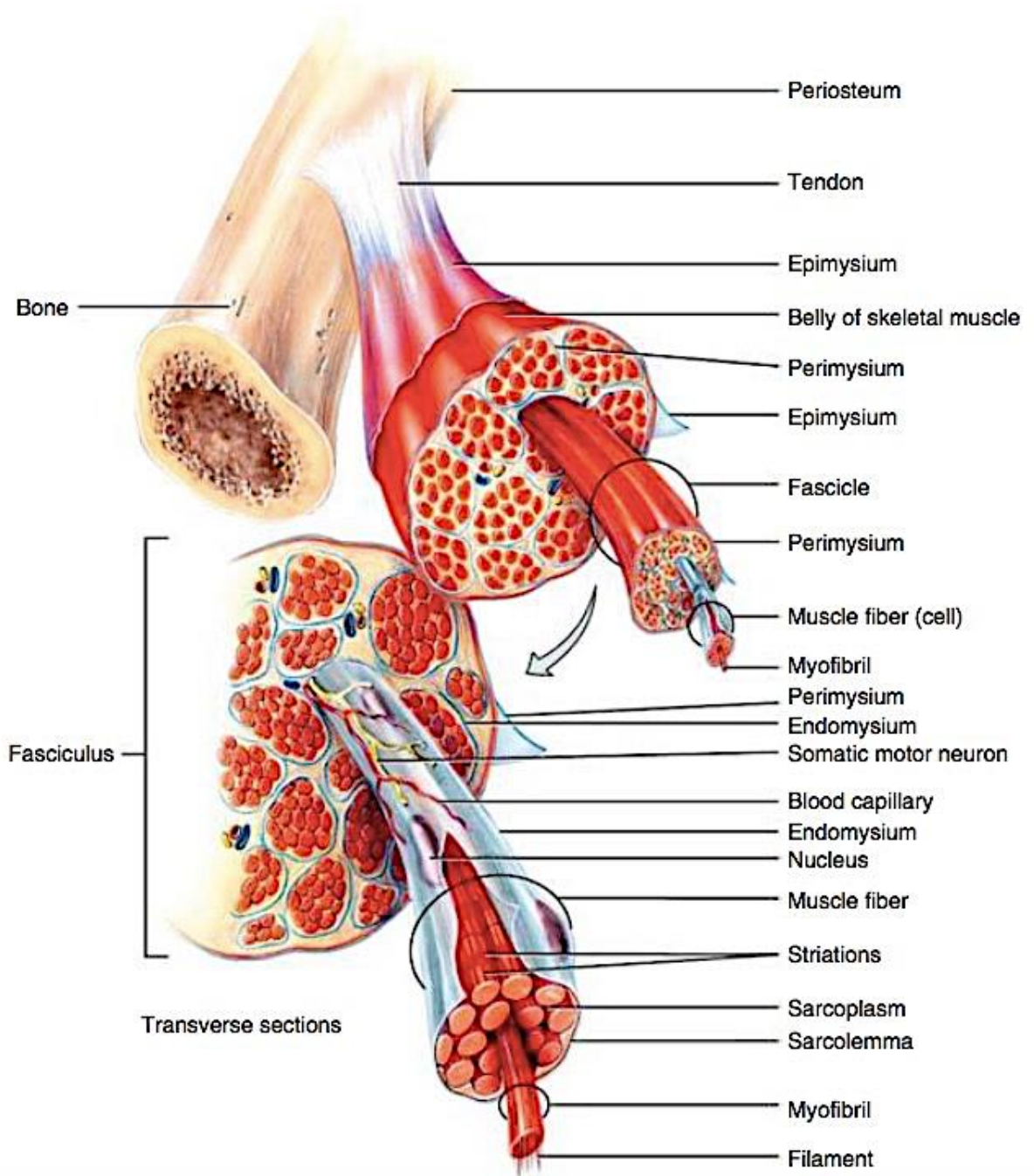


Figure 1.3. SkM gross anatomical structure

Schematic representation of the gross anatomical structure of SkM. Taken from MacLaren and Morton (2011).

1.3.2 Ultra-Structure of Skeletal Muscle

The myofibrils run adjacent to the entire length of the muscle cells which contain ~2000 myofibrils per myofibre, depending of the specific muscle (Jones *et al.*, 2004). Importantly, the myofibrils contain the contractile proteins, thick myosin and actin, which gives rise to the striation appearance of the myofibre (Huxley, 1953). As visualised in Figure 1.4, the sarcomeres containing the myosin and actin filaments are precisely organised. Indeed, the light isotropic (I) band highlights the area where only actin thin filaments are present. However, the dark anisotropic (A) band contains areas where only myosin is present (also known as the *H-zone*) or where there is an overlap of actin and myosin filaments (which demonstrates the darkest area of the sarcomere; Huxley, 1953; Jones, Round and de Haan, 2004). The *H-zone* is further dissected by the *M-line* which attaches the thick myosin filaments via the key myomesin/myomesin-2 (MacLaren & Morton, 2011). Finally, each sarcomere is separated by the *Z-disc/line* which comprises the essential structural cytoskeleton proteins nebulin, α -actinin and desmin, and also stabilises myosin filaments via the largest muscle protein, titin which has a protein size of ~3700 kDa (Krüger and Linke, 2011; see Figure 1.4).

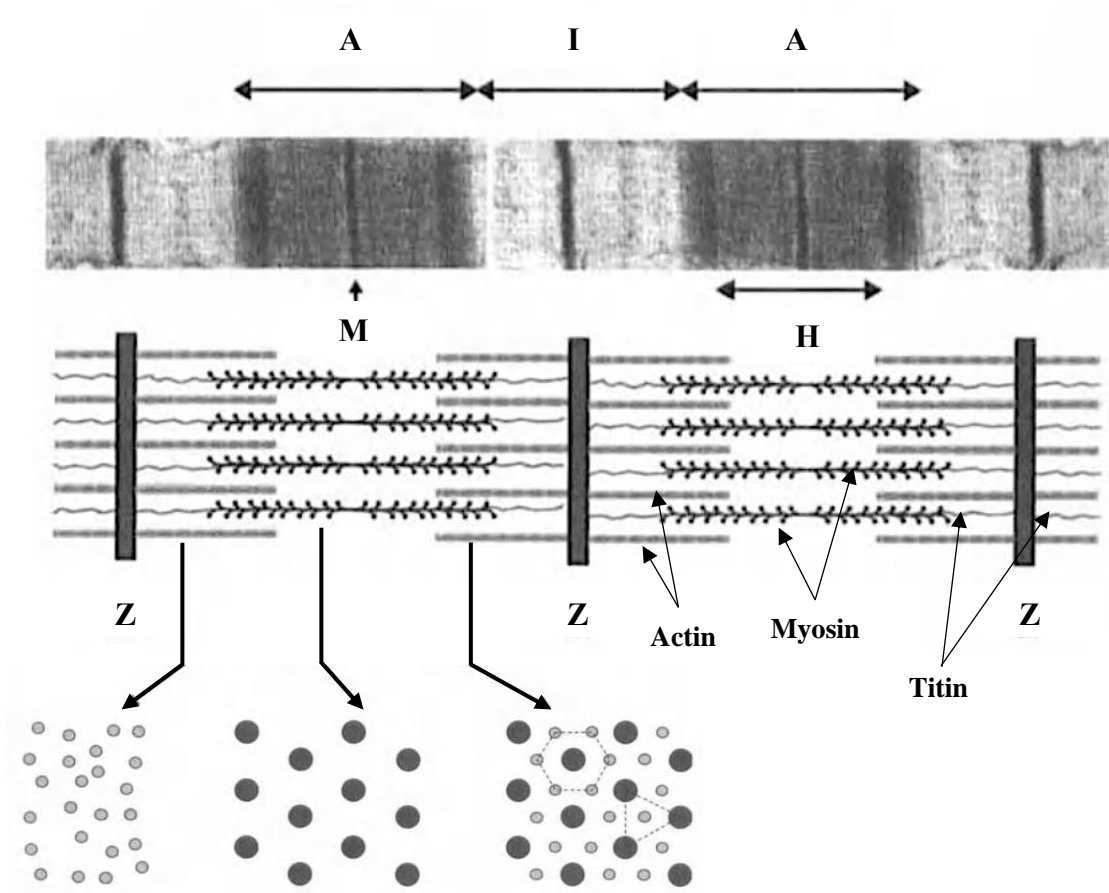


Figure 1.4. SkM sarcomere structure

Schematic representation of the sarcomere. Below represents cross-sections of the sarcomere containing only actin filaments (left), myosin filaments (middle) and overlap of actin and myosin (right). (A = anisotropic/dark band; I = isotropic/light band; H = H-zone; M = M-line; Z = Z-disc/line). Taken from Jones, Round and de Haan (2004).

1.4 Skeletal Muscle Function

1.4.1 Skeletal Muscle Contraction

As described in section 1.3.1 and 1.3.2, it is the well-organised structure of the myosin and actin filaments embedded within the myofibril which gives rise to the precise structure of the sarcomeres and orchestrate muscular contraction to initiate movement and subsequent force production. In order for muscle to contract, a series of events take place. Firstly, a neural signal (known as a nerve impulse) is generated from the central nervous system (CNS) which is sensed by the muscle via the neuromuscular junction (NMJ). It is here where the neurotransmitter acetylcholine (ACh) is released from the neural axons and is received by the ACh receptors located on the motor end plate on muscle which ultimately act as voltage-gate ion channels to permit influx and efflux of sodium and potassium, respectively (MacLaren & Morton, 2011). This results in an overall positive charge and thus depolarizes the plasma membrane which triggers the action potential along the transverse tubule (T-tubules) channels which initiates excitation-contraction coupling. Once the action potential is sensed by the myofibre, Ca^{2+} is released from the sarcoplasmic reticulum (SR) into the sarcoplasm which binds to troponin C on the actin filaments and directs the troponin-tropomyosin complex to expose the binding sites for the myosin heads to attach, enabling the sarcomere to undergo the 'sliding filament mechanism'. This mechanism is underpinned via ATP hydrolysis where the products (ADP and P_i) remain bound to myosin heads. Crossbridges are then formed via the attachment of myosin to the actin binding sites, after which P_i is released to enable tilting and rotation of the myosin heads which leads to a 'pulling' motion, inducing muscular contraction and subsequent force production. During muscle contraction, the I band length of the sarcomere shortens whilst the A band does not change (MacLaren & Morton, 2011). After completion of muscle contraction, there is a reuptake of Ca^{2+} ions into the SR which is regulated via the activity of the SR Ca^{2+} ATPase (SERCA), preparing the muscle for future contraction (Periasamy and Kalyanasundaram, 2007).

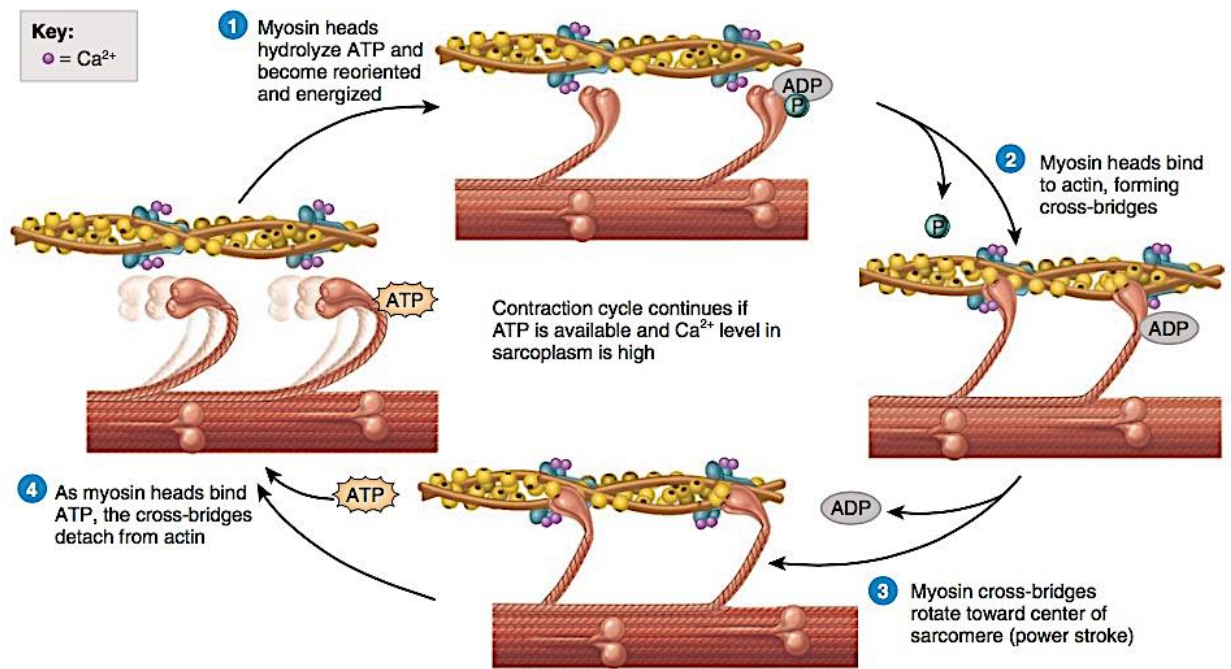


Figure 1.5. SkM contraction

Schematic representation of the cascade of events underpinning SkM contraction. Taken from Tortora and Derrickson (2012).

1.5 Key Regulatory Signalling Pathways Associated with Skeletal Muscle Hypertrophy and Atrophy

1.5.1 Positive Regulators of Skeletal Muscle Mass

The regulation of SkM mass is orchestrated via the synthesis and breakdown of muscle protein whereby muscle size increases when protein synthesis (MPS) exceeds protein breakdown rates (MPB) and represents a 'positive' net protein balance. Conversely, muscle mass is compromised when the net protein balance is 'negative', represented by greater protein breakdown versus protein synthesis rates. Such events are controlled by a number of well-characterised regulatory transcripts/proteins that interact with each other within specific cellular and molecular pathways. The most notable positive regulator of MPS/ribosome biogenesis (increased cellular capacity to undergo protein translation) and subsequent muscle mass is the mammalian target of rapamycin complex 1 (mTORC1) signalling pathway (see Figure 1.6). It

is important to note however that mTOR is difficult to directly measure given its large protein size. Previous researchers have therefore studied the activity of mTOR via measuring the activity of upstream regulators, Akt/PKB, and downstream effectors, p70S6K and 4E-BP1 (Baar & Esser, 1999; Baar *et al.*, 2000; Bodine *et al.*, 2001b; Drummond *et al.*, 2009). The first study to demonstrate the importance of mTOR for inducing SkM hypertrophy following RE subjected rodent plantar- and dorsiflexor muscles to high frequency (100 Hz) chronic electrical stimulation consisting of 10 sets \times 6 reps (3 s contractions per rep, each rep interspersed with 10 s rest and each set separated by 50 s rest) for 2 days/week for 6 \times weeks (Baar & Esser, 1999). Interestingly, increased p70S6K phosphorylation (a key downstream target of mTOR) was highly positively correlated ($r > 0.99$) with the \sim 14% increase in muscle mass post exercise (Baar & Esser, 1999). Soon after, the same group demonstrated that acute mechanical loading (6 cycles of 12% within 20 s, repeated 10 times with a 50 s rest between cycles) of C₂C₁₂ myotubes also demonstrated significant increases in phosphorylation of the protein translation initiator, p70S6K just 3 hrs post-loading (Baar *et al.*, 2000). To further test the assumption as to whether mTOR signalling was indeed key for SkM anabolism/hypertrophy, researchers administered rapamycin (a known inhibitor of mTOR, hence its chosen name ‘target of rapamycin’; Davies *et al.* 2000) prior to functional overload/synergistic ablation in rodents (Bodine *et al.*, 2001b) and acute RE in humans (Drummond *et al.*, 2009) which induced a blunted hypertrophic and protein synthetic response in both rodent and human SkM, respectively. To confirm the role of mTOR in load-induced SkM hypertrophy, Goodman and Hornberger’s group later showed that administration of rapamycin in mTOR-null mice (i.e. rapamycin-insensitive mice) did not prevent muscle hypertrophy (\sim 40% increase in muscle size in 14 days) following functional overload/synergistic ablation and that rapamycin only ablated the hypertrophic response in wild-type mice that were sensitive to rapamycin-induced inhibition of mTOR (Goodman *et al.*, 2011). Taken together, the aforementioned studies clearly demonstrate that mTOR is somewhat sensitive to mechanical loading/RE and is considered the key positive regulator of SkM anabolism and hypertrophy (Philp *et al.*, 2011). Another

controversial mechanism which may be critical for hypertrophy (together with repair and regeneration of SkM) is the regulation of the key muscle-specific satellite cells. However, this topic is discussed in more details in section 1.2 above.

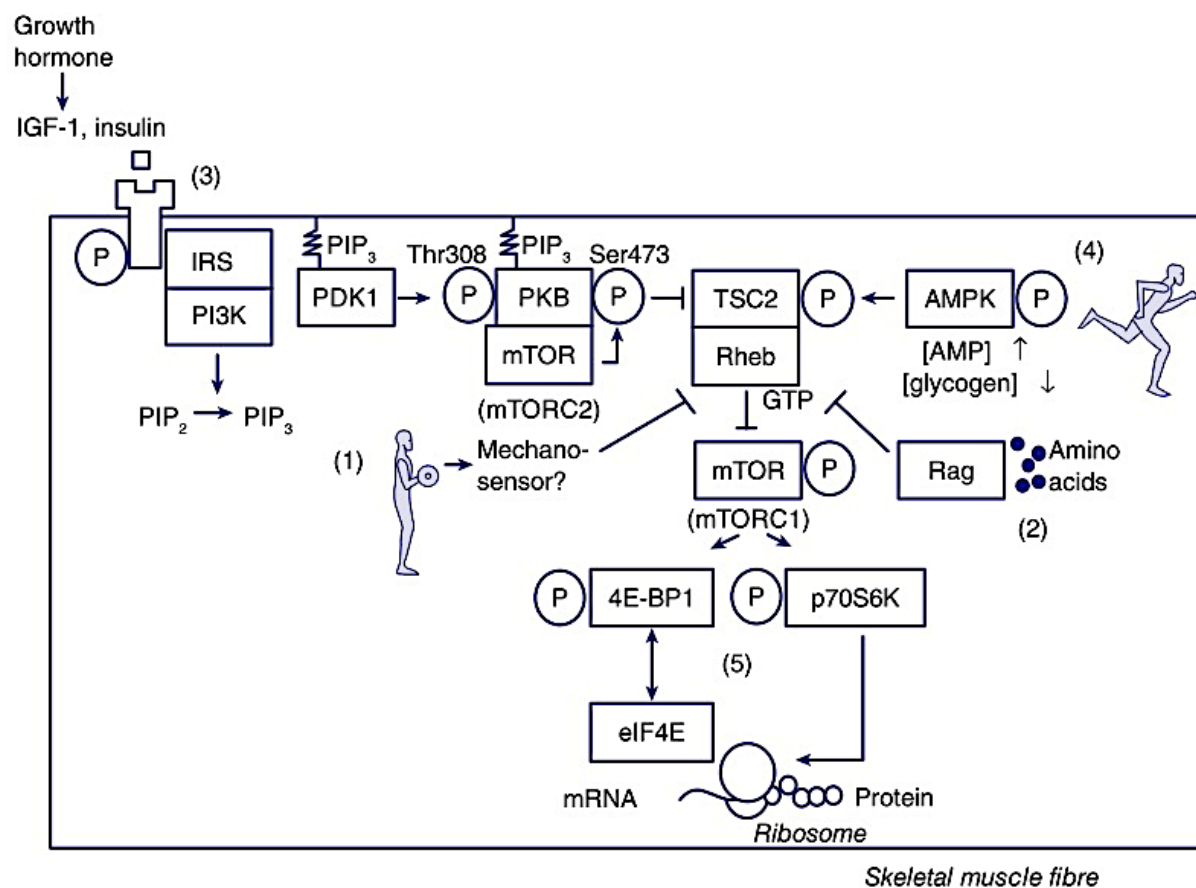


Figure 1.6. mTORC1 signalling pathway

Schematic representation of the regulatory mTORC1 signalling pathway, a well-characterised regulator of SkM mass. Taken from Wackerhage (2014).

1.5.2 Negative Regulators of Skeletal Muscle Mass

The key proposed mechanism which negatively regulates SkM mass is the myostatin/Smad signalling pathway (see Figure 1.7). Indeed, early work first demonstrated that cattle possessing a mutation of the myostatin (also referred to as growth differentiation factor-8, GDF-8) gene displayed a ‘doubling’ in SkM hypertrophy (McPherron & Lee, 1997) which was further exaggerated in myostatin mutant mice overexpressing the Follistatin related gene (FLRG – a known inhibitor of myostatin), resulting in a substantial ‘quadrupling’ increase in muscle size (Lee, 2007). Furthermore, others determined myostatin-specific downstream signalling in *ski* (a transcriptional repressor) transgenic mice, demonstrating that a reduction in Smad can also permit muscle growth by ~3-fold (Sutrave *et al.*, 1990). Despite the supraphysiological increases in muscle size observed following knockdown of myostatin/Smad, additional research reported compromised muscle quality, evidenced by a reduction in specific force (muscle force relative to muscle size or force/cross sectional area of muscle), regardless of increases in absolute force (Mendias *et al.*, 2006). *In-vitro* experiments also demonstrated that myostatin administration (which increased Smad 2/3 activity) reduced mTOR/p70S6K signalling (see section 1.5.1) and myotube size in human muscle derived cells (Trendelenburg *et al.*, 2009). Moreover, myostatin has been shown to be associated with FOXO signalling as suppression of the muscle-specific E3 ligase, MAFbx also resulted in reduced myostatin expression which ultimately enhanced cell differentiation and MyoD expression (Cong *et al.*, 2011). Interestingly, MAFbx (muscle atrophy F-box; FBXO32), together with MuRF-1 (muscle RING finger 1; Trim63) are well-characterised muscle-specific E3 ubiquitin ligases that are critical for the degradation of SkM proteins (Bodine *et al.*, 2001a; Bodine & Baehr, 2014). Therefore, their mechanistic roles and target proteins for degradation are discussed throughout subsequent chapters of this thesis (see Chapter 3, 5 and 6). Taken together, myostatin/Smad signalling and the activity of the muscle-specific atrogenes, MuRF1 and MAFbx are considered key regulators of SkM atrophy.

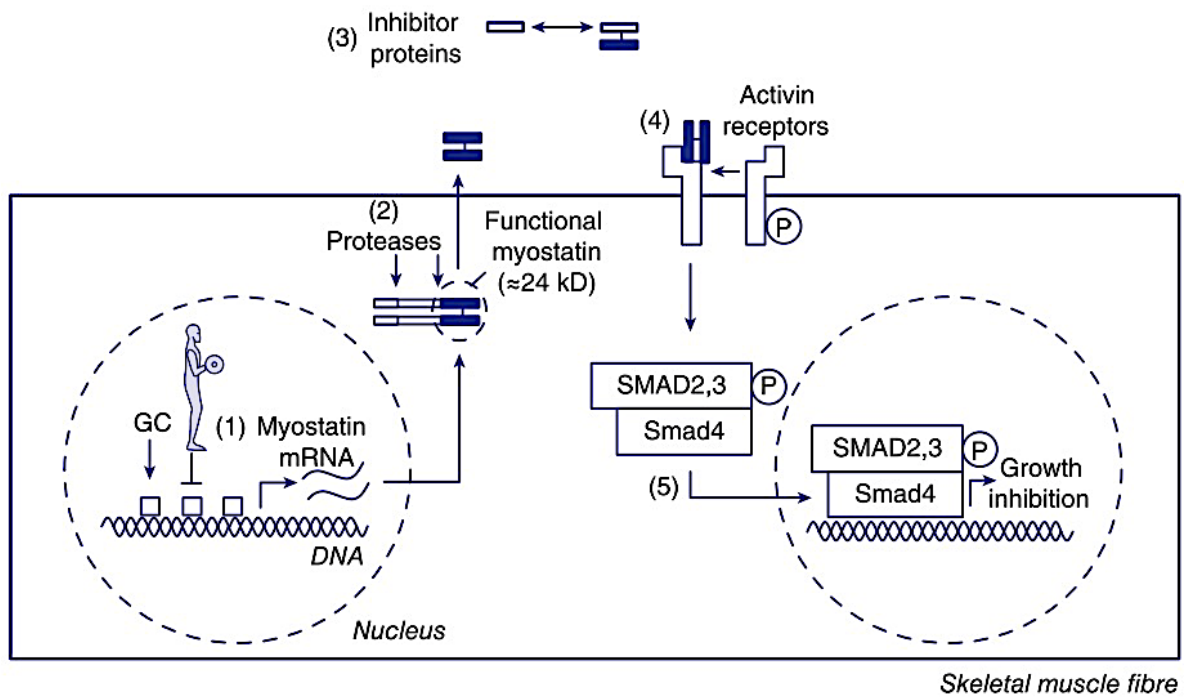


Figure 1.7. Myostatin/Smad signalling pathway

Schematic representation of the regulatory myostatin/Smad signalling pathway which is proposed as a negative regulator of SkM mass. Taken from Wackerhage (2014).

1.6 Epigenetics in Skeletal Muscle

1.6.1 Chromatin, Histones and DNA

The term ‘epigenetics’ (the Greek prefix ‘*epi*’ represents ‘above’ or ‘after’, gene/genetics) was first coined in 1942 by the embryologist, Conrad Waddington whom defined this area of research as the ‘whole complex of developmental processes’ which bridges the gap between the ‘genotype and phenotype’ (Waddington, 1942; Deichmann, 2016). Since the 1940’s however, the drastic increase in epigenetics research (specifically from the year 2000) has evolved our current understanding of this topic which has led to its’ redefinition of heritable changes in gene activity that are not a consequence of changes in the DNA sequence (Haig, 2012; Deichmann, 2016). Epigenetics involves the chemical regulation of histone, chromatin and DNA macromolecules which are located within the nucleus of eukaryotic cells. For this

reason, a brief introduction into their structure is first described before focusing on the key epigenetic modifications that modulate these macromolecules.

The nucleus within eukaryotic cells comprises the 23 pairs of chromosomes of which contain all of the genetic hereditary material (or the molecular blueprint) of each living cell. Each chromosome is made up of chromatin fibres which contain nucleosomes. The nucleosomes are small structures (~ 1 nm in diameter) which are commonly referred to as ‘beads on a string’ given their appearance (see Figure 1.8) as the DNA is wrapped around the core histone proteins which essentially act as scaffolds to enable condense packaging of the DNA molecules (see Figure 1.8). Within the nucleosomes, histone tails containing amino acid sequences extend from the central histone proteins which are prone to a number of post-translational modifications such as methylation (also referred to as ‘hyper’-methylation), demethylation (also referred to as ‘hypo’-methylation), acetylation (addition of a acetyl group), deacetylation (removal of an acetyl group) and phosphorylation (Ramakrishnan, 1997; Widmann *et al.*, 2019). Importantly however, histone modifications are determined via the chromatin state whereby condensed/closed (also termed heterochromatin) or decondensed/open chromatin (also termed euchromatin) prevents or enables such modifications and gene transcription to occur (Bannister & Kouzarides, 2011; Allis & Jenuwein, 2016).

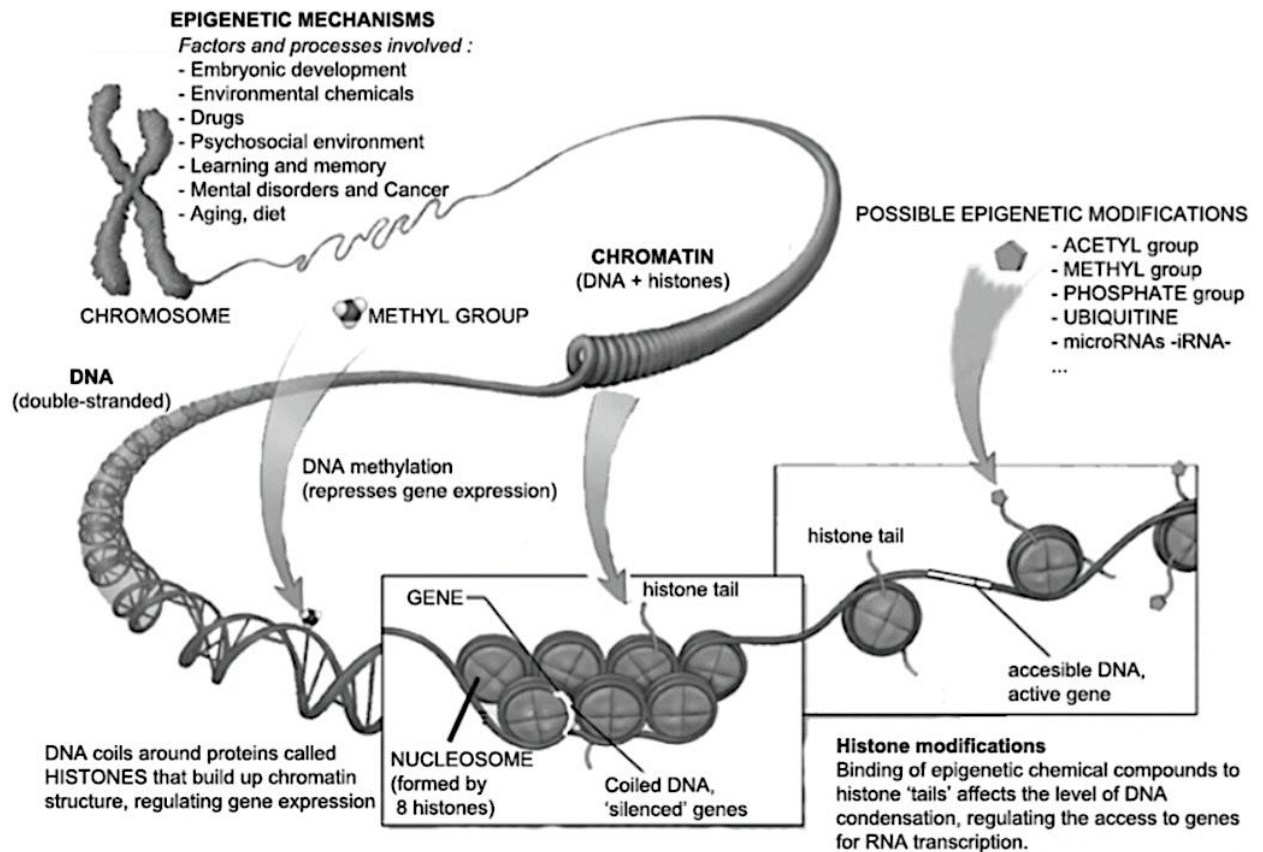


Figure 1.8. Chromatin, histones and DNA structure

Schematic representation of chromatin and nucleosomes extending from the chromosome.

Taken from González-Pardo and Marino (2013).

1.6.2 DNA Methylation

As described in section 1.6.1, histone proteins within the nucleosomes may be subject to various modifications that are dependent on whether the chromatin structures are loosely (i.e. euchromatin state enabling gene transcription) or tightly (i.e. heterochromatin state suppressing gene transcription) condensed. At the DNA level however, epigenetic modifications are predominantly induced by the biochemical process, DNA methylation. DNA methylation (also known as hypermethylation) occurs when a covalent methyl chemical group attaches to the 5th position of a cytosine nucleotide located within cytosine-phosphate-guanidine (CpG) base pairing sites which forms 5-methylcytosine (5-mC; see Figure 1.9). CpG sites are abundant within most regulatory gene promoters, referred to as CpG islands (Sharples and Seaborne,

2019; see Figure 1.9). DNA methylation within the promoter or enhancer regions of genes is capable of changing mRNA expression via two key distinct mechanisms. One mechanism involves the recruitment of CpG methyl binding proteins (MBD) when cytosine is methylated (hypermethylation) which inhibits binding of RNA polymerase, preventing gene transcription from occurring (Bogdanović & Veenstra, 2009). Additionally, recruitment of chromatin remodelling proteins, MecP-1/2, exhibits tightening of chromatin/heterochromatin which also prevents gene transcription (Jones *et al.*, 1998). Taken together, increased CpG DNA methylation, particularly within the promoter region of a gene is associated with a reduction in mRNA expression whereas demethylation (or hypomethylation) may permit gene transcriptional activity, therefore increasing gene expression. It is important to highlight the mechanisms by which DNA methylation is controlled which is nicely presented in recent work by our group (Sharples and Seaborne, 2019; see Figure 1.9). Increased/hypermethylation is accomplished via the enzymatic activity of the DNA methyltransferases (DNMT), DNMT-1, -3a and -3b. Specifically, DNMT1 is important for the maintenance of DNA methylation that may be retained during DNA replication whereas DNMT3a and 3b are responsible for *de novo* methylation, or the addition of ‘new’ methyl groups to cytosine residues which is achieved when a methyl group is cleaved from S-adenosyl methionine (SAM), producing 5mC and S-adenosyl homocysteine (SAH; Trasler *et al.*, 2003, Sharples and Seaborne, 2019; see Figure 1.9). Alternatively, demethylation/hypomethylation is catalysed by the ten-eleven translocation (TET) enzymes via oxidation of 5mC to 5-hydroxy-methyl-cytosine (5hmC; Delatte, Deplus and Fuks, 2014), or as a consequence of insufficient DNMT1 activity where methylation is passively lost during DNA replication (Sharples and Seaborne, 2019, Ito *et al.*, 2010; see Figure 1.9). Collectively, the present section demonstrates that DNA methylation is tightly regulated via the activity of key enzymes, DNMTs and TETs, which determines whether methylation is increased (hypermethylation) or decreased (hypomethylation) ultimately affecting subsequent

gene transcription. The following section will focus on the role of DNA methylation in SkM following exercise with a particular emphasis on the responses to mechanical loading/RE.

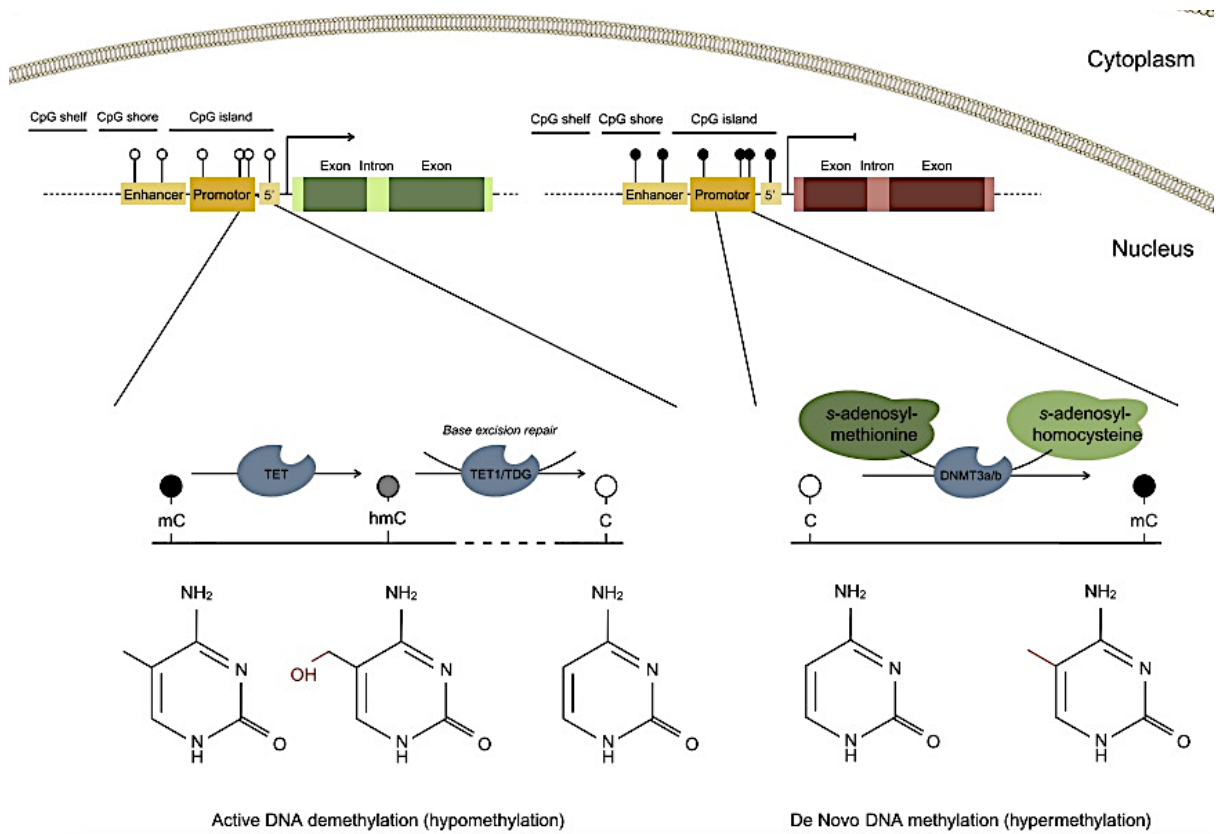


Figure 1.9. Mechanisms of DNA methylation

Schematic representation of the enzymatic reactions associated with increased (hypermethylation) or decreased (hypomethylation) DNA methylation. (CpG = cytosine-phosphate-guanine; TET = ten-eleven translocases; DNMT = DNA methyltransferases). Taken from Sharples and Seaborne (2019).

1.6.3 DNA Methylation and Exercise

Despite decades of research demonstrating the transcriptional regulatory roles in SkM adaptation following mechanical loading/RE (as described in chapters 3, 4 and 5 of this thesis ; Goldberg & Goodman, 1969; Goldberg *et al.*, 1975; Egan & Zierath, 2012), the importance of epigenetics, specifically DNA methylation has only more recently begun to emerge. Indeed, it was not until 2014 that researchers first showed that RE could indeed modulate the human DNA methylome. In this study, Rowlands and colleagues subjected middle-aged (49 ± 5 yrs) type II diabetic male and female humans to chronic RE (6-8 reps \times 2-3 sets \times 8 full body exercise, 3 days/week for 16 weeks) and demonstrated differential DNA methylation across 450K CpG sites at post- versus pre-exercise (Rowlands *et al.*, 2014). Interestingly, the authors reported more genes being hypomethylated versus hypermethylated, and that these differences were in genes associated with ‘cellular assembly and organization, cellular development, tissue morphology, and cardiovascular system development and function’ following pathway enrichment analysis (Rowlands *et al.*, 2014). It is also worth noting that the same study also demonstrated a global reduction in DNA methylation at post- versus pre-chronic endurance cycling exercise (40–60 min steady-state cycling exercise at 65%–85% of heart rate max, 3 days/week for 16 weeks) with pathway enrichment analysis suggesting that genes were associated with ‘lipid/carbohydrate metabolism, metabolic disease, cell death and survival, cardiovascular system development/function, and haematological system development/function’ (Rowlands *et al.*, 2014). This study therefore demonstrated for the first time that DNA methylation is regulated by mechanical loading/RE *in-vivo* which was influenced by the mode of exercise performed, evidenced by the different enriched pathways in RE vs. endurance exercise. Two years after, an Italian group of researchers reported a significant reduction in leukocyte-specific global DNA methylation following 12 weeks of chronic progressive RE (3 days/week, 10-12 reps \times 3-4 sets at 70% 1RM which was assessed via leg extension testing every 2 weeks) in male and female elderly humans (Dimauro *et al.*, 2016). Shortly after, DNA methylation in leukocytes was further investigated using genome-

wide array technology (450K CpG sites) to permit gene-specific methylation analysis following 8 weeks of chronic RE (3 days/week, 10-12 reps \times 3-4 sets at 80% 1RM ensuring 3 s contractions) in humans (Denham *et al.*, 2016). In support of previous findings, RE also evoked hypomethylation of genes which were associated with ‘cancer, axon guidance, diabetes’. Interestingly, a number of anabolic signalling-related genes were also hypomethylated including insulin-like growth factor I receptor (IGF-IR), growth hormone-releasing hormone (GHRH) and fibroblast growth factor 1 (FGF1), with the latter two genes also displaying corresponding increases in mRNA expression, further supporting the notion that epigenetic modifications are associated with changes in gene expression (Denham *et al.*, 2016). A year on, Robinson and colleagues analysed DNA methylation (450K array) profiles in young and old human SkM tissue following 12 weeks of either chronic RE, high-intensity interval training (HIIT) exercise or combined/concurrent exercise (Robinson *et al.*, 2017). Interestingly, DNA methylation did not significantly change (<10%), regardless of exercise type or age group (Robinson *et al.*, 2017). It is important to note however that only gene promoter DNA methylation was reported. Conversely, a study published within the same year demonstrated that RE was able to negate increased genome-wide hypermethylation induced by short term high fat feeding (consisting of >77% of total calorie intake) following bisulfite sequencing analysis (Laker *et al.*, 2017). Using more recent genome-wide technology that permits greater CpG methylation coverage (850K CpG sites), work by our group also reported significant total and gene-specific DNA hypomethylation in response to acute and 7 weeks of chronic RE (Seaborne *et al.*, 2018a, 2018b). Interestingly, a large number of these hypomethylated genes also demonstrated corresponding changes in mRNA expression whereby hypomethylation determined by genome wide analysis, with follow up analysis of candidate genes at the gene expression level following chronic exercise, were associated with increases in mRNA expression. For some genes, hypomethylation was retained during 7 weeks of detraining/unloading where muscle mass returned to baseline/pre-exercise levels of which further decreased following 7 week of retraining (where the greatest increase in muscle mass

occurred) which also corresponded with the greatest increase in mRNA expression (Seaborne *et al.*, 2018a). Suggestive of an ‘epigenetic memory’ (Sharples *et al.*, 2016b) at the DNA level since earlier exercise encounters resulted in an retained response during future RE. Another subset of genes in this study also demonstrated an inverse relationship between mRNA expression and DNA methylation whereby expression and methylation increased and decreased, respectively after chronic RE. Following detraining however, both gene expression and DNA methylation returned back to baseline levels after which the increased mRNA and decreased methylation was enhanced after reloading, further supporting the notion that DNA methylation may indeed regulate gene expression in response to exercise. Specific details of these regulated gene such as names and their gene expression profiles are reported within chapter 5 of this thesis where the transcriptional and epigenetic regulation of these genes are also assessed following acute and chronic loading/RE in in bioengineered/rodent SkM. Although Seaborne *et al.*, (2018) also assessed the genome-wide epigenetic responses to acute RE, there is still limited research that have studied the effects on DNA methylation after acute exercise/loading. Indeed, Zierath’s group demonstrated that acute endurance exercise (cycling exercise at 40 or 80% VO_{2peak} until 1,674 KJ) in humans induced promoter associated hypomethylation of key metabolic genes, PPAR- δ , PGC1- α and PDK4, all of which also displayed increased mRNA expression (Barrès *et al.*, 2012). It is also important to note however that altered DNA methylation of these genes only occurred after performing high intensity exercise (80% VO_{2peak}) and that exercise-induced alterations in DNA methylation may therefore be load/intensity dependent.

1.7 Introduction to Monolayer Cell Culture Mode

In-vitro SkM monolayer culture experiments have provided considerable insights into the cellular and molecular mechanisms underpinning many important biological processes in SkM. These experiments entail extraction of SkM cells from muscle biopsies using a number of techniques such as explant culture (Martin *et al.*, 2013), enzymatic digestion (Danoviz &

Yablonka-Reuveni, 2012) or a combination of both methods (Owens *et al.*, 2015; Turner *et al.*, 2019a). Alternatively, cells can be isolated from entire rodent muscle tissue which provides high cell yield or immortalised cells derived from humans (Mamchaoui *et al.*, 2011) and rodents (Yaffe & Saxel, 1977; Blau *et al.*, 1985) are considered useful for *in-vitro* experiments given their ability to infinitely grow without the risk of senescence as with primary cells. Furthermore, immortalized cells such as the commonly used C₂C₁₂ cell line have superior differentiation capacity and are 100% myogenic, suggestive that results derived from experiments using these cells are not influenced by changes in other cell sources present in muscle tissue (i.e. fibroblasts and small proportion of mesenchymal stem cells; Machida, Spangenburg and Booth, 2004). Once cells are readily available, they are grown in high serum growth media to ensure they are maintained within the cell cycle until they reach a desired confluent state (typically ~60-80%) upon which they are switched to low serum medium to enable cells to exit the cell cycle and differentiate into mature multinucleated myotubes (see Figure 1.10). These stages of culture essentially resemble the processes of SkM embryonic development (see section 1.1) and postnatal growth/regeneration *in-vivo* (see section 1.2). Traditionally however, SkM cells are cultured on rigid polystyrene plastic surfaces (~10⁶ kPa) which does not recapitulate the stiffness or elasticity of native SkM (~12 kPa), ultimately affecting myotube maturation as cells being to detach after contraction (Engler *et al.*, 2004; Gilbert *et al.*, 2010; Chiron *et al.*, 2012). There is also a lack of tension applied to the cells culture in monolayer which leads to the random, dysmorphic formation of myotubes that are not aligned in parallel as is observed *in-vivo* (Eastwood *et al.*, 1998; Smith *et al.*, 2012; see Figure 1.10). To overcome these issues, a number of research groups have developed engineered SkM which entails culturing muscle cells within a surrounding representative extracellular matrix that is under tension (ECM, described in section 1.8).

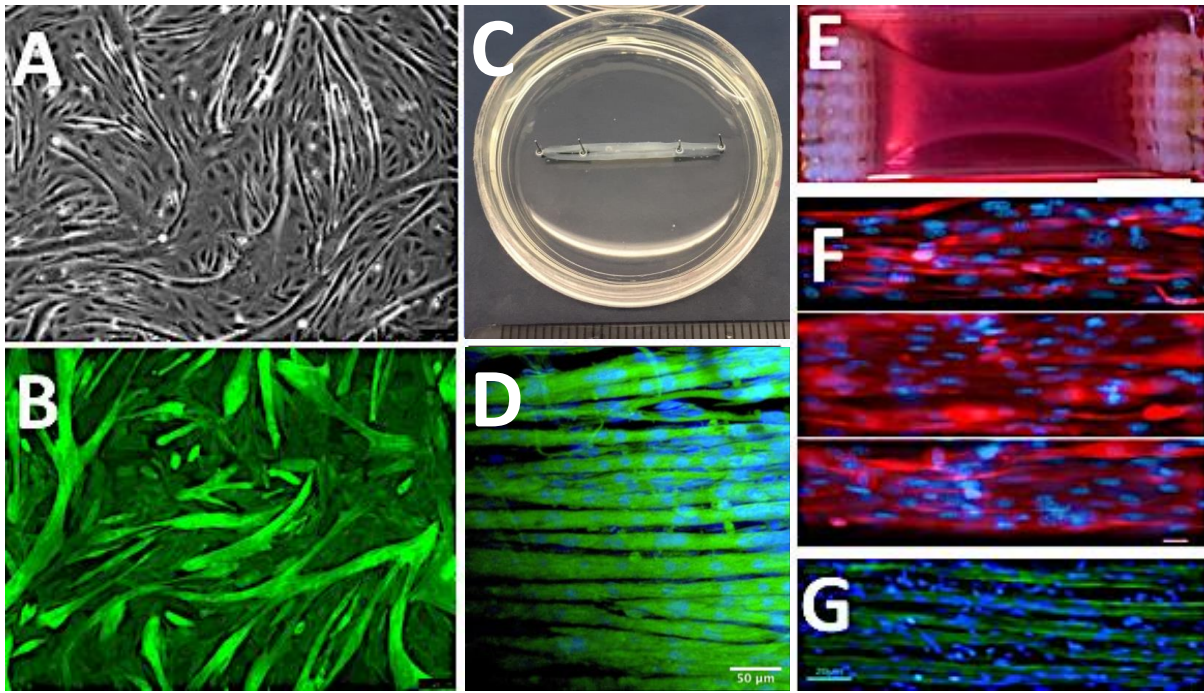


Figure 1.10. Myotube morphology in monolayer versus bioengineered SkM models

(A) Light and (B) fluorescent microscopic images (10 \times , actin-green) of C₂C₁₂ SkM cells cultured in monolayer and the resulting swirling myotube formations that occur when no tension is applied to cells (scale bar 100 μ m; unpublished images taken from our lab). (C) Macroscopic and (D) microscopic images of self-assembled fibrin bioengineered SkM (C₂C₁₂) displaying aligned myotube formation due to applied tension of the pinned silk sutures (scale bar 50 μ m). Fluorescent staining for actin (green) and nuclei (blue). Figures taken from (Seaborne *et al.*, 2019; Turner *et al.*, 2019a). (E) Microscopic and (F) macroscopic representation of type I collagen C₂C₁₂ bioengineered SkM (scale bar 10 μ m) taken from Player *et al.*, (2014), displaying myotube formation (red desmin, blue nuclei) due to unilateral tension applied by the A-frames (scale bar 20 μ m). (G) Fluorescently stained muscle fibres from *in-vivo* tissue (Figure originally from Smith *et al.*, 2012) suggesting that bioengineered muscle morphologically mimics native SkM tissue (scale bar 20 μ m) versus monolayer. Figure adapted from (Kasper *et al.*, 2018).

1.8 Introduction to Skeletal Muscle Bioengineering

Since initial pioneering work in the 1980's (Vandenburgh *et al.*, 1988; Vandenburgh & Karlisch, 1989) there has been incremental improvements in the development of bioengineered SkM for drug screening (Vandenburgh *et al.*, 2008) or studying muscle physiology in response to exercise (Khodabukus *et al.*, 2007, 2018b). However, there are a number of factors which influence the structure and function of these engineered muscles, including cell source (i.e., cell line, primary human/animal cells), media components (i.e., serum, protein crosslinkers, proteolytic inhibitors, antibiotics, nutrients), model (scaffold versus scaffold-free), ECM (synthetic versus biological) and the type of external stimulation applied to the resultant engineered muscle (i.e., electrical stimulation or mechanical loading). All of which are reviewed in Khodabukus and Baar, (2016). The following section however will briefly outline the most common biological ECM proteins used for the fabrication of bioengineered SkM whereas the influence of mechanical loading on these engineered tissues will be reviewed in chapter 3 of this thesis, as it is directly relevant to the experimental work conducted in this chapter.

1.8.1 Collagen

Collagen, is most abundant ECM protein in SkM, contributing to approximately 1-10% of dry muscle mass (Gillies & Lieber, 2011). Collagen type 1 makes up the majority of this and is therefore extensively used in tissue engineering research. The first studies to engineer animal (Vandenburgh *et al.*, 1988) and human (Powell *et al.*, 2002) SkM tissue embedded cells within a type 1 collagen matrix which enabled long term culture (~2-3 weeks), resulting in mature myotubes that were highly aligned in parallel between the points of tension. Producing engineered collagen engineered muscle typically involves mixing large quantities of cells in type 1 collagen derived from the rat tail to polymerise whereby cells are then differentiated into aligned mature myotubes over a given period (typically ~2 weeks) as seen in figure 1.10 (Cheema *et al.*, 2005; Mudera *et al.*, 2010; Player *et al.*, 2014). The large number of cells required to produce mature collagen constructs imposes several issues including throughput,

particularly if using human cells (~20-40 million cells per construct; Mudera *et al.*, 2010) which are usually limited. However, recent work by the same group has further optimised this system to enable the production of collagen bioengineered muscle using much lower seeding densities using rat ($\sim 5 \times 10^6$; Torii *et al.* 2018) cells or C₂C₁₂ and HMDCs which ranged from $10^4 - 2 \times 10^6$ cells/construct (Aguilar-Agon *et al.*, 2019; Capel *et al.*, 2019). It is important to note however that maturation and the quantity of material (i.e., protein) is compromised in the lower density constructs, evidenced by reduced myotube length, width and number and the need to use larger gel volumes for immunoblotting analysis, suggestive that collagen muscle may still therefore require the need for large quantities of cells. Despite this, there has been considerable progress continuously improving this model and is therefore still one of the most employed models in SkM bioengineering research.

1.8.2 Laminin

Laminin is the major non-collagenous protein within the basement membrane/basal lamina and is a critical cell adhesion molecule which connects the cytoskeleton to the ECM via the dystrophin-dystroglycan complex (Lewis *et al.*, 2001). Use of laminin is therefore deemed appropriate for use in monolayer culture and bioengineered SkM experiments. Indeed culturing rat SkM cells on laminin coated plates demonstrated superior cell attachment, proliferation and myotube maturation compared to cells cultured on collagen-coated plates (Foster *et al.*, 1987). In laminin bioengineered muscle, primary rodent SkM cells were subjected to electrical stimulation which resulted in specific forces of ~ 4.2 kN/mm² (Dennis *et al.*, 2001) compared to ~ 200 kN/m² in adult rodent SkM *in-vivo* (Close, 1972), suggestive that the lack of force production does not particularly render laminin muscle a functional engineered SkM model. Interestingly however, others have shown that culturing HMDCs in laminin hydrogels enabled the production of engineered muscle with similar stiffness to native muscle (~ 12 kPa) that could be transplanted into hindlimb of mice which improved muscle regeneration *in-vivo* (Gilbert *et al.*, 2010). Although force was not measured in this study, the low force production in earlier

work by Dennis *et al.*, (2001) may be a consequence of the model employed (self-assembled laminin muscle).

1.8.3 Fibrin

In conjunction with collagen and laminin, the naturally occurring polymer fibrin is also extensively within the literature of SkM tissue engineering research. Fibrin is a developmental matrix, important for the blood clotting after following wound injury and has proven a useful material for studying muscular development, diseases and the physiological response to exercise *in-vitro* (Yen-Chih Huang, Robert G. Dennis, Lisa Larkin, 2005; Huang *et al.*, 2006; Khodabukus *et al.*, 2007, 2015, 2018*b*, 2018*a*; Khodabukus & Baar, 2012; Heher *et al.*, 2015). Indeed, previous research has shown that fibrin engineered SkM displays similar stiffness/elasticity to native muscle (Chiron *et al.*, 2012) and that when subjected to electrical stimulation, displays much greater increases in maximal absolute ($\sim 800 \mu\text{N}$) and specific ($\sim 30 \text{ kN/m}^2$) forces (Huang *et al.*, 2005; Huang *et al.*, 2006) versus collagen and laminin engineered muscles, which increases myotube hypertrophy (Khodabukus *et al.*, 2018*a*). Furthermore, fibrin is able to secrete its own ECM, and bind a number of key growth factors which promote differentiation, including vascular endothelial growth factor (VEGF), basic fibroblast growth factor-2 (bFGF-2), alongside indirect binding of insulin-like growth factor-1 (IGF-I) ultimately improving maturation (Campbell *et al.*, 1999; Sahni *et al.*, 2003). Furthermore, cells are able to proliferate and migrate freely when cultured on fibrin. For this reason, much lower seeding densities are needed for producing mature engineered muscle versus collagen muscle whereby $\sim 10\text{-}18 \times 10^4$ C₂C₁₂ cell line or $\sim 2\text{-}4 \times 10^5$ human cells are required to produce a single self-assembling fibrin muscle construct (Khodabukus & Baar, 2009; Turner *et al.*, 2019*a*). Furthermore, use of PDMS moulds now permit even lower seeding densities when culturing fibrin muscle, however, at the expense of reduced construct size (Heher *et al.*, 2015; Khodabukus *et al.*, 2018*a*). Recent work by Bursac's group has more recently attempted to rectify this issue of using large primary SkM cell densities via using Pax7 overexpressed human pluripotent stem cells (hPSCs) which are much more readily available given their unlimited

proliferative potential versus human SkM cells that are at risk of senescence following multiple passages (Rao *et al.*, 2018). This will also open up exciting avenues for studying muscular diseases in representative *in-vitro* systems. It is also important to highlight a number of factors when using fibrin as the matrix in bioengineering. Indeed, studies have demonstrated batch variation in key fibrin constituents, fibrinogen and the protease thrombin and media components (i.e. streptomycin/glucose concentration and origin of serum), all of which ultimately effect muscle functionality and fibrinolysis rates (i.e. the breakdown of the fibrin via the fibrinolytic enzyme plasminogen; Khodabukus and Baar, 2009, 2015). However, fibrinolysis can be controlled via the administration of plasminogen inhibitors such as aprotinin, aminocaproic acid/amino-hexanoic acid, or using cross-linkers such as genipin, although genipin auto fluoresces, imposing difficulties for immunohistochemical analysis (Khodabukus and Baar, 2009). Therefore, these factors should be carefully considered according to the experimental aims of interest.

Whilst the present section demonstrates the advances made in bioengineered SkM systems over many years it is worth acknowledging a number of common issues faced in bioengineering research. Firstly, bioengineering can be costly and requires a greater level of time and expertise given the stringent techniques involved and the much greater culture time periods versus traditional monolater culture systems. Furthermore, there is little research that has used gene-specific knockdown or overexpression techniques to determine the mechanistic role a particular gene of interest. Indeed, the only study to the authors knowledge that has genetically manipulated gene expression in engineered muscle is that of Shahini *et al.*, (2018) whom overexpressed NANOG in replicatively aged (multiple population doubled, MPD) C₂C₁₂ cells (Sharples *et al.*, 2012, 2016a; Shahini *et al.*, 2018) cultured in a type 1 collagen matrix and demonstrated restoration of differentiation that was impaired in non-treated control cells. Despite this recent work, to the authors knowledge, there are no other studies to date, particularly in fibrin muscle that have manipulated gene expression in bioengineered SkM.

Therefore, monolayer culture models may prove beneficial in various scenarios given their cost effectiveness and simplicity relative to bioengineered culture methods, allowing experiments to be more easily repeated. Furthermore, required seeding densities are reduced in monolayer (Owens *et al.*, 2015) versus bioengineered SkM models (Bradey *et al.*, 2008; Mudera *et al.*, 2010; Martin *et al.*, 2013), enabling higher experimental throughput from the originating sample. Moreover, due to the absence of a surrounding matrix, cells cultured in monolayer may be more easily transfected to induce gene-specific silencing/overexpression to investigate their mechanistic role *in-vitro*. Therefore, use of either or both monolayer and bioengineering *in-vitro* systems in some circumstances would be beneficial, dependent upon the experimental aims of interest.

1.9 Thesis Aims and Objectives

The overarching aim of the present thesis was to investigate whether acute mechanical loading of murine bioengineered fibrin SkM could recapitulate the transcriptional and epigenetic responses that occur following loading/RE *in-vivo*. Therefore, a series of experiments were conducted to achieve a number of aims:

1. Firstly, in chapter 3, this thesis aimed to mechanically load C₂C₁₂ fibrin bioengineered SkM using distinct loading regimes and determine the mechano-responses using a novel bioreactor system, not previously used for loading SkM. This was accomplished via assessing mRNA expression of known mechano-sensitive genes that have also been shown to be regulated after mechanical loading in other bioreactors previously published.
2. Secondly, in chapter 4, using large scale genome-wide bioinformatics analysis of publicly available data sets, we aimed to identify which genes were frequently regulated across both the human transcriptome and methylome after RE in human SkM. This

would provide an appropriate subset of genes to investigate at the mRNA and DNA methylation level, to confirm if mechanical loading in fibrin bioengineered muscle mimicked the *in-vivo* loading response in the subsequent chapter (chapter 5 below).

3. In chapter 5, after identifying which genes were regulated across the transcriptome and methylome after RE in human SkM in chapter 4, the following aim was to assess the transcriptional and epigenetic response of these genes following mechanical loading in bioengineered SkM to establish whether loading fibrin engineered SkM *in-vitro* was a representative model that mimicked loading in humans and rodent muscle *in-vivo*.
4. Finally, in chapter 6 of this thesis, we aimed to induce gene-specific knockdown of the most upregulated gene (UBR5) identified after acute loading in bioengineered SkM alone and across all additional models and species of RE/loading (in chapter 5), in order to determine its mechanistic role following mechanical loading in human myotubes.

CHAPTER 2

Materials and Methods

2.1 Cell Culture

All cell culture procedures were undertaken in a Class II Microbiological Safety Cabinet (BSC; Kojair Biowizard Silverline, Finland) under aseptic conditions. All cells were sub-cultured and incubated in a HERAcell 150i CO₂ humidified incubator (Thermo Fisher Scientific, Denmark) at 37 °C and 5% CO₂ and were routinely monitored using an inverted light microscope (Olympus, CKX31, Japan).

2.2 Conventional Monolayer Cell Culture

2.2.1 The C₂C₁₂ Cell Line

All murine C₂C₁₂ mouse skeletal muscle (SkM) myoblasts were sourced from the American Tissue Culture Collection (ATCC; Rockville, USA) and were passaged (~P12) to increase cell yield and were stored in liquid nitrogen (LN₂) until required for experimentation. C₂C₁₂ cells are the C₁₂ sub-clone and daughter of the C₂ parental cell line, originally derived from the crush injured leg of the C3H mouse (Yaffe & Saxel, 1977; Blau *et al.*, 1985). The C₁₂ sub-clone was selected for their differentiation capability, hence the extensive use of this cell line for *in-vitro* SkM research. For bioengineered SkM experiments, C₂C₁₂ cells were first differentiated in monolayer culture over 7 days to determine their differentiation capacity (see Figure 2.1). Indeed, differential cloning of C₂C₁₂ cells has been shown to display high variation in myotube formation when cultured in fibrin bioengineered SkM (Khodabukus & Baar, 2009). Therefore, determining the differentiation potential in monolayer prior to using cells for tissue engineering purposes improved SkM construct maturation during bioengineered SkM experiments.

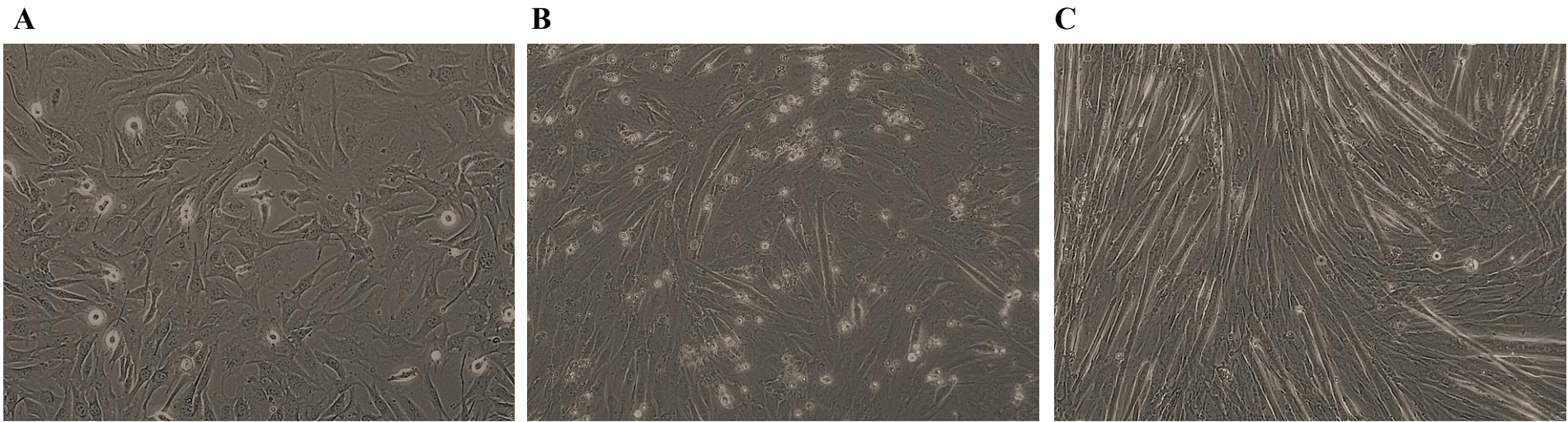


Figure 2.1. C₂C₁₂ myoblasts differentiation in monolayer

Murine C₂C₁₂ myoblasts cultured in differentiation medium (DM) at (A) 0 hrs, (B) 72 hrs and (C) 7 days (10× magnification, Olympus, CKX31).

2.2.2 Human Skeletal Muscle Derived Cells (HMDCs)

SkM tissue (~200 mg) was obtained from the vastus lateralis quadriceps muscle via a conchotome biopsy of consenting participants self-recruited from the university campus via email or verbal communication (see Table 2.1). All participants were considered healthy as determined by blood pressure, resting heart rate, and height and weight (for BMI) measurements, together with completion of a pre-biopsy medical history questionnaire. Muscle biopsies were undertaken in a designated biopsy suite in the Tom Reilly Building (TRB), Liverpool John Moores University, UK following participant recruitment and informed consent procedures. Ethical approval was granted for the collection of muscle tissue under the REC reference code [15/SPS/052].

Following sample collection, muscle tissue was immediately dissected in a sterile irradiated petri dish (100 mm, VWR, UK) using 2 × disposable sterile scalpels (No. 11, Swann-Morton, UK) and placed in sterile microfuge tubes (Ambion[®], Thermo Fisher Scientific Denmark) containing 1.5 ml of cool (4°C) transfer media (TM) composed of Ham's F-10 medium including 1 mM L-glutamine (LG; Thermo Fisher Scientific, Denmark), 0.1% heat inactivated fetal bovine serum (hiFBS; Gibco[™], South America Origin, Fisher Scientific, UK), 0.1% heat inactivated new born calf serum (hiNBCS; Gibco[™], New Zealand Origin, Fisher Scientific, UK), 100 U/ml penicillin (Lonza, UK), 100 µg/ml streptomycin (Lonza, UK), 2.5 µg/ml amphotericin B (Sigma-Aldrich, UK). Tubes containing the dissected tissue were then placed on ice and transported to the cell culture laboratory (Life Science Building, Liverpool John Moores University, UK) within 10 mins post-harvesting for subsequent cell isolation procedures.

Using a modified version of methods previously established (Crown *et al.*, 2000) the contents of the cryovial containing transfer media was emptied into an irradiated 100 mm × 15 mm

sterile petri dish (Sigma-Aldrich, UK) within a tissue culture hood. The excess transfer media was then removed followed by 3 × in phosphate buffered saline (1× PBS, Sigma-Aldrich, UK) washes and any visible connective and adipose tissue was removed using 2 × sterile scalpels. Five millilitres of 0.05% trypsin/0.02% ethylenediaminetetraacetic acid (trypsin/EDTA; Lonza, UK) was then added to the tissue where it was minced using sterile scalpels for 1-2 mins. The trypsin solution was pipetted into a sterile 100 ml polypropylene specimen pot (Fisher Scientific, UK) containing a 6 mm × 35 mm magnetic stir bar (VWR, UK) and placed on a heated (37°C) magnetic stirring platform at for 10 mins. This process was repeated before placing the homogenised tissue into a 15 ml sterile tube (Falcon[®], Fisher Scientific, UK) containing 2 ml heat inactivated horse serum (hiHS; Gibco[™], New Zealand Origin, Fisher Scientific, UK) to neutralise the trypsin. The tube was then centrifuged at 340 × g for 5 min at 24°C. Following centrifugation, the top 2.5 ml was discarded whilst the next 5 ml was seeded onto a pregelatinised (0.2% in dH₂O; Type A, Sigma-Aldrich, UK) T25 flask (Nunc[™], Thermo Fisher Scientific, Denmark) with 7.5 ml of human growth medium (HGM) composed of Ham's F-10 medium that includes 1 mM LG, 10% hiFBS, 10% hiNBCS, 4 mM LG, 100 U/ml penicillin, 100 µg/ml streptomycin and 2.5 µg/ml amphotericin B. Finally, the remaining contents were resuspended in 7.5 ml of fresh HGM and seeded on a separate pre-gelatinised (2 ml of 0.2% gelatin in dH₂O per T25 flask, incubated at RT for 15 mins). Both T25 flasks were then incubated for 5 days to allow cells to migrate out of the tissue explant and adhere to the culture flask surface. HGM was changed every 48 hrs until cells reached ~80% confluency (see Figure 2.2).

Table 2.1. SkM biopsy characteristics indicating participant number, age (in years), height (cm) and weight (kg) for BMI, biopsy procedure and muscle obtained, cell myogenicity (%) and final passage number used for mechanical loading.

Participant Number	Age of Donor (yrs)	Biopsy Procedure	Biopsy Location	Myoblast Proportion (%)
001	25	Conchotome	Vastus Lateralis	70.47
002	19	Conchotome	Vastus Lateralis	70.77
003	24	Conchotome	Vastus Lateralis	74.70

Final Cell Passage Number (P)	Body Mass (kg)	Height (cm)	Body Mass Index (BMI)
P8	79.25	179	24.87
P9	71.8	180	22.06
P7	75.1	183	22.40

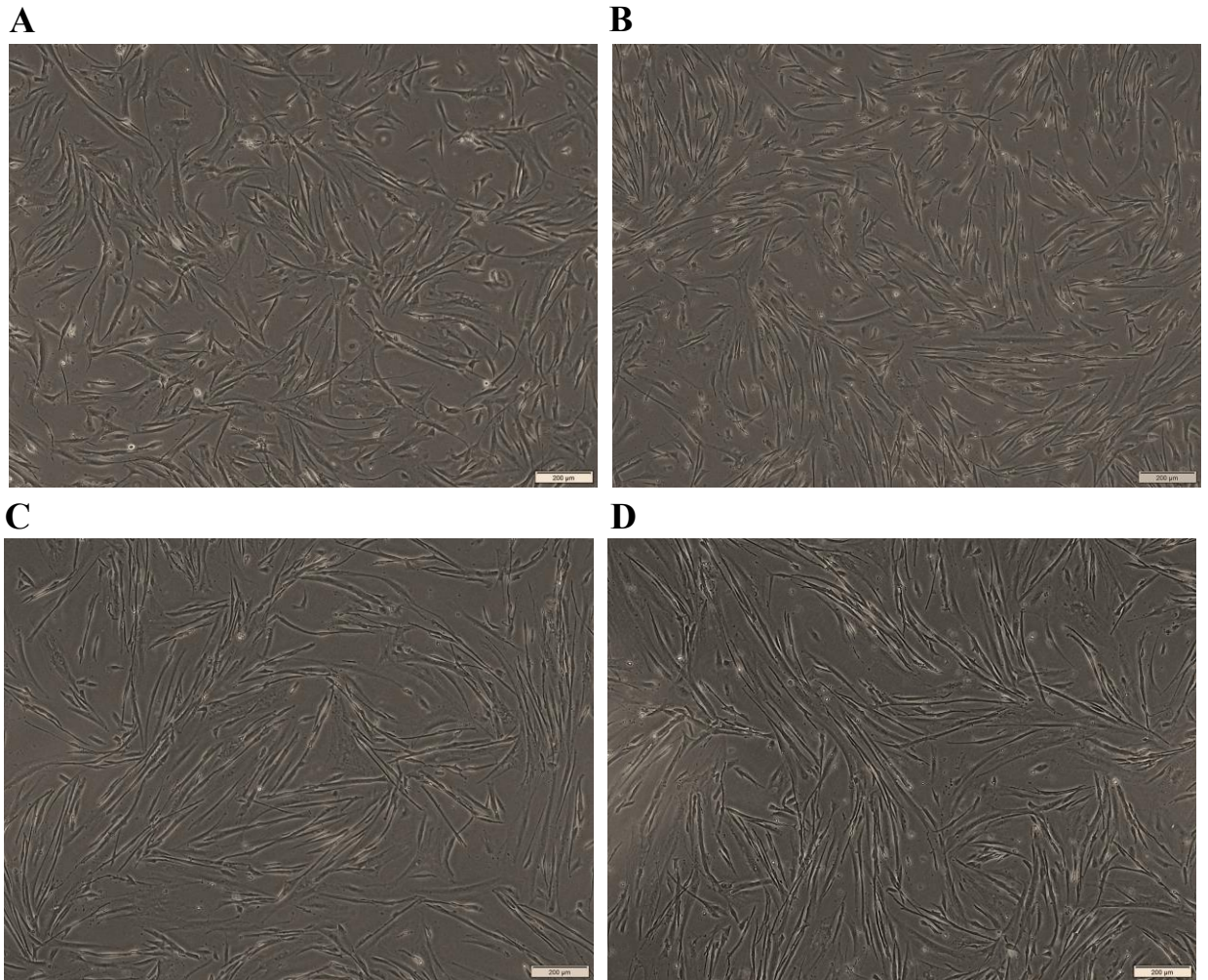


Figure 2.2. Differentiation of HMDCs in monolayer

Human skeletal muscle derived cells (HMDCs) at (A) 0 hrs, (B) 72 hrs, (C) 7 days and (D) 10 days in HDM (10× magnification, Olympus, CKX31).

2.2.3 Cell Counting

After trypsinising cells (see section 2.2.3), the suspension was homogenised $5 \times$ using a 19G hypodermic needle (Becton Dickinson, USA). Cells were then manually counted on a Neubauer haemocytometer (BLAUBRAND[®] Neubauer, Sigma-Aldrich, UK) using the trypan blue exclusion method whereby $10 \mu\text{l}$ of cell suspension was diluted with $10 \mu\text{l}$ 0.4% trypan blue stain (Sigma-Aldrich, UK) at a 1:1 ratio. The mixture was then pipetted onto either end of the haemocytometer, flooding both chambers via capillary action. Cells present within each quadrant were counted. Small, round and clearly visible cells were considered viable whereas larger, darker/blue stained cells were considered non-viable cells or debris and were therefore excluded from cell counts (see Figure 2.3) for the purposes of calculating seeding density of future experiments. To determine the concentration of cells (cells/ml) present within the cell suspension, the mean number of cells in $8 \times$ grids was calculated (average cell numbers per 0.1 mm^3 grid) which was multiplied by 2 (to account for the trypan blue dilution factor) and 10^4 (to convert the number of cells in 0.1 mm^3 to 1 cm^3). The total number of cells present within the cell suspension was calculated via simply multiplying the cells/ml by the cell suspension volume in ml (see Equation 2.1).

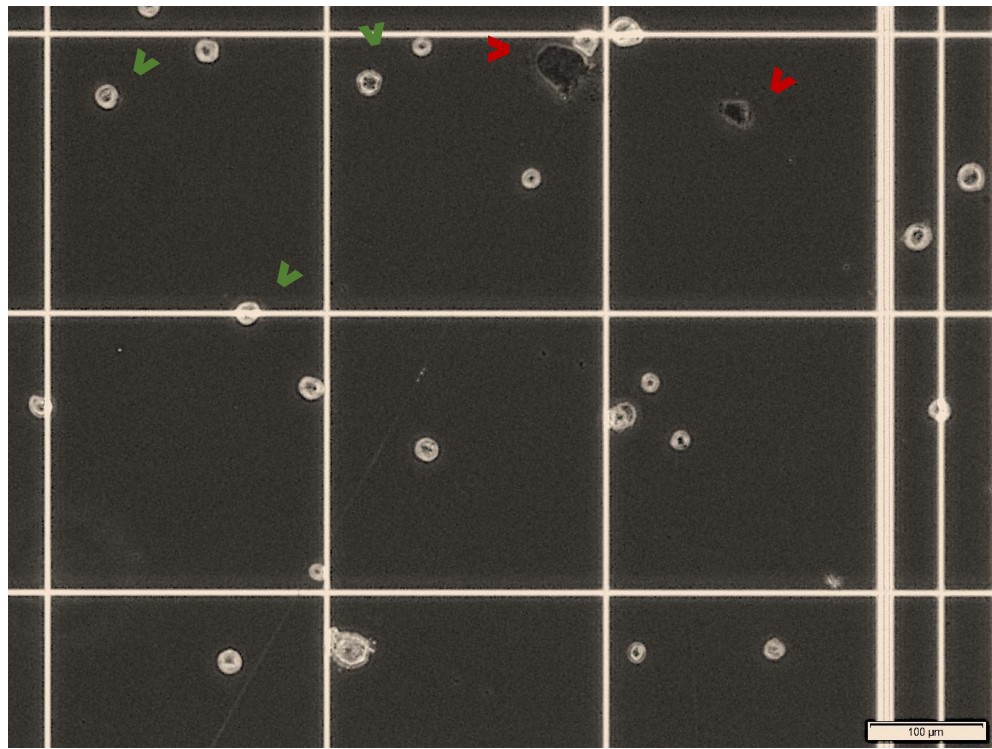


Figure 2.3. Cell counting using a Haemocytometer

An example of cells within a quadrant on a Haemocytometer. Each quadrant contains $16 \times$ grids and a total of $8 \times$ quadrants were counted. Only viable cells (GREEN arrows) were included for all cell counts and nonviable cells/debris (RED arrows) were excluded (10 \times magnification, Olympus, CKX31).

Cell Counting Equation

$$\text{Cells/ml} = \text{Average of 8 grids} \times \text{dilution factor (2)} \times 10^4 \text{ cells/ml}$$

$$\text{Total number of cells} = \text{Cells/ml} \times \text{cell suspension volume (ml)}$$

Cell Seeding Density Equation

$$\text{Cell suspension required (ml)} = \frac{\text{Desired cell concentration (cells/ml)}}{\text{current cell concentration (cells/ml)}} \times \text{required cell suspension volume (ml)}$$

Equation 2.1. An example of equations used to calculate cell concentrations (cells/ml), the total number of cells and the desired cell concentration for seeding cells.

2.2.4 Cell Cryopreservation and Resuscitation

Once counted (see section 2.2.4), GM/HGM was added to existing cell suspension to ensure a concentration of 1×10^6 cells/ml (for C₂C₁₂ cells) or 5×10^5 cells/ml (for HMDCs). Dimethyl sulfoxide (DMSO; Sigma-Aldrich, UK), a cryoprotectant that prevents ice crystal formation, was added at 10% of the total cell suspension volume (Lovelock & Bishop, 1959) before distributing the cell suspension into labelled (name, cell type, passage number, concentration and date) 2 ml cryovials (Simport™, Fisher Scientific, UK). The cryovials were transferred to a cryopreservation container ('Mr Frosty', Thermo Fisher Scientific, Denmark) containing 200 ml of isopropanol (Sigma-Aldrich, UK) and was placed in a -80°C freezer for 24 hrs to ensure a gradual freezing rate (-1°C/min) before storing in liquid nitrogen (LN₂). When resuscitating cells, a cryovial was removed from LN₂, mist sprayed with 70% industrial methylated spirits (IMS) and placed in a BSC to thaw at RT. Cell suspension was then pipetted onto a pre-gelatinised T75 flask(s) (5 ml of gelatin per T75, incubated at RT for 15 mins) containing 20 ml of preheated (37°C) HGM/GM and incubated at 37°C, 5% CO₂ to allow cell attachment and proliferation over the ensuing days. The time to reach ~80% confluency varied for HMDCs given inter-individual differences in cell growth. However, 1×10^6 of C₂C₁₂ cells typically reached ~80% confluency at approximately 72 hrs.

2.2.5 Differentiation of C₂C₁₂ Cells in Monolayer Culture

As described in section 2.2.1, C₂C₁₂ cells were differentiated in monolayer culture over 7 days to first assess their differentiation capacity before using for SkM tissue engineering purposes (see Figure 2.1). This was to determine which stocks of C₂C₁₂ cells demonstrated the greatest increase in myotube formation and would therefore be sub-cultured within a fibrin muscle during bioengineered SkM experiments. During the initial monolayer experiments, various stocks of C₂C₁₂ cells were first sub-cultured to ~80% confluency in T75 flasks. Once ~80% confluency was attained, cells were trypsinised and seeded on pre-gelatinised 6-well plates (1 ml of gelatin per well, incubated at RT for 15 mins) at a density of 8×10^4 /ml in 2 ml of GM

(see Equation 2.1). Well plates were incubated for 24 hrs to reach ~80% confluency before switching to differentiation medium (DM) composed of high glucose DMEM, 2% hiHS, 2 mM LG, 100 U/ml penicillin and 100 µg/ml streptomycin and was topped up with 1 ml of GM at 72 hrs. The differentiation experiment was terminated at 7 days.

2.2.6 Differentiation of Human Skeletal Muscle Derived Cells

HMDCs were seeded onto fibronectin (F1141, Sigma-Aldrich, UK) at a concentration of 10 µg/ml in PBS (1×) to promote cell attachment 6-well plates at a concentration of 9×10^4 cells/ml in 2 ml of HGM (see Equation 2.1). Once cells had reached ~80% confluency (typically 2-3 days), HGM was switched to 2 ml human differentiation media (HDM) composed of Ham's F-10 medium that includes 1 mM LG, 2% hiFBS, 4 mM LG, 100 U/ml penicillin, 100 µg/ml streptomycin and 2.5 µg/ml amphotericin B. Each well received an additional 1 ml of HDM at 72 hours and 7 days. The differentiation time course was terminated at day 10 (see Figure 2.2).

2.3 Dosing of UBR5 siRNA in Human Myotubes

2.3.1 Principle

RNA interference (RNAi) is a natural mechanism that has become a popular tool for manipulating the activity of a target gene in order to characterise its mechanistic role both *in-vitro* and *in-vivo*. This mechanism can be induced experimentally via transfecting cells or tissue with small (typically 21 nucleotides long) synthetic double stranded (ds) RNA molecules known as short interfering RNA's (siRNA; Tuzmen *et al.*, 2007). Delivery of siRNA into cells can be achieved using cationic lipids (e.g. lipofectamine) or using physical methods (e.g. electroporation; Oliveira, Storm and Schiffelers, 2006). Once inside the cell, siRNA's bind to the protein argonaute to form the RNA-induced silencing complex (RISC). The siRNA 'guide' strand directs RISC to target mRNA transcripts with complimentary sequences to the bound

siRNA molecule. mRNA is then cleaved and degraded, resulting in transcriptional silencing of the target gene (see Figure 2.4; Tuzmen *et al.*, 2007).

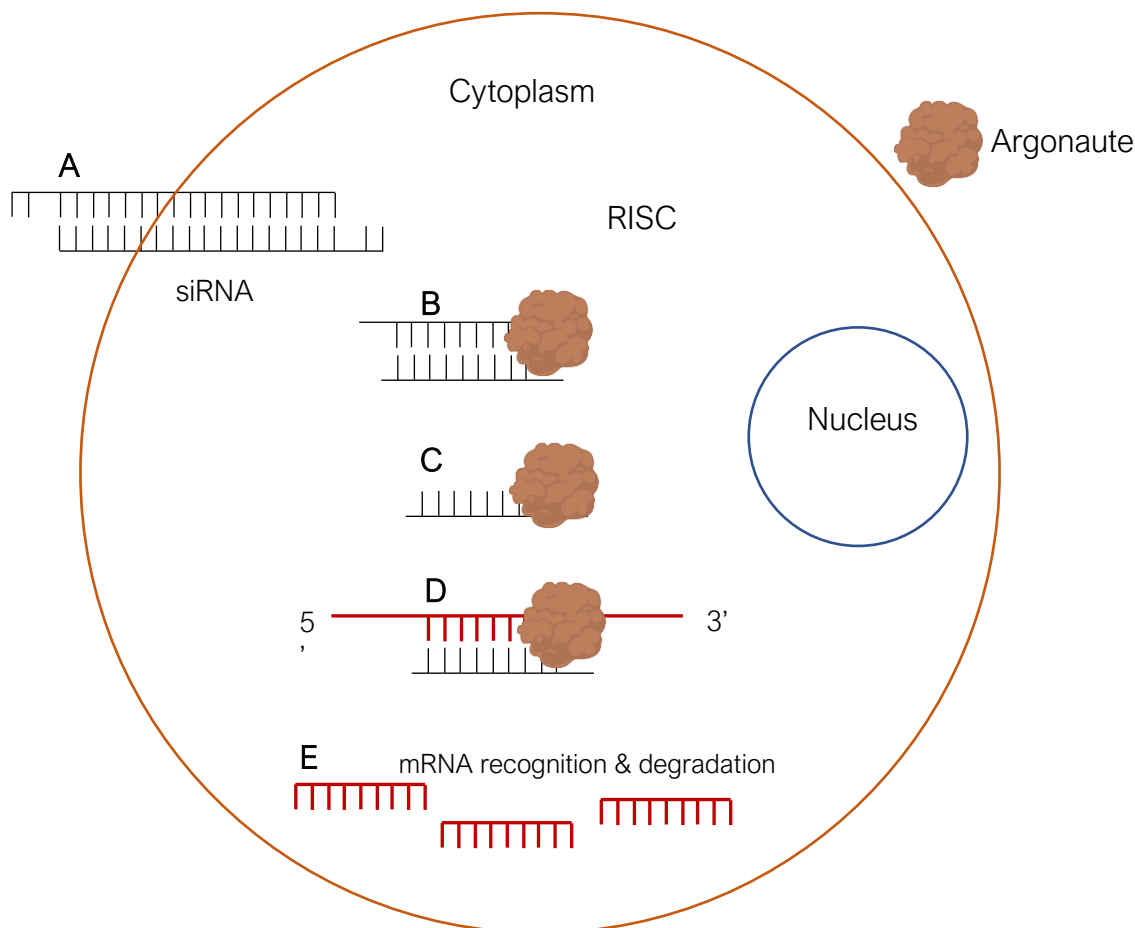


Figure 2.4. Mechanisms of siRNA silencing

Synthetic double stranded (ds) RNA molecules known as short interfering RNA's (siRNA) are delivered into the cell using lipid (e.g., lipofectamine) or physical methods (e.g., electroporation). **(B)** Once inside the cell, siRNA's bind to the argonaute protein to form the RNA-induced silencing complex (RISC). **(C)** The 'guide' strand is then cleaved from the ds siRNA molecule which **(D)** directs RISC to target mRNA transcripts with complimentary sequences to the bound siRNA molecule. **(E)** mRNA is then cleaved and degraded, resulting in transcriptional silencing of the target gene. Schematic representation was adapted from the Qiagen 'Flexible RNAi Technologies' handbook.

2.3.2 Procedure

Throughout this thesis, 4 × synthetic siRNAs (Flexitube GeneSolutions™, Qiagen, UK) were transfected into human myotubes (see section 2.2.7) to target various regions of the 10900 bp UBR5/EDD1 human gene in order to maximise post-transcriptional gene silencing potential (see Table 2.2). Each of the 4 × siRNA lyophilised pellets (1 nmol) were diluted in 100 µl of RNase-free H₂O to ensure a 10 µM stock solution. For siRNA validation experiments, cells were also transfected with a negative control siRNA (AllStars Negative Control siRNA™, Qiagen, UK) to confirm whether changes in gene expression were specific to the gene of interest. The AllStars Negative Control siRNA™ pellet (5 nmol) was reconstituted in 1 ml of RNase-free H₂O to ensure a 5 µM stock solution. HiPerFectTransfection™ (Qiagen, UK) reagent containing a blend of cationic and neutral lipids was used to facilitate uptake of siUBR5 and negative control siRNA into differentiated cells. For siUBR5 validation experiments, human myotubes (see Section 2.2.7) from 3 participants (see Table 2.1) were washed 2 × in PBS and subjected to 1 of 4 conditions; Flexitube GeneSolutions™ (siUBR5) alone, AllStars Negative Control siRNA™ (negative siRNA) alone, HiPerFectTransfection™ (transfection reagent) alone and HDM alone. For the siUBR5 condition, 1 µl of each target siRNA was diluted in 1 ml of HDM containing 12 µl transfection reagent to ensure a 10 nmol working solution. Negative control cells received 2 µl of negative siRNA in 1 ml of HDM containing 12 µl transfection reagent to ensure a 10 nmol working solution. The transfection reagent alone condition consisted of 12 µl of transfection reagent in 1 ml of HDM and the final condition received 1 ml of HDM only. After dosing, cells were incubated for 3 hrs before lysing with TRIzol for subsequent RNA isolation (see section 2.8.1). UBR5 expression was analysed via quantitative real-time polymerase chain reaction (qRT-PCR; see section 2.9.4) where the mean cycle threshold (C_T) value of duplicates for each sample of each condition was analysed to confirm knockdown efficiency. Given the gene knockdown efficiency was low following validation experiments (-25.72 ± 4.72%) using a concentration of 10 nmol, siRNA concentrations were increased to 20 nmol (1.5 µl of each target siRNA diluted in 750 µl of

HDM containing 9 μ l transfection reagent) during subsequent experiments and were able to confirm efficient knockdown of UBR5 ($-77.39 \pm 0.74\%$) as demonstrated in experimental chapter 6.

Table 2.2. UBR5/EDD1 (NM_015902, 10900 bp length) siRNA target sequences

Product Name	Target Sequence
Hs_EDD1_3	CTGGTATTTCTTCAATGCCGA
Hs_EDD1_2	CCAAATCTAGAGTGTATCCAA
Hs_EDD1_1	TTCAACTTAGATCTCCTGAAA
Hs_EDD_2	CAGGTATGCTTGAGAAATAAT

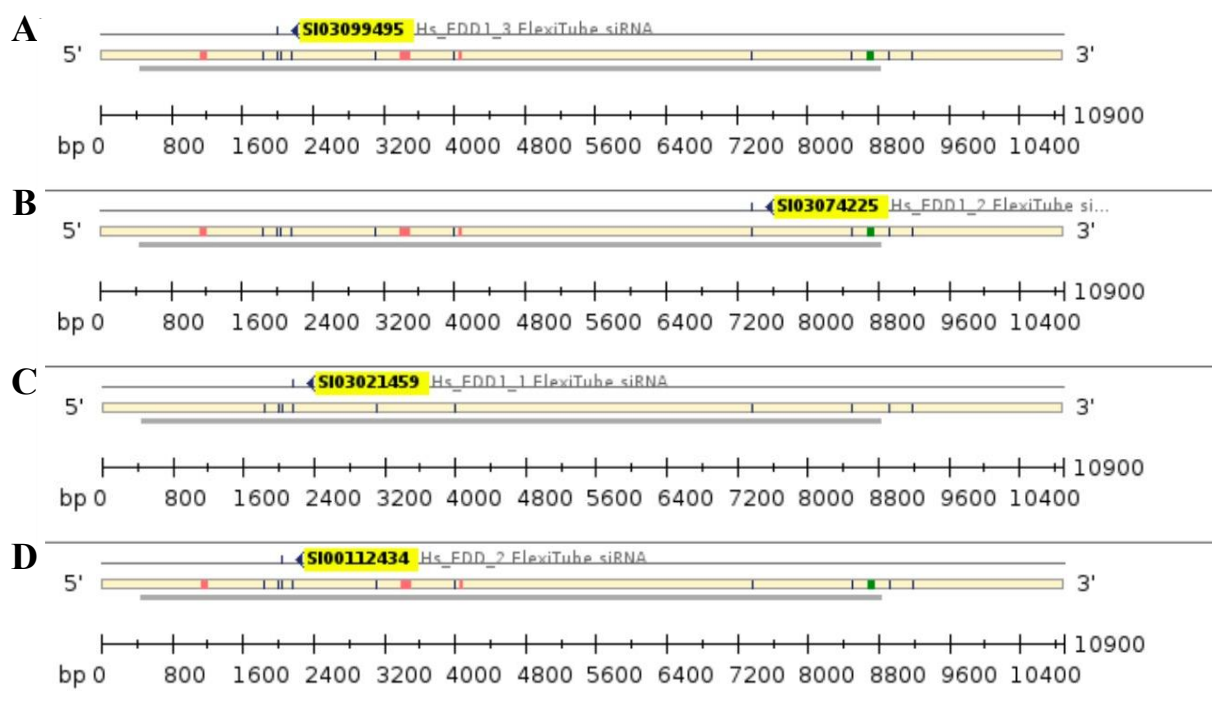


Figure 2.5. UBR5 siRNA target sequence locations

Graphical representation of the 4 \times siUBR5 sequence locations, targeting various regions of the 10900 bp UBR5 human gene. (A) Hs_EDD1_3. (B) Hs_EDD1_2.03 (C) Hs_EDD1_1. (D) Hs_EDD_2.

2.4 Bioengineered Fibrin Skeletal Muscle Constructs

The materials and methods used for tissue engineering purposes throughout this thesis have been described extensively elsewhere (Seaborne *et al.*, 2019; Turner *et al.*, 2019a) and the following sections have therefore been adapted from this published work throughout. Given batch variations in fibrin constituents (Khodabukus & Baar, 2009, 2016), batch catalogue numbers for each reagent are included throughout.

2.4.1 Preparation of Reagents

All reagents stored at -20°C were thawed at RT prior to use. Reagents were never freeze-thawed and were therefore only used once. Fibrinogen from Bovine Plasma (F8630, Sigma-Aldrich, UK) was dissolved at 20 mg/ml in pre-heated (37°C) Ham's F12-K media (Sigma-Aldrich, UK) in a 100 mm specimen pot(s) containing a magnetic stir bar and was incubated at 37°C on a magnetic stirrer for 2 hours. Fibrinogen solution was then sterile vacuum filtered (0.22 µm, Merck™ Stericup™, Fisher Scientific, UK), aliquoted into 2 ml Eppendorf's (Eppendorf, Germany) and stored at -20°C. Thrombin from Bovine Plasma (T4648, Sigma-Aldrich, UK) was dissolved at 200 U/ml in high glucose DMEM. Thrombin solution was then sterile filtered (0.22 µm, Fisher Scientific, UK), aliquoted into 0.5 ml microfuge tubes (250 µl) and stored at -20°C. Aprotinin from Bovine Lung (A3428, Sigma-Aldrich, UK) was dissolved at 10 mg/ml in distilled water (dH₂O), sterile filtered (0.22 µm), aliquoted into 0.5 ml microfuge tubes (250 µl) and stored at -20°C. Six (6)-Aminocaproic Acid (6AA; A7824, Sigma-Aldrich, UK) was dissolved at 50 mg/ml in dH₂O, sterile filtered (0.22 µm), aliquoted into 2 ml Eppendorf's and stored at -20°C. L-Ascorbic Acid (LAA; A4403, Sigma-Aldrich, UK) was dissolved in high glucose DMEM at a concentration of 50 mM, sterile filtered (0.22 µm), aliquoted into 0.5 ml microfuge tubes (500 µl) and stored at 4°C. L-Proline (LP; P8865, Sigma-Aldrich, UK) was dissolved in sterile PBS (1×) at a concentration of 50 mM, sterile filtered (0.22 µm), aliquoted into 0.5 ml microfuge tubes (500 µl) and stored at 4°C.

2.4.2 Preparation of Culture Dishes

Easy-Grip 35 mm culture dishes (BD Falcon[®], VWR, UK) were coated with approximately 1.5 ml of sylgard (Sylgard[™] 184 Elastomer Kit, Dow Corning, USA) using a 20 ml syringe without needle. Sylgard coated dishes were then left to cure for 2-3 days with the lids removed and stored for a further two weeks before use. Silk suture thread (Ethicon Mersilk, 2.0, Portugal) was then trimmed to 6 mm lengths and was pinned 12 mm apart using 0.15 mm Minutien pins (Entomoravia, Czech Republic; see Figure 2.6). Culture dishes, including lids, were then filled with 70% IMS and left to sterilise and air-dry overnight under UV light (programmed to 1 hr) within a culture hood.

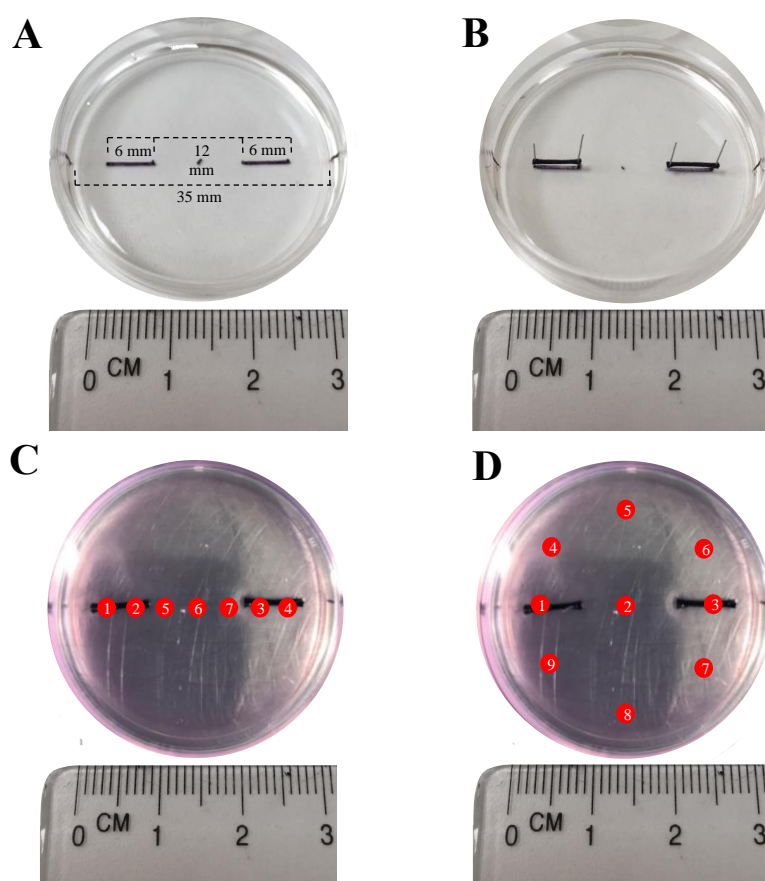


Figure 2.6. Fabrication of fibrin bioengineered SkM

Depicts (A) marked sylgard coated culture dish with (B) silk sutures pinned in place. (C) Depicts thrombin solution placement to ensure sutures are saturated and (D) indicates pipetting fibrinogen dropwise prior to gentle agitation to ensure even distribution across the cell culture dish surface. Taken from Turner *et al.*, (2019).

2.2.1 Preparation and Maintenance of Fibrin Skeletal Muscle Constructs

Once the culture dishes were thoroughly sterilised, 500 μ l of thrombin solution consisting of 50 μ l/ml thrombin, 8 μ l/ml aprotinin in GM containing 0.5 mg/ml 6AA was added to each dish, covering the sutures (outside to inside) first and then across the centre to join both sutures. Each plate was then agitated to ensure even distribution across the culture dish surface (see Figure 2.6). Two-hundred microliters of stock fibrinogen was then added dropwise to each plate (see Figure 2.6) and left to incubate for at RT for 10 mins before transferring to an incubator (37°C, 5% CO₂) for one hour to polymerise. Following polymerisation, C₂C₁₂ cells were seeded onto the fibrin gel at $5-9 \times 10^4$ cells/ml in 2 ml GM containing 0.5 mg/ml 6AA and 50 μ M of both LAA and LP. GM was changed every 48 hrs until cells were ~90% confluent, at which point the media was switched to DM containing 1 mg/ml 6AA, 50 μ M of both LAA and LP. Following 48 hrs in DM, fibrin gels were washed 2 \times with PBS and media was changed to maintenance medium (MM) composed of high glucose (4.5 g/l) DMEM that includes 4 mM LG, 3.5% hiFBS, 3.5% hiNBCS, 2 mM LP, 100 U/ml penicillin, 100 μ g/ml streptomycin, 1 mg/ml 6AA, 50 μ M LAA and 50 μ M LP. MM was changed every 48 hrs and 0.5 ml was added on days where media was not changed until muscle constructs had matured into cylindrical-like 'mini-muscles' containing aligned myotubes at day 14 days (see Figure 2.7).

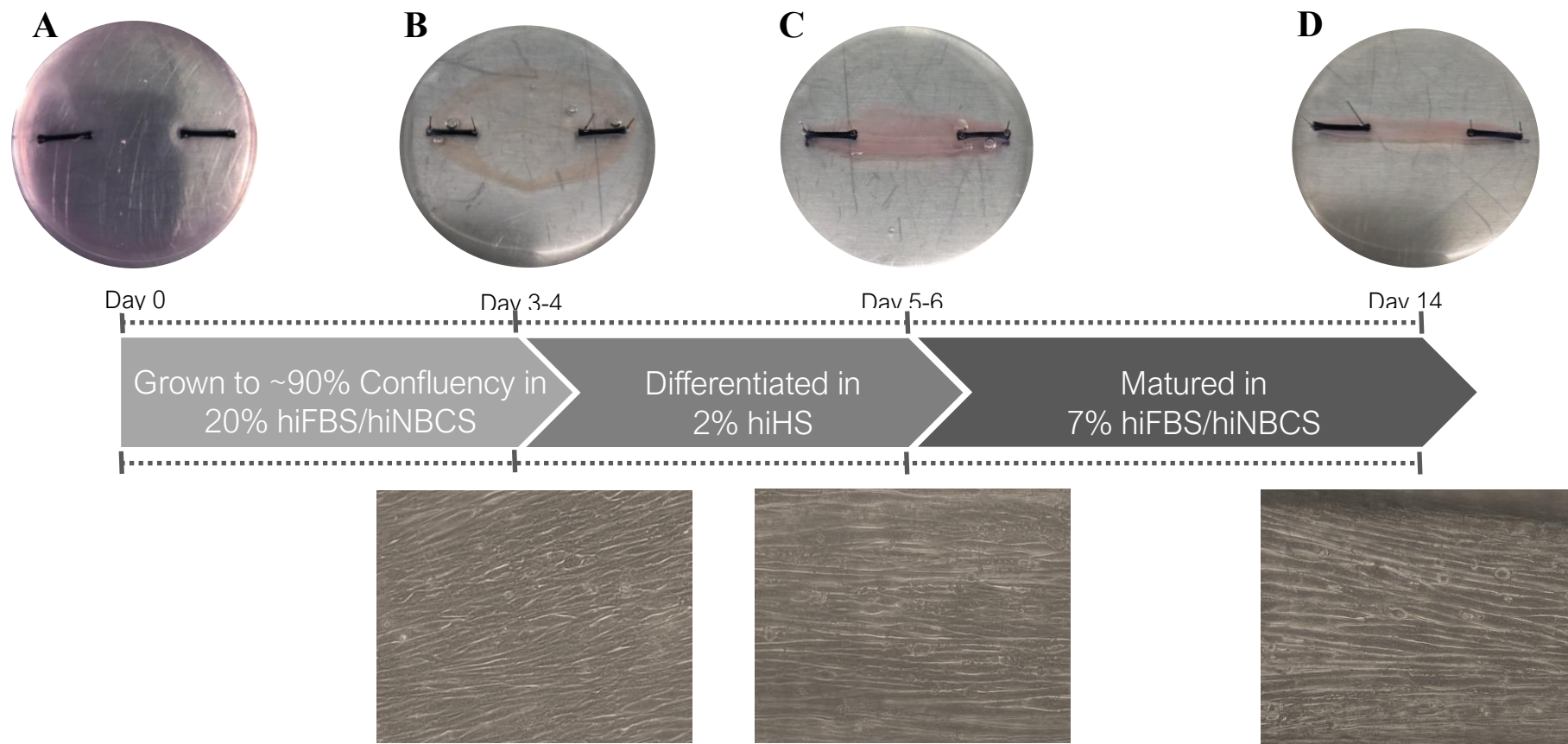


Figure 2.7. Differentiation of C₂C₁₂'s in fibrin bioengineered SkM

Macroscopic image of polymerised gel at (A) 0 days. Macro- and microscopic images of C₂C₁₂ fibrin constructs (B) 3-4 days, (C) 5-6 days and (D) 14 days in culture (10× magnification, Olympus, CKX31).

2.5 Mechanical Loading of Fibrin Skeletal Muscle Constructs

2.5.1 The TC-3 Bioreactor System

Throughout this thesis, the TC-3 tension bioreactor (EBERS Medical Technology, Spain) was used to mechanically load fibrin SkM constructs. The TC-3 bioreactor is a commercially available system that is able to apply both mechanical and/or electrical stimuli to loaded tissues *in vitro* (see Figure 2.8). Tissues may be mechanically loaded via applying tension, compression or hydrostatic pressure in order to simulate forces applied to tissue *in vivo*. Although electrical stimulation was not employed throughout this thesis, the system now also has the capacity to induce coordinated mechanical and electrical inputs due to customised software modifications made by our lab.

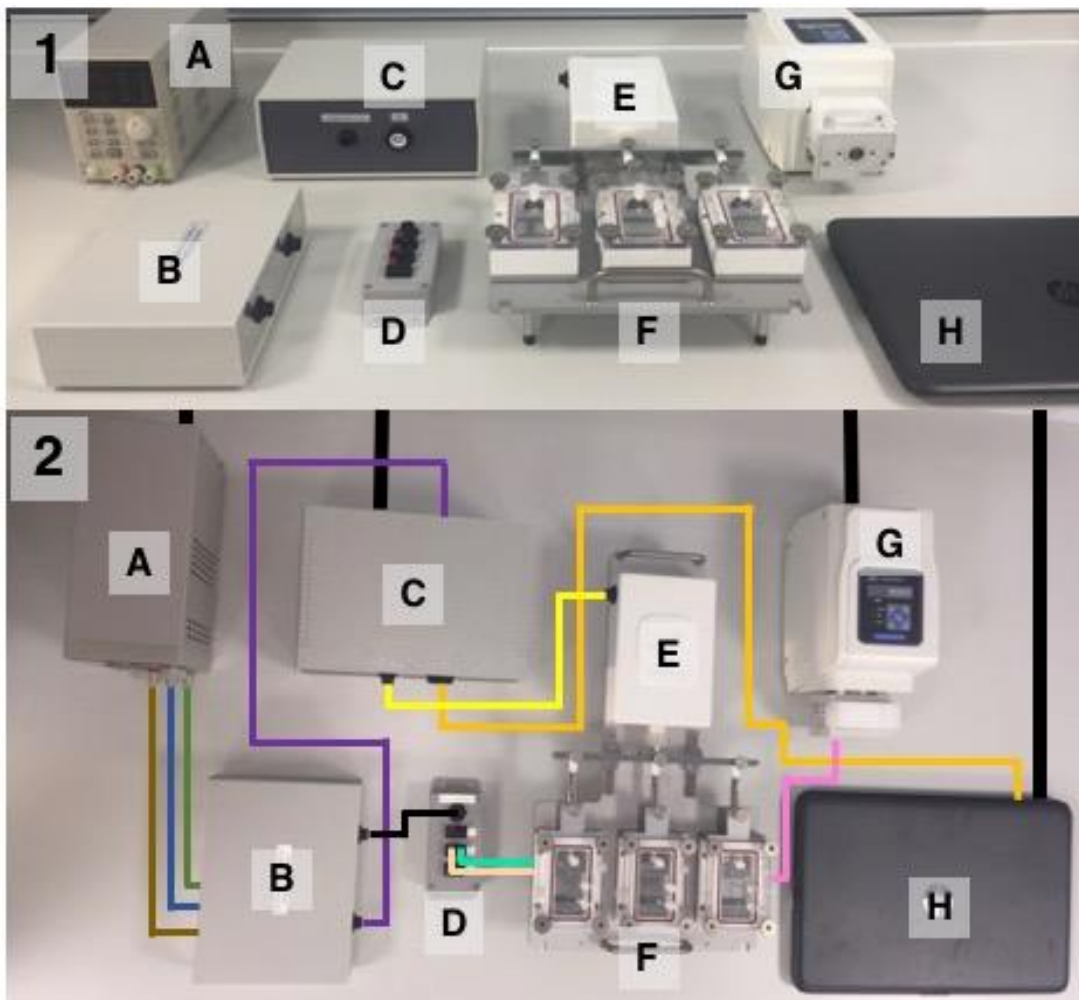


Figure 2.8. Example of the TC-3 bioreactor

An example of the TC-3 bioreactor system (EBERS Medical Technology, Spain) allowing mechanical loading, electrical stimulation, and perfused cell culture media into a cell culture chamber that can all be housed into a humidified CO₂ incubator. (A) Electrical stimulation module, (B) electrical stimulation output box, (C) control module, (D) electrode anode/cathode splitter, (E) bioreactor mechanical stimulation box, (F) bioreactor culture chambers, (G) peristaltic pump/perfusion box, (H) laptop and controlling software. (2) Black—mains power; orange—laptop (G) to control module (C); yellow—control module (C) to bioreactor mechanical stimulation box (E); brown—anode (+ve) from electrical stimulation module (A) to electrical stimulation output box (B); green—neutral from electrical stimulation module (A) to electrical stimulation output box (B); blue—cathode (-ve) from electrical stimulation module to electrical stimulation output box (B); purple—control module (C) to electrical stimulation module (B); red—electrical stimulation output box (B) to electrode anode/cathode splitter (D); peach/gold—anode (+ve) from electrode anode/cathode splitter (D) to bioreactor culture chambers (F); light blue—cathode (-ve) from electrode anode/cathode splitter (D) to bioreactor cell culture chambers (F); pink—perfusion box (G) to bioreactor cell culture chambers (F). Taken from (Kasper *et al.*, 2018; Turner *et al.*, 2019a).

2.5.2 Procedure

Once fibrin SkM constructs were considered mature at day 14, pins were removed using 2 × sets of angled surgical tweezers (Sigma-Aldrich, UK) and the gels (including sutures) were transferred to the bioreactor chamber(s), ensuring a 12 mm (resting length) gap between the medial edge of either clamp. Muscle constructs were then submerged in 20 ml of MM. Typically, 3-5 muscle constructs were clamped within each chamber (see Figure 2.9). Assembled chambers containing the bioengineered muscles were then attached to the bioreactor system, housed in a humidified incubator (37°C, 5% CO₂) to undergo mechanical

stimulation (see Figure 2.9). Using the TC-3 control software (EBERS Medical Technology, Spain), the resting length (12 mm) was programmed before adjusting the ‘velocity’ and ‘frequency’ mode settings for the desired stretch regime (see Figure 2.10). The specific velocity and frequency mode settings will be specified within the methods section of each experimental chapter.

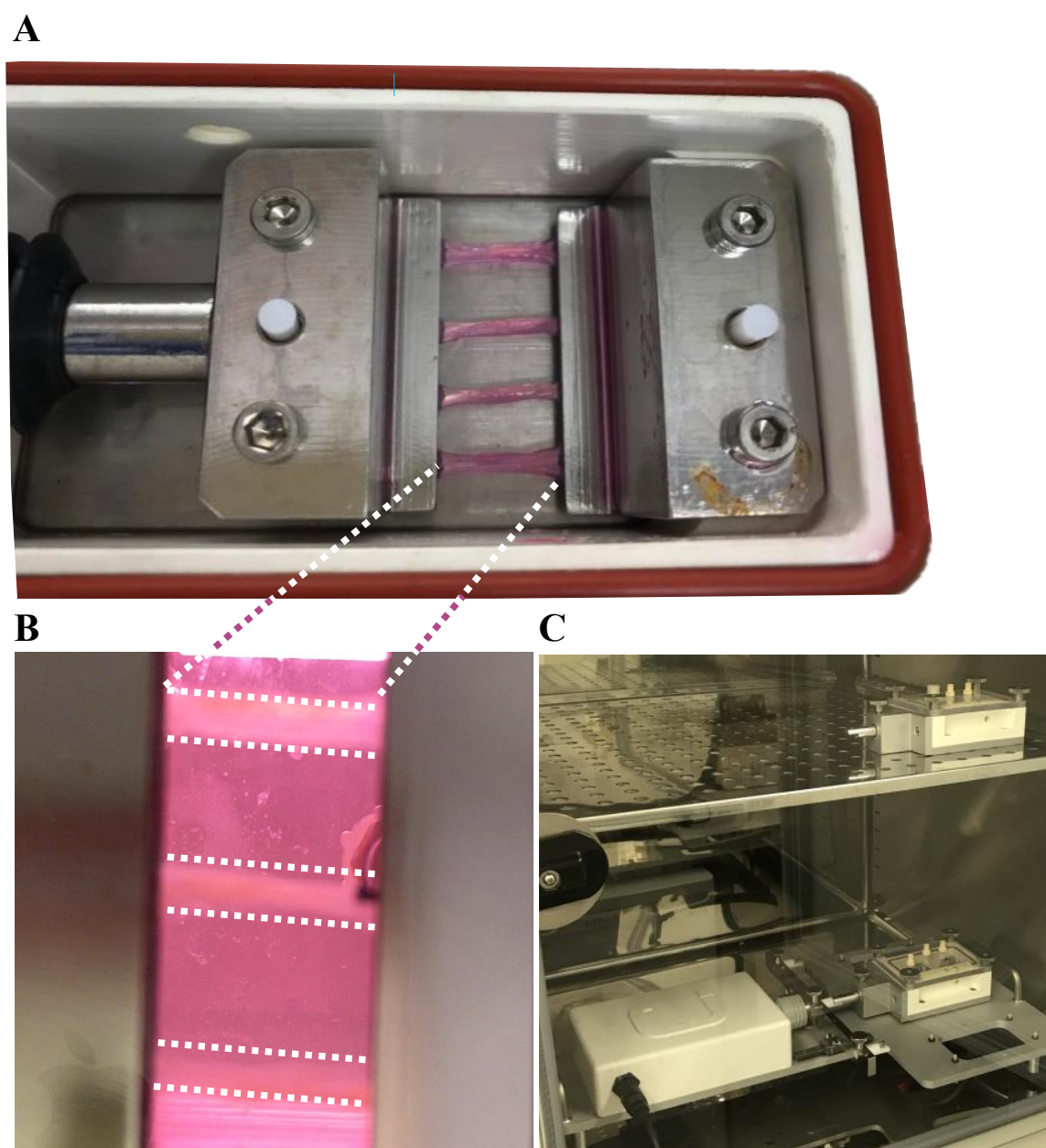


Figure 2.9. Mechanical loading of fibrin bioengineered SkM

(A) $4 \times C_2C_{12}$ fibrin constructs clamped within a bioreactor chamber (B) to undergo mechanical loading (B; white dashed lines outline the SkM constructs) whilst (C) incubating at $37^\circ C/5\%$.

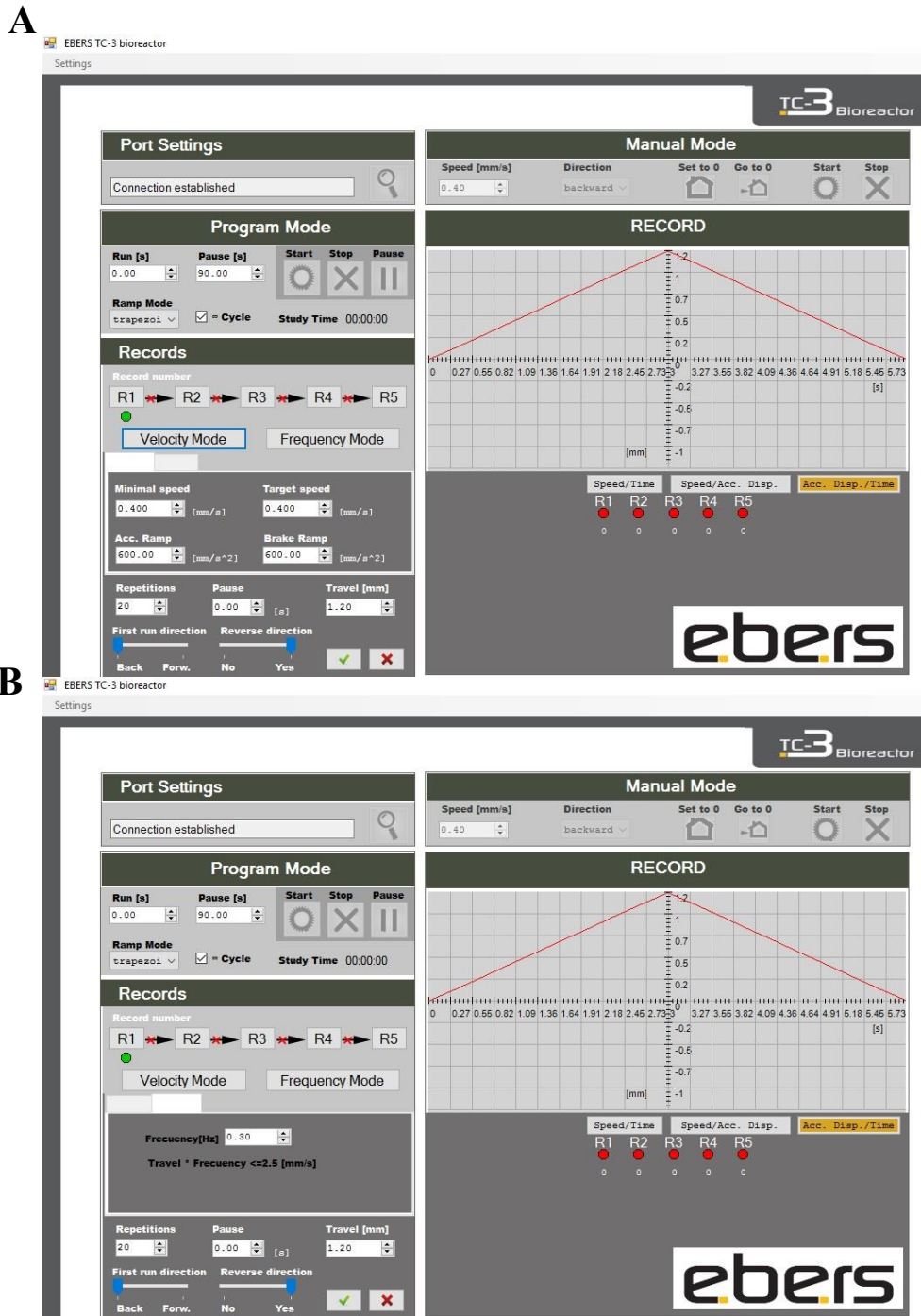


Figure 2.10. Velocity and frequency mode settings

EBERS TC-3 Software. Mechanical stretch navigation menu for adjusting (A) velocity and (B) frequency mode settings. Taken from (Turner *et al.*, 2019a).

2.6 Mechanical Loading of Human Myotubes

2.6.1 The Flexcell® FX-5000™ Tension System

In chapter 6, the Flexcell® FX-5000™ Tension system (Dunn Laborstechnik, Germany) was used to apply mechanical loading to human myotubes *in-vitro*. The Flexcell® FX-5000™ Tension system enables the application of defined equibiaxial, uniaxial and gradient mechanical strain (cyclic or static) to cells flexible-bottomed culture plates (BioFlex®, Dunn Laborstechnik, Germany). This is achieved via regulated vacuum pressure which deforms the flexible silicon membrane on which cells are cultured on (see Figure 2.11).

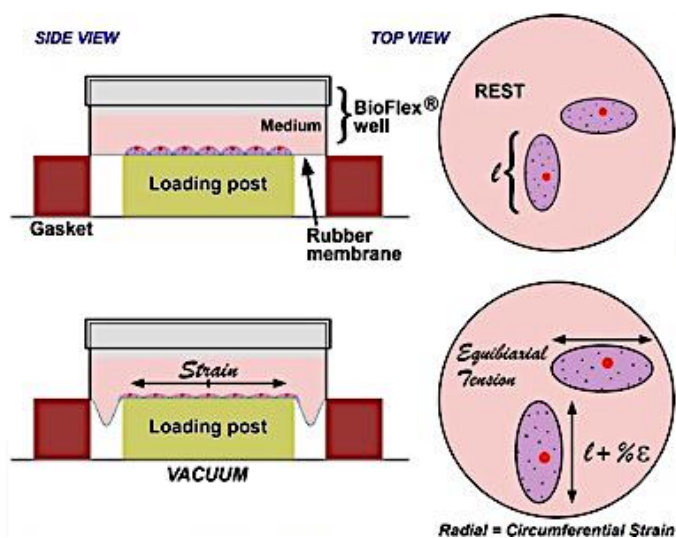


Figure 2.11. Equibiaxial loading of cells in monolayer

Schematic of cultured cells undergoing equibiaxial strain on BioFlex® well plates. Taken from the Flexcell International Corporation website (<https://www.flexcellint.com/category/tension>).

2.6.2 Differentiation of Human Myotubes on BioFlex® Culture Plates

BioFlex® culture plates (25 mm; Dunn Labortechnik, Germany) were first coated with 1 ml of fibronectin (F1141, Sigma-Aldrich, UK) at a concentration of 10 µg/ml in PBS (1×) to promote cell attachment. Fibronectin coated well plates were then incubated at 37°C for 1 hr. Following incubation, excess fibronectin was aspirated, and each well was rinsed 2 × with PBS. HMDCs were then seeded at a density of 9×10^4 cells/ml in 2 ml of HGM. Once cells reached ~80% confluency, HGM was switched to HDM to enable differentiation into multinucleated myotubes over the ensuing 10 days (see section 2.2.7). Each well was topped up with 1 ml of HDM at 72 hrs and 7 days. Once mature, cells were treated prior to mechanical loading (see section 2.3).

2.6.3 Mechanical Loading of Human Myotubes Using the Flexcell® FX-5000™ Tension System

Loading posts were first lubricated (Loctite, Germany) before placing the Flexcell® FX-5000™ Tension base plate in a humidified incubator (37°C, 5% CO₂). BioFlex® culture plates were assembled to the base plate ready for mechanical loading (see Figure 2.12). Myotubes were subject to a low frequency (0.15 Hz with sine wave) intermittent stretch regime which consisted of 4 × 10 reps with 90 s rest between sets, representing 1 × exercise (see Figure 2.12). There was a total of 5 exercises, each interspersed with a 3.5 min rest interval, totalling a regime of 60 mins. Non-loaded myotubes acted as controls and were also assembled to the Flexcell® base plate, however, the vacuum entry was sealed with tape to avoid any unwanted stretch. All cells were lysed for RNA (see section 2.8.1) and protein (see section 2.11) immediately post (~30 mins) and 3 hrs post stretch. Puromycin was first incorporated into myotubes before lysing for protein for a measure of global protein synthesis (see section 2.11).

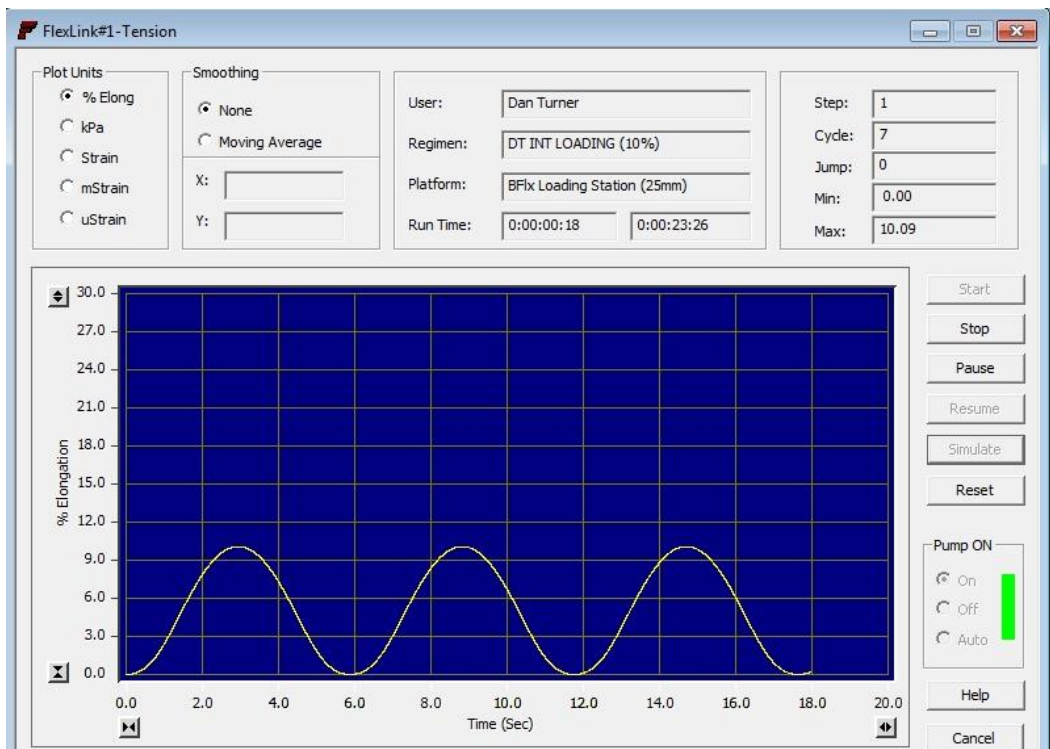
A**B**

Figure 2.12. Mechanical loading of human myotubes

(A) Human myotubes mechanically loaded on BioFlex[®] well plates within a humidified incubator (37°C/5%). (B) Example of the sine wave profile during the mechanical loading regime.

2.7 Immunochemistry and Microscopy

2.7.1 Principle

Immunochemistry is a method typically employed to detect a particular protein of interest in cells (immunocytochemistry, ICC) and tissue (immunohistochemistry, IHC) via the use of fluorescent-labelled antibodies which bind to their target antigens. This technique enables researchers to visualise the localisation and morphology (i.e. the size and shape of the cell) of individual cell components which are maintained during immunochemistry procedures (Coons *et al.*, 1942).

Samples are first 'fixed' using crosslinking reagents (e.g., formaldehyde/formalin) which form bridges or organic solvents (e.g., methanol and acetone) to dehydrate cells and remove lipids in order to retain cytoskeletal morphology. Specific reagents such as Triton X-100 are then used for permeabilising the cell membrane, enabling antibodies to penetrate into the sample and bind to the antigen of interest. Serum, specifically that derived from the same species in which the secondary antibody was raised is used for 'blocking', preventing any unwanted binding of the primary antibody to non-specific sites within the sample which may lead to background staining. Permeabilising and blocking are usually undertaken together for time efficiency.

There are two major classes of antibodies used within immunochemistry, namely polyclonal and monoclonal antibodies. *Polyclonal* antibodies are raised *in-vivo*, whereby animals are injected with the antigen of interest which allows B lymphocytes to produce quantities of the antibody which are later purified from the serum. Similarly, *monoclonal* antibodies are generated via immunising the host with the antigen. However, hybridomas derived from the fusion of lymphocytes of the animal spleen and myeloma cells are expanded in culture, forming a single clone (Köhler & Milstein, 1976). Monoclonal antibodies have high specificity as they are epitope specific and may therefore be considered preferable for therapeutic drug development. However, polyclonal antibodies have a higher antibody affinity as they recognise

multiple epitopes on a given antigen, suggesting a greater robust protein detection. The use of either antibody may therefore be determined based on the application of interest.

Once the samples are permeabilised and 'blocked', a primary antibody is added which binds to the protein/antigen of interest. Following primary incubation, the antibody is removed, and the sample is washed several times. A secondary antibody conjugated to a fluorophore (fluorescent dye), which is raised against the host species in which the primary antibody was raised, is then added to the sample to enable detection of the antigen using fluorescence microscopy by absorbing and emitting light at specific wavelengths.

2.7.2 Immunostaining Human Skeletal Muscle Derived Cells

Cells within 6-well plates were washed $3 \times$ TBS ($1\times$; Sigma-Aldrich, UK) and fixed and dehydrated in ice-cold methanol:acetone:TBS (25:25:50) for 15 mins then a further 15 mins in methanol:acetone (50:50) only. Following $3 \times$ further washes, 6-well plates were wrapped in parafilm and stored at 4°C until required for immunostaining.

Following fixation, cells were permeabilised in 0.2% Triton X-100 (Sigma-Aldrich, UK) and blocked in 5% goat serum (Sigma-Aldrich, UK) in TBS for 90 mins. Cells were then washed $3 \times$ in TBS and incubated overnight (4°C) in 300 μl of anti-desmin (ab15200, Abcam, UK) primary antibody made up in TBS, 2% goat serum and 0.2% Triton X-100 at concentrations of 1:50. After overnight incubation, the primary antibody was removed and cells were washed $3 \times$ in TBS. Cells were then incubated at RT for 3 hrs in 300 μl secondary antibody solution containing anti-rabbit TRITC (T6778, Sigma-Aldrich, UK) at a concentration of 1:75 in $1\times$ TBS, 2% goat serum and 0.2% Triton X-100 to counterstain myoblasts. After a further $3 \times$ TBS washes, 300 μl of DAPI (D1306, Thermo Fisher Scientific, Denmark) was added to the cells at a concentration of 300 nM for 30 mins to counterstain myonuclei. Once stained, 2 ml of TBS was added to each well and culture plates were sealed with parafilm and covered with foil and were stored at 4°C until required for fluorescence imaging.

2.7.3 Immunostaining Bioengineered Skeletal Muscle

Bioengineered SkM constructs were fixed using methanol and acetone as described in section 2.7.2. The fixation method used will be described within the methods section of each experimental chapter throughout this thesis. Following fixation, pins were removed, and constructs were transferred to 2 ml Eppendorf tubes using 2 × sets of angled tweezers (see Figure 2.13). Gels were then permeabilised (0.2% Triton X-100) and blocked (5% goat serum) in TBS (1×) for 90 min and incubated overnight (4°C) in 250 µl of Phalloidin-FITC antibody (P5282, Sigma-Aldrich, UK) at a concentration of 50 µg/ml. After overnight incubation, the antibody was aspirated, and gels were washed 3 × in TBS before adding 250 µl of DAPI (300 nM) for 90 mins to counterstain myonuclei. When immunostaining for desmin, antibody concentrations and incubation durations were the same as that described in section 2.7.2 for HMDCs cultured in 6-well plates. Once stained, muscle constructs were transferred to non-sylgard coated culture dishes containing 2 ml of TBS and were wrapped in parafilm and foil and stored at 4°C until required for fluorescence imaging.



Figure 2.13. Immunostaining fibrin bioengineered SkM

Fixed SkM constructs ($n = 4$) were transferred to 2 ml Eppendorf's held in place using blue tac. Windows were carved longitudinally to enable easy access of gels. Green circles highlight muscle constructs.

2.7.4 Microscopy and Image Analysis

Immunostained cells and SkM constructs were visualised using either an inverted fluorescence (Nikon, Eclipse Ti-S, Japan) or confocal (Olympus IX83, Japan) microscope and were imaged using corresponding software (Nikon, NIS Elements and FV10-ASW 4.2 for fluorescence and confocal microscopy, respectively). Microscopy equipment/procedures is detailed within the methods section of each experimental chapter. Myoblasts and myotubes were visualised using FITC (Phalloidin-FITC, Excitation: 495 nm, Emission: 513 nm) and TRITC (Desmin, Excitation: 557 nm, Emission: 576 nm) filters and myonuclei was visualised using a DAPI filter

cube (Excitation: 358 nm, Emission: 461 nm). All immunostained samples were imported to Fiji/ImageJ (version 2.0.0) software for subsequent analysis. Primary heterogenous cell populations were characterised via counting the total number of myoblasts (red) overlapping nuclei (blue) and dividing this by the total number of nuclei (see Figure 2.14).

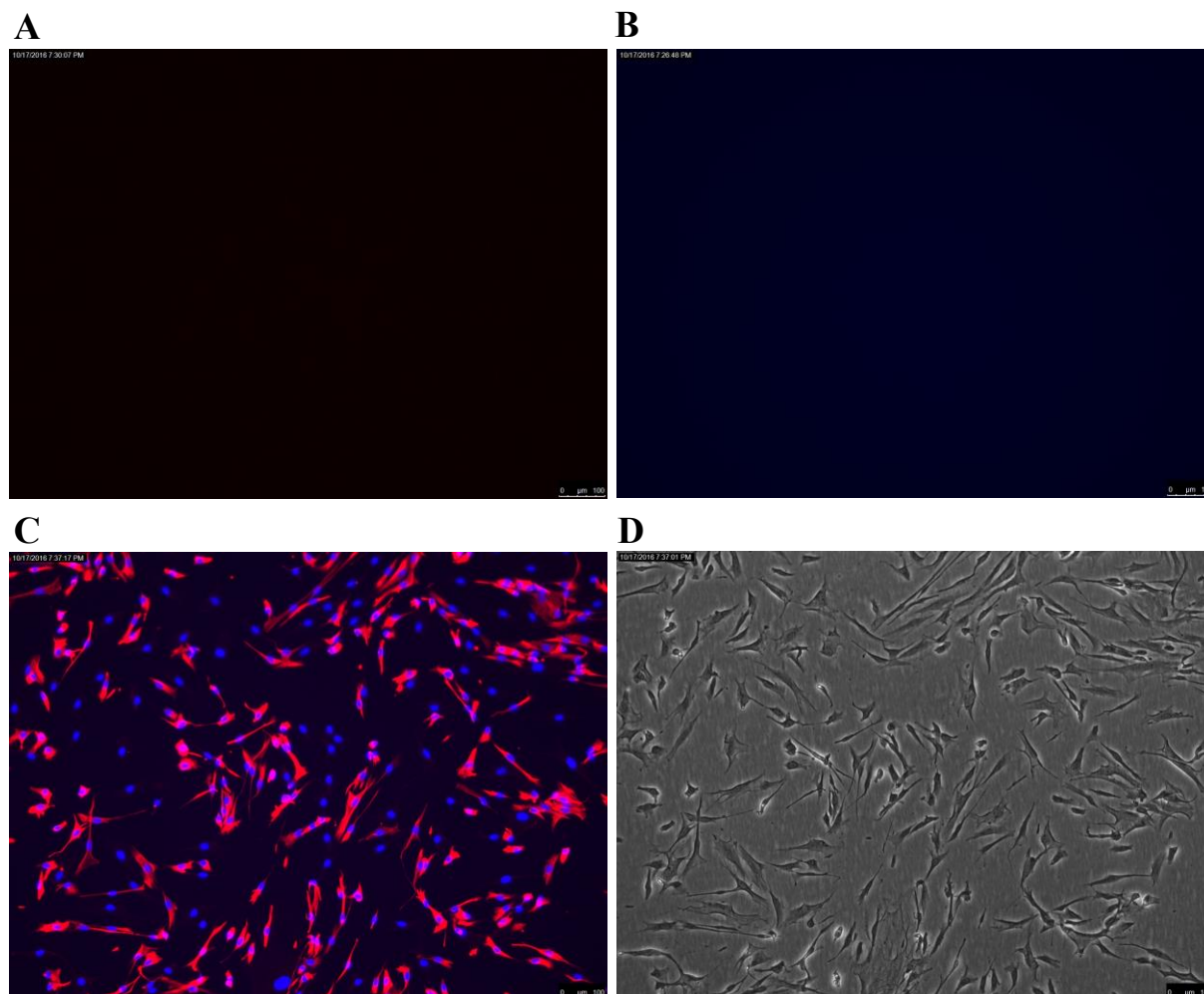


Figure 2.14. Immunostaining of HMDCs for determining myogenic population

Example of immuno-stained (A-C) and bright-field (D) microscopic images of HMDCs (Nikon, Eclipse Ti-S, 10× magnification scale bar = 100 μm) stained with (A) primary antibody only (anti-desmin), (B) secondary antibody (anti-rabbit TRITC) or (C) desmin (red) and myonuclei (blue). Myogenicity (%) was calculated via dividing the sum of all desmin positive cells by the total number of blue/nuclei cells present.

2.8 Lysing and Homogenising Bioengineered Skeletal Muscle Tissue for RNA and DNA

Following cessation of mechanical loading, SkM constructs were removed from the bioreactor chambers and transferred to MagNA Lyser green bead tubes (Roche, MagNA Lyser, USA) containing 600 μ l of Buffer RLT and 6 μ l β -Mercaptoethanol (β -ME) lysis buffer if samples were co-purified for RNA and DNA using the AllPrep RNA/DNA Mini Kit (Qiagen, UK). Alternatively, samples were dissected in two halves using sterile scalpels and each part was either submerged in 1 ml TRIzol (Invitrogen™, Thermo Fisher Scientific, Denmark) or 180 μ l buffer ATL with 20 μ l proteinase K (DNeasy Blood and Tissue Kit, Qiagen, UK) if solely purifying RNA or DNA, respectively. DNA samples were incubated at 56°C in the lysis buffer (180 μ l buffer ATL with 20 μ l proteinase K) for 3 hrs. Both RNA and DNA lysates were then placed into a MagNA Lyser instrument (Roche, MagNA Lyser, USA) and were vigorously disrupted (6 m/s for 40 seconds, repeated 3 \times with samples placed on ice for 5 mins after each disruption) to ensure sufficient homogenisation, tissue/cell lysis and the release of nucleic acids. The tissue lysates were then pipetted into nuclease-free tubes and stored in -20°C until required for RNA extraction (see sections 2.9.1 and 2.9.2).

2.8.1 Lysing Human Myotubes for RNA

Cultured myotubes were thoroughly washed 2 \times in PBS and 300 μ l TRIzol was added to each well. Myotubes were left to incubate in lysis buffer for 5 mins before mechanically dissociating cells from the well surface using an autoclaved polypropylene cell scraper. Lysed myotubes were then pipetted into nuclease-free tubes and stored at -20°C until required for RNA extraction.

2.9 RNA Extraction and Quantitative Real-Time Polymerase Chain Reaction (qRT-PCR)

2.9.1 RNA Extraction Using the AllPrep RNA/DNA Mini Kit

RNA extraction using the commercially available AllPrep RNA/DNA Mini Kit (Qiagen, UK) was conducted according to the manufacturers' instructions. All procedures, including centrifugation, were performed at RT. Homogenised tissue and cell lysates were thawed at RT and centrifuged for 3 mins at maximum speed ($20,000 \times g$). The supernatant was transferred to AllPrep DNA spin columns placed in a 2 ml collection tube. The supernatant was then centrifuged for 30 s at $8,000 \times g$. The DNA spin column was placed into a fresh 2 ml collection tube and stored at 4°C for later DNA extraction (see section 2.10.1). One volume ($600 \mu\text{l}$) of 70% molecular grade ethanol (Sigma-Aldrich, UK) diluted in dH_2O was added to the flow-through. The mixture was then transferred to a RNeasy spin column placed in a 2 ml collection tube and centrifuged for 15 s at $8,000 \times g$. The column membrane was washed several times with Buffer RW1 (1 \times) and Buffer RPE (2 \times), centrifuging samples in between each wash for 15 s at $8,000 \times g$ with a longer duration of 2 mins following the final wash. Finally, the RNeasy spin column was placed in a 1.5 ml nuclease-free collection tube and $31 \mu\text{l}$ of nuclease-free H_2O was added before centrifuging the samples for 1 min at $8,000 \times g$ to elute the RNA. The final elution step was repeated using a separate collection tube to increase RNA yield without compromising final RNA concentrations. Samples were vortexed and stored at -20°C until required for qRT-PCR (see section 2.9.4).

2.9.2 RNA Extraction Using TRIzol

All procedures, including centrifugation were performed at 4°C when purifying RNA using TRIzol. TRIzol is a monophasic reagent containing phenol and guanidine isothiocyanate, which maintains RNA integrity via inhibiting RNase activity whilst simultaneously disrupting and dissolving cellular components during cell/tissue lysis and homogenisation (see sections 2.8

and 2.8.1). Once lysed, 200 μ l of chloroform (Sigma-Aldrich, UK) was added to each sample which was shaken vigorously by hand to separate the sample into a lower red organic layer (containing phenol and chloroform), a cloudy interphase layer (containing little RNA with the majority DNA) and a clear upper aqueous layer (containing RNA). The samples were then centrifuged ($12,000 \times g$ for 15 minutes at 4°C) and the upper aqueous layer containing RNA was carefully extracted (avoiding direct contact with the interphase) and pipetted into a new RNase-free tube. RNA was then supplemented with 1 volume of isopropanol which was briefly vortexed and incubated at RT for 10 min. The samples were then centrifuged at $12,000 \times g$ for 10 mins at 4°C , forming a cell pellet containing RNA. Excess isopropanol was carefully removed, and the pellet washed with 75% molecular grade ethanol. The sample was then centrifuged for a final time at a lower speed ($7,500 \times g$) and duration (8 mins). Finally, the excess ethanol was removed, and the pellet resuspended in 21 μ l storage solution (Ambion[®] RNA Storage Solution, Invitrogen[™], Thermo Fisher Scientific, Denmark). Samples were vortexed and stored at -20°C until required for RNA extraction.

2.9.3 Assessment of RNA Concentration and Purity

RNA concentration and purity were assessed using a spectrophotometer (Nanodrop[™] 2000, Thermo Fisher Scientific, Denmark). One microliter of extracted RNA was pipetted onto the Nanodrop probe and the amount of ultraviolet (UV) light absorbed at 260 nm, the wavelength at which nucleic acids best absorb light, was measured by a photodetector to determine the concentration inferred using the Beer-Lambert law (see Equation 2.2). Following assessment of RNA concentration, the purity or RNA 'quality' was determined from the ratio of absorbance at 260 nm to 280 nm, the wavelengths at which RNA/DNA and protein best absorb UV light, respectively. Highly purified RNA is indicated by a A_{260}/A_{280} ratio of 2. Other potential contaminants include ethanol, phenol or guanidine, which are measured at 230 nm. Therefore, the A_{260}/A_{230} ratio is also measured where a reading >1.5 is preferred. RNA concentrations

and purities are reported within the methods section of each experimental chapter throughout this thesis.

$$A = \epsilon C l$$

Where:

A = absorption at 260 nm

ϵ = the molar extinction coefficient (40 $\mu\text{g/ml}$ for RNA and 50 $\mu\text{g/ml}$ for dsDNA)

l = the path length of the spectrophotometer

C = concentration of RNA/DNA

Equation 2.2 Quantifying RNA and DNA concentrations using spectrophotometry

Quantitative Real-Time Polymerase Chain Reaction (qRT-PCR)

2.9.4 Principle

In order to produce functional proteins and therefore alter the muscle phenotype, a gene must first be transcribed in the nucleus to produce a messenger ribonucleic acid (mRNA) which is later translated into protein within the ribosome. The amount of a gene expressed typically (yet not exclusively) translates to the amount of protein produced which may influence the overall structure and function of SkM tissue. Assessment of mRNA regulation in response to a given stimulus has therefore become of particular interest in cellular and molecular physiology/biology. Since DNA is a very large molecule with such limited copies, assessment of mRNA expression proved difficult until the 1980's where polymerase chain reaction (PCR), a technique widely used to amplify specific fragments of the DNA, was introduced by Kary Mullis who later won the Nobel prize in chemistry in 1993 (Mullis & Faloona, 1987).

Following isolation of mRNA from tissue or cells (see sections 2.9.1 and 2.9.2), the single stranded RNA (ssRNA) must be reverse transcribed to form a complimentary DNA (cDNA) before the target sequence is amplified. In order for reverse transcription (RT) to occur,

oligonucleotides (dNTPs) are added to the ssRNA using the enzyme reverse transcriptase and cDNA is synthesised from the 3' to 5' end of the mRNA molecule. Once synthesised, the DNA is amplified via three distinct steps, all of which represent 1 cycle of a PCR reaction that is repeated numerous times (30-40 cycles) to produce ~ 1 bn copies of the target sequence. These steps include: 1) *Denaturation* whereby the double stranded DNA (dsDNA) is subjected to high temperatures (95°C) in order to separate the DNA into two strands exposing the 3' end of the DNA. 2) *Annealing* of primers then occurs whereby the temperature is lowered (optimal temperature is primer specific, with all the primers used herein designed to anneal at approximately 60°C) to enable binding of short sequence (approximately 18-30 bp) primers to the DNA strands. 3) *Extension* then takes place. Here, *Taq* polymerase, an enzyme derived from the bacterium species, *Thermus Aquaticus* that is able to withstand such high temperatures, binds to the primers and synthesises the complimentary strand using free dNTPs.

During each PCR cycle, a fluorescent dye or probe, binds to each dsDNA molecule after primers anneal to the 3' end. The amount of light excited and emitted from the fluorescent molecule is able to provide a 'real-time' measurement of DNA amplification as the amount of light measured by a fluorometer within the PCR thermocycler instrument is directly proportional to the amount of targeted DNA produced. This can easily be quantified following each PCR run, according to the number of cycles required to exceed the fluorescence cycle threshold (C_T) self-reported. Thus, generally, the lower the C_T value, the higher the expression levels as the fluorescence being detected earlier above background fluorescence reflects the larger amount of starting nucleic acid material. Conversely, the higher the cycle number, the later detection of fluorescence above background levels reflecting a lower starting abundance of the nucleic acid material. The resultant C_T values of the target gene in each sample are then compared to the C_T values of a housekeeper/reference gene (one of which should remain consistent, regardless of any given stimulus) to determine either absolute or relative quantities (Schmittgen & Livak, 2008).

2.9.5 Procedure

Throughout this thesis, a one-step PCR kit (QuantiFast SYBR[®] Green RT-PCR Kit, Qiagen, UK) was used to analyse mRNA expression whereby the cDNA synthesis and PCR steps were performed in the same reaction tube for time efficiency and reduced risk of cross contamination. Reaction tubes were either prepared manually by hand or automatically using the QIAgility robot instrument (Qiagen, Crawley, UK). Each reaction included 50% SYBR[®] Green master mix (containing HotStarTaq DNA polymerase, RT-PCR buffer, SYBR green fluorescent dye and ROX passive reference dye) 1% reverse transcriptase (RT) mix and 0.75% of forward and 0.75% reverse primer, with the remaining 47.5% as diluted RNA sample (7.37 ng/ μ l in nuclease-free H₂O). The preparation method (i.e., manual or automatic using the QIAgility robot), alongside the specific volumes (μ l) of PCR reagents and RNA sample used per reaction will be specified within the methods section of each experimental chapter. Prepared reaction tubes were then transferred to a PCR thermal cycler (Rotor-Gene 3000Q, Qiagen, UK) to undergo reverse transcription/cDNA synthesis (hold 50°C for 10 min), transcriptase inactivation and initial denaturation (95°C for 5 min) followed by 40 \times amplification cycles consisting of; 95°C for 10 s (denaturation), 60°C for 30 s (annealing and extension).

2.9.6 Quantification of Relative Gene Expression

Following the completion of 40 \times PCR cycles, melt curve analysis was first performed to ensure only the gene(s) of interest was amplified (see section 2.9.4.4). Sample efficiencies were also analysed and will be reported within the methods section of each experimental chapter. An efficiency value of 2 represents a 2-fold increase (100% which is derived from dividing the efficiency value by 2 and multiplying by 100) of amplicon with each PCR cycle. To obtain the raw C_T values for each sample, a threshold line was self-adjusted on the amplification curve according to where an exponential rise in fluorescence occurred (see Figure 2.15). The C_T values were used to quantify relative gene expression using the comparative Delta Delta C_T

($\Delta\Delta C_T$) equation (Schmittgen & Livak, 2008) against a reference gene and a control group (see Equation 2.3 and Table 2.3).

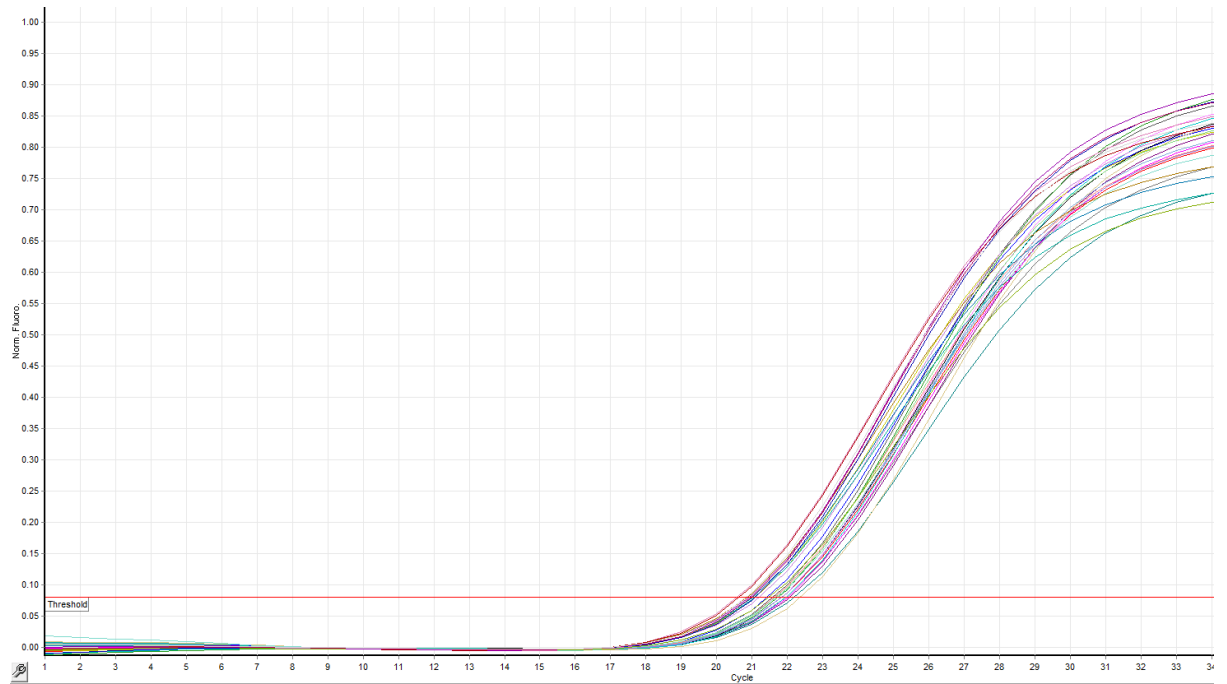


Figure 2.15. Analysis of raw C_T values for gene expression

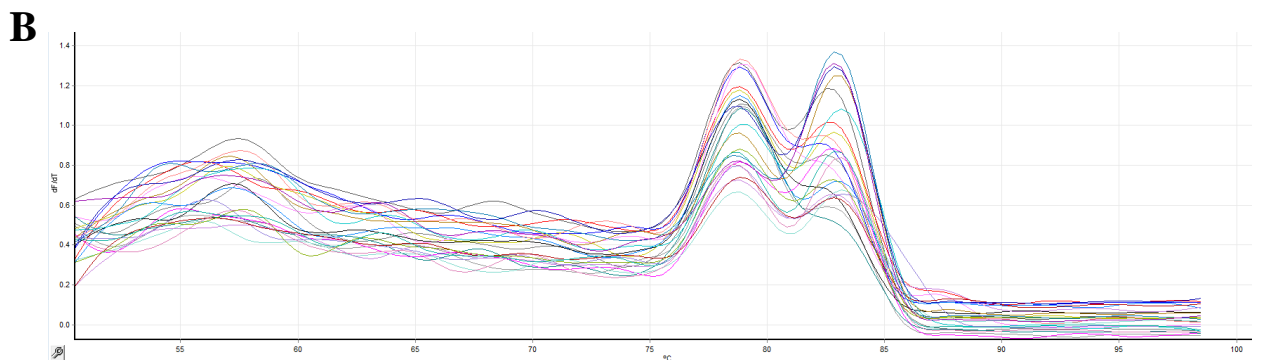
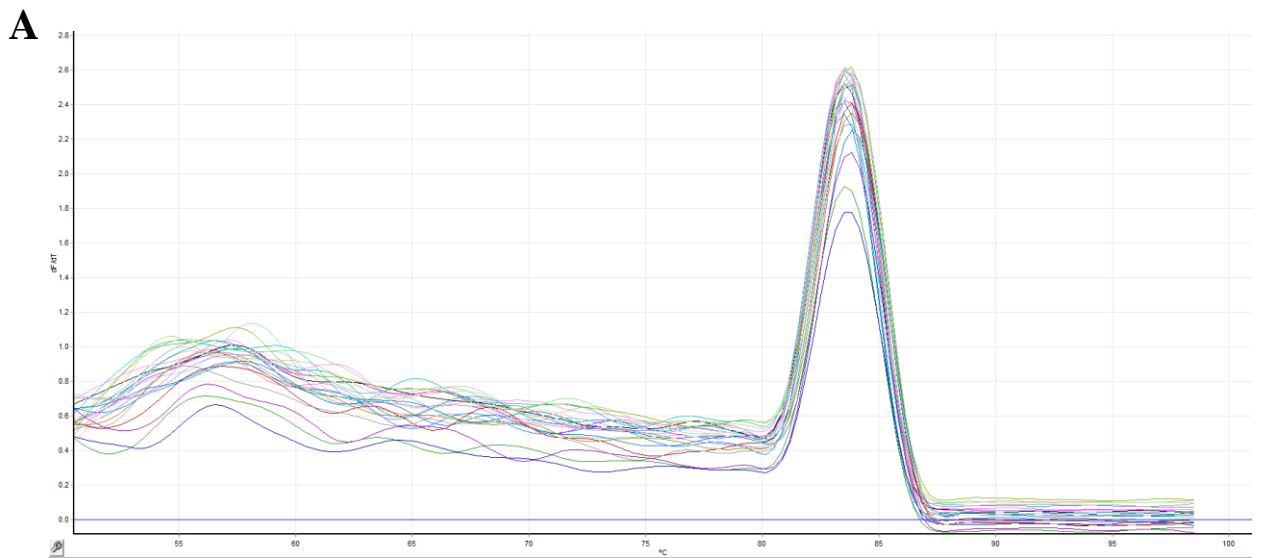


Figure 2.16. Melt curve analysis to determine specific target amplification

An example of melt curves analysed to determine primer specificity. (A) displaying a single peak which suggest no unspecific amplification whereas (B) a double peak suggests amplification of unintended targets and/or primer dimer issues.

Delta Delta C_T ($\Delta\Delta C_T$) Equation:

1. $\Delta C_T = C_T (\text{Target Gene}) - C_T (\text{Target Gene})$
2. $\Delta\Delta C_T = \Delta C_T (\text{Target Sample}) - \Delta C_T (\text{Control Sample})$
3. $2^{-\Delta\Delta C_T}$ (normalised expression ratio)

Equation 2.3. An example of the Delta Delta C_T ($\Delta\Delta C_T$) equation used to calculate relative gene expression against a reference gene and control group.

Table 2.3. Quantifying mRNA expression using the $\Delta\Delta C_T$ method

Calculation for quantifying the normalised gene expression ratio using the Delta Delta C_T ($\Delta\Delta C_T$) equation (Schmittgen & Livak, 2008).

Sample	Mean C_T (Target Gene)	Mean C_T (Reference Gene)	ΔC_T	$\Delta\Delta C_T$	($2^{\Delta\Delta C_T}$)
Sample 1 (Control)	21.34	18.22	3.12	0.00	1.00
Sample (Test)	19.18	18.00	1.18	-1.94	3.83

2.9.7 Primer Design

All primers were self-custom designed according to a number of specific guidelines (Dieffenbach, Lowe and Dveksler, 1993; see Table 2.4) and were manufactured and ordered via Sigma-Aldrich (UK). All stock (desalted) primers were suspended in TE buffer (pH 8.0, Ambion®, Invitrogen, California, USA) to ensure a concentration of 100 μM . For genes with multiple transcript variants, primers were designed to target all mRNA sequences of the main

transcript and its variants to enable a global measure of gene expression. This was performed using the Clustal Omega Multiple Sequence Alignment program (<https://www.ebi.ac.uk/Tools/msa/clustalo/>) to identify gene regions which shared the same sequence across all transcript variants. After primer design, specificity was confirmed via performing a Basic Local Alignment Search Tool (BLAST) online (<http://blast.ncbi.nlm.nih.gov/>) search and following melt curve analysis. Melt curve analysis determines the melting temperature (T_m) and confirms that only the gene of interest was amplified (indicated by a single peak) without amplification of unintended targets (indicated by a double melt curve peak; see Figure 2.15). Primers sequences for the gene(s) of interest are described in the methods section of each experimental chapter.

Table 2.4. Primer design guidelines.

Considerations	Guidelines
Primer Length	18-24 bp
Temperature Melt (T _m)	Between 56-62°C to ensure optimal annealing temperatures
GC Content (%)	~50% GC content 3 or more GC bases were avoided in the last 5 bases at the 3' end of the primer was avoided
Amplicon Length	Less than 200 bp
General Considerations	Primers should span an exon-intron boundary Mismatches at the 3' end should be voided There should be no complimentary nucleotides at the 3' end for prime pairs

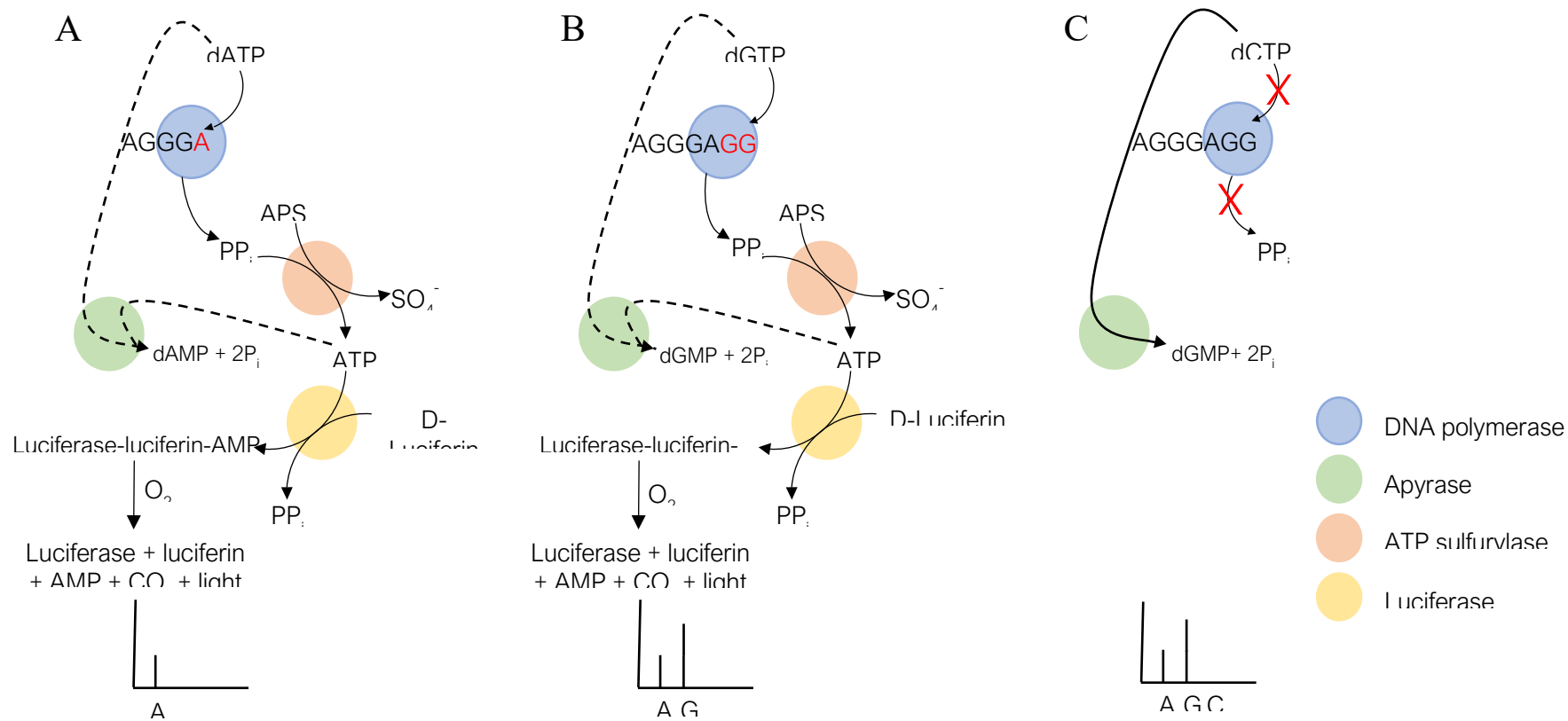


Figure 2.17. Mechanisms of pyrosequencing for DNA methylation

Example of the cascade of events during a pyrosequencing reaction. **(A)** Incorporation of a dATP into the DNA template. PP_i is released and is converted to ATP which provides the necessary energy to oxidise luciferin, producing a light signal. **(B)** Represents the addition of 2 × complementary dGTPs resulting in a double peak. **(C)** Depicts no incorporation of the dCTP due to non-complementary base pairs. The nucleotide is therefore degraded by the enzyme apyrase, resulting in no peak. Schematic adapted from Tost and Gut (2007).

2.10 Loci-Specific Pyrosequencing

2.10.1 Principle

Pyrosequencing technology quantitatively determines the methylation status of DNA in real-time via a series of biochemical reactions catalysed by four key enzymes. This is achieved through the release of pyrophosphate (PP_i) when a complementary free nucleotide (dNTP) is incorporated into the DNA template via DNA polymerase (see Figure 2.17). PP_i is then converted to ATP via ATP sulfurylase, providing the necessary energy for oxidising luciferin via the enzyme luciferase. These reactions result in a light signal which is displayed as a pyrogram peak. The enzyme apyrase degrades any unincorporated dNTP's during each reaction. The pyrogram peak intensity is directly proportional to the number of complementary dNTP's added to the DNA template (Tost & Gut, 2007). For example, the incorporation of 2 × dNTPs results in a double peak whereas no incorporation results in no peak displayed (see Figure 2.17).

2.10.2 Procedure

Pyrosequencing assays were purchased from EpigenDX (Hopkinton, USA) and were designed to assess the methylation status of 6 × CpG sites in the Intron 1 region of the mouse UBR5 gene. PCR bias testing was first performed via mixing unmethylated DNA control and methylated DNA at various ratios (0, 5, 10, 25, 50, 75 and 100%). Percentage of methylation following bias testing was highly correlated with the expected methylation ($R^2 = 0.9161$). Five-hundred nanograms of DNA was bisulfite converted (see section 2.10.4) and amplified via PCR as per the manufacturer's instructions (HotStar Taq Polymerase, Qiagen). Briefly, each 30 μl reaction consisting of: 3 μl (1×) of 10× PCR buffer (containing 15 mM MgCl₂), 1.8 μl (3 mM) of 25 mM MgCl₂, 0.6 μl (200 μM) of 10 mM dNTPs, 0.6 μl (6 pmol) of forward and reverse primers (10 μM), 0.15 μl (0.75 U) HotStar Taq Polymerase (5 U/μl) and 1 μl of bisulfite treated DNA was amplified as follows: 95°C for 15 mins (initial denaturation) followed by 45 × cycles of 95°C for 30 s (denaturation); 55°C for 30 s (annealing); 68°C for 30 s (extension) followed

by a final 5 minutes at 68°C. After amplification, 6-15 µl of PCR sample was mixed with a binding solution composed of 2-3 µl streptavidin sepharose beads HP (GE Healthcare Life Sciences), 40 µl 2× binding buffer (Qiagen, UK) and 15 µl dH₂O. PCR products were then purified, washed, denatured with a 0.2 µM NaOH solution and rewashed using the Pyrosequencing Vacuum Prep Tool (Pyrosequencing, Qiagen, UK) as per the manufacturer's instructions. Sepharose beads were released into annealing buffer (Qiagen, UK) containing 0.5 µM of sequencing primer. Once annealed, PCR products were sequenced using the PSQ 96HS System (Qiagen, UK) following the manufacturer's instructions and analysed using QCpG 92 software (Qiagen, UK).

2.11 Targeted Next Generation Bisulfite Sequencing

2.11.1 Principle

As with pyrosequencing, targeted next generation bisulfite sequencing (tNGBS) is a 'sequencing by synthesis' method which uses Ion Torrent™ technology to quantitatively assess the methylation status of a number of target genes at any given time. However, ion torrent sequencing relies on the release of hydrogen ions (H⁺) when complementary free nucleotides (dNTPs) are incorporated into the DNA template by DNA polymerase (Rothberg *et al.*, 2011). Firstly, a semiconductor chip is flooded with free dNTPs which fills each microwell containing a bead with DNA fragments (see Figure 2.18). If the dNTP is complementary to the DNA template, H⁺ is released which increases the pH. The pH is sensed by an ion sensor and converted into a voltage signal which is proportional to the number of nucleotides added to the DNA template (see Figure 2.18). For example, the incorporation of 2 × dNTPs releases 2 × H⁺ and a double bp is recorded whereas entry of non-complementary dNTPs results in no voltage recorded.

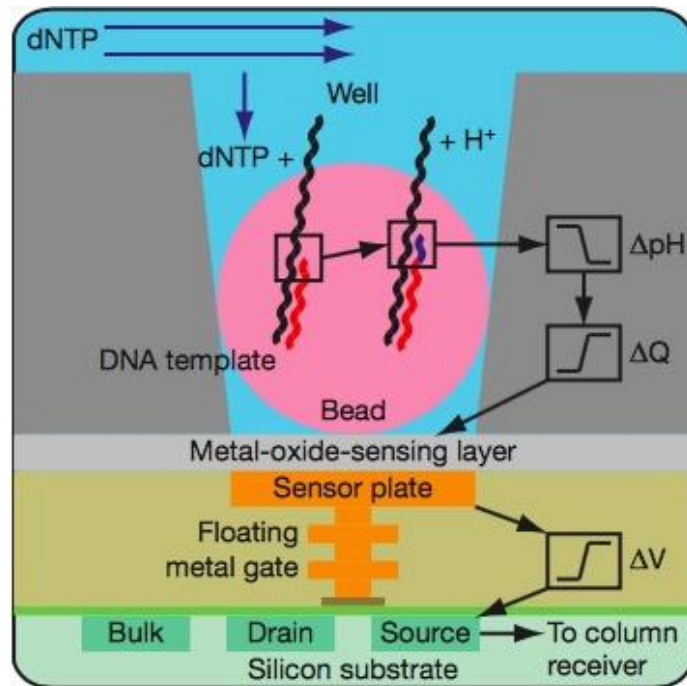


Figure 2.18. Mechanisms of tNGBS for DNA methylation

A simplified schematic of a bead containing fragments of the DNA template within each microwell and the underlying on sensor and electronics. When dNTPs complimentary to the DNA template are flood the microwell, H⁺ are released leading to a change in pH (ΔpH) which induces a change in surface potential of the sensing layer and a change in potential (ΔV). Schematic taken from (Rothberg *et al.*, 2011).

2.11.2 Procedure

Targeted Next Generation Bisulfite Sequencing (tNGBS) assays were purchased from EpigenDX (Hopkinton, USA) and the same assay design algorithm was used as that for pyrosequencing. Assays were designed to target various regulatory regions of mouse genes; MSN, TIMP3, WNT9a, CTTN, GSK3 β , PAX3, AGTR1a, BICC1, GRIK2, TRAF1, STAG1, ODF2 and UBR5. Two-hundred and fifty nanograms of DNA was first bisulfite converted (see section 2.10.4) and amplified via multiplex PCR. Each 20 μl PCR reaction was composed of 5 U HotStar Taq Polymerase (Qiagen, UK), 0.2 μM of forward and reverse primers for the gene of interest and 2 μl of bisulfite treated DNA. All PCR products were verified and quantified using the QIAxcel Advanced System (Qiagen, UK). Prior to library preparation, PCR products from the same sample were pooled and purified using QIAquick PCR Purification Kit columns

(Qiagen, UK). Libraries were then prepared using a custom method (EpigenDx, Hopkinton, USA). Library molecules were purified using Agencourt AMPure XP beads (Beckman Coulter, USA) and quantified using the Qiagen QIAxcel Advanced System. Template preparation and enrichment were performed using the Ion Chef system (Thermo Fisher Scientific, Denmark) using Ion 520TM and Ion 530TM.ExT Chef reagents (Thermo Fisher Scientific, Denmark). Enriched template-positive library molecules were then sequenced on the Ion S5TM sequencer using an Ion 530TM sequencing chip (Thermo Fisher Scientific, Denmark). FASTQ files from the Ion Torrent S5 server were aligned to the local reference database using open-source Bismark Bisulfite Read Mapper with the Bowtie2 alignment algorithm. Methylation levels were calculated in Bismark by dividing the number of methylated reads by the total number of reads. If a data set displayed less than 30 reads, the results were considered unreliable and were therefore excluded from further analysis.

2.12 Lysing for Protein and Puromycin Incorporation for Global Protein Synthesis

2.12.1 Principle

Traditionally, muscle protein synthesis (MPS) rates are measured after administering an amino acid tracer labelled with either a stable or radioactive isotope. This is achieved via constant infusion or administering as a ‘flooding dose’. The rate at which the labelled amino acid is synthesised within the muscle is then assessed (Fiorotto *et al.*, 2012). More recently however, a nonradioactive technique known as the surface sensing of translation (SUnSET) technique was developed to enable the investigation of global and single cell protein synthesis rates both in cultured cells (Schmidt *et al.*, 2009) and tissue (Goodman & Hornberger, 2013). This method involves the incorporation of the antibiotic puromycin that is a structural analogue of tyrosyl-tRNA and can therefore be incorporated into translating polypeptide chains at low concentrations. As the incorporation of puromycin into nascent peptide chains results in the

termination of peptide elongation, the rate at which puromycin-labelled polypeptides (detected using anti-puromycin antibodies) are formed acts as an effective measure of MPS.

2.12.2 Procedure

Puromycin was incorporated into loaded and non-loaded human myotubes to serve as a marker for measurement of global MPS. Following mechanical loading, existing media was aspirated and 2 ml of fresh preheated HDM containing 10 µg/ml of puromycin (P7255, Sigma-Aldrich, UK) was added to each well and incubated at 37°C, 5% CO₂ for 15-30 mins. After incubation, media containing puromycin was aspirated and each well was thoroughly washed 3 × PBS. One-hundred microliters of ice-cold RIPA buffer (10× stock, diluted 1:10 with dH₂O, Sigma-Aldrich, UK) containing protease and phosphatase inhibitors (Pierce™, Thermo Fisher, Denmark) was then added to 2 × wells per condition and placed on ice for 10 mins. Lysed cells were then scraped and transferred to a 2 ml Eppendorf and centrifugation at 16,000 × g for 10 mins (4°C). The supernatant was then transferred to a new Eppendorf tube to undergo sonication for 1 min before proceeding with protein quantification (see section 2.12).

2.13 Quantification of Protein Concentration Using the Bicinchoninic Acid (BCA)

Protein Assay

2.13.1 Principle

Cell lysates were quantified for protein using the bicinchoninic acid (BCA) protein assay. This method relies on the reduction of the cuprous ion, Cu⁺² to Cu⁺¹ using protein in an alkaline solution (Smith *et al.*, 1985). Here, 2 × BCA molecules join with one Cu⁺¹ ion resulting a purple-coloured solution which is influenced by four key amino acids; cysteine, cystine, tryptophan and tyrosine. The colour density is determined by the amount of protein present in the samples whereby a dark purple solution suggests a higher protein concentration and vice

versa. Protein present in each sample can be then be quantified via absorbance at 540-590 nm using a plate reader.

2.13.2 Procedure

The BCA assay was performed using a commercially available kit (23225, Pierce™, Thermo Fisher, Denmark) according to the manufacturer's instructions. Standards were first made up using a 1 ml ampule of 2 mg/ml bovine serum albumin (BSA) to ensure known protein concentrations of 2000, 1500, 1000, 750, 500, 250, 125 and 25 µg/ml in dH₂O. This enabled the determination of protein concentrations based on a standard curve generated using a plate reader (CLARIOstar® Plus, BMG LABTECH, Germany). The BCA working reagent was prepared by mixing reagent A (sodium carbonate, sodium bicarbonate, bicinchoninic acid and sodium tartrate in 0.1 M of sodium hydroxide) with reagent B (4% cupric sulphate) at a ratio of 1:50. Ten microliters of standard and a blank (dH₂O) was pipetted into a 96-well plate in triplicates and 10 µl of raw sample was added in duplicates. Using a multichannel pipette, 190 µl of working reagent was added to each well to ensure a total volume of 200 µl. The well plate was then sealed with parafilm and incubated at 37°C for 30 mins to initiate the biuret reaction. Following incubation, the samples were cooled to RT for 5 mins before quantifying protein using a CLARIOstar® Plus plate reader at a wavelength of 562 nm.

2.14 Acetone Protein Precipitation

After protein quantification using the BCA assay, protein concentrations were considerably low for all samples (0.54 ± 0.11 µg/µl in 100 µl). Therefore, acetone protein precipitation procedures were carried out in attempt to increase the concentration:volume ratio and enable the required amount of protein (~20 µg) to be loaded during SDS-PAGE and western blot procedures (see section 2.14). This method entailed adding 5 volumes (~ 500 µl) of acetone to each sample and incubating at -20°C for 1 hr. After incubation, samples were centrifuged at $5,000 \times g$ for 5 mins. The supernatant was then removed, and samples were left to air-dry in a

fume hood for 5 mins. Finally, samples were resuspended in 50 μ l of ice-cold 1 \times RIPA buffer (10 \times stock, diluted 1:10 with dH₂O, Sigma-Aldrich, UK) containing protease and phosphatase inhibitors (Pierce™, Thermo Fisher, Denmark).

2.15 SDS-PAGE and Western Blot

2.15.1 Sample Preparation

Despite attempting to increase protein concentration:volume ratio as described in section 2.13, protein concentrations post-precipitation were still considerably low with significant variability ($0.38 \pm 0.37 \mu\text{g}/\mu\text{l}$). Therefore, 4 \times laemmli buffer (Bio-Rad Laboratories, USA) composed of 62.5 mM Tris-HCl (pH 6.8), 10% glycerol, 1% SDS, 0.005% Bromophenol Blue was added directly to protein lysates. SDS is added for protein denaturation and to negatively charge proteins to enable separation according to size. Glycerol increases the density of the sample and ensures the sample remains in the well when loaded. β -ME reduces both inter and intra-molecular disulphide bonds when heated. Bromophenol blue is added for ease of sample detection when loading and running the sample during gel electrophoresis. Tris-HCl ensures the buffer is at the required pH, in this case pH 6.8. After dilution, samples were placed on a heat block for 10 mins at 95°C and then placed on ice for a further 10 mins. All samples were then vortexed, ready for separation (see section 2.13.2).

2.15.2 Procedure

Precast gels (4-15%, Mini-PROTEAN® TGX Stain-Free™, Bio-Rad Laboratories, USA) were first assembled to an electrophoresis chamber (Bio-Rad Laboratories, USA) filled with 1 \times running buffer (10 \times 0.25 M Tris, 1.92 M Glycine, 1% SDS diluted in dH₂O, National Diagnostics, USA). Ten microliters of molecular weight marker (peqGOLD, Protein Marker II, VWR, UK) was loaded into the first well followed by the addition of 25 μ l of each sample in

subsequent wells ready to undergo separation via gel electrophoresis (15 minutes at 100 V, followed by 60 minutes at 150 V). Electrophoresis was terminated once all samples had transferred through the entire gel. Gels were then removed from the chambers and imaged using a ChemiDoc system (Bio-Rad Laboratories, USA). After imaging, the gels were sandwiched between transfer paper and nitrocellulose membrane using a Trans-Blot[®] Turbo[™] RTA Mini Nitrocellulose Transfer Kit (Bio-Rad Laboratories, USA) and placed in a trans-blot turbo transfer system (Bio-Rad Laboratories, USA) for 7 mins. After transfer, nitrocellulose membranes were imaged using the ChemiDoc system to determine total protein. Membranes were washed 3 × 5 mins in Tris-buffered saline (0.19 M Tris pH 7.6, 1.3 M NaCl) containing 0.1% Tween[®] 20 (TBST, Sigma-Aldrich, UK). Membranes were then blocked for 1 hr at room temperature (RT) in 5% non-fat dry milk (Sigma-Aldrich) made up in TBST. After blocking, 5 ml of anti-puromycin antibody (MABE343, Merck Millipore, USA) made up at 1:10000 in blocking buffer (5% non-fat dry milk in TBST) was added to the membranes and incubated overnight on a rocker (4°C). After overnight incubation, membranes were washed 3 × 5 mins in TBST and a secondary antibody (rabbit anti-mouse IgG, ab6728, Abcam, UK) made up at 1:1000 in blocking buffer, was added and incubated at RT for 2 hrs. Membranes underwent a final 3 × TBST washes before adding 1 ml of chemiluminescence signal solution (SuperSignal[®] West Pico Enhancer/Peroxide Solution, Thermo Scientific, UK) to visualise proteins using the ChemiDoc system.

2.16 Statistical Analysis

All statistical analysis throughout this thesis was conducted using either a statistical package for the social sciences software (SPSS, version 25.0, SPSS Inc, USA), MiniTab Statistical Software (Minitab, Version 18, USA) or GraphPad Software (Prism, Version 7.0a, San Diego, CA). The software used, alongside the specific statistical tests conducted is specified within the methods section of each experimental chapter.

CHAPTER 3

Characterisation of a Novel Bioreactor System for Mechanically Loading Fibrin Bioengineered Skeletal Muscle

3.1 Introduction

Skeletal muscle (SkM) is an extremely mechano-sensitive tissue, responsive to both loading and unloading activity. Indeed, mechanical loading/resistance exercise (RE) is considered one of the most potent stimuli to influence SkM growth (Goldberg, 1967), remodelling (Benjamin & Hillen, 2003; Franchi *et al.*, 2017) and strength (Sale, 1988). Conversely, muscle mass and function are somewhat diminished with inadequate loading, for example, during spaceflight, aging (sarcopenia) (Hughes *et al.*, 2001; Morse *et al.*, 2005) and periods of immobilization/bed rest (Dirks *et al.*, 2016). Since SkM is crucial for locomotion and whole body metabolism, a reduction in tissue size and function may be detrimental, leading to earlier onset of disability (Laukkanen *et al.*, 1995), morbidity (Kalyani *et al.*, 2014) and all-cause mortality (Ruiz *et al.*, 2008), thus highlighting the clinical importance of SkM tissue. Understanding the cellular and molecular mechanisms that regulate muscle mass and function are therefore of paramount importance for characterising optimised loading (i.e., RE) regimes which evoke the greatest anabolic response and for the potential development of pharmacological interventions which target genes involved in the regulation of SkM mass.

3.1.1 Models for Investigating the Mechanisms of Mechanical Loading *In-Vivo*

Throughout the literature, a number of *in-vivo* and *in-vitro* models have been employed for investigating the physiological responses to mechanical loading. Seminal *in-vivo* work by Goldberg first demonstrated that overloading the plantaris and soleus muscles via removal of the gastrocnemius tendon (termed compensatory hypertrophy/synergistic ablation) in hypophysectomised rats increased muscle mass by 20 and 40%, respectively within just 5 days post tenotomy (Goldberg, 1967). This rapid growth response was directly proportional to the amount of labelled amino acids incorporated in the growing muscles (Goldberg, 1968), and an increase in total protein synthesis (Goldspink, 1977). Since this early work, several others have employed this model for studying satellite cell activation and proliferation (Schiaffino *et al.*, 1972; Rosenblatt & Parry, 1992), growth and maturation (Esser & White, 1995), as well as the

molecules which govern this extreme increase in muscle mass (Goodman *et al.*, 2011; You *et al.*, 2019). Despite the extensive use of this model within the literature, the substantial gains observed are somewhat supraphysiological since RE results in an increase in muscle size of approximately 1–2% per week (Baar & Esser, 1999; Seaborne *et al.*, 2018a). Furthermore, a high level of expertise is required to conduct the surgeries and numerous animals are required to undertake each experiment which may be costly and not in line with the UK governments ‘National Centre for the Replacement Refinement & Reduction of Animals in Research (NC3Rs)’ aims of reducing the number of animals in scientific research (Prescott & Lidster, 2017).

In humans, the cellular and molecular responses to mechanical loading in SkM are assessed via obtaining muscle biopsies for downstream analysis (Phillips *et al.*, 1997) whereas scanning technology (i.e. dual-energy X-ray absorptiometry [DXA], computer tomography [CT] and magnetic resonance imaging [MRI]) are used to detect changes at the whole SkM tissue level (Franchi *et al.*, 2018). A combination of both methods are typically employed within translational research (Seaborne *et al.*, 2018a). After a SkM biopsy, the amount of tissue obtained is typically limited given a needle biopsy yields a total ~20–30 mg’s, whereas a conchotome biopsy can yield ~100–250 mg of tissue (Turner *et al.*, 2019a). The need for repeated biopsies may therefore be necessary, especially if one wishes to explore multiple time points. Despite advances in bioptic techniques, the procedure itself can potentially mask any intervention-induced changes in mRNA (Friedmann-bette *et al.*, 2012) and protein (Caron *et al.*, 2011) expression, particularly if several biopsies are taken over a short time frame. Therefore, *in-vitro* techniques may prove beneficial if a number of acute time points are to be explored without the risk of inducing changes in the variables of interest due to the methods employed.

3.1.2 Monolayer Culture Models for Investigating the Mechanisms of Mechanical Loading *In-Vitro*

Methods for studying the mechanical load-induced responses in SkM *in-vitro* involves the use of bioreactors to stretch immortalised (Baar *et al.*, 2000; Hornberger *et al.*, 2005) and/or primary (Vandeburgh & Kaufman, 1979; Powell *et al.*, 2002) muscle cells which can be routinely isolated via explant culture (Martin *et al.*, 2013), enzymatic digestion (Danoviz & Yablonka-Reuveni, 2012) or a combination of both methods (Owens *et al.*, 2015; Turner *et al.*, 2019a).

Vandeburgh and Kaufman (1979) first applied an external mechanical loading stimulus to cultured cells in monolayer, whereby differentiated 12-day old embryonic chick myotubes cultured on an elastic silicone membrane underwent 18 hrs of multiaxial/stretch (10%), resulting in an increase in amino acid uptake, total/myofibrillar protein synthesis and myotube size (Vandeburgh and Kaufman, 1979; Vandeburgh and Kaufman, 1980). The same group (Vandeburgh, 1988; Vandeburgh *et al.*, 1989) and others (Eastwood *et al.*, 1996, 1998b; Mudera *et al.*, 2000) later developed this model using a computerised step motor to enable the application of various stimulatory patterns which mimic the mechanical tension experienced *in-situ* (i.e. stretch-relaxation also termed cyclic stretch or continuous passive stretch which mimics bone elongation). Since, others have employed similar models to determine some important mechanisms involved in mechanical load-induced muscle development, anabolism and hypertrophy. Indeed, using a system based on the design of the horizontal computerised cell stimulator, Baar and colleagues demonstrated that acute uniaxial cyclic stretch (12%) of C₂C₁₂ cells in monolayer significantly increased the phosphorylation of the well-characterised protein translation initiator, p70S6K (Baar *et al.*, 2000), a ribosomal kinase which was earlier shown to be highly correlated ($r = 0.998$) with increased muscle hypertrophy following chronic RE in rat muscle (Baar & Esser, 1999). It is important to highlight several limitations of culturing/loading cells in traditional monolayer culture models. Firstly, cells are

grown on stiff substrates which can detach from the plastic culture surface after short term differentiation, affecting subsequent myotube maturation (Engler *et al.*, 2004; Gilbert *et al.*, 2010). Given the lack of tension applied to cells in monolayer culture, myotubes form random and swirling formation which do not recapitulate the morphology of myofibres *in-situ* which are uniaxially aligned in the direction of tension (see Figure 1.10). As a consequence, contraction of cells causes non-uniaxial force production, making it difficult to measure SkM function (Brevet *et al.*, 1976; Wehrle *et al.*, 1994). Since force production is the primary function of SkM (Baar, 2005), the inability to assess such measures, together with the aforementioned environmental and morphological issues with traditional monolayer culture systems has led to the development of bioengineered SkM. Despite these limitations, it is also important to acknowledge the benefits surrounding monolayer culture models. Specifically, monolayer culture is cost effective and requires less technical or complicated culture systems compared to bioengineered 3D culture methods, allowing consistent experiments to be more routinely performed. Furthermore, required seeding densities are lower in monolayer (Owens *et al.*, 2015) versus bioengineered SkM models (Bradey *et al.*, 2008; Mudera *et al.*, 2010; Martin *et al.*, 2013) which is an important consideration when initial cell stocks are limited, particularly of precious primary cells that senesce if continually passaged. Moreover, cells cultured in monolayer may easily be transfected to induce gene-specific silencing/overexpression to investigate their mechanistic role(s), and while such methods in bioengineered SkM have been performed, they are not yet as well-characterised (Shahini *et al.*, 2018). Therefore, careful consideration between the use of monolayer versus bioengineered culture systems are important based on the individual studies aims and the appropriate research design to address those aims.

3.1.3 Mechanical Loading of Bioengineered SkM *In-Vitro*

Pioneering work conducted by Vandenburg's group first demonstrated that suspending embryonic avian SkM cells onto a collagen gel prolonged cell survival (2-3 weeks) compared

to traditional monolayer culture, leading to the formation of mature myotubes/fibres evidenced by the presence of a representative basal lamina, well-organised contractile machinery and myonuclei located on the periphery of the myofibres (Vandenburgh *et al.*, 1988). The first studies to engineer human bioengineered muscle also presented similar morphological characteristics to *in-vivo* muscle tissue, given the improved maturation and presence of myotubes along the direction of the longitudinal axis (Powell *et al.*, 2002; Mudera *et al.*, 2010; Chiron *et al.*, 2012; Martin *et al.*, 2013). Although myotube maturation and morphology are somewhat improved when cultured in a representative extracellular matrix (ECM) under tension, there is a necessity for an external mechanical and/or electrical input to further improve muscle maturation in bioengineered SkM which is achieved via the use of bioreactor devices (see Figure 3.1). Indeed, both cyclic and passive stretch of embryonic avian pectoralis muscle cultured on collagen-coated elastic substratum's has been shown to result in greater cell proliferation and myotube size (Vandenburgh & Karlisch, 1989; Vandenburgh *et al.*, 1989). Furthermore, the same group demonstrated that a combination of both mechanical stimulatory patterns applied to human engineered myotubes suspended in a collagen/matrigel matrix led to an increase in myotube diameter (~12%) and area (~40%; Powell *et al.*, 2002). Several others later mechanically loaded bioengineered SkM to determine the mechanisms underpinning load-induced anabolism (Cheema *et al.*, 2005), matrix remodelling (Auluck *et al.*, 2005) and maturation (Heher *et al.*, 2015). However, very few have compared the responses to various loading regimes to determine the optimal regime which elicits the greatest anabolic response. To bridge this gap, Player and colleagues cultured C₂C₁₂ myoblasts in 3D collagen constructs over 14 days, resulting in highly aligned myotubes in parallel prior to loading (Player *et al.*, 2014; see Figure 1.10). Collagen constructs were then subjected to either static (10% stretch held for 1 hr to mimic synergistic ablation/compensatory hypertrophy, see Section 3.1.1) or ramp (10% stretch attained over a 1 hr period) load using a modified version of the well-characterised t-CFM bioreactor system (Mudera *et al.*, 2000; Auluck *et al.*, 2005; Cheema *et al.*, 2005; Player *et al.*, 2014). Interestingly, static loading increased IGF-I and MMP-9

expression and decreased IGFBP-5 expression, with no significant change in catabolic genes, MuRF-1, MAFbx and myostatin. Taken together, this was suggestive of a positive anabolic response and perhaps a potential increase in myotube hypertrophy if this expression profile was maintained over a longer period. Indeed, combining both ramp and static load (15% stretch attained over a 1 hr period and held for a further 2 hrs) in the same model significantly increased myotube size and force production which was concomitant with upregulation of IGF-I and MMP-2 mRNA and increased phosphorylation of Akt, p70S6K, 4EBP-1 protein synthetic signalling (Aguilar-Agon *et al.*, 2019).

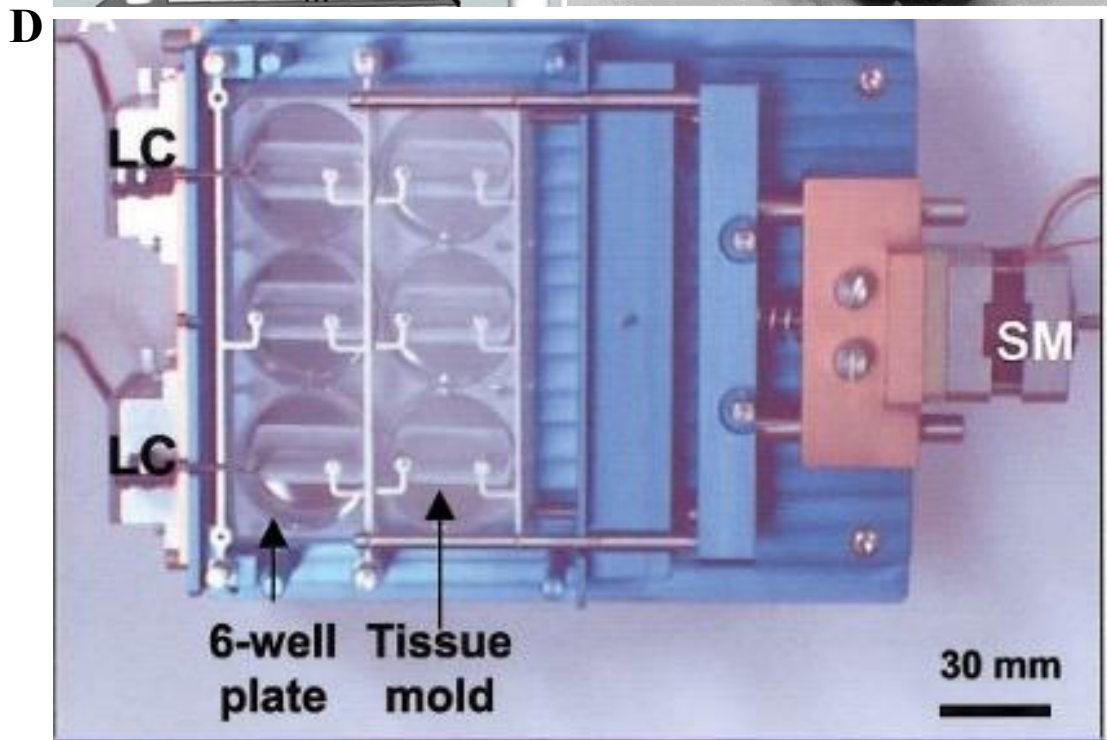
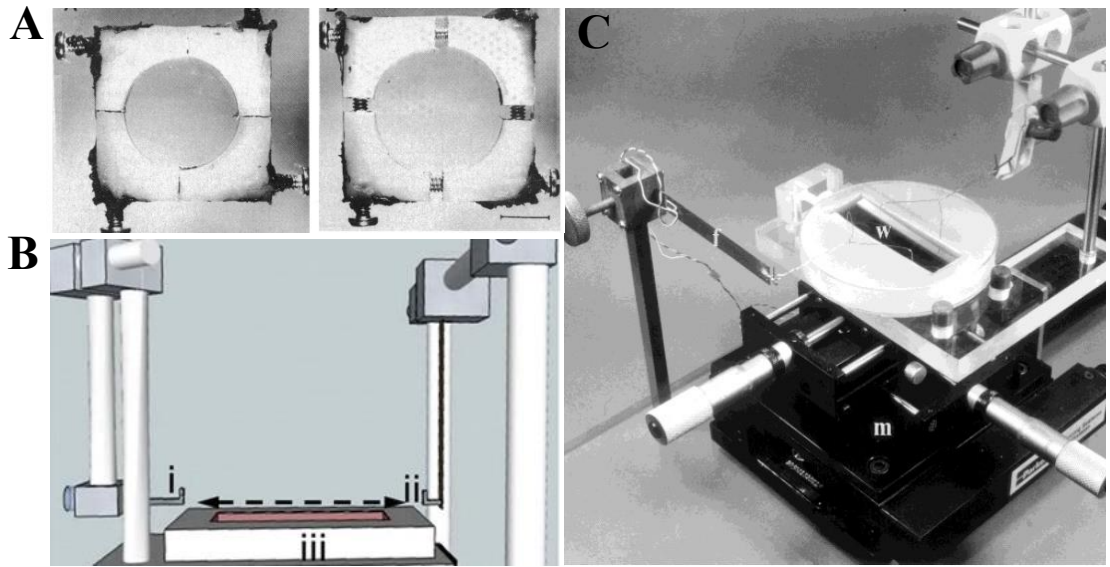


Figure 3.1. Bioreactor used for loading cells and bioengineered tissues

A number of bioreactors used to apply mechanical loading to cultured cells. (A) Cells cultured on elastic membrane are stretched multiaxially via expansion of the surrounding frames (left image - unstretched, right image - stretched by 10%) (taken from Vandeburgh and Kaufman 1979). (B) A more recent bioreactor used to apply uniaxial stretch to engineered muscle using a computerised step motor (taken from Player et al. 2014). (C) An example of the original tensioning culture force monitor (t-CFM; taken from Eastwood et al. 1998). (D) A system which enables uniaxial stretch of engineered tissues cultured in 6-well plates with higher throughput (taken from Powell et al. 2002). (E) The commercially available Flexcell[®] FX-5000[™] Tension system (Dunn Labortechnik, Germany) used to apply both uniaxial and multiaxial load to cells cultured on flexible-bottomed 6-well plates.

Although mechanical loading of bioengineered SkM has served a useful tool for investigating the mechano-responses to external load, a regime which more closely mimics RE *in-vivo* is yet to be determined. Furthermore, the mechano-responses to loading have predominantly been investigated in collagen engineered muscle (Lewis *et al.*, 2001; Powell *et al.*, 2002; Auluck *et al.*, 2005; Cheema *et al.*, 2005; Mudera *et al.*, 2000; Player *et al.*, 2014; Capel *et al.*, 2019) with little use of fibrin as the matrix (Heher *et al.*, 2015; Kim *et al.*, 2019). Indeed, the only studies to the authors knowledge either loaded C₂C₁₂ fibrin bioengineered muscle during differentiation (Heher *et al.*, 2015) or to assess contractile force and ECM remodelling with or without simultaneous electrical stimulation (Kim *et al.*, 2019). Others have also demonstrated that fibrin engineered muscle structure (i.e. stiffness and myotube alignment) is similar to native SkM in the absence of loading (Chiron *et al.*, 2012; Martin *et al.*, 2013). Despite collagen (specifically isoform type 1) being the most prevalent matrix protein within native SkM, fibrin may prove advantageous for tissue engineering, owing to the lower required seeding densities, culture time

(Yen-Chih Huang, Robert G. Dennis, Lisa Larkin, 2005; Huang *et al.*, 2006; Khodabukus & Baar, 2009) and gel stiffness (~12 kPa) which is similar to that of intact muscle (Chiron *et al.*, 2012). Moreover, fibrin directly binds vascular endothelial growth factor (VEGF) and basic fibroblast growth factor-2 (bFGF-2), alongside indirect binding of insulin-like growth factor-1 (IGF-I), all of which improve maturation (Campbell *et al.*, 1999; Sahni & Francis, 2000; Sahni *et al.*, 2003).

3.1.4 Aims and Objectives

As mentioned in section 3.1.3, static (Player *et al.*, 2014; Aguilar-Agon *et al.*, 2019) and cyclical/intermittent (Cheema *et al.*, 2005) loading of bioengineered SkM has demonstrated changes in mechano-sensitive/anabolic gene expression, albeit in collagen muscle. Therefore, the aim of the present chapter was to characterise the response of these known mechano-responsive genes to distinct mechanical loading regimes (i.e. static loading versus intermittent loading which more closely mimics RE *in-vivo*) in fibrin muscle using a bioreactor that has not been previously used for loading engineered SkM (TC-3 Tension Bioreactor, EBERS Medical Technology, Spain; see section 2.5.1). The objective was to confirm that loading of C₂C₁₂ fibrin engineered SkM was responsive to mechanical loading using the previously uncharacterised TC-3 bioreactor system. This would assist in the initial validation of whether this bioreactor is a relevant and comparable system for loading fibrin engineered SkM, and for its subsequent use in future chapters.

3.2 Methods

3.2.1 Cell Culture

C₂C₁₂ cells were sub-cultured in gelatin coated T75 flasks containing 20 ml of GM until ~80% confluency was attained (see sections 2.2.1 and 2.2.3). Cells were then trypsinised (see section 2.2.3), counted (see section 2.2.4) and reseeded into new flasks until the required number of

cells were obtained for fabrication of SkM constructs (see section 3.2.2). All cells throughout this chapter were used at passage 10 (P10).

3.2.2 Fabrication of Fibrin Skeletal Muscle Constructs

Fibrin SkM constructs were prepared as previously described in section 2.4 (Seaborne *et al.*, 2019; Turner *et al.*, 2019a). Following polymerisation, C₂C₁₂ cells were seeded onto the fibrin matrix at a density of 5×10^4 cells/ml in 2 ml GM (see section 2.2.4). GM was changed every 48 hrs until the cells had reached ~90% confluency, whereby GM was switched to DM for 48 hrs to initiate differentiation. After 48 hrs in DM, media was replaced with MM for the remainder of the experiment at which point, gels were fixed (see section 2.7.3) or removed from the sylgard culture dishes to undergo mechanical loading (see section 3.2.3).

3.2.3 Mechanical Stimulation of Fibrin Skeletal Muscle Constructs

After 14 days in culture, fibrin gels were removed from the culture dishes and transferred to the TC-3 bioreactor chambers (see section 2.5). The chambers containing the engineered muscle constructs were assembled to the bioreactor system, placed in a humidified incubator at 37 °C, 5% CO₂, ready to undergo mechanical loading (see Figure 2.7). Constructs acting as controls (CON, $n = 3$ replicate cultures) were kept at resting length (12 mm) for 1 hr whereas loaded constructs were subject to 10% (1.2 mm) strain, a percentage tension which has been shown to increase myotube hypertrophy (Powell *et al.*, 2002), differentiation (Heher *et al.*, 2015) and an increased anabolic response at the transcription level (Player *et al.*, 2014) in bioengineered muscle. The intermittent loading regime (INT, $n = 3$ replicate cultures) consisted of 4 sets \times 10 repetitions (frequency of 0.3 Hz, 0.4 mm/s), each set interspersed with 90 s rest, representing 1 of 5 'exercises'. Each exercise was separated by 3.5 mins rest whereby constructs were kept at resting length. Constructs subjected to static loading (STAT, $n = 4$ replicate cultures) were held

at 10% of resting length for 1 hr to mimic mechanical overload (Player *et al.*, 2014), similar to that observed in *in-vivo* synergistic ablation/compensatory hypertrophy (Goldberg, 1967).

3.2.4 Immunohistochemistry (IHC)

SkM constructs were fixed in methanol:acetone as described in section 2.7.2. Following fixation, fibrin gels were removed from the culture dishes and transferred to 2 ml Eppendorf tubes ready for immunostaining (see section 2.7.3). SkM constructs were stained for the cytoskeletal intermediate filament protein, desmin (red) and myonuclei (blue) was determined using DAPI (see section 2.7.2). Stained gels were then visualised using an inverted fluorescence microscope (Nikon, Eclipse Ti-S, Japan) to confirm the formation of highly aligned multinucleated myotubes (see Figure 3.2).

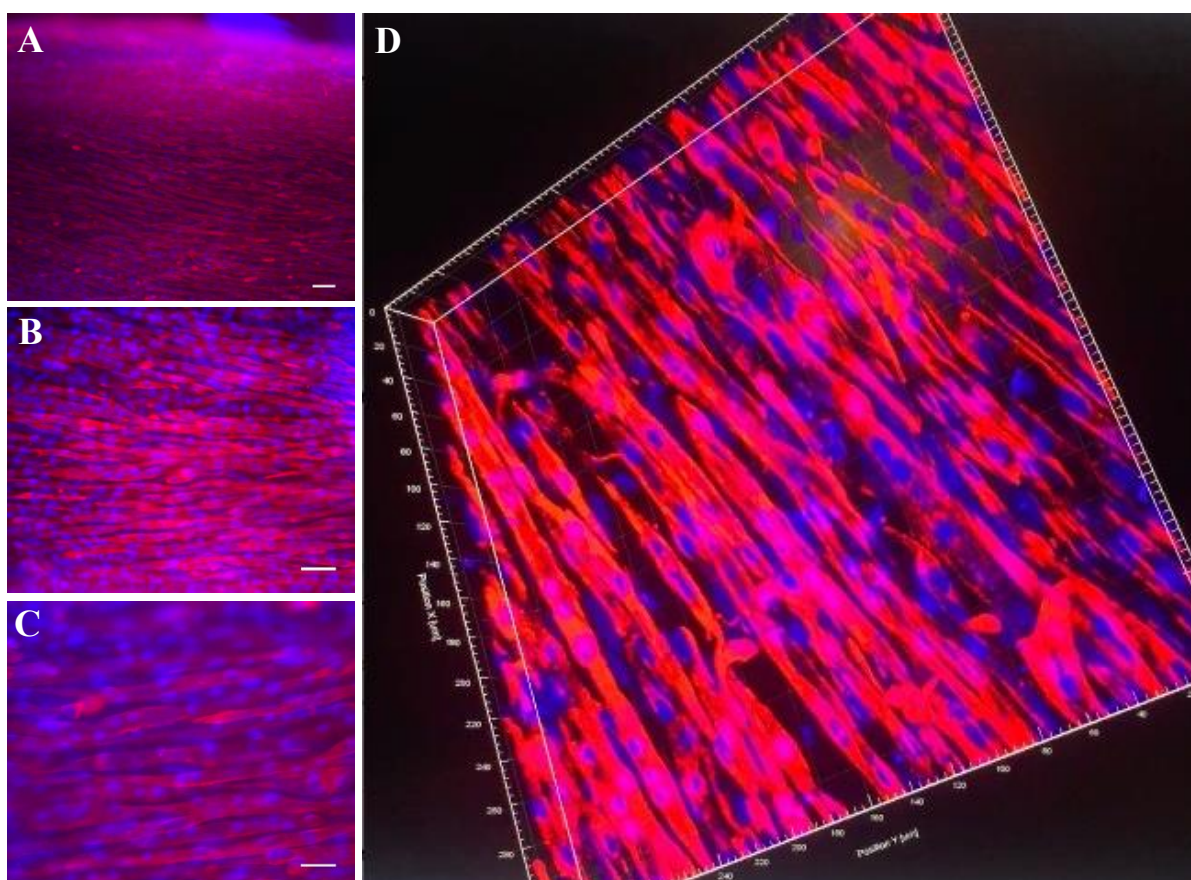


Figure 3.2. Immunostained fibrin bioengineered SkM

Immuno-stained microscopic (Nikon, Eclipse Ti-S) images of C₂C₁₂ bioengineered fibrin muscle constructs at (A) 10× (scale bar = 50 μm) (B) 20× (scale bar = 20 μm) and (C) 40× (scale bar = 20 μm) magnification. (D) Z-stack confocal (Olympus, IX83) microscopic image (40× magnification). Constructs were stained for desmin (red) and myonuclei (blue) (taken from Turner *et al.* 2019a).

3.2.5 RNA Extraction and Quantitative Real-Time Polymerase Chain Reaction (qRT-PCR)

Three hours post mechanical loading, gels were removed from the bioreactor chambers and lysed in 1 ml TRIzol (see section 2.8) for subsequent RNA extraction (see section 2.9.2). RNA concentration (387.23 ± 20.30 ng/μl) and purity ($2 \pm 0.01_{A260/A280}$) was assessed using a Nanodrop (see section 2.9.3). Samples were then diluted in nuclease-free H₂O to ensure a concentration of 70 ng in 9.5 μl (7.37 ng/μl) which was added to 10.5 μl of master mix composed of 10 μl SYBR green, 0.2 μl of reverse transcriptase (RT) mix and 0.15 μl of both forward and reverse primers in PCR reaction tubes (0.1 ml strips and caps, Qiagen, UK). All samples/genes were ran in duplicate. Primer sequences and locations for the genes analysed throughout this chapter are described in Table 3.1. After preparation, reaction tubes were transferred to a PCR thermal cycler for amplification (see section 2.9.4.2). Once amplified, gene expression was quantified using the DDCT ($\Delta\Delta C_T$) equation (Schmittgen & Livak, 2008) against the mean C_T values of the reference gene, RP-IIβ (16.73 ± 0.39 , with low variation of 2.37%) and a non-loaded control (CON) group (see section 2.9.4.3). PCR efficiencies for the reference gene ($91.95 \pm 3.4\%$, with low variation of 3.71%) and genes of interest ($93.44 \pm 8.6\%$, with a variation of 9.2%) were similar.

Table 3.1 Mouse primers for assessing mechano-responsive genes after loading in bioengineered SkM

Target Gene	Primer Sequence (5'-3' end)	Product	Reference
		Length	Sequence Number
MHC-1	F: CGGTCGAAGTTGCATCCCTA R: TTCTGAGCCTCGATTGCTC	149	NM_030679.1
MHC-2	F: GCGAAGAGTAAGGCTGTCCC R: GGCGCATGACCAAAGGTTTC	76	NM_001039545.2
MHC-4	F: AGGAGGCTGAGGAACAATCC R: TTCTCCTGTCACCTCTCAACA	192	NM_010855.3
MHC-7	F: TGTGCTACCCAGCTCCAAG R: CTGCTTCCACCTAAAGGGCTG	77	NM_080728.2
IGF-1	F: CACACCTCTTCTACCTGGCG R: CCACAATGCCTGTCTGAGGT	189	NM_001314010.1
IGF-1Ea	F: GCTTGCTCACCTTTACCAGC R: AATGTACTTCCTTCTGGGTCT	300	NM_010512
MGF	F: GCTTGCTCACCTTTACCAGC R: AAATGTACTTCCTTTCCTTCTC	353	NM_010512.5
IGFBP-2	F: GATCTCCACCATGCGCCTTC R: TGTCACAGTTGGGGATGTGC	77	NM_001310659.1
IGFBP-5	F: GAAGAGGTGGTGACAGAG R: TGACAACAAGATCGGGAA	104	NM_010518.2
MMP-2	F: GACAAGTTCTGGAGATAC R: TAATAAGCACCTTGAAG	155	NM_008610.2
MMP-9	F: CTGGCAGAGGCATACTTG R: GCCGTAGAGACTGCTTCT	76	NM_013599.2
MyoD	F: CATTCCAACCCACAGAAC R: GGCGATAGAAGCTCCAA	125	NM_010866.2
Myogenin	F: CCAACTGAGATTGTCTGTC	173	NM_031189.2

	R: GGTGTTAGCCTTATGTGAAT		
MuRF-1	F: GAGGGCCATTGACTTTGGGA	97	NM_001039048.2
	R: TTTACCCTCTGTGGTCACGC		
MAFbx	F: TCGACTGCCATCCTGGATTC	104	NM_133521.1
	R: TTCTTTTGGGCGATGCCACT		
RP-IIβ	F: GGTCAGAAGGGAACTTGTGGTAT	197	NM_153798.2
	R: GCATCATTAATGGAGTAGCGTC		

3.2.6 Statistical Analysis

All statistical analysis was conducted using SPSS software (version 25, SPSS Inc, USA). A one-way between subjects' ANOVA was used to detect statistical differences in gene expression between conditions. A pair-wise comparison post-hoc test was performed using Tukey HSD where main effects for condition occurred. The alpha value of significance was set at $P < 0.05$. All data is represented as the mean \pm standard error of mean (SEM).

3.3 Results

3.3.1 Myosin Heavy Chain (MHC) mRNA Expression After Mechanical Loading

The mRNA expression of myosin heavy chain (MHC) genes, MHC-1, MHC-2, MHC-4 and MHC-7, encoding for contractile proteins, MHC-IIx, MHC-IIa, MHC-IIb and MHC-1, respectively, were first determined in loaded (INT and STAT) and non-loaded (CON) constructs.

MHC-1 Expression

There was no significant main effect for condition on MHC-1 mRNA expression ($F_{2,9} = 2.30$, $P = 0.17$), despite a greater increase following STAT (1.34 ± 0.18) versus INT (0.87 ± 0.19 , 95% CI = -1.15 to 0.21, $P = 0.17$) and CON (1.01 ± 0.09 , 95% CI = -0.34 to 1.02, $P = 0.37$; see

Figure 3.3). There was also no statistical difference between INT and CON conditions (95% CI = -0.86 to 0.59, $P = 0.85$).

MHC-2 Expression

As with MHC-1, there was no significant main effect for condition on MHC-2 mRNA expression ($F_{2,8} = 2.36$, $P = 0.18$), despite an increase following STAT (1.5 ± 0.18) versus INT (1.11 ± 0.18 , 95% CI = -1.12 to 0.33, $P = 0.29$) and CON (1.02 ± 0.14 , 95% CI = -1.21 to 0.24, $P = 0.18$; see Figure 3.3). Furthermore, there was no statistical difference between INT and CON conditions (95% CI = -0.64 to 0.81, $P = 0.93$).

MHC-4 Expression

There was no significant main effect for condition on MHC-4 mRNA expression ($F_{2,9} = 0.38$, $P = 0.7$), with no significant difference between CON (1.02 ± 0.15) versus INT (1.29 ± 0.41 , 95% CI = -1.38 to 0.83, $P = 0.76$) and STAT (1.3 ± 0.17 , 95% CI = -1.31 to 0.75, $P = 0.72$; see Figure 3.3). There was also no statistical difference between INT and STAT conditions (95% CI = -1.04 to 1.03, $P = 1$).

MHC-7 Expression

There was no significant main effect for condition on MHC-7 expression ($F_{2,9} = 0.82$, $P = 0.48$), with no statistical difference between CON (1.07 ± 0.3) versus INT (0.94 ± 0.22 , 95% CI = -1.5 to 1.76, $P = 0.97$) and STAT (1.56 ± 0.45 , 95% CI = -2.01 to 1.04, $P = 0.64$; see Figure 3.3). Furthermore, there was no significant difference between INT and STAT conditions (95% CI = -2.14 to 0.91, $P = 0.49$).

Overall, the present section suggests that neither acute STAT nor INT loading was able to induce a significant change in myosin heavy chain mRNA expression, despite a non-significant increase after STAT for all isoforms analysed herein. This could be due to the acute loading stimulus applied and that chronic loading may induce significant changes in MHC mRNA

expression in bioengineered SkM. However, MHC gene expression following chronic loading in fibrin engineered SkM warrants future investigation.

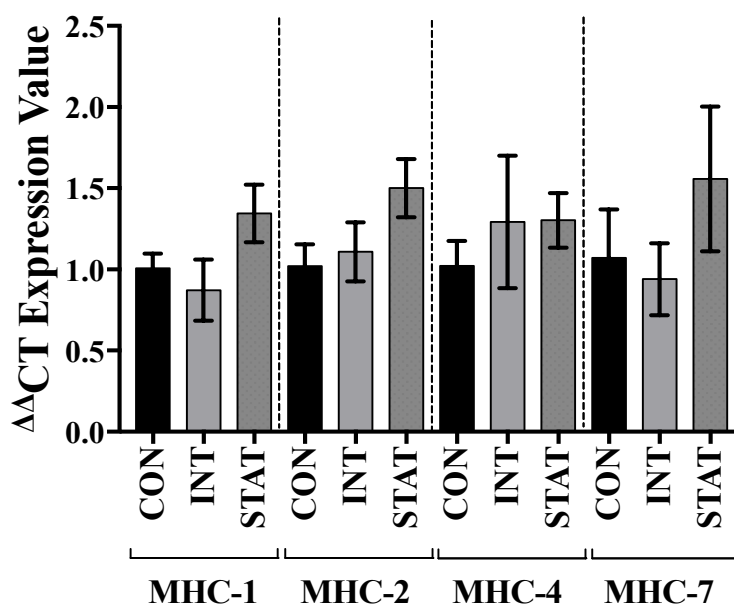


Figure 3.3. MHC mRNA expression after mechanical loading

Myosin heavy chain mRNA expression in loaded (INT, $n = 3$ and STAT, $n = 4$) and non-loaded (CON, $n = 3$) bioengineered SkM constructs. There was no significant main effect for loading on myosin heavy chain-1, 2, 4 or 7 mRNA expression ($P > 0.05$). Data is presented as mean \pm standard error of mean (SEM).

3.3.2 IGF-1, IGF-IEa and MGF mRNA Expression After Mechanical Loading

To investigate the response of known transcripts associated with the anabolic response to loading in bioengineered SkM (Cheema *et al.*, 2005; Player *et al.*, 2014), mRNA expression of total mature IGF-I and isoforms, IGF-IEa and MGF were quantified following the contrasting INT/STAT regimes.

IGF-I Expression

There was no significant main effect for condition on IGF-I mRNA expression ($F_{2,9} = 1.36$, $P = 0.32$), despite a greater increase following INT (1.58 ± 0.40) versus STAT (1.02 ± 0.25 , 95%

CI = -0.56 to 1.66, $P = 0.36$) and CON (1 ± 0.04 , 95% CI = -0.61 to 1.76, $P = 0.38$; see Figure 3.4). There was also no statistical difference between STAT and CON (95% CI = -1.09 to 1.13, $P = 1$).

IGF-IEa

There was a significant main effect for condition on IGF-IEa mRNA expression ($F_{2,9} = 13.71$, $P < 0.01$) which was greatest following INT (2.97 ± 0.37) versus STAT (1.31 ± 0.28 , 95% CI = 0.53 to 2.79, $P = 0.01$) and CON (1 ± 0.07 , 95% CI = 0.76 to 3.18, $P = 0.01$; see Figure 3.4). However, there was no statistical difference between STAT and CON (95% CI = -0.82 to 1.44, $P = 0.72$).

MGF

As with IGF-IEa, there was a significant main effect for condition on MGF mRNA expression ($F_{2,9} = 17.67$, $P < 0.01$) which significantly increased following INT (2.18 ± 0.1) versus STAT (1.17 ± 0.19 , 95% CI = 0.42 to 1.77, $P = 0.01$) and CON (1.01 ± 0.08 , 95% CI = 0.63 to 2.07, $P < 0.01$; see Figure 3.4). However, there was no statistical difference between STAT and CON (95% CI = -0.41 to 0.93, $P = 0.53$).

Despite the non-significant increase in IGF-1 mRNA expression following INT loading, the present section suggests that INT loading elicited the greatest anabolic response given isoforms, IGF-IEa and MGF demonstrated a significant increase in mRNA expression after INT versus STAT and CON.

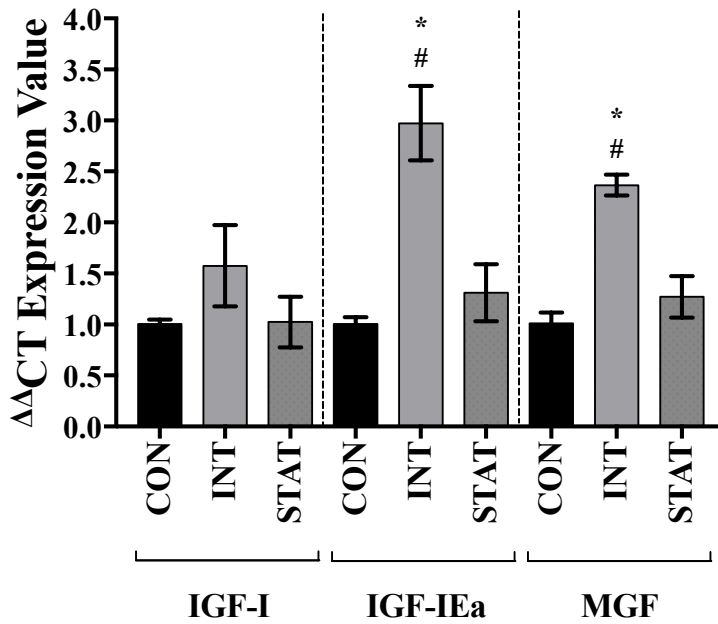


Figure 3.4. IGF-I, IGF-IEa and MGF mRNA expression after mechanical loading

IGF-I, IGF-IEa and MGF mRNA expression in loaded (INT, $n = 3$ and STAT, $n = 4$) and non-loaded (CON, $n = 3$) bioengineered SkM. There was no significant main effect for loading on IGF-1 mRNA expression ($P > 0.05$), however, IGF-IEa and MGF mRNA was significantly upregulated after INT versus CON (*) and STAT (#) loading ($P < 0.05$). Data is presented as mean \pm standard error of mean (SEM).

3.3.3 IGFBP-2 and IGFBP-5 mRNA Expression After Mechanical Loading

Following determination of the transcriptional IGF-I responses after loading, mRNA expression of IGF binding protein genes, IGFBP-2 and IGFBP-5 were also quantified due to previous studies demonstrating an altered response to loading in bioengineered muscle (Player *et al.*, 2014).

IGFBP-2

There was no significant main effect for condition on IGFBP-2 mRNA expression ($F_{2,9} = 0.97$, $P = 0.43$), despite a non-significant reduction following INT (0.73 ± 0.25) versus STAT (1.25 ± 0.27 , 95% CI = -1.61 to 0.58, $P = 0.40$) and CON (1.06 ± 0.26 , 95% CI = -1.49 to 0.84, $P =$

0.7; see Figure 3.5). There was also no statistical difference between STAT and CON (95% CI = -0.9 to 1.28, $P = 0.87$).

IGFBP-5

As with IGFBP2, there was no significant main effect for condition on IGFBP-5 mRNA expression ($F_{2,8} = 1.23$, $P = 0.36$), despite a reduction following INT (0.8 ± 0.09) versus STAT (1.31 ± 0.38 , 95% CI = -1.5 to 0.49, $P = 0.33$), and CON (1 ± 0.04 , 95% CI = -1.2 to 0.8, $P = 0.82$; see Figure 3.5). There was also no statistical difference between STAT and CON (95% CI = -0.69 to 1.3, $P = 0.64$).

Collectively, the present section demonstrates that neither loading regime elicited a significant response in IGFBP-2 and -5 mRNA expression. Interestingly however, the non-significant reduction in mRNA following INT coincides with the non-significant increase in IGF-1 and upregulation of IGF-IEa and MGF after INT (see section 3.3).

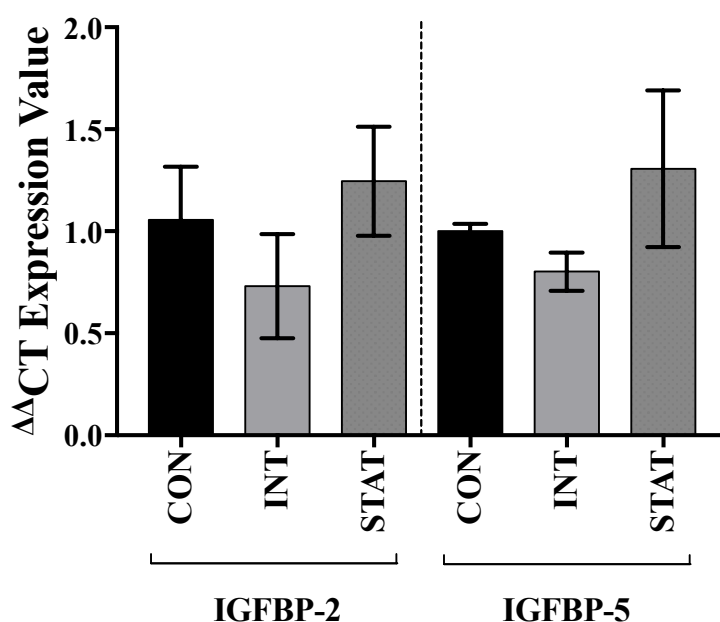


Figure 3.5. IGFBP-2 and IGFBP-5 mRNA expression after mechanical loading

IGFBP-2 and -5 mRNA expression in loaded (INT, $n = 3$ and STAT, $n = 4$) and non-loaded (CON, $n = 3$) bioengineered SkM. There was no significant main effect for loading on IGFBP-2 and -5 mRNA expression ($P > 0.05$). Data is presented as mean \pm standard error of mean (SEM).

3.3.4 MMP-2 and MMP-9 mRNA Expression After Mechanical Loading

The mRNA expression of matrix remodelling genes, MMP-2 and MMP-9 were investigated to determine whether such loading regimes in fibrin muscle had the potential to initiate ECM turnover as shown previously after loading in engineered collagen muscle (Mudera *et al.*, 2000; Auluck *et al.*, 2005; Player *et al.*, 2014).

MMP-2

There was no significant main effect for condition on MMP-2 mRNA expression ($F_{2,9} = 0.25$, $P = 0.79$) with no statistical differences between CON (1 ± 0.05) versus INT (1.15 ± 0.02 , 95% CI = -0.8 to 0.51, $P = 0.8$) and STAT (1.03 ± 0.2 , 95% CI = -0.64 to 0.58, $P = 0.99$; see Figure 3.6) together with no significant difference between INT and STAT (95% CI = -0.49 to 0.73, $P = 0.84$).

MMP-9

Interestingly, there was a significant main effect for loading on MMP-9 mRNA expression ($F_{2,9} = 9.69$, $P = 0.01$) with the greatest increase observed after INT (1.89 ± 0.32) versus STAT (0.89 ± 0.03 , 95% CI = 0.29 to 1.7, $P = 0.01$) and CON (1.01 ± 0.09 , 95% CI = 0.13 to 1.63, $P = 0.03$; see Figure 3.6). However, there was no statistical difference between STAT and CON (95% CI = -0.82 to 0.59, $P = 0.88$).

Taken together, the present data suggests that INT loading evoked the greatest ECM turnover response in following mechanical loading in fibrin bioengineered SkM. This was evidenced by the significant increase in MMP-9 mRNA expression observed following INT versus STAT and CON.

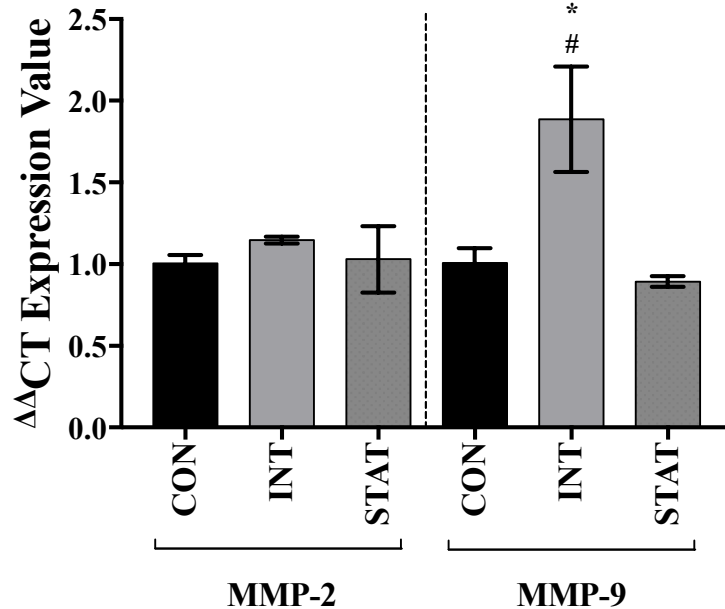


Figure 3.6. MMP-2 and MMP-9 mRNA expression after mechanical loading

MMP-2 and MMP-9 mRNA expression in loaded (INT, $n = 3$ and STAT, $n = 4$) and non-loaded (CON, $n = 3$) bioengineered SkM. There was no significant main effect for loading on MMP-2 mRNA expression ($P > 0.05$), however, MMP-9 mRNA was significantly upregulated after INT versus CON (*) and STAT (#) loading ($P < 0.05$). Data is presented as mean \pm standard error of mean (SEM).

3.3.5 MyoD and Myogenin mRNA Expression After Mechanical Loading

Given the importance of the well-characterised myogenic regulatory factors, myoD and myogenin during development and regeneration following damaging stimuli, their mRNA expression was analysed in response to distinct loading regimes.

MyoD

There was no significant main effect for condition on myoD mRNA expression ($F_{2,8} = 1$, $P = 0.42$), despite an elevation following INT (1.38 ± 0.23) versus CON (1.01 ± 0.11 , 95% CI = -

1.2 to 0.45, $P = 0.41$) and STAT (1.14 ± 0.21 , 95% CI = -0.58 to 1.1, $P = 0.64$; see Figure 3.7). There was also no statistical differences between CON and STAT (95% CI = -0.95 to 0.7, $P = 0.89$).

Myogenin

There was no significant main effect for condition on myogenin mRNA expression ($F_{2,8} = 1.23$, $P = 0.36$), despite a lower expression in CON (1.03 ± 0.18) versus INT (2.02 ± 0.62 , 95% CI = -2.94 to 0.97, $P = 0.33$) and STAT (1.65 ± 0.44 , 95% CI = -2.57 to 1.34, $P = 0.62$; see Figure 3.7). There was also no statistical differences between INT and STAT (95% CI = -1.59 to 2.32, $P = 0.84$).

The present data demonstrates that mechanical loading of fibrin bioengineered SkM did not evoke a significant change in myoD or myogenin, despite a slight increase following INT versus STAT and CON.

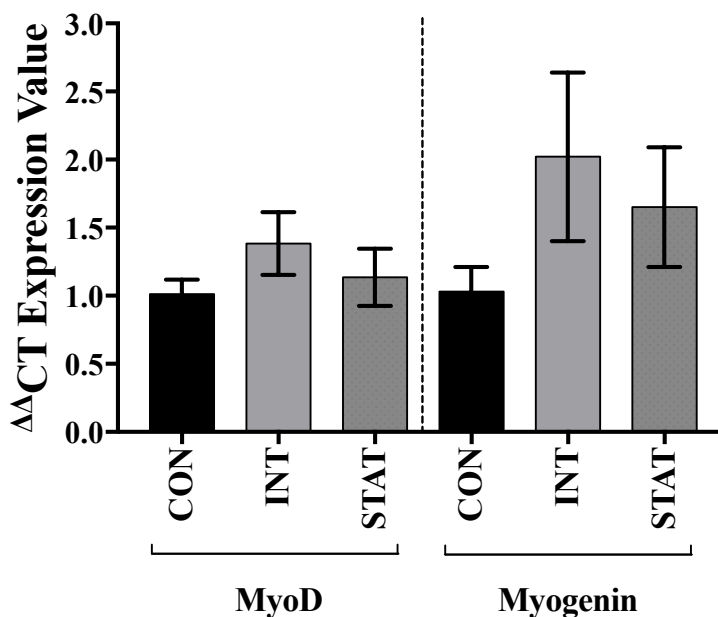


Figure 3.7. MyoD and myogenin mRNA expression after mechanical loading

MyoD and myogenin mRNA expression in loaded (INT, $n = 3$ and STAT, $n = 3$) and non-loaded (CON, $n = 3$) bioengineered SkM. There was no significant main effect for loading on myoD and myogenin mRNA expression ($P > 0.05$). Data is presented as mean \pm standard error of mean (SEM).

3.3.6 MuRF-1 and MAFbx mRNA Expression After Mechanical Loading

After analysing the acute anabolic response to the loading regimes employed herein, the expression of the well-characterised E3 ubiquitin ligases MuRF-1 and MAFbx involved in muscle atrophy were examined.

MuRF-1

There was no significant main effect for loading regime on MuRF-1 mRNA expression ($F_{2,8} = 4.48, P = 0.06$), despite lower mRNA expression in CON (1.01 ± 0.11) versus INT (2.72 ± 0.31 , 95% CI = -3.66 to 0.25, $P = 0.08$) and STAT (2.61 ± 0.71 , 95% CI = -3.55 to 0.36, $P = 0.1$; see Figure 3.8). There was also no statistical differences between INT and STAT (95% CI = -1.85 to 2.06, $P = 0.98$).

MAFbx

As with MuRF-1, there was no significant main effect for condition on MAFbx mRNA expression ($F_{2,8} = 2.11, P = 2.02$), despite in a non-significant increase following STAT (1.8 ± 0.41) versus INT (1.21 ± 0.24 , 95% CI = -1.81 to 0.63, $P = 0.36$) and CON (1.02 ± 0.13 , 95% CI = -2 to 0.43, $P = 0.1$; see Figure 3.8). There was also no statistical significance between INT and CON (95% CI = -1.41 to 1.02, $P = 0.88$).

Data reported herein clearly demonstrates an increase in MuRF-1 and MAFbx mRNA expression following mechanical loading. Interestingly however, such changes failed to reach statistical significance, potentially due to the large variation observed within loading conditions (i.e. INT and STAT). Future studies should therefore consider increasing sample size to determine whether mechanical loading of fibrin muscle is indeed able to induce a significant change in gene expression that could be representative of the acute upregulatory response observed following mechanical overload *in-vivo* (Baehr *et al.*, 2014).

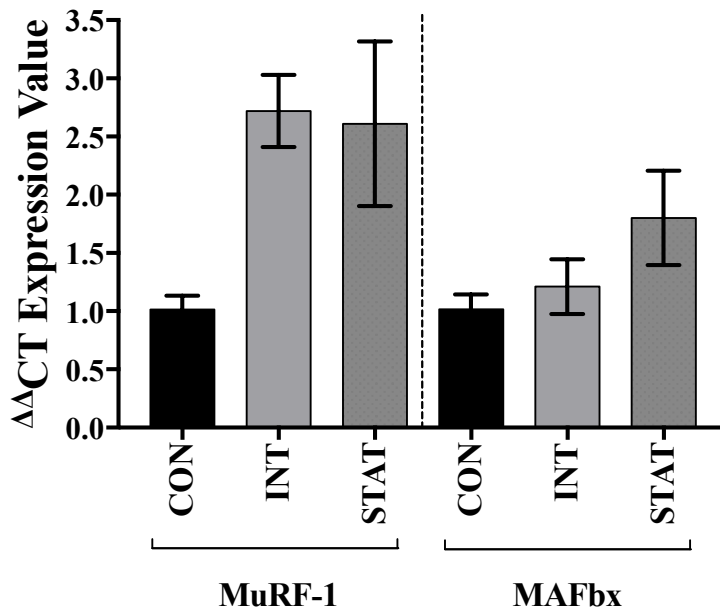


Figure 3.8. MuRF-1 and MAFbx mRNA expression after mechanical loading

MuRF-1 and MAFbx mRNA expression in loaded (INT, $n = 3$ and STAT, $n = 3$) and non-loaded (CON, $n = 3$) bioengineered SkM. There was no significant main effect for condition on MuRF-1 and MAFbx mRNA expression ($P > 0.05$). Data is presented as mean \pm standard error of mean (SEM).

3.4 Discussion

The aim of the present chapter was to characterise the use of a novel bioreactor system for loading bioengineered SkM *in-vitro*. Therefore, targeted gene expression of known mechano-responsive genes *in-vivo* that have also been shown to be regulated after loading collagen muscle using previously published bioreactor systems (Mudera *et al.*, 2000; Cheema *et al.*, 2005; Player *et al.*, 2014; Aguilar-Agon *et al.*, 2019) were assessed after loading in fibrin engineered SkM. Specifically, genes involved in SkM maturation/phenotype, anabolism/hypertrophy, atrophy and SkM/ECM remodelling were compared after static (STAT) and intermittent (INT) loading in murine fibrin bioengineered SkM using the TC-3 bioreactor. The comparison of STAT and INT loading which mimic synergistic ablation/compensatory hypertrophy and acute eccentric lengthening exercise *in-vivo*, respectively also enabled the characterisation of which regime elicits the greatest anabolic response to loading in mature fibrin bioengineered SkM.

3.4.1 Myosin Heavy Chain (MHC)-1, 2, 4 and 7 mRNA Expression After Loading

Mechanical load-induced mRNA changes of myosin heavy chains (MHC)-1, 2, 4 and 7 which encode for contractile proteins, MHC-IIx, IIa, IIb and I, respectively were first assessed. MHCs are cytoskeleton proteins which determine the stage of maturation during embryogenesis and the muscle phenotype in adult tissue. During the developmental stages, embryonic (MHC-3) and slow (MHC-7) isoforms are firstly expressed, followed by MHC-8 (perinatal) during the foetal and neonatal stages where fast (MHC-1, 2 and 4) isoform expression becomes prominent during late foetal myogenesis (Schiaffino & Reggiani, 2011; Chal & Pourquié, 2017). Mechanical loading has been shown to alter MHC phenotypic expression whereby a single bout of RE was sufficient in upregulating expression of MHC-1, 2 and 7 in human SkM with, MHC1 (IIx) considered the most responsive (~75% increase versus ~40% and 45% increase in MHC-7 and MHC-2, respectively; Willoughby & Nelson, 2002). Mechanical loading fibrin muscle within the present chapter failed to recapitulate such findings since neither regime elicited a significant alteration in MHC expression (see Figure 3.3). It is worth noting however that changes in MHC expression was only prevalent 6 hrs post exercise (versus pre and 30 mins post), suggestive that the discrepancies in results may not necessarily be a consequence of the model and/or regimes employed herein, but possibly the timepoint at which MHC mRNA was analysed in loaded engineered muscle (3 hrs post). Furthermore, Sugiura *et al.*, (1993) observed alterations in MHC isoforms following synergistic ablation in 6 week old Wistar rats whereby tenotomy of the gastrocnemius muscle resulted in a decrease in MHC-IIb with a concomitant increase in MHC-IIx and MHC-I in the plantaris muscle (Sugiura *et al.*, 1993). However, overload of the soleus muscle increased MHC-I only, highlighting the influence of the originating muscle phenotype. Such findings therefore make direct comparisons to MHC expression within the present chapter difficult since C₂C₁₂ cells used herein are derived from the thigh muscle of C3H mice which is composed of mixed muscle fibres.

3.4.2 IGF-IEa and MGF mRNA Expression Significantly Increased After Loading

To determine which loading regime elicits the greatest anabolic response in fibrin bioengineered muscle, mRNA expression of known anabolic genes, insulin-like growth factor I (IGF-I) together with isoforms, IGF-IEa and mechano-growth factor (MGF; IGF-IEb in rodents and IGF-IEc in humans) were investigated. IGF-I is a growth factor with a pivotal role in inducing SkM hypertrophy, alongside stimulating cell proliferation and differentiation (Florini *et al.*, 1996). Despite IGF-I being primarily produced in the liver as an endocrine hormone, Matheny and colleagues highlighted the importance of local production of IGF-I from the muscle, reporting similar strength gains following 16 weeks of RE in severely liver IGF-I deficient (~80%) mice compared to wild-type mice (Matheny *et al.*, 2009). Furthermore, local infusion of IGF-I in rat tibialis anterior (TA) muscle resulted in a ~9% increase in lean mass compared to the contralateral control TA muscles (Adams & McCue, 1998). An associated increase in IGF-I mRNA expression following mechanical loading of bioengineered muscle has also been observed, whereby stretching mature (14 days in culture) C₂C₁₂ type 1 collagen constructs significantly increased IGF-I mRNA expression, specifically in response to static load (10% stretch for 1 hr) versus continuous (increased stretch over 1 hr until 10% load was attained) and non-loading constructs (Player *et al.*, 2014). Such findings would oppose those presented herein considering IGF-I mRNA expression was not significantly regulated in response to STAT versus CON and INT (see Figure 3.4). Furthermore, IGF-1 was not significantly altered following INT, despite a modest increase versus CON and STAT (see Figure 3.4).

IGF-IEa and mechano-growth factor (MGF) are splice variants of the IGF-I gene and have different modes of action in SkM (Yang *et al.*, 1996; Goldspink, 1999; Yang & Goldspink, 2002). The mechano-sensitive isoform, MGF enhances C₂C₁₂ cell proliferation (independent of IGF-I receptor) but inhibits terminal differentiation, whilst IGF-IEa promotes cell

differentiation (Yang & Goldspink, 2002; Matheny & Nindl, 2011). Furthermore, single legged knee extension RE (10 × 6 reps, 80% 1RM) significantly increased MGF, but not IGF-IEa expression in young human muscle, supporting the notion that the MGF isoform is markedly upregulated in response to mechanical loading (Hameed *et al.*, 2003). Cheema and colleagues (2005) assessed MGF and IGF-IEa expression in response to 12 hrs of 10% cyclic (1, 5 and 10 cycles/hr) and ramp (10% stretch for 10 min [held for remaining 11 hr 50 mins], 1 hr [held for remaining 11 hr] and 12 hr) stretch in C₂C₁₂ type 1 collagen 3D matrices (maintained in DM over 6 days; Cheema *et al.*, 2005). Both IGF-IEa and MGF expression were greatest when constructs were subject to 10% ramp stretch over 1 hr (and held at 10% for the remaining 11 hr). During cyclic stretch, IGF-IEa expression decreased in a dose dependant manner whereas MGF expression significantly increased at a rate of 10%/hr (1 cycle/hr) relative to unloaded static controls. Therefore, this study was suggestive of a suitable anabolic response following ramp stretch whereas MGF and IGF-IEa expression within the present chapter was greatest following INT loading in fibrin muscle (see Figure 3.4). Such opposing findings may be a consequence of the level of maturation given a low percentage (5%) of myotubes were identified within Cheema *et al.* (2005), suggestive that constructs were not fully mature and perhaps represented a model of muscle development during bone growth (e.g. ramp stretch) and the results cannot therefore be necessarily extrapolated to the effect of mechanical loading on mature myotubes.

3.4.3 IGFBP-2 and IGFBP-5 mRNA Expression After Loading

After examining IGF-I, IGF-IEa and MGF gene expression, mRNA of IGF binding proteins, 2 (IGFBP-2) and 5 (IGFBP-5), were assessed given their importance in modulating IGF-I action, having stimulatory and inhibitory effects both *in-vivo* (Rehfeldt *et al.*, 2010) and *in-vitro* (Sharples & Stewart, 2011; Sharples *et al.*, 2013). Indeed, IGFBP-2 binds extracellularly to IGF-I with high affinity which subsequently reduces IGF-I binding to its receptor (IGF-IR) and downstream signalling of the MAPK and Akt pathway, responsible for cell proliferation and

differentiation, respectively (Florini *et al.*, 1996; Coolican *et al.*, 1997; Li *et al.*, 2000) and are involved in protein synthesis/hypertrophy in response to mechanical overload *in-vivo* (Miyazaki *et al.*, 2011). Work from our laboratory also demonstrated impaired Akt signalling and C₂C₁₂ cell differentiation when neutralising IGFBP-2, which was subsequently restored following knockdown of the downstream target, phosphatase tensin homologue (PTEN), evidenced by the increase in myotube hypertrophy (Sharples *et al.*, 2013). *In-vivo*, mice overexpressing IGFBP-2 also displayed higher fat mass and lower lean mass and myofibre size as a result of reduced satellite cell proliferation (identified via a reduction in marker Ki67; Rehfeldt *et al.*, 2010). Furthermore, IGF-I and IGFBP-5 expression significantly increased and decreased, respectively following mechanical overload of the mouse soleus muscle (Awede *et al.*, 1999). In humans, isometric leg strength is also compromised in older men possessing higher serum IGFBP-2 concentrations (van den Beld *et al.*, 2003), demonstrating the relationship between increased IGFBP-2 and impaired muscle function. Such findings corroborate with the increase in IGF-I and decrease in IGFBP-5 expression following static load (1 hour of 10% stretch) in bioengineered collagen muscle constructs (Player *et al.*, 2014). However, the imposed anabolic response may be compromised given IGFBP-2 was also elevated, reducing the affinity of IGF-1 to its receptor and downstream signalling of MAPK/ERK and Akt pathway. The modest increase in IGF-I and isoforms, MGF and IGF-IEa (see Figure 3.5) following INT within the present chapter coincided with the lowest, albeit non-significant reduction in IGFBP-2 and IGFBP-5 mRNA expression (see Figure 3.5), indicating that INT loading of fibrin muscle results in the greatest anabolic response. In contrast, IGF-I and IGFBP's demonstrated a non-significant increase and decrease in mRNA expression, respectively in response to STAT showing a consistent correlation between gene regulatory networks of both IGF-I and its binding proteins following mechanical loading. The present chapter therefore suggests that MAPK and Akt signalling may be enhanced following INT stretch which may result in protein synthesis and subsequent muscle hypertrophy if such expression was maintained overtime. However, MAPK and Akt signalling in fibrin muscle,

alongside interactions between IGF-I and IGFBP's that have been explored within monolayer culture (Sharples *et al.*, 2013) warrant future investigation in bioengineered SkM.

3.4.4 mRNA Expression of the Matrix Remodelling Gene, MMP-9 Significantly Increased After Loading

Given the importance of matrix remodelling for cell migration and fusion during muscle development and regeneration (Lewis *et al.*, 2000), expression of the matrix metalloproteinases (MMPs), MMP-2 (gelatinase A) and MMP-9 (gelatinase B) were assessed. MMP-2 and MMP-9 are highly expressed in single muscle derived cells (Lewis *et al.* 2000) and are key for degradation of basement membrane proteins during matrix remodelling (Lewis *et al.*, 2001). Under resting condition, MMP-2 is constitutively expressed in SkM, which is further upregulated following mechanical stretch (Mudera *et al.*, 2000; Auluck *et al.*, 2005). Indeed, ramp (15% for 6 hours) but not cyclic (1.5 min stretch, 1.5 min hold followed by 1.5 min release of stretch for 6 hrs) stretch induced a significant increase in MMP-2 expression in human masseter muscle suspended onto 3D collagen sponges (Auluck *et al.*, 2005). Furthermore, 4 hrs of ramp and static load combined (15% stretch attained over 1 hr and held for an additional 3 hrs) significantly increased MMP-2 expression 21 hrs post stretch in C₂C₁₂ collagen engineered muscle which coincided with increased myotube width and fusion index (Aguilar-Agon *et al.*, 2019). In the present chapter however, no significant difference in MMP-2 expression was observed, regardless of the stretch regime employed (see Figure 3.6).

MMP-9 expression is upregulated following muscle damaging stimuli (Carmeli *et al.*, 2004). Under nondamaging conditions (i.e. muscle development) however, the absence of MMP-9 in female null mice significantly altered muscle fibre CSA and fibre type distribution compared to wild-type mice with no change in type IV collagen or hindlimb twitch force, suggestive that decreased MMP-9 may attenuate perinatal and postnatal growth (Mehan *et al.*, 2011). Others have also observed an altered muscle fibre CSA in MMP-9 overexpressed mice, resulting in

larger TA and soleus muscle CSA, alongside increased fibre diameter and isometric muscle strength (Dahiya *et al.*, 2011). Taken together, these studies highlight the associated upregulation in MMP-9 and muscle hypertrophy, strength and matrix remodelling, although the exact mechanisms underpinning these responses are yet to be determined. *In-vitro*, Player and colleagues observed a significantly higher MMP-9 expression following static versus ramp load (Player *et al.*, 2014). Interestingly however, combined ramp and static loading (15% stretch attained over 1 hr and held for an additional 3 hrs) using the same model (C₂C₁₂ collagen engineered muscle) failed to replicate such findings given no change in MMP-9 mRNA was observed (Aguilar-Agon *et al.*, 2019). In fibrin engineered muscle, MMP-9 expression was greatest following INT versus STAT, suggestive of an elevated signal for matrix remodelling that would potentiate muscle hypertrophy if the upregulated expression was chronically maintained (see Figure 3.6). Despite the discrepancies in MMP-9 expression in response to mechanical load, both studies demonstrated that MMP-9 is mechano-sensitive in bioengineered muscle, regardless of the matrix in which cells are cultured in.

3.4.5 mRNA Expression of the Myogenic Regulatory Factors, MyoD and Myogenin After Loading

Seminal work in the 1980's first described the importance of the myogenic regulatory factors (MRFs), myoD and myogenin for myogenic determination and differentiation, respectively (Davis *et al.*, 1987; Wright *et al.*, 1989). Since, these basic helix-loop-helix (bHLH) transcription factors have received considerable attention to further determine their roles during developmental myogenesis and satellite cell function and regeneration in adult/mature muscle (reviewed extensively in Zammit, 2017). Several groups have also investigated the mechano-responses following passive stretch in rodents (Gomes *et al.*, 2006; Peviani *et al.*, 2007) and RE in humans (Willoughby & Nelson, 2002; McKay *et al.*, 2008). Indeed, passive stretching of the rat soleus muscle via manually holding the ankle in full dorsiflexion for 10 × 1 mins

(each stretch interspersed with 30 s rest) induced a ~1.7-fold increase whereas continuous stretch for 30 mins induced a ~3.5-fold increase in MyoD gene expression at 24 hrs post but not immediately, 8, 48, 72 or 168 hrs (Gomes *et al.*, 2006; Peviani *et al.*, 2007). In humans, performing 300 × maximal knee extensions (30 × 10 reps, each set interspersed with 1 min rest) induced a 2-fold increase in myoD just 4 hrs post exercise which dropped by 24 hrs and remained stable from thereon (~120 hrs post; McKay *et al.*, 2008). Interestingly however, myogenin significantly increased at 4 hrs (~2.2-fold) but peaked at 72 hrs (~2.8-fold) and remained elevated at 120 hrs post (~2.5-fold). Such findings suggests myoD may be acutely regulated following damaging stimuli to enable satellite cell activation and therefore initiate regeneration, whereas myogenin is more present during the latter stages where myoblasts terminally differentiate to repair the damage portion of the muscle fibre (Zammit, 2017). *In-vitro*, mechanically stretching (15% for 1 s followed by 1 s rest for ~48 hrs) C₂C₁₂ cells differentiated on collagen-coated flexible-bottomed 6-well plates significantly increased expression of both myoD and myogenin after 24 hrs of stretch (Abe *et al.*, 2009). Despite an elevation in myoD and myogenin following INT loading in the present chapter, this increase did not reach statistical significance and therefore did not support the aforementioned previous findings (see Figure 3.8). It is important to note however that expression of myoD (Seward *et al.*, 2001) and myogenin (Loughna & Brownson, 1996) is muscle and fibre type specific and may partially explain discrepancies observed when compared to *in-vivo* rodent studies (Gomes *et al.*, 2006; Peviani *et al.*, 2007). Indeed, passive stretch was conducted in the rat soleus muscles that have different fibre type compositions to the C3H mice thigh muscles of which C₂C₁₂ cells are derived. Furthermore, the direction of stretch (i.e. multiaxial versus uniaxial) has also been shown to induce differential mechano-responses even when using the same C₂C₁₂ cell line cells (Hornberger *et al.*, 2005), making direct comparisons between stretch in these disparate *in-vitro* model difficult. Additionally, the loading duration and/or timepoint at which mRNA expression was assessed throughout this chapter may not have been long enough to detect any significant changes. Finally, myoD and myogenin are more highly expressed in

single satellite cells than mature myofibres as they commit to differentiate (myoD) and during differentiation (myogenin). Therefore, any changes in myoD and/or myogenin observed after exercise may be a consequence of changes in satellite cells rather than mature myofibres.

3.4.6 Expression of E3 Ubiquitin Ligases, MuRF-1 and MAFbx After Loading

MuRF-1 (muscle RING finger 1; Trim63) and MAFbx (muscle atrophy F-box; FBXO32) are two muscle-specific E3 ubiquitin ligases which have been extensively characterised in SkM, and shown to target muscle specific proteins for degradation, specifically during various atrophic conditions (Bodine *et al.*, 2001a; Bodine & Baehr, 2014). Indeed, MuRF-1 and MAFbx mRNA expression significantly increased following denervation, immobilisation and hindlimb unloading-induced atrophy of the rat gastrocnemius muscle within 14 days of post treatment (Bodine *et al.*, 2001a). Furthermore, administering rat medial gastrocnemius muscle tissue with interleukin-1 (IL-1) and dexamethasone and treating differentiated C₂C₁₂ cells with a MAFbx adenovirus upregulated mRNA expression and reduced myotube size (Bodine *et al.*, 2001a). Finally, denervation of the TA and gastrocnemius muscles (via cutting the sciatic nerve) resulted in a 36% and 56% muscle sparing in MuRF-1 and MAFbx KO versus wild-type mice, respectively which coincided with increased fibre size (in MAFbx null mice only) at 14 days post-surgery. Such findings using various models of atrophy therefore highlights the importance of these atrogenes during episodes of severe muscle loss (Bodine & Baehr, 2014). Interestingly, work from the same group suggests a potential role for these genes during remodelling post mechanical loading given expression of both MuRF-1 and MAFbx are increased in mice plantaris muscles after 1 day of overload (tenotomy of the soleus and gastrocnemius muscles) which is reduced thereon ~14 days, with MAFbx dropping below basal levels at 7 and 10 day post tenotomy (Baehr *et al.*, 2014; Bodine & Baehr, 2014). To test this assumption *in-vitro*, MuRF-1 and MAFbx was assessed following STAT and INT loading in fibrin engineered SkM. Despite an elevation in MAFbx following STAT and MuRF-1 in

response to both loading regimes, neither loading protocol induced statistically significant changes (see Figure 3.9). Others have also reported no increase in MuRF-1/MAFbx mRNA following ramp or static loading (Player *et al.*, 2014) or when both regimes were performed simultaneously (Aguilar-Agon *et al.*, 2019) in collagen C₂C₁₂ engineered muscle.

3.5 Conclusion

The present chapter clearly demonstrates that INT loading (which more closely resembles acute RE *in-vivo*) of fibrin bioengineered SkM using a novel bioreactor was able to induce comparable transcriptional responses to those observed following loading in collagen muscle using the t-CFM bioreactor system (Mudera *et al.*, 2000; Cheema *et al.*, 2005; Player *et al.*, 2014; Aguilar-Agon *et al.*, 2019). Moreover, the mechano-transcriptional responses in loaded fibrin muscle were also similar to reported changes in targeted gene expression after RE/loading *in-vivo*. Indeed, IGF1-IEa and MGF significantly increased following INT versus CON and STAT with a modest, albeit non-significant increase and reduction in mature IGF-1 and binding proteins, IGFBP-2 and 5. Furthermore, an increase in the matrix remodelling gene, MMP-9 alongside a non-statistical increase in RING E3 ligases MuRF-1 and MAFbx suggests that these genes may help initiate the remodelling process following mechanical loading in engineered fibrin muscle. Since the present chapter has characterised the cell culture methods, loading regime and transcriptional response of known ‘mechano-sensitive’ candidate genes using the TC-3 bioreactor, the next experimental chapter (chapter 4) will conduct extensive *in-silico* and bioinformatic genome-wide analysis to determine the associated transcriptomic and epigenetic response to acute loading/RE in human SkM. The most significantly regulated transcripts at the mRNA and DNA methylation level identified in chapter 4 will then be assessed in response to mechanical loading in fibrin bioengineered SkM using the bioreactor and loading regime employed herein. This approach will enable a direct comparison of the mechano-response to loading in murine fibrin bioengineered muscle versus loading/RE in human SkM and therefore

determine whether loading bioengineered SkM is able to mimic the transcriptional and DNA epigenetic response to loading/RE in human SkM *in-vivo*.

CHAPTER 4

Transcriptomic and Epigenomic Analysis of Acute Resistance Exercise in Human Skeletal Muscle

4.1 Introduction

Skeletal muscle (SkM) displays a high level of plasticity, undergoing considerable hypertrophy following repetitive bouts of resistance exercise (RE)/mechanical loading (Goldberg, 1967; Phillips *et al.*, 1997; Seaborne *et al.*, 2018a) or atrophy during periods of disuse as a result of injury or ageing (reviewed in Sharples *et al.*, 2015; Sharples, Stewart and Seaborne, 2016). Several transcriptome-wide studies have provided significant insights into the gene regulatory networks that regulate SkM anabolism and hypertrophy following acute (MacNeil *et al.*, 2010; Raue *et al.*, 2012; Murton *et al.*, 2014; Vissing & Schjerling, 2014; Lundberg *et al.*, 2016) and chronic (Liu *et al.*, 2010a; MacNeil *et al.*, 2010; Raue *et al.*, 2012; Phillips *et al.*, 2013; Thalacker-Mercer *et al.*, 2013; Murton *et al.*, 2014; Vissing & Schjerling, 2014) RE, respectively. However, little is known whether such alterations across the transcriptome correspond to epigenetic changes at the DNA level.

As discussed in section 1.6, epigenetics represents changes in gene function that are not due to alterations in the DNA sequence itself but involves the addition or removal of specific molecules on the DNA or the surrounding histone proteins that may ultimately determine the level of gene expression. Epigenetics is influenced by several environmental factors including diet and exercise, specifically in SkM as evidenced in previous work by our group (Seaborne *et al.*, 2018a) and others (Barrès *et al.*, 2012). A major key epigenetic modification, known as DNA methylation involves the attachment (also known as ‘hyper’-methylation) or detachment (also referred to as ‘hypo’-methylation) of a covalent methyl chemical tag on the 5’ position of a cytosine residue within cytosine-guanidine dinucleotide base pairing sites (CpG site). As described in section 1.6, increased CpG methylation (hypermethylation), particularly within the promoter regions of a gene is able to inhibit binding of RNA polymerase or tightening of the chromatin (termed heterochromatin), ultimately preventing gene transcription from occurring (Bogdanović & Veenstra, 2009). Conversely, reduced DNA methylation (hypomethylation) is

able to expose regulatory regions of a gene to permit gene transcription, subsequently increasing mRNA expression (Sharples & Seaborne, 2019).

Previous work by our group analysed the DNA methylome (850K CpG sites) following acute (4 sets \times 10 reps of 5 exercises) and chronic (3 days/per week for 7 weeks) RE/loading followed by 7 weeks of unloading (cessation of RE) and a further 7 weeks reloading (3 days/per week for 7 weeks) in untrained humans (Seaborne *et al.*, 2018a, 2018b). Within this study, clusters of genes previously uncharacterised in SkM were epigenetically altered after chronic training (evoking a \sim 6.5% increase in lower limb lean mass) and further retraining (evoking a \sim 12.5% versus baseline; Seaborne *et al.*, 2018a, 2018b). Indeed, one gene cluster (including genes; RPL35a, BICC1, ZFP2, UBR5, HEG1, PLA2G16, SETD3 and ODF2 which are described in chapter 5) demonstrated increased gene expression and reduced DNA methylation after training, with a larger increase in mRNA expression and greater reduction in methylation after further retraining. Interestingly, another group of genes (including genes; AXIN1, TRAF1 and GRIK2 which are also described in chapter 5) demonstrated increased and decreased mRNA expression and DNA methylation, respectively after chronic RE which was retained during detraining (where muscle mass reduced back to baseline levels) and further regulated after retraining. Finally, a number of genes were epigenetically modified after just one single bout of RE with reduced methylation being retained after 7 weeks of chronic training and retraining, suggesting a potential important role for these genes in ‘muscle memory’ (Seaborne *et al.*, 2018a, 2018b).

The gene expression responses to mechanical loading in bioengineered SkM are typically determined via assessing the mRNA expression of well-characterised mechano-sensitive genes. Considering the role of epigenetics in SkM has only more recently begun to emerge, there has previously been no attempt to establish the epigenetic responses to mechanical loading in bioengineered SkM. Therefore, identifying the most frequently regulated genes across

transcriptome-wide human RE studies which are also epigenetically regulated across the methylome would provide a more comprehensive list of relevant genes to assess at the transcript and epigenetic level following mechanical loading in engineered SkM. This would firstly validate the use of loading C₂C₁₂ fibrin bioengineered muscle *in-vitro* as a representative model of loading/RE *in-vivo*. Moreover, if loading bioengineered SkM recapitulates the epigenomic and transcriptomic responses to loading/RE *in-vivo*, this would potentially demonstrate a plausible *in-vitro* model for studying the mechanistic regulation of load-induced anabolism/muscle growth via gene-specific overexpression, knockdown and hormonal or pharmacological manipulation.

4.1.1 Aims and Hypothesis

The aims of the present chapter were to therefore identify genes which were significantly expressed across the human transcriptome after acute RE in all published human transcriptome data sets to date (April 2018), and further determine whether such alterations in gene expression corresponded to changes at the DNA level of the same genes across the methylome from Seaborne *et al.*, (2018). To achieve this, publicly available transcriptome-wide data files that compared pre- versus post-acute RE in humans were pooled to enable the detection of mechano-sensitive genes. The significantly expressed genes across all studies were then mapped against the DNA methylome data derived from previously published work by our group (Seaborne *et al.*, 2018a, 2018b). Gene expression and DNA methylation patterns identified herein would therefore enable identification of which genes to examine after mechanical loading in bioengineered SkM throughout subsequent chapters of this thesis. It was hypothesised that a number of genes, previously known and unknown to be epigenetically regulated in response to acute RE *in-vivo* would be identified.

4.2 Methods

4.2.1 Identification of Transcriptomic Studies

The pooled transcriptome-wide studies analysed after acute RE in humans are summarised in Table 4.1. All transcriptomic data files included throughout the present chapter were derived from a publicly available database (Gene Expression Omnibus, [GEO]) which were deposited before April 2018 (time of the first analysis). Studies were selected according to a number of inclusion and exclusion criteria to enable a suitable comparison across all acute RE transcriptomic studies. Indeed, only healthy adult male humans were included to ensure a similar population when mapping the transcriptomic data with the previously published methylome array data from our group (Seaborne *et al.*, 2018a). Furthermore, RE only array data files and not aerobic or concurrent exercise data were included, due to RE being associated with muscle growth versus these other modes of exercise. For sampling timepoints, biopsies obtained within 24 hrs post-acute exercise were included and samples collected after 24 hrs were therefore excluded. Given the variation in post-exercise timepoints at which samples were collected between and within studies (with only 2 studies sampling at the same post-exercise timepoint; see Table 4.1), all samples obtained within the first 24 hrs post-exercise were pooled and contributed to the same ‘post-exercise’ condition. Any study with less than 10,000 gene probe-sets annotated by ‘gene symbol’ were also excluded since these studies used earlier gene array platforms with a low number of gene transcripts analysed versus more recent data sets which enabled an analysis of approximately 15,000 gene transcripts, detailed later.

Table 4.1. Transcriptome-wide acute RE studies pooled for comparative analysis

Details of all transcriptomic studies analysed throughout the present chapter including each studies PubMed ID (PMID) and gene expression omnibus (GEO) accession numbers, the array platform and exercise intervention employed, timepoint(s) at which muscle biopsies were collected (all obtained from the vastus lateralis quadricep muscle) and general notes highlighting the samples that were removed from each study according to the inclusion and exclusion criteria outlined in section 4.2.1. Note that only two studies (MacNeil *et al.*, 2010; Lundberg *et al.*, 2016) sampled at the same post-exercise timepoint (i.e. 3 hrs). All biopsies which were collected ~24 hrs post-acute RE were therefore pooled to ensure an adequate sample number for the post-exercise condition.

Acute RE Studies	PMID	GEO	Array Platform	Exercise Protocol	Timepoint(s)	Notes
(MacNeil <i>et al.</i> , 2010)	20502695	GSE19062	GPL6255 Illumina humanRef-8 v2.0	Eccentric quadricep exercise. 15 sets × 10 reps, maximal resistance of knee flexion at 120°/s. 1 min rest between sets.	Pre, 3 hrs Post	The E2 supplement group was removed. Only the placebo/no supplement group was analysed.
(Raue <i>et al.</i> , 2012)	22302958	GSE28422	GPL570 [HG U133_Plus_2]	Bilateral quadricep knee extension. 3 sets × 10 reps at 70-75% of 1RM.	Pre, 4 hrs Post	Elderly male/female and young female adult acute/chronic RE groups were removed. Only the young male adult group analysed.
(Vissing & Schjerling, 2014)	25984345	GSE59088	GPL6244 [HuGene-1_0- st]	3 individual quadricep exercises. 4 × sets at 12 RM. 1.5 mins rest between exercises.	Pre, 2.5 & 5 hrs Post	The endurance exercise group was removed. Only pre- and post-acute RE were analysed.
(Murton <i>et al.</i> , 2014)	24265280	GSE45426	GPL570 [HG U133_Plus_2]	Quadricep knee extensions. 5 sets × 30 maximal isokinetic contractions at 180°/s. 1 min rest between sets.	Pre, 24 hrs Post	Non-exercise group was removed. Pre/post-acute RE group used for the analysis.

Lundberg et al. (2016)	27101291	GSE74194	GPL17692 [HuGene-2_1- st]	Quadri- ceps knee extensions. 4 sets × 7 reps (70% 1RM). 2 mins rest between sets.	3 hrs Post Only	No relevant 'pre', as the comparison was 'post'- acute RE from one limb (that performed RE) versus the contralateral limb that underwent both RE plus endurance exercise. Post RE limb samples used for the analysis only. RE+ endurance limb samples were therefore removed.
---------------------------	----------	----------	---------------------------------	---	--------------------	--

4.2.2 Bioinformatic Pooled Transcriptome Analysis

All transcriptomic data files were downloaded from the National Institutes of Health (NIH) GEO data base and imported into Partek Genomics Suite software (version 7.18.0518, Partek Inc. Missouri, USA) as .CEL or .TXT files. The relevant gene array platform annotation file was then assigned to the appropriate data set. All intensity values were Log transformed (if not done so already upon downloading) prior to continuing. The highest-scoring probe set was selected whenever more than one probe set was detected for a given gene. This was to enable a comparison of the unambiguous expression estimate of an individual gene, and to compare across different studies and array platforms. Such methods have previously been considered appropriate when accounting for altered hybridisation efficiency across multiple probe sets for the same gene and across array platforms (Li *et al.*, 2011; Gravendeel *et al.*, 2012). To enable direct comparisons of gene expression between studies, the common gene symbol annotations across all studies were identified. This enabled filtering of each individual data set by gene symbols that were uniformly shared across the different array platforms, allowing a comparison of identical genes across all studies. Samples were then defined as ‘pre’ or ‘post’ acute RE, also in line with the inclusion/exclusion criteria stated in section 4.2.1. Quality assurance (QA) and control (QC) analyses were undertaken on all data sets using principal component analysis (PCA), box/whisker charts and sample frequency/density plots by lines to identify sample outliers and to analyse the normal distribution of intensity values (see Figure 4.1). Samples were considered outliers if they fell outside 2 standard deviations (SD) from the centroid using ellipsoids as well as showing different distribution patterns to the samples of the same condition (pre/post) or within each study. All outliers were subsequently removed from further analysis. Batch correction was performed using Partek Genomics Suite ‘Remove Batch Effects’ tool (uses ANOVA approach) to account for any differences in sample processing or array platform methods between studies. This method has previously been identified as an appropriate batch correction tool when dealing with data of non-trivial size (i.e. large number of samples per condition; Nygaard, Rødland and Hovig, 2016). A detailed description of the QA/QC and batch

removal can be seen in the appropriate figure legend (see Figure 4.1). Detection of differentially expressed genes was then performed on Partek Genomics Suite software (version 7.18.0518, Partek Inc. Missouri, USA) using an ANOVA and a gene list of all the significantly ($P \leq 0.01$) up/downregulated genes was created.

4.2.3 Overlapping the Pooled Transcriptome with the DNA Methylome

Using Venn diagram analysis, the significant differentially regulated gene lists generated from the pooled transcriptomic gene expression analysis described in section 4.2.2 were overlapped with the significantly differentially modified CpG sites lists from the methylome array data file (Seaborne *et al.*, 2018a). Genome-wide DNA methylation data was processed as previously described (Seaborne *et al.*, 2018a, 2018b). Briefly, raw .IDAT files were processed on Partek Genomic Suite software (version 6.6, Partek Inc. Missouri, USA) and background normalisation was performed via the Subset-Quantile Within Array Normalisation (SWAN) method (Maksimovic *et al.*, 2012) and imported using the MethylationEPIC_v-1-0_B2.bpm manifest file. This analysis enabled the comparison of genes that were both up/downregulated at the mRNA expression level and hypo/hypermethylated at the DNA level after acute RE. Also, to determine the association of genes that were up/down regulated in the comparative transcriptome analysis after acute RE that were hypo/hypermethylated at the DNA level.

4.2.4 Pathway Analysis

Using statistically generated gene expression and CpG data (see section 4.2.3), KEGG signalling pathway analysis (Kanehisa, 1997; Kanehisa *et al.*, 2016, 2017; see results/figures in section 4.3 for significance level of enrichment P values) was performed in Partek Genomic Suite software and Partek Pathway (version 7.18.0518, Partek Inc. Missouri, USA). Once significant enrichment was determined via Venn diagram analysis, regulated pathways identified both in the transcriptome and methylome analysis were overlapped.

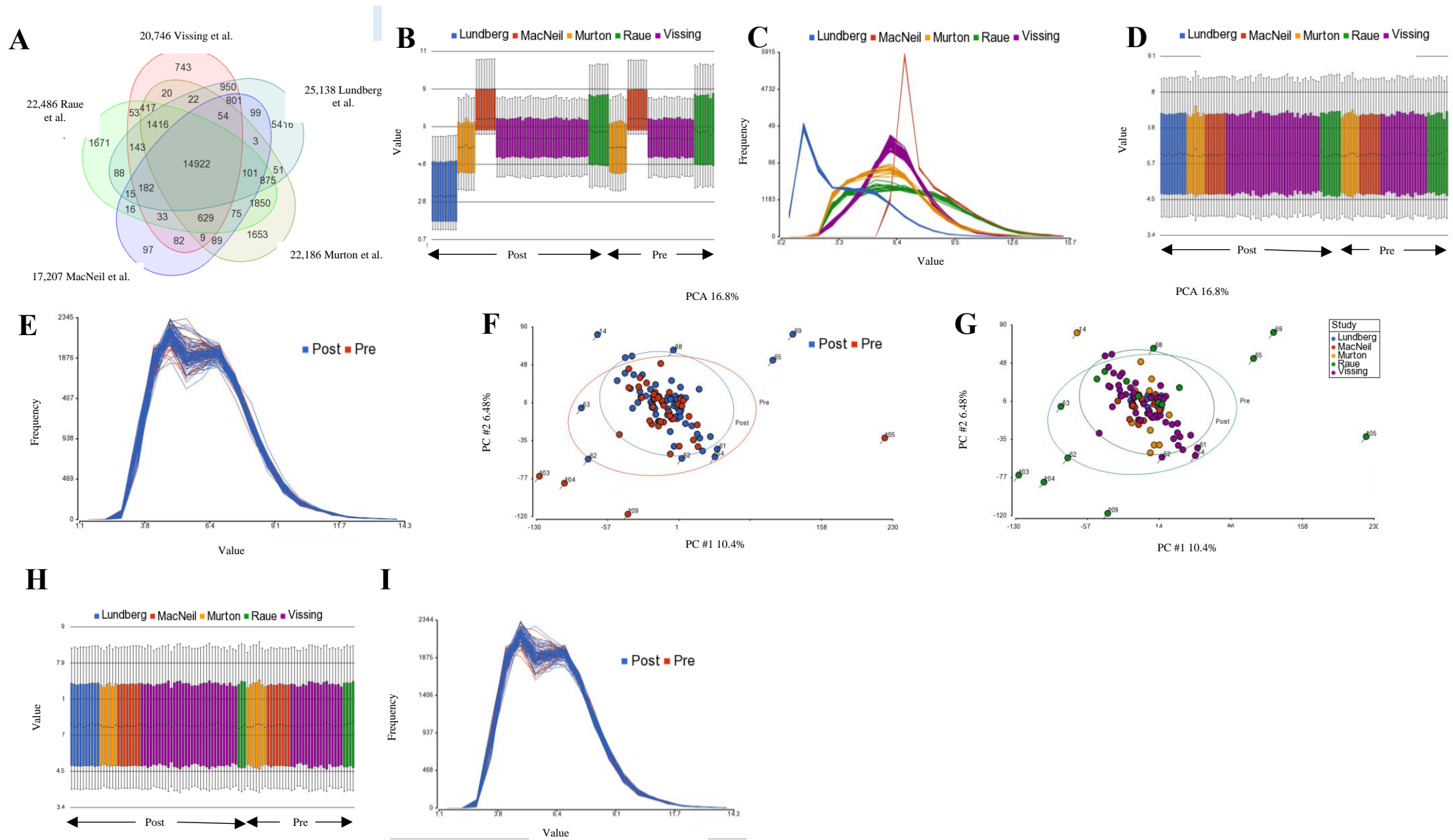


Figure 4.1. QC/QA, Venn diagram and PCA analysis

(A) Venn diagram analysis identified 14,992 shared annotated genes by 'gene symbol' across all pooled transcriptomic studies after acute RE. The number of genes identified in Murton *et al.*, (2014) and Raue *et al.*, (2012) are depicted as different despite both studies using the same array platform. This is due to the highest probe set analysis (see section 4.2.2) altering the number of genes that could be compared in the present chapter. (B) Box/whisker charts and (C) frequency/density plots by lines prior to batch correction enabled detection signal/value variation as a result of batch effects across studies. (D) Box/whisker chart and (E) frequency normalisation plots by lines post batch correction. (F) PCA by sampling timepoint (pre/post) and (G) PCA by study post batch correction. Samples located outside 2 SD of the centroid value using ellipsoids were identified as outliers and were removed (depicted by line strikethrough) prior to analysis. (H) Depicts sample box/whisker chart and (I) frequency plot by lines after batch correction and with outlier samples (highlighted in F/E) removed.

4.3 Results

4.3.1 Pooled Transcriptome Analysis Overlapped with the Methylome in Human Skeletal Muscle After Acute Resistance Exercise

In total, 110 gene arrays were included for the pooled transcriptome analysis in the present chapter, all of which were derived from all pre- and post-exercise SkM biopsies across the 5 studies analysed (see Table 4.1). This included 41 baseline (pre) samples and 69 post-acute RE samples (37 pre/57 post after outlier removal). All 5 studies analysed herein identified 14,992 of the same annotated genes by 'gene symbol' (see Figure 4.1A). Relevant QA/QC and outlier removal is depicted in figure 4.1 and described in the corresponding figure legend. Downstream gene expression analysis of the transcriptome data across all 5 studies demonstrated that 1,802 genes were significantly differentially modified ($P \leq 0.01$) after acute RE (full gene list described in Supplementary File 4.1A). Out of these genes, 866 were upregulated and 936 genes were downregulated. Out of the 866 upregulated genes, 270 of these genes were also hypomethylated (see Figure. 4.2A; full gene list described in Supplementary File 4.1B) which equated to 355 different CpG sites on these 270 genes as some individual genes had more than one CpG site that was hypomethylated per gene (full gene list described in Supplementary File 4.1C). Furthermore, 216 out of the 866 upregulated genes were hypermethylated. Out of the 936 downregulated genes, 216 were also hypermethylated (see Figure 4.2B; full gene list described in Supplementary File 4.1D) which equated to 268 different CpG sites on these 216 genes given some genes had more than one hypomethylated CpG site per gene (full gene list described in Supplementary File 4.1E). Furthermore, 298 out of the 936 downregulated genes were hypomethylated.

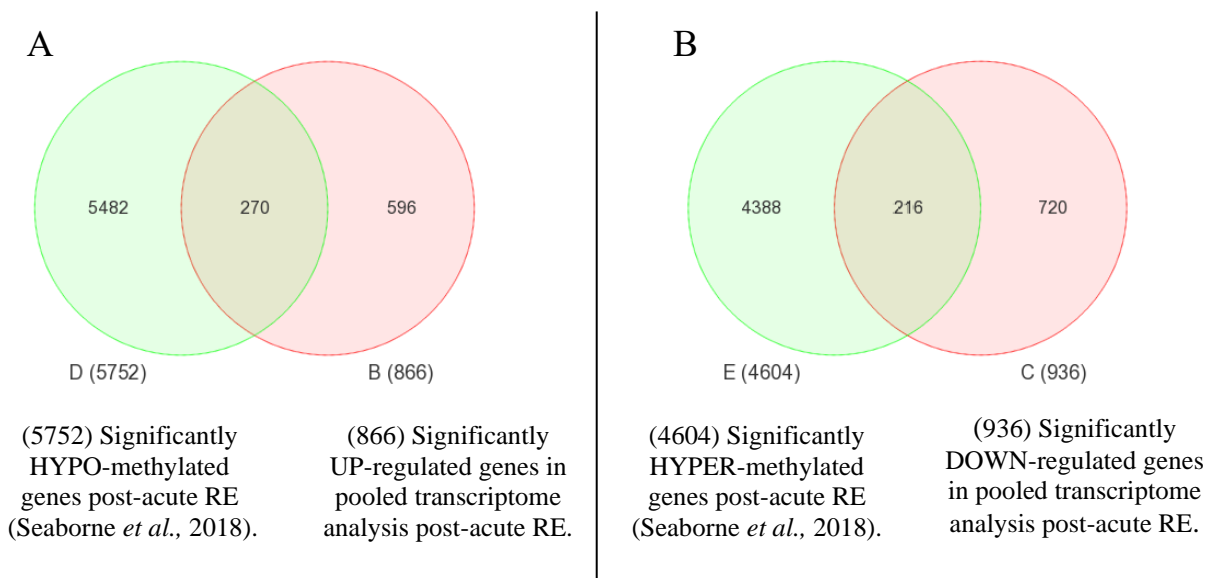


Figure 4.2. Analysis of upregulated/hypomethylated and downregulated/hypermethylated genes after acute RE in human SkM

Venn diagram analysis identified **(A)** out of the 866 upregulated genes, 270 of these genes were also hypomethylated across the methylome (Seaborne *et al.*, 2018a, 2018b) and **(B)** out of the 936 genes that were downregulated across the pooled transcriptome, 216 of these genes were also hypermethylated in the methylome data following acute RE in humans (Seaborne *et al.*, 2018a, 2018b). Venn diagrams were created using Partek Genomics Suite software (version 7.18.0518, Partek Inc. Missouri, USA).

4.3.2 Genes Associated with Cancer Pathways are Enriched in Both the Transcriptome and Methylome Data Sets in Human Skeletal Muscle After Acute Resistance Exercise

KEGG Pathway analysis of the top 20 pathways included 483 genes that were differentially expressed with statistical significance at post versus pre-exercise ($P \leq 0.01$) and significantly enriched (Enrichment P value ≤ 0.003). Out of these 483 genes, 35% (168 genes) were genes associated with 5 different enriched ‘cancer’ pathways including ‘Proteoglycans in cancer’, ‘Transcriptional misregulation in cancer’, ‘Colorectal cancer’, ‘Small cell lung cancer’ and ‘Pathways in cancer’ (full list of all enriched pathways across the transcriptome are described

in Supplementary File 4.2A). While the ‘cancer’ term is not relevant to analysis of healthy SkM tissue, these cancer pathways e.g. KEGG term ‘pathways in cancer’ incorporates well described molecular pathways in the regulation of SkM mass such as; focal adhesion, MAPK signalling, PI3K-Akt-mTOR signalling, p53 signalling, Jak-STAT signalling, TGF- β and Notch signalling. Indeed, in a closer analysis of the specific genes (detailed below), they were specifically related to pathways associated with matrix/actin structure and remodelling, mechano-transduction, TGF- β /calcium/IL-6/retinoic acid signalling and protein synthesis as described below. As some of the same genes were also present in more than one of these KEGG cancer pathways, 106 out of the total 168 genes were unique and were either up- (69 cancer genes) or down-regulated (37 cancer genes) after acute RE across all 5 ‘cancer pathways’. Pathway analysis on the methylome-wide data also identified ‘Proteoglycans in cancer’ and ‘Pathways in cancer’ as significantly enriched ($P \leq 0.001$), appearing within the top 20 KEGG pathways list after acute RE (full list of all enriched pathways across the methylome are described in Supplementary File 4.2B; schematic representation of upregulated/hypomethylated and downregulated/hypermethylated cancer genes are displayed in Figure 4.3). Comparison of the pathway diagrams demonstrated that there was a larger proportion of upregulated versus downregulated genes included in ‘Pathways in Cancer’ and ‘Proteoglycans in cancer’ for the pooled transcriptome analysis (see Supplementary File 4.2C and D, respectively). A larger number of hypomethylated versus hypermethylated CpGs within ‘Pathways in Cancer’ and ‘Proteoglycans in cancer’ were also observed (see Supplementary File 4.2E and F, respectively). Other than ‘pathways in cancer’ and ‘proteoglycans in cancer’, no other top 20 KEGG pathway was enriched in both the pooled transcriptome and methylome analysis (full list of all enriched pathways across the transcriptome and methylome are described in Supplementary File 4.2A and B, respectively). Out of the genes up (69) and downregulated (37) across these ‘cancer’ pathways (full gene list described in Supplementary File 4.2G and H, respectively), these genes were overlapped with those which were hypo- and hypermethylated, respectively across the methylome after acute RE (Seaborne *et al.*, 2018a)

(see Figure 4.3A and B). This analysis identified 23 transcripts that were upregulated in the pooled transcriptome analysis that also demonstrated significant hypomethylation of the same gene following acute RE (see Figure 4.4A; full gene list described in Supplementary 4.2I/J). This related to 29 CpG sites mapping to the 23 transcripts (as some genes had more than 1 CpG site modification per gene) (full gene list with CpG sites described in Supplementary File 4.2J). The genes identified included: MSN, FOS, THBS1, ITPR3, TIMP3, RARA, FLNB, LAMA5, RASSF5, CRK, SMAD3, STAT3, COL4A1, ITGA2, WNT9A, ITGB3, KDR, ADCY3, CTTN, CD63, DOT1L, F2RL3 and GSK3 β (see Figure 4.4A; full gene list described in Supplementary File 4.2I/J). The largest proportion (57%) of the CpG's were located in a promotor region for the same gene (for at least one of their gene transcripts; full gene list with CpG sites described in Supplementary File 4.2J). In SkM, 13 out of 23 genes are associated with matrix/actin structure or remodelling and mechano-transduction (MSN, THBS1, TIMP3, FLNB, LAMA5, CRK, COL4A1, ITGA2, ITGB3, CD63, CTTN, RASSF5, F2RL3), 3 genes associated with TGF- β signalling (SMAD3, FOS, WNT9A), 2 genes with calcium signalling (ITPR3, ADCY3), and 1 gene with IL-6 signalling (STAT3), protein synthesis (GSK3 β) and retinoic acid signalling (RARA). Finally, 12 genes that were downregulated in the comparative transcriptomic analysis were also hypermethylated in (see Figure 4.4B; full gene list described in Supplementary File 4.2K/L). Here, 14 CpG sites were identified in the methylome analysis as some genes had more than 1 CpG site modification (full gene list with CpG sites described in Supplementary File 4.2L). This included genes: RUNX1T1, GAB1, ESR1, LAMA3, NANOG, SMO, ANK3, GADD45G, DROSHA, ATM, APAF1 and AGTR1 (see Figure 4.4B; full gene list described in Supplementary File 4.2K), with varied functions in SkM (see section 4.4). Again, the largest proportion (64%) of the CpG's were also located in a promotor region for the same gene (for at least one of their gene transcripts; full gene list with CpG sites described in Supplementary File 4.2L).

Figure 4.3. ‘Pathways- and proteoglycans in cancer’ were significantly enriched pathways across the human transcriptome and methylome after acute RE

KEGG pathway analysis of the top 20 enriched pathways identified (A) ‘pathways in cancer’ and (B) ‘proteoglycans in cancer’ as significantly enriched across both the pooled transcriptome and the methylome (Seaborne *et al.*, 2018a). For mRNA expression, genes highlighted in ‘GREEN’ represent ‘upregulated’ genes whereas genes highlighted in ‘RED’ represent ‘downregulated’ genes. For DNA methylation, genes highlighted in ‘BLUE’ represent ‘hypomethylated’ genes, genes highlighted in ‘YELLOW’ represent ‘hypermethylated’ genes. Figures were created using Partek Genomics Suite software (version 7.18.0518, Partek Inc. Missouri, USA).

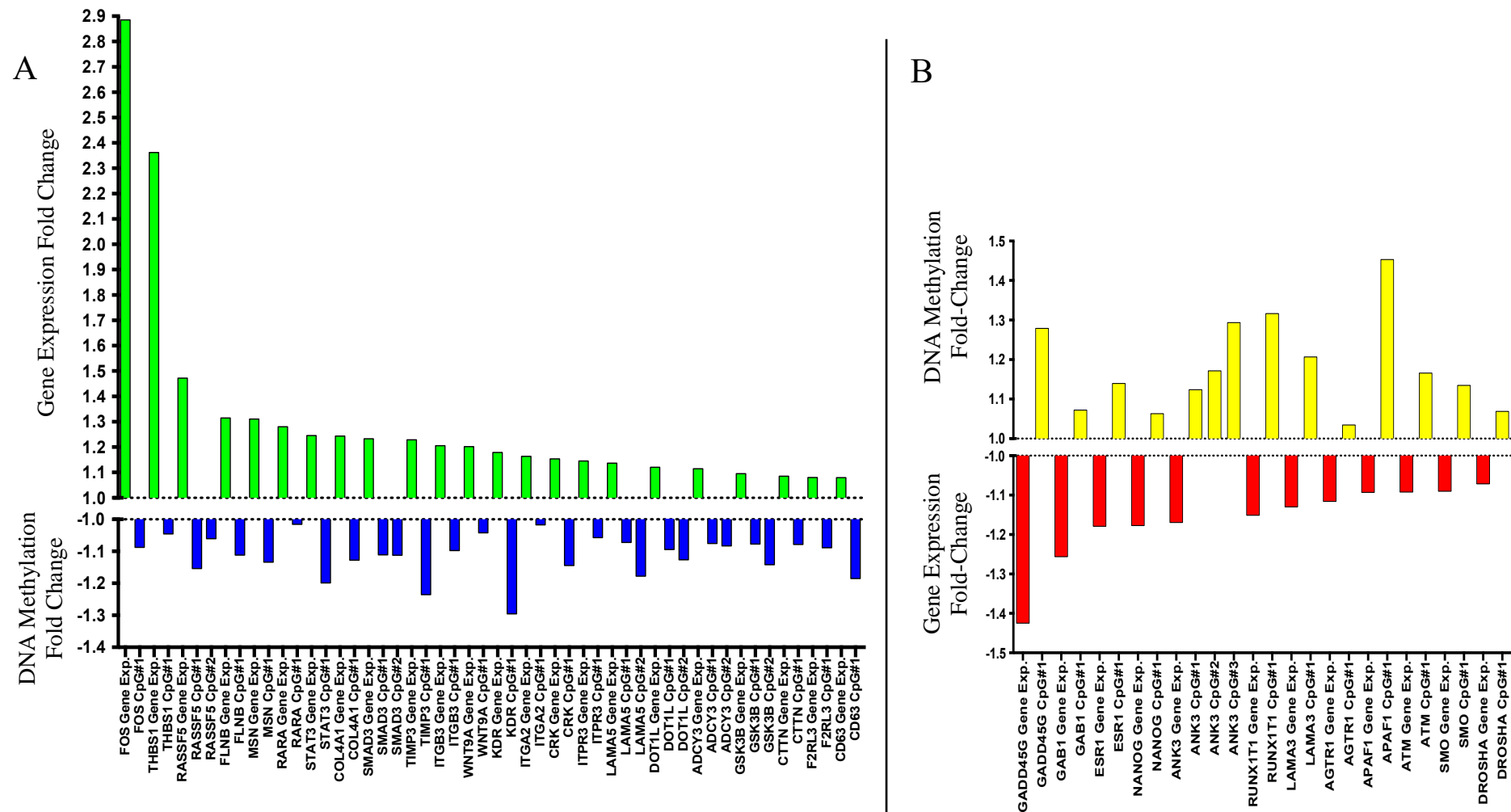


Figure 4.4. Upregulated/hypomethylated and downregulated/hypermethylated enriched in cancer genes after acute RE in humans

(A) Depicts ‘cancer’ pathway genes upregulated (GREEN bars) in pooled transcriptomic studies ($P \leq 0.01$) and hypomethylated (BLUE bars) ($P \leq 0.05$) after acute RE. (B) Depicts ‘cancer’ genes that were downregulated (RED bars) and hypermethylated (YELLOW bars) across the pooled transcriptome and methylome (Seaborne *et al.*, 2018a), respectively after acute RE in humans. Figures were created in Partek Genomics Suite software (version 7.18.0518, Partek Inc. Missouri, USA).

4.4 Discussion

In the present chapter, extensive bioinformatic analysis was undertaken in order to identify genes that were differentially expressed with statistical significance across publicly available transcriptome studies after acute RE in human SkM. Pooled data sets were then overlapped with the DNA methylome data derived from previously published work by our group (Seaborne *et al.*, 2018a) in attempt to identify novel genes/gene pathways that were also epigenetically modified at the DNA methylation level after acute RE *in-vivo*. Transcriptionally and epigenetically modified genes identified herein would therefore enable the detection of suitable genes to analyse after acute mechanical loading in bioengineered SkM throughout subsequent chapters of this thesis. This would further enable the validation of whether acute mechanical loading of bioengineered SkM *in-vitro* induces similar responses to RE *in-vivo*.

Following acute RE, 866 up- and 936 down-regulated genes were identified. Out of the 866 upregulated genes, 270 were also hypomethylated and out of the 936 downregulated genes, 216 were also hypermethylated. After KEGG pathway analysis, genes associated with ‘pathways in cancer’ and ‘proteoglycans in cancer’ were significantly enriched in both the pooled transcriptome analysis and methylome data after acute RE. This resulted in 23 upregulated and 12 downregulated ‘cancer’ genes that were also hypo- and hypermethylated, respectively. The largest proportion of CpG sites on both the upregulated/hypomethylated (57%) and downregulated/hypermethylated (64%) ‘cancer’ genes were promoter associated. DNA methylation, specifically within the promotor region of coding genes, is known to be an important regulator of downstream transcript expression, due to manipulation of RNA polymerase to bind to gene regulatory regions for gene transcription to occur (Bogdanović & Veenstra, 2009). The present chapter therefore identifies an important role for promoter-associated DNA methylation within human SkM after just an acute bout of exercise, supporting previous findings following both acute resistance (Seaborne *et al.*, 2018a) and aerobic (Barrès *et al.*, 2012) exercise in humans.

4.4.1 Enriched Upregulated and Hypomethylated Cancer Genes Involved in ECM/Actin Structure/Remodelling and Mechano-Transduction in Human Skeletal Muscle After Acute Resistance Exercise

Of the 23 upregulated/hypomethylated genes identified across the transcriptome after acute RE, a large proportion (13 out of 23) were associated with ECM/actin structure and remodelling as well as mechano-transduction in SkM.

Actin Structure and Remodelling Genes

Genes that were upregulated/hypomethylated after acute RE that are involved in actin structure and remodelling include; MSN, FLNB and CTTN. MSN (also known as moesin) is part of the ezrin-radixin-moesin (ERM) protein family involved in crosslinking actin filaments with the plasma membrane and has been linked with dystrophy-associated fibrosis in mice and young human muscle via SMAD3/TGF- β signalling (Pines *et al.*, 2017). Furthermore, a recent study reported hypomethylation of moesin in lifelong active aged individuals versus aged sedentary individuals (Sailani *et al.*, 2019), however, no studies have yet investigated mRNA expression or DNA methylation directly in response to exercise. Another actin-plasma membrane crosslinker identified as upregulated and hypomethylated in the present chapter is FLNB (Filamin B). Whilst mutations in Filamin isoforms, A (FLNA) and C (FLNC) are associated with variety of hereditary diseases (i.e. circulatory, CNS and skeletal systems), FLNB mutations are solely associated with skeletal system deformities, suggesting an importance for FLNB in skeletal development (Xu *et al.*, 2017). In SkM, deletion of the FLNB hinge-1 region improved myotube formation in C₂C₁₂ cells, indicative that FLNB is important for myoblast differentiation, although the exact mechanisms remain unknown (Van Der Flier *et al.*, 2002). In addition to FLNB, CTTN (Src substrate cortactin) was also upregulated across the human transcriptome after both acute and chronic RE in recently published work by our group (Turner *et al.*, 2019b). CTTN contributes to the formation of the actin cytoskeleton whereby siRNA

knockdown completely abolishes actin formation and glucose uptake in L6 myotubes (Nazari *et al.*, 2011). Despite upregulation and hypomethylation of both FLNB and CTTN after acute RE in the present chapter, no other studies have directly investigated the roles of these genes in response to exercise or loading in bioengineered muscle.

ECM Structure and Remodelling Genes

Of the upregulated/hypomethylated genes involved in structure/remodelling of the ECM, these include THBS1, TIMP3, ITGA2, ITGB3, LAMA5 and COL4A1. THBS1 (Thrombospondin-1) is a large adhesive glycoprotein that binds to fibrinogen and ECM proteins, fibronectin, laminin, collagen and integrins. In SkM, THBS1 is considered anti-angiogenic whereby chronic (12 days) administration of a THBS1 mimetic (which targets the CD36 THBS1 receptor) in mice resulted in a 20, 11 and 35% decrease in capillarity of the gastrocnemius, plantaris and soleus muscles, respectively (Audet *et al.*, 2013). VEGF protein expression also decreased (140% and 62% in gastrocnemius and soleus, respectively with no change in the plantaris) whereas serum VEGF and endogenous THBS1 remained unchanged, suggestive that alterations were mediated via the CD36 receptor (Audet *et al.*, 2013). Others have reported that THBS1 null mice are protected from high fat diet-induced weight gain (fat and total mass) and insulin resistance (Inoue *et al.*, 2013). In relation to exercise, THBS1 mRNA increased after both acute aerobic exercise (45 mins at 70% VO_{2max}) and chronic concurrent exercise (4 days/week for 12 weeks; 2 × HIIT [1 × 7 min cycling intervals at 85% HR_{max} , 1 × 2 mins intervals at >90% HR_{max}], 2 × RE [3 sets × 8 upper/lower body exercises] sessions) in humans (Hjorth *et al.*, 2015). However, this may be a consequence of the HIIT exercise and not RE given no change in gene expression was observed after acute RE (3 × 12 reps at 70% 1-RM on leg press and extension exercises) alone in young and old human muscle (Wessner *et al.*, 2019). The same acute RE study also reported no significant change in TIMP3 or ITGA2 mRNA expression, albeit ITGB3 expression increased in young but not aged human muscle (Wessner *et al.*, 2019). TIMP3 (tissue inhibitor of metalloproteinase 3) is a member of the TIMP protein family

(TIMP1-4) which regulate MMP activity and matrix homeostasis. TIMP3 mRNA and protein expression has been shown to decrease during C₂C₁₂ myoblast differentiation whereas overexpression inhibits myotube formation via reduced TNF α release, P38 MAPK activity and myogenin mRNA expression (Liu *et al.*, 2010b). Furthermore, TIMP3 expression is reduced in regenerating CTX-injured and overloaded soleus mouse muscle (Liu *et al.*, 2010b) which is interesting given TIMP3 was upregulated across the human transcriptome in the present chapter. ITGA2 (Integrin alpha-2/beta-1) is a major integrin collagen binding transmembrane receptor which mediates cell-ECM adhesion and signalling. ITGA2 has a similar structure to ITGA1, however has opposing actions via activating distinct signalling pathways (Kang *et al.*, 2011). In SkM, high fat feeding-induced insulin resistance was prevented in ITGA2 but not ITGA1 null mice, potentially due to reduced accumulation of collagen and increased vascularisation in KO vs. wild-type rodents (Kang *et al.*, 2011). Furthermore overexpression of ITGA2 in human osteosarcoma cells (Ivaska *et al.*, 1999) and primary human fibroblasts (Langholz *et al.*, 1995) also increased collagen expression when cultured on 3D collagen matrices, highlighting the associated integrin-collagen interaction in various cell types. Similarly, ITGB3 (Integrin subunit beta-3) is a binding receptor for ECM proteins fibronectin and vitronectin and is highly expressed in craniofacial muscle cells, particularly during cell migration but not differentiation (Sinanan *et al.*, 2008). Despite the reported roles of these integrin genes in response to exercise, nutrition and during cell culture, the present chapter demonstrates that ITGA2 and ITGB3 are also regulated at both the mRNA and DNA methylation level after acute RE in humans. LAMA5 (laminin subunit alpha-5) and COL4A1 (Collagen type IV alpha-1 chain) which are isoforms of the laminin and collagen ECM proteins, respectively are a further two ECM structure/remodelling genes identified as upregulated and hypomethylated after RE in the present chapter. The greater abundance of LAMA5 in dystrophic muscle has been demonstrated (Patton *et al.*, 1999), albeit, this may be a consequence of muscle regeneration given its high expression in various types of muscle dystrophies (DMD, LGMD, CMD and EMD) and in regenerating mouse muscle after crush

(Patton *et al.*, 1999) and CTX (Rayagiri *et al.*, 2018) injury. Moreover, LAMA5 was expressed 7 days post-CTX administration in injured but not undamaged muscle and in single EDL mouse myofibres after 72 hrs in culture with little expression at 0 hrs, further suggesting an important role in muscle regeneration (Rayagiri *et al.*, 2018). COL4A1 is a major component of the basement membrane and is increased after acute resistance (10 sets \times 10 reps of quadriceps eccentric-lengthening) and chronic aerobic (6-7 \times 20 s cycling sprints at 170% VO_{2max} , 4 days/week for 6 weeks) exercise (Hyldahl *et al.*, 2015). Furthermore, COL4A1 mRNA was reduced after 14 days of hindlimb unloading in the soleus muscles of young (3 months) Wistar rats which increased after 7 days reloading (Kanazawa *et al.*, 2017). Interestingly however, this trend was not observed in old (20 months) rats suggestive that COL4A1 is important for matrix remodelling after exercise and injury in SkM, albeit aging attenuates the synthesis of collagen during recovery from atrophy (Kanazawa *et al.*, 2017). Despite evidence suggesting a role for these genes in matrix structure and remodelling after exercise and injury, the present chapter is the first to report changes in LAMA5 and COL4A1 DNA methylation patterns after RE which are inverse to expression patterns identified at the mRNA level.

Mechano-Transduction genes

Genes that were upregulated and hypomethylated after acute RE across the human transcriptome are also involved in mechano-transduction. These include genes CRK (also known as proto-oncogene) and CD63 (also known as CD63 antigen). CRK is an adapter protein involved in ERK, JNK and p38 MAPK signalling and has been shown to regulate cell adhesion via activation of FAK in C₂C₁₂ cells (Goel & Dey, 2002). CD63 functions as a cell surface glycoprotein receptor for TIMP1 and is involved in integrin/FAK/Akt signalling. Indeed, knockdown of CD63 (via shRNA) in epithelial MCF10A cells cultured on 3D matrigel matrices reduced cell surface binding of TIMP1 (Jung *et al.*, 2006). Furthermore, researchers have demonstrated increases in CD63 protein expression following acute high-intensity aerobic exercise in rats (Oliveira *et al.*, 2018), although to the authors knowledge, no one has yet

confirmed the effects of CD63 following RE at the transcript and/or epigenetic level. Despite findings demonstrating the importance of these actin/ECM structure/remodelling genes in satellite cell regulation and after aerobic and/or RE at the mRNA and protein level, there is a paucity of data suggesting that such genes are epigenetically modified. The present chapter therefore provides novel mechanistic findings that frequently regulated genes/gene pathways identified across the human transcriptome after acute RE in humans are also differentially methylated and that this occurs via hypomethylation and upregulation of genes associated with structure and remodelling of the matrix and cytoskeleton as well as mechano-transduction in SkM.

Genes, RASSF5 (Ras association domain-containing protein 5 also referred to as RAPL) and F2LR3 (also referred to as Proteinase-activated receptor 4, PAR-4) were 2 out of 23 genes that were upregulated and hypomethylated in the present chapter. RASSF5 is a tumour suppressor gene and despite no known role in SkM, is associated with extension of microtubules in HUVEC cells (Fujita *et al.*, 2005). F2LR3 is part of the G receptor protein family which binds thrombin and trypsin and has been shown to have limited effects on fusion in primary rodent muscle cells (Chinni *et al.*, 1999). However, together with RASSF5, no previous studies have examined the mechano-responses to acute RE at either the transcript or methylation level. DOT1L (disruptor of telomeric silencing-like, also known as Kmt4) was also upregulated and hypomethylated in the present chapter. DOT1L is a methyltransferase which mediates histone 3 lysine-79 (H3K79) methylation and is crucial for embryonic development and muscle function via regulation of dystrophin in mouse cardiomyocytes and C₂C₁₂ muscle cells (Nguyen *et al.*, 2011). In SkM tissue, proteomic analysis revealed that DOT1L was reduced in muscle wasting COPD patients whereas muscle-specific knockdown in human SkM satellite cells increased p21^{WAF1/Cip1} involved in cellular senescence (Lakhdar *et al.*, 2017). The present chapter, together with previous work therefore suggests that DOT1L is important for muscle growth and maintenance and that a reduction may potentially be a contributor to sarcopenia via

decreased and increased dystrophin and p21 expression, respectively. However, its role in ageing SkM warrants future investigation. Such experiments may be achieved via genetic manipulation of DOT1L *in-vivo* to determine whether successful muscle-specific knockdown or overexpression has significant effects on muscle weight and/or fibre size (i.e. CSA) in aged rodent SkM.

4.4.2 Enriched Upregulated and Hypomethylated Cancer Genes Involved in Protein Synthesis and TGF- β , Calcium, Retinoic and IL-6 Signalling in Human Skeletal Muscle After Acute Resistance Exercise

In the present chapter, a further 8 ‘cancer’ genes were significantly upregulated and hypomethylated across the human transcriptome and methylome after acute RE. This included genes associated with protein synthesis (GSK3 β), TGF- β (FOS, SMAD3, WNT9A), calcium (ITPR, ADCY3), IL-6 (STAT3) and retinoic acid (RARA) signalling.

Protein Synthesis

GSK3 β (Glycogen synthase kinase-3 beta) is a downstream target of Akt and once phosphorylated, becomes inactivated and regulates protein synthesis via controlling the activity of eukaryotic initiation factor 2B (eIF2B) (Glass, 2003; Léger *et al.*, 2006). Inhibition of GSK3 β regulates myogenesis during C₂C₁₂ differentiation (Litwiniuk *et al.*, 2016) and recovery from atrophy in mice (Pansters *et al.*, 2015). In humans, GSK3 β protein phosphorylation is significantly increased (~40%) in response to chronic (2 days/week for 4 weeks, 3 days/week for 4 weeks) RE-induced hypertrophy (~10% increase in quadricep CSA) with phosphorylation decreasing by ~30% after 8 weeks detraining-induced atrophy (~5% reduction in CSA) (Léger *et al.*, 2006). Moreover, recent studies have highlighted that basal GSK3 β protein content is greater in lifelong aged physically active versus physically inactive humans, although no difference was observed in promoter-related DNA methylation (Sailani *et al.*, 2019). Furthermore, no studies have yet determined whether GSK3 β is epigenetically modified

directly after exercise in SkM. The present chapter therefore demonstrates for the first time that GSK3 β is regulated at the mRNA and DNA level after acute RE in human SkM.

TGF- β Signalling

TGF- β (transforming growth factor beta) signalling is fundamental for a number of biological processes such as cell growth, differentiation and development and is important in SkM mass regulation and exercise adaptation. To the authors knowledge however, the present chapter is the first to report simultaneous genetic (upregulation) and epigenetic (hypomethylation) regulation of a number of genes involved in TGF- β signalling after acute RE in human SkM. One of the genes is FOS (c-FOS) which has been demonstrated to increase at the mRNA and protein level immediately after 30 mins of running in humans (Puntschart *et al.*, 1999) and after acute RE in rats (Chen *et al.*, 2002) and humans (Trenerry *et al.*, 2007). Despite evidence reporting epigenetic alterations of c-Fos in response to electroconvulsive stimulation in the brain (Dyrvig *et al.*, 2012), there is limited evidence investigating epigenetic changes of FOS in SkM after exercise. Recent evidence suggests the JNK/SMAD (intracellular signal transducer and transcriptional modulator) axis is critical for exercise adaptation. Indeed, increased and suppressed JNK/SMAD activity was associated with increased muscle size after RE and enhanced oxidative/endurance capacity after aerobic exercise, respectively, therefore acting as a molecular switch in response to different modes of exercise (Lessard *et al.*, 2018). Such findings are contradictory to previous research highlighting that SMAD3 (Smad family member 3), is increased after denervation in mice whereas muscle-specific knock-down prevents muscle atrophy (Tando *et al.*, 2016). It is worth noting however that knock-down induced changes were only observed at the protein and not mRNA level. The present chapter therefore demonstrates novel findings that SMAD3 is transcriptionally and epigenetically regulated after acute RE in humans. Finally, WNT9a (Wingless-Type MMTV Integration Site Family, Member 9A) which functions via the canonical Wnt/beta-catenin signalling pathway was also upregulated and hypomethylated in the present chapter. WNT9a is also considered

important in differentiation of SkM satellite cells whereby RNA sequencing and subsequent targeted mRNA expression analysis revealed that WNT9a, together with TGF- β 2 and FGFR4, was key for development of SkM (Zhang *et al.*, 2018). Interestingly, work from the same lab later mapped the transcriptome data derived from their previous work (Zhang *et al.*, 2018) across the methylome of the same mouse samples and demonstrated promoter-associated hypomethylation of WNT9a with corresponding transcriptional upregulation at earlier stages of development (6 weeks), however WNT9a was downregulated and hypermethylated during the later stages (Zhang *et al.*, 2019a). Taken together, previous and current findings highlight the importance of WNT9a during SkM development and RE in humans, further supporting the notion that TGF- β /Wnt signalling is involved in critical muscle-specific biological events.

Calcium, IL-6 and Retinoic Signalling

In the present chapter, calcium signalling-related genes were also upregulated and hypomethylated after acute RE in humans. This included ITPR3 (also known as IP3R - Inositol 1,4,5-trisphosphate receptor type/isoform 3) and ADCY3 (also referred to as adenylylate cyclase 3). ITPR3, present in satellite cells, has been associated with Ca²⁺ release which contributes to increased muscle fibre growth and NMJ stabilisation (Powell *et al.*, 2003). Transcriptomic and proteomic analysis also revealed that ITPR3 was upregulated after acute high intensity exercise in horses (Bryan *et al.*, 2017) and in differentiated muscle but not adipose precursor cells derived from the latissimus dorsi of pigs (Zhang *et al.*, 2019b). The present chapter however is the first demonstrate changes in ITPR3 after exercise in human muscle at both the mRNA and DNA level. Despite the lack of research demonstrating a distinct role for ADCY3 in SkM, adenylylate cyclase's catalyse the production of the signalling molecule cAMP via G-protein signalling which regulate Ca²⁺-dependent insulin secretion in HEK cells (Ding *et al.*, 2004). Furthermore, DNA methylation is altered in adipose tissue following chronic high fat feeding in mice (Li *et al.*, 2018). However, there is currently a paucity of data surrounding the role of ADCY3 in SkM. STAT3 (also known as signal transducer and activator of transcription factor

3) is downstream of both IL-6 and TGF- β and has been examined in response to load-induced hypertrophy and muscle dystrophies (recently reviewed in Guadagnin *et al.*, 2018). Indeed, research has shown increased STAT3 phosphorylation after an acute bout of RE in Wistar rats (Begue *et al.*, 2013), albeit, recent evidence has shown that STAT3 phosphorylation is not altered after acute RE in humans and is not required for overload-mediated hypertrophy in rodent SkM (Pérez-schindler *et al.*, 2017). IL-6 has been shown to promote DNA methylation of STAT3 in human colon cancer cells (Yang *et al.*, 2010). However, to the authors knowledge, the present chapter is the first to report epigenetic changes in the IL-6/STAT3 signalling pathway in SkM. Finally, the nuclear receptor RARA (Retinoic acid receptor alpha) has been shown to modulate human myoblast differentiation (El Haddad *et al.*, 2017). Indeed, RARA treated cells displayed reduced myogenic regulatory factor expression and myotube formation whereas enhanced differentiation was observed after knock-down (El Haddad *et al.*, 2017). To the authors knowledge, there is no previous evidence to suggest that any of these calcium/IL-6/retinoic acid signalling genes are differentially methylated in SkM following acute RE and the present chapter therefore suggests a potential role for DNA methylation in modulating the acute transcriptional response after RE in humans.

4.4.3 Enriched Downregulated and Hypermethylated Cancer Genes Identified in Human Skeletal Muscle After Acute Resistance Exercise

Of the 35 regulated ‘cancer’ across the human transcriptome, the present chapter demonstrates that 12 of these genes were downregulated and hypermethylated. These included genes, GADD45G, ATM, APAF1, RUNX1T1, GAB1, LAMA3, NANOG, SMO, ANK3, DROSHA, AGTR1 and ESR1 which have several opposing functions within SkM, although with the exception of those relating to apoptosis (GADD45G, ATM, APAF1), are not inter-linked. RUNX1T1 (Partner Transcriptional Co-Repressor 1) encodes corepressor proteins which suppress gene transcription in myeloid cells, although its role in SkM remains elusive. GAB1 (GRB2 Associated Binding Protein 1) is part of the IRS-1 protein family and is involved in cell

growth and muscle development. Indeed, c-Met dependant GAB1 signalling is crucial for muscle development whereby forelimb and diaphragm muscle formation is completely ablated in GAB1 deficient mice (Sachs *et al.*, 2000). As with LAMA5 (described in section 4.4.1), LAMA3 (laminin subunit alpha-3) is a major structural basement membrane protein. However, in SkM, researchers reported no change in LAMA3 mRNA during satellite cell regeneration in rodents after CTX injury (Rayagiri *et al.*, 2018) or acute RE in young and aged humans (Wessner *et al.*, 2019). Such findings are confounding given LAMA3 was significantly downregulated and hypermethylated after acute RE in the present chapter. NANOG (Nanog Homeobox) is important in cell proliferation and self-renewal and maintains pluripotency of embryonic stem cells. Interestingly, recent evidence demonstrates the importance of NANOG in muscle/satellite cell differentiation whereby overexpression in collagen 1 bioengineered SkM improved myogenic potential in highly passaged (>40 passages) C₂C₁₂ cells which displayed reduced myotube formation and suppressed MRF (myoD, myog, MRF4, myf5, mef2a/c) mRNA expression in untreated cells (Shahini *et al.*, 2018). Despite research reporting methylation changes in testicular tumour cell line (Nettersheim *et al.*, 2011) and primary epithelial (Zhou *et al.*, 2017) cells, the present chapter is the first to demonstrate epigenetic regulation of NANOG in SkM which coincided with alterations at the mRNA level after acute RE. SMO (Smoothed, Frizzled Class Receptor) is G-protein receptor involved in signal transduction. SMO, downstream of the sonic hedgehog protein complex, is expressed in chick pectoralis muscle during maturation and during proliferation and differentiation in C2 cell line cells suggesting a role in muscle development and myotube formation (Elia *et al.*, 2007). Others have also shown that downregulation of SMO in colon cancer cell lines is associated with increased promoter methylation (Zhu *et al.*, 2004), however, no studies have reported such findings in SkM. ANK3 (Akyrin 3) is a membrane-actin cytoskeleton crosslinker protein and is expressed in SkM (Peters *et al.*, 1995), associated with muscle development and myopathies (reviewed in Tee and Peppelenbosch, 2010). To the authors knowledge however, the present chapter presents, for the first time, simultaneous mRNA and DNA methylation changes in

human muscle after exercise. DROSHA (also known as Drosha Ribonuclease III) catalyses the initial stages of miRNA biogenesis (Lee *et al.*, 2003) and has been shown to increase (35%) at the mRNA level 3 hrs post-acute aerobic exercise (60 mins cycling at $\sim 70\%$ VO_{2peak}) in young males (Russell *et al.*, 2013). Interestingly however, DROSHA was downregulated and hypermethylated after RE in the present chapter, suggestive that regulation of this gene may be dependent on the mode of exercise performed. Furthermore, there is currently no evidence to suggest that changes at the mRNA level may be somewhat attributable to changes at the DNA level. AGTR1 (angiotensin II receptor type I) is part of the G protein receptor family and has been shown to be mechano-responsive in different cells. Indeed, mechanical loading increased AGTR1 in HEK cells (Yasuda *et al.*, 2008) and cardiomyocytes, alongside cardiac tissue (Zou *et al.*, 2004). Interestingly however, AGTR1 mRNA expression was reduced in the present chapter after acute RE in human SkM. Furthermore, muscle specific knock-down in rodent SkM prolonged life span and improved repair and regeneration of the TA muscles after cryoinjury (Yabumoto *et al.*, 2015), suggestive that AGTR1 may have pleiotropic effects which are tissue-specific. In regards to DNA methylation, researchers have reported increased promoter-associated DNA methylation in lung tumour vs. non-tumour tissue (Chen *et al.*, 2017), however the present chapter is the first to report AGTR1 hypermethylation patterns in human SkM, specifically after RE. PAX3 (paired box 3), together with PAX7 is highly expressed in quiescent and activated SkM progenitor cells which drives them to the myogenic lineage (Relaix *et al.*, 2005). PAX3 is therefore crucial for myogenesis whereby expression activates the key MRF, myoD (Relaix *et al.*, 2006). Studies have also demonstrated DNA hypermethylation in human rhabdomyosarcoma muscle tissue (Kurmasheva *et al.*, 2005) and myoblasts (Tsumagari *et al.*, 2013). To the authors knowledge however, the present chapter is the first to report hypermethylation of PAX3 in SkM, specifically after RE. Finally, ESR1 (estrogen receptor 1) was downregulated and hypermethylated in the present analysis, where others have demonstrated muscle weakness in ESR1 mutant female mice (Collins *et al.*, 2018), yet, overexpression has been shown induce a shift in muscle fibre type to a slow muscle fibre

phenotype (Chen *et al.*, 2016). Therefore, a reduction observed in adult male humans in the present chapter may therefore be associated with reduced slow fibre formation and subsequently may be conducive to faster fibre formation, previously identified to occur after RE. The associated hypermethylation and downregulation of ESR1 and its role in fibre type transition however warrants further investigation. Such experiments may be achieved via subjecting ESR1 mutant and overexpressed rodents to resistance (i.e. chronic high-frequency [100 Hz] electrical stimulation or mechanical overload/synergistic ablation to induce a fast muscle fibre type transition) and/or endurance (i.e. chronic low-frequency electrical stimulation [10 Hz] or wheel running to induce a slow muscle fibre type transition) exercise followed by the assessment of muscle function/force *ex-vivo*, fibre type (using histological techniques) and ESR1 DNA methylation (via tNGBS or pyrosequencing). This would enable the characterisation of ESR1 mRNA expression and DNA methylation on muscle fibre type transition in response to different modes of exercise.

4.5 Limitations

It is worth noting a key limitation of the acute RE analysis performed in the present chapter. Specifically, the post-acute RE samples pooled for transcriptomic analysis included samples taken immediately post and ~24 hrs post whereas the samples derived from the methylome data were collected just 30 minutes post RE (Seaborne *et al.*, 2018a, 2018b). This was due to very few transcriptomic studies sampling at the same timepoint and therefore pooling all post-RE datasets across studies up to 24 hrs post enabled an adequate sample number. Furthermore, recent work by our group demonstrated that DNA methylation changes observed just 30 mins post-acute RE in humans correlate with changes in mRNA expression after acute RE and even after chronic training and retraining (Seaborne *et al.*, 2018a, 2018b). However, a time-course that includes multiple timepoints at both the transcriptomic and methylome level is required to directly investigate the temporal relationship between DNA methylation and gene expression after acute RE.

4.6 Conclusion

The present chapter provides novel mechanistic findings that differentially expressed genes identified across the human transcriptome are also epigenetically altered at the DNA methylation level after acute RE in human SkM. Specifically, mRNA expression and DNA methylation of genes enriched in ‘cancer’ pathways were significantly modified across the human transcriptome and DNA methylome after acute RE in humans. These genes are known to have specific roles in SkM including ECM/actin structure and remodelling, TGF- β /calcium/IL-6/retinoic acid signalling as well as mechano-transduction. As described in section 4.5, future studies should assess transcriptome-wide gene expression and DNA methylation across multiple timepoints to directly investigate their temporal relationship in response to acute RE in human SkM. Furthermore, the present analysis was performed in young male humans only and future experiments should aim to investigate the differential transcriptional and epigenetic responses to exercise in young female and aged female/male humans to expand our current knowledge of the molecular mechanisms of exercise-induced SkM adaptation across wider populations. Finally, performing integrative transcriptomic/methylomic and proteomic analysis in SkM following RE would also enable the detection of whether such acute changes at the transcript and DNA methylation level correspond to functional changes at the protein and whole tissue (i.e. muscle/fibre size) level. Despite such possible questions arising from the present chapter, the data reported herein provides a detailed account of which genes to assess in regards to mRNA expression and DNA methylation after mechanical loading in fibrin bioengineered SkM (chapter 5) using the TC-3 bioreactor which was characterised in chapter 3. Analysis of mRNA expression and DNA methylation in fibrin muscle will enable the validation of whether loading bioengineered SkM *in-vitro* mimics the transcriptional and epigenetic response to RE/loading in human SkM *in-vivo*.

CHAPTER 5

**The Transcriptional and Epigenetic Regulation of
Murine Fibrin Bioengineered Skeletal Muscle in
Response to Mechanical Loading**

5.1 Introduction

Skeletal muscle (SkM) is a highly abundant (constituting approximately ~40% of overall body mass; Janssen *et al.*, 2000) and malleable tissue, displaying functional and morphological changes in the presence or absence of mechanical loading. Indeed, muscle size and strength are enhanced in response to resistance exercise (RE)/mechanical loading (Goldberg, 1967; Baar & Esser, 1999; Seaborne *et al.*, 2018a) whereas SkM mass and function are somewhat compromised during periods of unloading, such as that during aging (Hughes *et al.*, 2001; Morse *et al.*, 2005), spaceflight (Edgerton *et al.*, 1995) and bed rest (Dirks *et al.*, 2016).

Despite the well-established role of transcriptional activity during load-induced SkM hypertrophy (Goldberg & Goodman, 1969), the importance of epigenetics, specifically DNA methylation, has only more recently begun to emerge (Sharples & Seaborne, 2019). As described in section 4.1, DNA methylation is a key epigenetic modification and is characterised by the addition (hypermethylation) or removal (hypomethylation) of covalent methyl groups located within cytosine nucleotide bases of cytosine-guanidine base pairing (CpG) sites. The presence or absence of these methyl tags, specifically within the promotor or enhancer regions of coding genes, is able to permit (via hypomethylation) or prevent (via hypermethylation) gene transcription, ultimately controlling the level of gene expression (described in Sharples, Stewart and Seaborne, 2016; Sharples and Seaborne, 2019).

Recently published work by our group investigated differential genome-wide (850K CpG sites) DNA methylation responses after acute and chronic RE in untrained humans, followed by several weeks of unloading and reloading (Seaborne *et al.*, 2018a). Interestingly, a number of genes were epigenetically altered after just one single bout of RE, displaying significant hypomethylation which preceded increases in gene expression after chronic loading and reloading (Seaborne *et al.*, 2018a). As described in chapter 4 of this thesis, the methylome array data (Seaborne *et al.*, 2018a) was then mapped against publicly available transcriptomic data

files derived from the acute human RE studies to date (April 2018), in order to determine whether frequently regulated genes across the human transcriptome after acute RE were also epigenetically modified at the DNA level. Interestingly, a number of genes enriched in cancer pathways (i.e. ‘pathways in cancer’ and ‘proteoglycans in cancer’) were either upregulated/hypomethylated (23 genes) or downregulated/hypermethylated (12 genes), supporting the notion that a single bout of exercise alone is able to induce inversely associated transcriptional and epigenetic changes in SkM.

As discussed in section 3.1.1, rodent models such as functional overload/synergistic ablation have been extensively used for studying the molecular mechanisms underpinning the anabolic/hypertrophic response to mechanical loading *in-vivo* (Goldberg, 1967; Bodine *et al.*, 2001a; Goodman *et al.*, 2011). However, a recent model developed by our group using electrical peroneal and tibial nerve stimulation to enable co-contraction of the plantar- and dorsi-flexor hindlimb muscles, respectively has been shown to induce significant increases in rodent SkM mass. Indeed, high frequency (100 Hz) intermittent stimulation of the plantar-flexors which places considerable load on the dorsi-flexor muscles evoked a 14% and 19% increase in TA SkM mass and fibre CSA, respectively after 4 weeks of stimulation (Schmoll *et al.*, 2018; Seaborne *et al.*, 2019). This method (termed ‘SpillOver’ stimulation) therefore provides a useful novel *in-vivo* rodent model for studying the molecular responses to RE.

The molecular responses following mechanical loading in bioengineered SkM are typically determined via assessing the mRNA (Player *et al.*, 2014) and more recently, protein phosphorylation (Aguilar-Agon *et al.*, 2019) of well-characterised mechano-sensitive genes/proteins. However, there is limited data that has used such isolated *in-vitro* models to assist in characterising the activity of potential novel mechano-responsive genes. Indeed, recent work by our group mechanically loaded murine fibrin bioengineered SkM (the same model used throughout this thesis) to investigate the response of the E3 ubiquitin ligase, UBR5,

following acute anabolic stimuli (Seaborne *et al.*, 2019). Interestingly, UBR5 mRNA expression increased to a similar extent following acute RE/loading in human (~1.7-fold) and bioengineered (~1.6-fold) SkM, with no change in DNA methylation observed in either model of loading/RE (Seaborne *et al.*, 2018a, 2019). With the exception of this previous work, there has previously been no attempt to study the epigenetic responses to loading in bioengineered SkM. Indeed, if loading of fibrin C₂C₁₂ bioengineered SkM resembles the transcriptional and epigenetic responses to loading of SkM *in-vivo*, this system would provide a representative *in-vitro* model for studying the underlying mechanisms underpinning load-induced anabolism and hypertrophy.

5.1.1 Aims and Objectives

The aims of the present chapter were therefore: To determine whether transcriptional and epigenetic responses in loaded C₂C₁₂ bioengineered muscle *in-vitro* (using the INT loading regime and the TC-3 bioreactor characterised in chapter 3) mimics those identified in chapter 4, as well as changes observed previously after RE in humans (Seaborne *et al.*, 2018a, 2018b), and after chronic stimulation/RE in rodents *in-vivo* (Schmoll *et al.*, 2018; Seaborne *et al.*, 2019). This will help validate or invalidate whether mechanical loading of C₂C₁₂ bioengineered muscle is a representative *in-vitro* model of loading/RE *in-vivo*.

Given that mRNA and DNA methylation is altered after just a single bout of resistance (described in chapter 4 of this thesis and Seaborne *et al.*, 2018a) and endurance (Barrès *et al.*, 2012) exercise *in-vivo*, it was hypothesised that acute mechanical loading of fibrin bioengineered SkM may also evoke transcriptional and epigenetic changes at the mRNA and DNA level, respectively of regulated genes across the human transcriptome and methylome and that these would mimic the responses identified after loading/RE in human and rodent SkM *in-vivo*.

5.2 Methods

5.2.1 Cell Culture

C₂C₁₂ cells were expanded in T75 culture flasks as described in sections 2.2.1 and 2.2.3. Once 80% confluency was attained, cells were trypsinised (see section 2.2.3) and counted (see section 2.2.4) for subsequent fabrication of SkM constructs (see section 5.2.2). All cells throughout this chapter were used at passage 10 (P10).

5.2.2 Fabrication of Fibrin Skeletal Muscle Constructs

Preparation of fibrin SkM constructs is described in section 2.4 and in previously published work by our group (Seaborne *et al.*, 2019; Turner *et al.*, 2019a). C₂C₁₂ cells were then seeded onto the pre-polymerised fibrin matrix at a density of 9×10^4 cells/ml in 2 ml GM (see section 2.2.4). GM was changed every 48 hrs until the ~90% confluency was attained after which fibrin gels were washed 2 × in PBS before switching to DM for 48 hrs to initiate differentiation. DM was then replaced with MM for a further 10 days (see Figure 2.5) at which point, gels were fixed (see section 2.7.3) or removed from the sylgard culture dishes to undergo mechanical loading (see section 5.2.3).

5.2.3 Mechanical Loading of Fibrin Skeletal Muscle Constructs

After a total of 14 days in culture, fibrin gels were transferred from the culture dishes to the TC-3 bioreactor chambers (see section 2.5) and were clamped into position (12 mm resting length) before filling each chamber with 20 ml of MM (see Figure 5.1A). The chambers containing the engineered muscle were then assembled to the mechanical stimulation unit, placed in a humidified incubator at 37°C, 5% CO₂, ready to undergo mechanical loading (see Figure 5.1B). Constructs acting as controls (CON) were kept at resting length for 1 hr whereas loaded constructs were subject to intermittent loading (INT) as described in section 3.2.3. Briefly, the INT regime consisted of 4 sets × 10 repetitions (frequency of 0.3 Hz, 0.4 mm/s) at

10% stretch, representing 1 of 5 ‘exercises’. Each set of 10 repetitions was interspersed with a 1.5 min rest and each exercise was separated with 3.5 mins rest whereby constructs were kept at resting length.

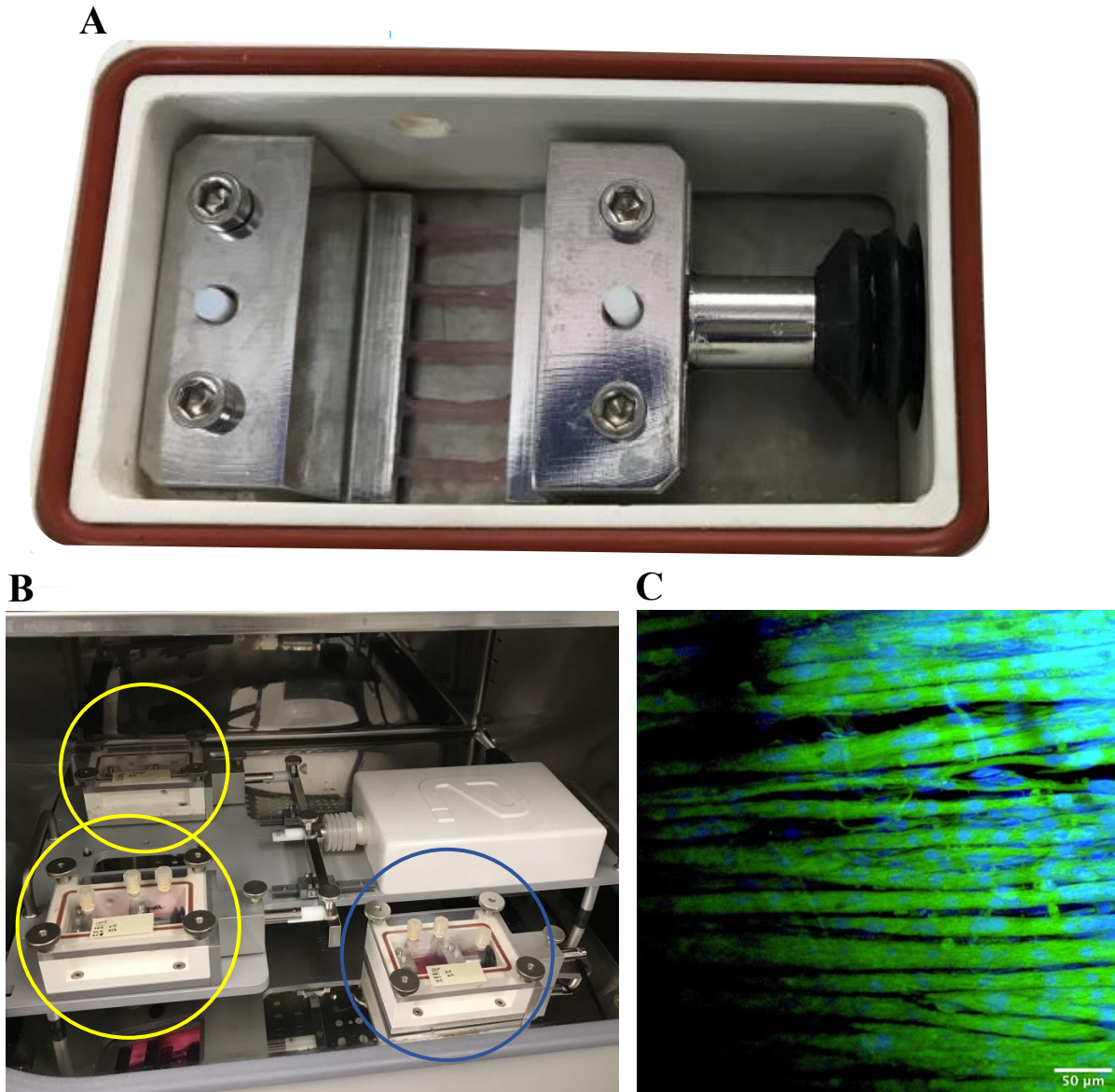


Figure 5.1. Mechanical loading and immunostaining of fibrin bioengineered SkM

(A) C₂C₁₂ fibrin constructs ($n = 5$ replicate cultures per time point) were clamped within the bioreactor chambers to (B) undergo mechanical loading whilst incubating at 37°C/5% (yellow and blue circled chambers represent those within INT and CON conditions, respectively). (C) C₂C₁₂ bioengineered fibrin muscle constructs were immuno-stained for f-actin (phalloidin-FITC, green) and myonuclei (DAPI, blue) and imaged using confocal microscopy (Olympus IX83, Japan; 20×, scale bar = 50 µm; taken from Seaborne *et al.*, 2019).

5.2.4 Chronic High-Frequency Electrical Stimulation in Rats

In order to compare the loading response in fibrin engineered muscle with the responses to RE in rodent SkM, adult (6 months) male Wistar rats were subject to high frequency (100 Hz) electrical stimulation as previously described in published work by our group (Schmoll *et al.*, 2018; Seaborne *et al.*, 2019). Briefly, rodents were equipped with an implantable stimulator connected to electrodes placed near the common peroneal and tibial nerves. Dorsiflexor muscles were then loaded via resisting against the plantarflexors during the electrical stimulation protocol. Dorsiflexor and plantar-flexor muscles were intermittently stimulated once a day for 4 weeks (5 sets \times 10 reps, each rep lasted 2 s with a 2 s rest between reps and 2.5 mins rest between sets), evoking a 14% and 19% increase in TA SkM weight and fibre CSA, respectively (Schmoll *et al.*, 2018). Following cessation of electrical stimulation, RNA was isolated from the TA muscle of the stimulated and contralateral unstimulated (control) limbs ($n = 5$) using the TRIzol method as described in section 2.8. Experimental procedures were conducted according to permissions within a project license granted under the British Home Office Animals (Scientific Procedures) Act 1986.

5.2.5 Acute and Chronic Resistance Exercise in Humans

In order to compare the genetic and epigenetic responses to loading in bioengineered SkM with those following RE in humans, 8 healthy young (27.6 ± 2.4 yrs) males were subjected to both acute and chronic RE as described in previously published work by our group (Seaborne *et al.*, 2018a, 2018b). Briefly, following a week of familiarisation, untrained male participants performed an acute bout of RE consisting of several lower body exercises (4 sets \times 10 reps, ~ 90 – 120 s rest between sets and ~ 3 mins rest between exercises). This was repeated 3 times per week for a total of 7 weeks (chronic RE), evoking a 6.5% ($\pm 1\%$) increase in lower limb lean mass as determined via dual-energy x-ray absorptiometry (DEXA) scanning technology.

RNA was isolated using the TRIzol method as described in section 2.8 and in the original published work (Seaborne *et al.*, 2018a, 2018b). Ethical approval was granted by the NHS West Midlands Black Country, UK, Research Ethics Committee (NREC approval no. 16/WM/0103).

5.2.6 Immunohistochemistry (IHC)

SkM constructs were fixed in methanol:acetone as described in section 2.7.2. Following fixation, fibrin gels were removed from the culture dishes and transferred to 2 ml Eppendorf tubes ready for immunostaining (see section 2.7.3) for f-actin (phalloidin-FITC, green) and myonuclei (DAPI, blue) as described in section 2.7.3. Immunostained gels were then visualised using a confocal fluorescence microscope (Olympus IX83, Japan) and imaged using supporting software (FV10-ASW 4.2, Olympus, Japan) as described in section 2.7.4 to illustrate the alignment of mature myotubes in the direction of uniaxial tension (see Figure 5.1C).

5.2.7 RNA Extraction and Quantitative Real-Time Polymerase Chain Reaction (qRT-PCR)

Following cessation of mechanical loading, engineered muscles ($n = 5$ replicate cultures per time point) were removed from the bioreactor chambers at 30 mins, 3 hrs and 24 hrs post-loading. SkM constructs used for assessing mRNA expression of genes identified in chapter 4 were lysed in 600 μ l of Buffer RLT containing 6 μ l β -Mercaptoethanol (β -ME) as described in section 2.8 ready for RNA isolation using the AllPrep RNA/DNA Mini Kit (see section 2.9.1). Bioengineered muscles analysed for transcript expression of genes identified after 30 mins post-acute RE in previously published work by our group (Seaborne *et al.*, 2018a) were dissected down the middle to ensure two separate parts. One part was then placed in 1 ml TRIzol (see section 2.8) for subsequent RNA extraction (see section 2.9.2). RNA concentrations and purities were assessed using a Nanodrop (see section 2.9.3) which were greater following isolations using the AllPrep Mini Kit ($4.1 \pm 2.42 \mu\text{g conc.}$; $2.05 \pm 0.03_{\text{A260/A280}}$) versus the

traditional TRIzol method ($1.92 \pm 0.65 \mu\text{g}$ concentration; $1.88 \pm 0.12_{A260/A280}$). Once isolated, samples were diluted in Nuclease-free H₂O to ensure a concentration of 35 ng in 4.75 μl (7.37 ng/ μl) which was added to 5.25 μl of master mix composed of 5 μl SYBR green, 0.1 ml of reverse transcriptase (RT) mix and 0.075 μl of both forward and reverse primers in PCR reaction tubes (0.1 ml strips and caps, Qiagen, UK). All primer sequences and locations for the genes analysed in bioengineered, rat and human SkM are described in Tables 5.1-5.5 in the thesis appendices. After preparation, reaction tubes were transferred to a PCR thermal cycler to undergo amplification (see section 2.9.4.2). All gene expression was relativized using the DDCT ($\Delta\Delta C_T$) method as described in section 2.9.4.3 (Schmittgen & Livak, 2008). For bioengineered SkM, the pooled C_T values from the non-loaded controls (CON) at each individual time point (30 mins, 3 hrs and 24 hrs) were used as the calibrator condition and were relativised to the mean C_T value of the reference gene, RP-II β (18.64 ± 0.74 , with a low 3.97% variation). For rat SkM, the contralateral non-stimulated limb for each animal and the mean reference gene (Pol2ra) C_T value across all rodents (24.12 ± 0.67 with low 2.78% variation) was used for the $\Delta\Delta C_T$ equation. For human SkM, gene expression was also quantified using the $\Delta\Delta C_T$ equation which included each individuals baseline (pre RE) C_T value and mean C_T value for reference gene, RPL13a across all participants (20.48 ± 0.64 , with low variation 3.17%). PCR efficiencies across all species were similar for reference genes (bioengineered = $92.24 \pm 5.43\%$, with 5.88% variation; rodent = $94.5 \pm 4.27\%$ with 4.52% variation) and genes of interest (bioengineered = $93.64 \pm 5.91\%$ with low variation 6.31%; rodent = $93 \pm 4.92\%$, with 5.29% variation).

5.2.8 DNA Isolation, Bisulfite Conversion and Targeted DNA Methylation

Samples were lysed in 600 μl of Buffer RLT containing 6 μl β -ME if DNA was extracted using the AllPrep RNA/DNA Mini Kit (see section 2.10.1), specifically when analysing the DNA methylation of genes identified in chapter 4. Remaining dissected tissue was lysed (see section 2.8) and purified (see section 2.10.2) using a DNeasy spin column kit for samples used to assess

the DNA methylation status of genes previously described in published work by our group (Seaborne *et al.*, 2018a). As with RNA, DNA concentrations and purities were assessed using a Nanodrop (see section 2.9.3). However, concentrations and A260/A280 ratios were similar between AllPrep Mini (2.68 ± 1.95 $\mu\text{g conc.}$; $1.89 \pm 0.06_{\text{A260/A280}}$) and DNeasy (2.46 ± 0.8 $\mu\text{g conc.}$; $1.78 \pm 0.1_{\text{A260/A280}}$) spin column kits. Stock DNA was diluted in Nuclease-free dH₂O to ensure 500 ng at a concentration of 20 ng/ μl ready for bisulfite conversion using the EZ-96 DNA Methylation Kit (Zymo Research Corp., USA) as described in section 2.10.4. Bisulfite converted DNA was then analysed for DNA methylation using targeted next generation bisulfite sequencing (tNGBS, as described in section 2.10.6) or loci-specific pyrosequencing (as described in section 2.10.5). Specifically, tNGBS assays were designed to target numerous regulatory regions of mouse genes; MSN, TIMP3, WNT9a, CTTN, GSK3 β , PAX3, AGTR1a and UBR5 3 hrs post-loading and genes; BICC1, GRIK2, TRAF1, STAG1, ODF2 and UBR5 30 mins post-loading (see section 2.10.6). Furthermore, additional pyrosequencing was undertaken to assess the methylation status of 6 \times CpG sites in the intron 1 region of the mouse UBR5 gene (see section 2.10.5).

5.2.9 Statistical Analysis

A multivariate analysis of variance (MANOVA) was conducted using a statistical package for the social sciences software (SPSS[®], version 24.0, Chicago) to determine main effects for groups of genes between conditions (CON vs. INT), across time (30 mins, 3 and 24 hrs). A two-way mixed ANOVA (2×3) was performed using Minitab[®] software (Version 18, USA) to detect statistical significant interactions for condition and time. Post-hoc analysis (Fisher LSD) was carried out to confirm statistical significance between condition (CON vs. INT) and within time (30 mins vs. 3 hrs vs. 24 hrs), respectively whenever significant interactions were observed. A one-way ANOVA was conducted to detect differences in mRNA expression between models of loading/RE (RE/loading in bioengineered and human SkM, and chronic RE/electrical stimulation in humans/rats). When comparing expression of genes previously

identified in across models of loading, follow up post-hoc analyses (with Tukey HSD correction) enabled detection of where main effects occurred. However, unpaired *t*-tests were conducted to determine where main effects for occurred for regulated genes identified in chapter 4. This was because the mean expression value across all transcriptomic studies analysed in chapter 4 was obtained and not mean expression values for each individual study employed. Therefore, a post-hoc analysis could not be performed to compare individual models of loading. Finally, unpaired *t*-tests were carried out to determine mRNA expression between conditions (CON vs. INT) at 30 mins post-loading in fibrin bioengineered SkM alone for previously identified genes (Seaborne *et al.*, 2018a) and also for CpG DNA methylation at 30 mins (UBR5, ODF2, BICC1, GRIK2, STAG1, TRAF1) and 3 hrs (UBR5, MSN, WNT9a, GSK3 β , CTTN, TIMP3) post-loading in bioengineered SkM. The alpha value of significance was set at $P \leq 0.05$. All data is presented as the mean \pm standard error of mean (SEM).

5.3 Results

5.3.1 mRNA Expression of Genes that are Upregulated/Hypomethylated After Resistance Exercise in Human Skeletal Muscle were Assessed After Loading in Bioengineered Muscle

In the present chapter, mRNA expression of genes which were upregulated and hypomethylated across the human transcriptome and methylome in chapter 4 were investigated at 30 mins, 3 and 24 hrs post-acute mechanical loading in bioengineered SkM. Specifically, genes involved in ECM/actin structure and remodelling (MSN, CTTN, FLNB, TIMP3, ITGB3, LAMA5, COL4A1, THBS1), mechano-transduction (CRK, CD63), protein synthesis (GSK3 β) and TGF- β (FOS, SMAD3, WNT9A), calcium (ITPR, ADCY3), IL-6 (STAT3) and retinoic acid (RARA) signalling were analysed. Collective mRNA expression of all upregulated/hypomethylated genes assessed after loading in bioengineered SkM is presented in Figure 5.2.

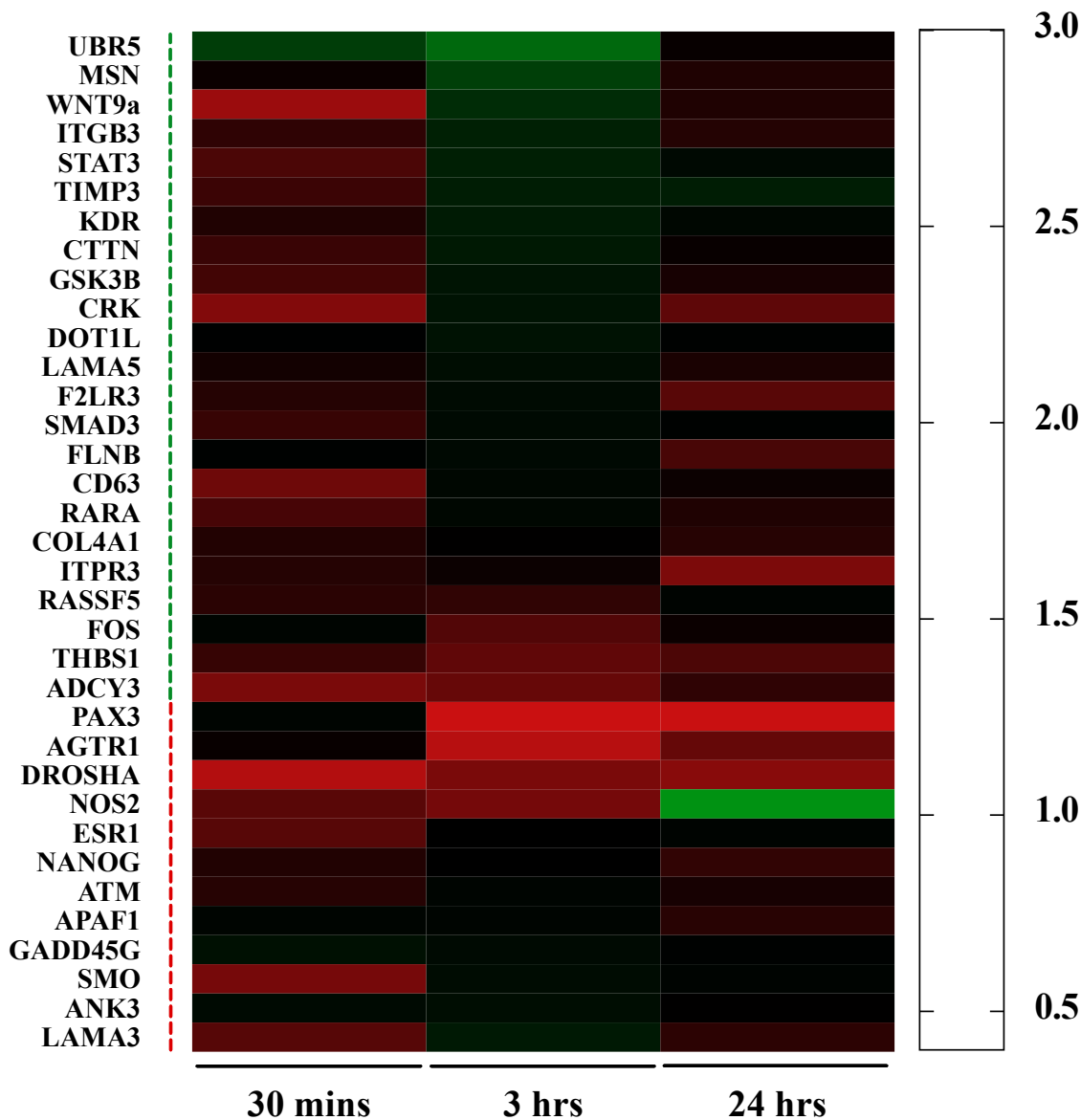


Figure 5.2. Heat map representation of temporal change in mRNA expression after mechanical loading in bioengineered SkM

mRNA expression of upregulated/hypomethylated (green dotted line indicated on the left y-axis) and downregulated/hypermethylated (red dotted line indicated on the left y-axis) genes identified in chapter 4, however, following mechanical loading in bioengineered SkM ($n = 5$ replicate cultures/muscles per condition [CON and INT) and time point [30 mins, 3 and 24 hrs]). Transcript expression was assessed at 30 mins, 3 hrs and 24 hrs post-loading (as indicated on the x-axis) and fold-change was determined via relativising mRNA expression in loaded (INT) versus non-loaded (CON) fibrin muscle for each separate timepoint (30 mins, 3 hrs or 24 hrs). The colour density represents the level of fold-change in mRNA expression (as indicated

on the right y-axis). Upregulated/hypomethylated genes identified in chapter 4 were graphed in order of the greatest (i.e. UBR5) to lowest (i.e. ADCY3) increase in mRNA expression at 3 hrs post-loading. Conversely, downregulated/hypermethylated genes identified in chapter 4 were graphed in order of the greatest (i.e. PAX3) to lowest (i.e. LAMA3) reduction in mRNA expression at 3 hrs post-loading in bioengineered SkM.

Actin Structure and Remodelling Genes

There was a significant main effect for loading ($F_{1,23} = 6.62$, $P = 0.02$) and time ($F_{2,23} = 15.83$, $P < 0.001$) on MSN transcript expression with a significant interaction ($F_{2,23} = 12.82$, $P < 0.001$). Expression was significantly increased at 3 hrs (1.43 ± 0.15) relative to 30 mins (0.99 ± 0.04 , $t = -4.62$, 95% CI -0.64 to -0.24, $P < 0.001$) and 24 hrs (0.96 ± 0.04 , $t = -5.05$, 95% CI -0.66 to -0.28, $P < 0.001$) with no difference between 30 mins and 24 hrs ($t = 0.28$, 95% CI -0.17 to 0.22, $P = 0.79$). Transcript expression was significantly greater after INT vs. CON at 3 hrs post (1.06 ± 0.17 CON vs. 1.8 ± 0.08 INT, $t = 5.67$, 95% CI 0.47 to 1.01, $P < 0.001$) with no difference between conditions at 30 mins (1.01 ± 0.07 CON vs. 0.97 ± 0.05 INT, $t = -0.3$, 95% CI -0.33 to 0.25, $P = 0.77$) and 24 hrs post-loading (1.01 ± 0.08 CON vs. 0.9 ± 0.04 INT, $t = -0.81$, 95% CI -0.38 to 0.17, $P = 0.43$; see Figure 5.3).

There was no significant main effect for loading ($F_{1,22} = 0.35$, $P = 0.56$) on CTTN transcript expression but there was for time ($F_{2,22} = 15.46$, $P < 0.001$) with no significant interaction ($F_{2,22} = 2.89$, $P = 0.08$). Mean expression at 3 hrs (1.26 ± 0.04) was significantly greater than that at 30 mins (0.93 ± 0.05 ; $t = -5.29$, 95% CI -0.46 to -0.2, $P < 0.001$) and 24 hrs (1 ± 0.05 , $t = -4.18$, 95% CI -0.38 to -0.13, $P < 0.001$) with no significant difference between 30 mins and 24 hrs ($t = -1.27$, 95% CI -0.20 to 0.05, $P = 0.22$). There was no significant difference in mRNA expression post-loading at 30 mins (1.01 ± 0.05 CON vs. 0.83 ± 0.07 INT, $t = -1.97$, 95% CI -0.36 to 0.01, $P = 0.06$), 3 hrs (1.19 ± 0.06 CON vs. 1.31 ± 0.04 INT, $t = 1.42$, 95% CI -0.06 to 0.31, P

= 0.17) and 24 hrs (1.01 ± 0.09 CON vs. 0.98 ± 0.04 INT, $t = -0.48$, 95% CI -0.21 to 0.13, $P = 0.64$; see Figure 5.3).

For FLNB transcript expression, there was no significant main effect for condition ($F_{1,23} = 0.37$, $P = 0.55$) nor time ($F_{2,23} = 2.7$, $P = 0.09$), with no significant interaction ($F_{2,23} = 3.05$, $P = 0.07$). Mean expression at 30 mins (1.01 ± 0.05) was not significantly different versus 3 hrs (1.06 ± 0.04 ; $t = -0.63$, 95% CI -0.19 to 0.1, $P = 0.53$) and 24 hrs (0.90 ± 0.06 , $t = 1.55$, 95% CI -0.04 to 0.26, $P = 0.13$), however, mRNA expression was significantly lower at 24 hrs versus 3 hrs ($t = -2.26$, 95% CI -0.3 to -0.01, $P = 0.03$). There was no significant difference in mRNA expression post-loading at 30 mins (1.01 ± 0.06 CON vs. 1.02 ± 0.11 INT, $t = 0.09$, 95% CI -0.21 to 0.23, $P = 0.93$) and 3 hrs (1 ± 0.03 CON vs. 1.11 ± 0.07 INT, $t = 1.12$, 95% CI -0.09 to 0.31, $P = 0.28$), however, mRNA was significantly lower in INT vs. CON at 24 hrs (1.01 ± 0.08 CON vs. 0.79 ± 0.08 INT, $t = -2.29$, 95% CI -0.43 to -0.02, $P = 0.03$; see Figure 5.3).

ECM Structure and Remodelling Genes

There was a significant main effect for loading ($F_{1,23} = 4.25$, $P = 0.05$) and time ($F_{2,23} = 4.39$, $P = 0.02$) on TIMP3 expression with a significant interaction ($F_{2,23} = 5.09$, $P = 0.02$). Mean mRNA expression at 30 mins (0.94 ± 0.08) was significantly lower than 3 hrs (1.19 ± 0.08 , $t = -2.6$, 95% CI -0.52 to -0.00, $P = 0.05$) and 24 hrs (1.19 ± 0.09 , $t = -2.6$, 95% CI -0.52 to -0.00, $P = 0.05$) post-loading with no significant difference between 3 hrs and 24 hrs ($t = -0.02$, 95% CI -0.25 to 0.25, $P = 1$). There was no statistical significance between CON vs. INT at 30 mins (1.03 ± 0.12 CON vs. 0.83 ± 0.08 INT, $t = -1.41$, 95% CI -0.51 to 0.1, $P = 0.17$), although expression was greater following INT at 3 hrs (1.01 ± 0.08 CON vs. 1.36 ± 0.07 INT, $t = 2.55$, 95% CI 0.07 to 0.63, $P = 0.02$) and 24 hrs post-loading (1.01 ± 0.07 CON vs. 1.36 ± 0.14 INT, $t = 2.59$, 95% CI 0.07 to 0.64, $P = 0.02$; see Figure 5.3).

There was no significant main effect for condition ($F_{1,23} = 0.10, P = 0.75$) on ITGB3 transcript expression, albeit, there was a significant main effect for time ($F_{2,23} = 5.47, P = 0.01$) with a significant interaction ($F_{2,23} = 5.44, P = 0.01$). Mean expression 3 hrs (1.21 ± 0.09) was significantly greater than that at 30 mins ($0.96 \pm 0.08, t = -2.83, 95\% \text{ CI } -0.46 \text{ to } -0.07, P = 0.001$) and 24 hrs ($0.95 \pm 0.05, t = -2.83, 95\% \text{ CI } -0.46 \text{ to } -0.07, P = 0.01$) with no difference between 30 mins and 24 hrs ($t = -0.06, 95\% \text{ CI } -0.19 \text{ to } 0.19, P = 0.96$). Transcript expression was significantly greater following INT at 3 hrs ($1.03 \pm 0.11_{\text{CON}} \text{ vs. } 1.4 \pm 0.06_{\text{INT}}, t = 2.91, P = 0.01, 95\% \text{ CI } 0.03 \text{ to } 0.7$) with no difference between CON vs. INT at 30 mins ($1.04 \pm 0.13_{\text{CON}} \text{ vs. } 0.86 \pm 0.09_{\text{INT}}, t = -1.29, 95\% \text{ CI } -0.46 \text{ to } 0.11, P = 0.21$) and 24 hrs post-loading ($1.02 \pm 0.08_{\text{CON}} \text{ vs. } 0.9 \pm 0.03_{\text{INT}}, t = -0.96, 95\% \text{ CI } -0.39 \text{ to } 0.14, P = 0.35$; see Figure 5.3).

There was no significant main effect for loading ($F_{1,23} = 0, P = 0.99$) nor time ($F_{2,23} = 1.68, P = 0.21$) on LAMA5 transcript expression with no significant interaction ($F_{2,23} = 1.43, P = 0.26$). Mean expression at 30 mins (0.98 ± 0.04) was not significantly different versus 3 ($1.09 \pm 0.06; t = -1.49, 95\% \text{ CI } -0.27 \text{ to } 0.04, P = 0.15$) and 24 hrs ($0.96 \pm 0.05, t = 0.11, 95\% \text{ CI } -0.15 \text{ to } 0.17, P = 0.91$). Furthermore, there was no statistical significance between 3 and 24 hrs ($t = -1.66, 95\% \text{ CI } -0.27 \text{ to } 0.03, P = 0.11$). There was no significant difference in mRNA expression post-loading at 30 mins ($1 \pm 0.05_{\text{CON}} \text{ vs. } 0.94 \pm 0.08_{\text{INT}}, t = -0.57, 95\% \text{ CI } -0.29 \text{ to } 0.17, P = 0.58$), 3 ($1.02 \pm 0.09_{\text{CON}} \text{ vs. } 1.16 \pm 0.09_{\text{INT}}, t = 1.38, 95\% \text{ CI } -0.07 \text{ to } 0.36, P = 0.18$) or 24 hrs ($1.01 \pm 0.06_{\text{CON}} \text{ vs. } 0.92 \pm 0.07_{\text{INT}}, t = -0.8, 95\% \text{ CI } -0.3 \text{ to } 0.13, P = 0.44$; see Figure 5.3).

There was a significant main effect for condition ($F_{1,19} = 7.89, P = 0.01$) on COL4A1 transcript expression, albeit, there was no significant main effect for time ($F_{2,19} = 0.56, P = 0.58$) with no significant interaction ($F_{2,19} = 2.17, P = 0.14$). Mean expression at 30 mins (1.01 ± 0.08) was not significantly different versus 3 ($1.01 \pm 0.07; t = 0.05, 95\% \text{ CI } -0.2 \text{ to } 0.21, P = 0.96$) and 24 hrs ($1.1 \pm 0.09, t = -0.88, 95\% \text{ CI } -0.29 \text{ to } 0.12, P = 0.39$). Furthermore, there was no statistical significance between 3 and 24 hrs ($t = 0.96, 95\% \text{ CI } -0.11 \text{ to } 0.29, P = 0.35$). There was no

significant difference in mRNA expression between CON vs. INT at 30 mins ($1.12 \pm 0.1_{\text{CON}}$ vs. $0.9 \pm 0.12_{\text{INT}}$, $t = -1.60$, 95% CI -0.52 to 0.07, $P = 0.13$) and 3 hrs ($1.02 \pm 0.1_{\text{CON}}$ vs. $1 \pm 0.11_{\text{INT}}$, $t = -0.17$, 95% CI -0.3 to 0.26, $P = 0.87$). However, COL4A1 expression was significantly lower at 24 hrs post-loading ($1.31 \pm 0.07_{\text{CON}}$ vs. $0.89 \pm 0.06_{\text{INT}}$, $t = -3.03$, 95% CI -0.72 to 0.13, $P = 0.01$; see Figure 5.3).

There was a significant main effect for loading ($F_{1,19} = 11.3$, $P = 0.003$) and time ($F_{2,19} = 5.33$, $P = 0.02$) on THBS1 expression with a significant interaction ($F_{2,19} = 3.59$, $P = 0.05$). Mean mRNA expression at 30 mins (1 ± 0.07) was significantly greater than that at 24 hrs (0.77 ± 0.03 , $t = 3.26$, 95% CI 0.08 to 0.39, $P = 0.004$) post-loading with no significant difference between 3 hrs (0.88 ± 0.07) and 30 mins ($t = 1.87$, 95% CI -0.02 to 0.27, $P = 0.08$) and 24 hrs ($t = -1.49$, 95% CI -0.25 to 0.04, $P = 0.15$). Mean mRNA expression was significantly lower at 30 mins ($1.15 \pm 0.06_{\text{CON}}$ vs. $0.84 \pm 0.07_{\text{INT}}$, $t = -3.13$, 95% CI -0.52 to -0.1, $P = 0.01$) and 3 hrs ($1.02 \pm 0.08_{\text{CON}}$ vs. $0.72 \pm 0.07_{\text{INT}}$, $t = -3.11$, 95% CI -0.5 to -0.1, $P = 0.01$) post INT loading with no difference between CON vs. INT at 24 hrs post-loading ($0.75 \pm 0.07_{\text{CON}}$ vs. $0.78 \pm 0.04_{\text{INT}}$, $t = 0.28$, 95% CI -0.19 to 0.25, $P = 0.78$; see Figure 5.3).

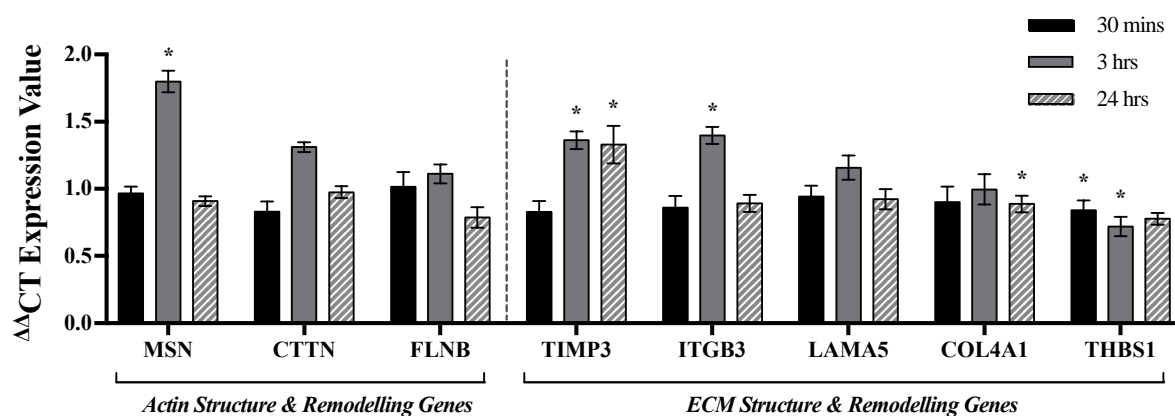


Figure 5.3. mRNA expression of actin/ECM structure and remodelling related genes after loading in bioengineered SkM

Gene expression of actin (i.e. MSN, CTTN, FLNB) / ECM (i.e. TIMP3, ITGB3, LAMA5, COL4A1, THBS1) structure and remodelling related genes was assessed at 30 mins, 3 hrs and 24 hrs post-loading in loaded (INT) and non-loaded (CON) bioengineered SkM ($n = 5$ replicate

cultures/muscles per condition [CON and INT] and time point [30 mins, 3 and 24 hrs]). (*) depicts significant mRNA expression fold-change after INT relative to CON at the same relative timepoint ($P \leq 0.05$). Data is presented as mean \pm standard error of mean (SEM).

Mechano-Transduction Genes

There was no significant main effect for condition ($F_{1,18} = 1.87$, $P = 0.19$) on CRK transcript expression, albeit, there was a significant main effect for time ($F_{2,18} = 4.16$, $P = 0.03$) with a significant interaction ($F_{2,18} = 6.04$, $P = 0.01$). Mean expression 30 mins (0.77 ± 0.07) was significantly lower than that at 3 hrs (1.09 ± 0.13 , $t = -2.88$, 95% CI -0.58 to -0.09, $P = 0.01$), however there was no significant difference at 30 mins vs. 24 hrs (0.91 ± 0.08 , $t = -1.57$, 95% CI -0.42 to 0.06, $P = 0.13$), nor 3 vs. 24 hrs ($t = -1.44$, 95% CI -0.38 to 0.07, $P = 0.17$). Furthermore, there was no statistical difference in transcript expression between CON vs. INT at 30 mins (0.89 ± 0.07 CON vs. 0.62 ± 0.09 INT, $t = -1.02$, 95% CI -0.38 to 0.13, $P = 0.32$) and 3 hrs (0.93 ± 0.12 CON vs. 1.24 ± 0.21 INT, $t = 1.1$, 95% CI -0.12 to 0.39, $P = 0.29$), however mRNA significantly reduced after 24 hrs post-loading (1.14 ± 0.09 CON vs. 0.72 ± 0.02 INT, $t = -2.42$, 95% CI -0.51 to -0.04, $P = 0.02$; see Figure 5.4).

There was no significant main effect for condition ($F_{1,23} = 3.41$, $P = 0.08$) on CD63 transcript expression, albeit, there was a significant main effect for time ($F_{2,23} = 5.22$, $P = 0.01$) with a significant interaction ($F_{2,23} = 4.67$, $P = 0.02$). Mean expression 30 mins (0.86 ± 0.07) was significantly lower than that at 3 (1.05 ± 0.06 , $t = -3.19$, 95% CI -0.35 to -0.07, $P = 0.004$) and 24 hrs (0.98 ± 0.04 , $t = -2.14$, 95% CI -0.28 to -0.004, $P = 0.13$) with no difference 3 and 24 hrs ($t = -1.08$, 95% CI -0.2 to 0.06, $P = 0.29$). Furthermore, mRNA expression significantly reduced after loading at 30 mins (1 ± 0.05 CON vs. 0.68 ± 0.05 INT, $t = -3.38$, 95% CI -0.53 to -0.13, $P = 0.003$), however there was no difference in CON vs. INT at 3 (1.02 ± 0.09 CON vs. 1.09 ± 0.07 INT, $t = 0.74$, 95% CI -0.12 to 0.26, $P = 0.47$) and 24 hrs post-loading (1 ± 0.03 CON vs. 0.96 ± 0.07 INT, $t = -0.42$, 95% CI -0.23 to 0.15, $P = 0.68$; see Figure 5.4).

Protein Synthesis

There was no significant main effect for loading ($F_{1,23} = 0.06$, $P = 0.8$) on GSK3 β mRNA expression, albeit there was for time ($F_{2,23} = 6.97$, $P = 0.004$) with a significant interaction ($F_{2,23} = 6.8$, $P = 0.01$). GSK3 β mean expression was significantly greater at 3 hrs (1.13 ± 0.06) versus 30 mins (0.92 ± 0.06 , $t = -3.57$, 95% CI -0.35 to -0.09, $P = 0.002$) and 24 hrs (0.97 ± 0.03 , $t = -2.69$, 95% CI -0.29 to -0.04, $P = 0.01$) with no difference between 30 mins and 24 hrs ($t = -0.96$, 95% CI -0.19 to 0.07, $P = 0.35$). Transcript expression was significantly lower in INT vs. CON at 30 mins ($1.01 \pm 0.07_{\text{CON}}$ vs. $0.8 \pm 0.04_{\text{INT}}$, $t = -2.26$, $P = 0.03$, 95% CI -0.4 to -0.02). However, expression was greater after INT loading at 3 hrs ($1.01 \pm 0.08_{\text{CON}}$ vs. $1.25 \pm 0.07_{\text{INT}}$, $t = 2.79$, 95% CI 0.06 to 0.42, $P = 0.01$) with no difference between conditions at 24 hrs post-loading ($1 \pm 0.04_{\text{CON}}$ vs. $0.93 \pm 0.04_{\text{INT}}$, $t = -0.85$, 95% CI -0.25 to 0.11, $P = 0.41$; see Figure 5.4).

TGF- β Signalling

There was a significant main effect for condition ($F_{1,17} = 18.21$, $P = 0.001$) and time ($F_{2,17} = 12.49$, $P < 0.001$) on FOS mRNA expression with a significant interaction ($F_{2,17} = 3.89$, $P = 0.04$). Mean expression at 30 mins (1.66 ± 0.2) was statistically greater than that at 3 (1.04 ± 0.15 , $t = 3.87$, 95% CI 0.26 to 0.88, $P = 0.001$) and 24 hrs (1 ± 0.06 , $t = 4.82$, 95% CI 0.37 to 0.95, $P < 0.001$) with no difference between 3 and 24 hrs ($t = -0.66$, 95% CI -0.36 to 0.19, $P = 0.52$). Interestingly, transcript expression significantly reduced after INT loading at 30 mins ($2.02 \pm 0.08_{\text{CON}}$ vs. $1.3 \pm 0.25_{\text{INT}}$, $t = -3.34$, 95% CI -1.18 to -0.27, $P = 0.004$) and 3 ($1.42 \pm 0.16_{\text{CON}}$ vs. $0.76 \pm 0.06_{\text{INT}}$, $t = -3.27$, 95% CI -1.09 to -0.23, $P = 0.01$) with no difference between conditions at 24 hrs post-loading ($1.04 \pm 0.14_{\text{CON}}$ vs. $0.97 \pm 0.1_{\text{INT}}$, $t = -0.41$, 95% CI -0.42 to 0.29, $P = 0.69$; see Figure 5.4).

There was no significant main effect for condition ($F_{1,23} = 0.13$, $P = 0.72$), nor time ($F_{2,23} = 1.63$, $P = 0.22$) on SMAD3 mRNA expression with no significant interaction ($F_{2,23} = 1.7$, $P =$

0.2). Mean expression at 30 mins (0.93 ± 0.05) was not statistically different than that at 3 (1.06 ± 0.04 , $t = -1.76$, 95% CI -0.3 to 0.02, $P = 0.09$) and 24 hrs (1.02 ± 0.07 , $t = -1.27$, 95% CI -0.26 to 0.06, $P = 0.22$) with no difference between 3 and 24 hrs ($t = -0.51$, 95% CI -0.2 to 0.12, $P = 0.62$). Furthermore, transcript expression was not statistically different between CON and INT at 30 mins (1.01 ± 0.07 CON vs. 0.84 ± 0.05 INT, $t = -1.50$, 95% CI -0.41 to 0.07, $P = 0.15$) and 3 (1 ± 0.04 CON vs. 1.12 ± 0.06 INT, $t = 1.1$, 95% CI -0.12 to 0.34, $P = 0.28$) and 24 hrs post-loading (1.03 ± 0.13 CON vs. 1.02 ± 0.07 INT, $t = -0.15$, 95% CI -0.24 to 0.21, $P = 0.88$; see Figure 5.4).

There was no significant main effect for condition ($F_{1,23} = 0.03$, $P = 0.865$) on WNT9a mRNA expression, albeit, there was for time ($F_{2,23} = 11.97$, $P < 0.001$) with a significant interaction ($F_{2,23} = 12.63$, $P < 0.001$). Mean WNT9a expression at 3 hrs (1.28 ± 0.13) was greater than that at 30 mins (0.81 ± 0.1 , $t = -4.79$, 95% CI -0.71 to -0.28, $P < 0.001$) and 24 hrs (0.96 ± 0.05 , $t = -3.21$, 95% CI -0.53 to -0.12, $P = 0.004$) with no difference between 30 mins and 24 hrs ($t = -1.67$, 95% CI -0.39 to 0.04, $P = 0.11$). Furthermore, transcript expression was significantly lower in INT vs. CON at 30 mins (1.03 ± 0.11 CON vs. 0.55 ± 0.04 INT, $t = -3.18$, 95% CI -0.79 to -0.17, $P = 0.004$) but was greater at 3 hrs post (1.01 ± 0.08 CON vs. 1.56 ± 0.17 INT, $t = 3.82$, 95% CI 0.25 to 0.84, $P = 0.001$) with no difference between conditions 24 hrs (1.01 ± 0.08 CON vs. 0.9 ± 0.07 INT, $t = -0.75$, 95% CI -0.4 to 0.18, $P = 0.46$; see Figure 5.4).

Calcium Signalling

There was a significant main effect for condition ($F_{1,22} = 9.87$, $P = 0.01$) on ITPR3 transcript expression, albeit, there was no significant main effect for time ($F_{2,22} = 3.28$, $P = 0.06$) with no significant interaction ($F_{2,22} = 2.72$, $P = 0.09$). Mean expression at 24 hrs (0.82 ± 0.06) was significantly lower than that at 3 hrs (0.99 ± 0.05 ; $t = -2.41$, 95% CI -0.32 to -0.02, $P = 0.03$) post-loading with no significant difference between 30 mins (0.96 ± 0.07) and 3 hrs ($t = -0.49$, 95% CI -0.19 to 0.12, $P = 0.63$) nor 30 mins vs. 24 hrs ($t = 1.91$, 95% CI -0.01 to 0.28, $P =$

0.07). There was no significant difference in mRNA expression post-loading at 30 mins (1.02 ± 0.11 CON vs. 0.89 ± 0.07 INT, $t = -1.26$, 95% CI -0.34 to 0.08, $P = 0.22$) and 3 hrs (1.02 ± 0.09 CON vs. 0.96 ± 0.02 INT, $t = -0.52$, 95% CI -0.27 to 0.16, $P = 0.61$). However, gene expression was significantly lower at 24 hrs post-loading (1 ± 0.04 CON vs. 0.64 ± 0.02 INT, $t = -3.78$, 95% CI -0.57 to -0.17, $P = 0.001$; see Figure 5.4).

There was a significant main effect for condition ($F_{1,23} = 16.94$, $P < 0.001$) on ADCY3 transcript expression, albeit, there was no significant main effect for time ($F_{2,23} = 0.94$, $P = 0.4$) with no significant interaction ($F_{2,23} = 0.79$ $P = 0.46$). There was no significant difference in mean mRNA expression at 30 mins (0.85 ± 0.09) vs. 3 hrs (0.86 ± 0.07 , $t = -0.29$, 95% CI -0.21 to 0.15, $P = 0.77$) and 24 hrs (0.94 ± 0.07 , $t = -1.29$, 95% CI -0.29 to 0.07, $P = 0.21$) nor between 3 and 24 hrs ($t = 1.03$, 95% CI -0.09 to 0.26, $P = 0.31$). Gene expression significantly reduced after loading at 30 mins (1.02 ± 0.11 CON vs. 0.64 ± 0.05 INT, $t = -3.03$, 95% CI -0.65 to -0.12, $P = 0.01$) and 3 hrs (1.02 ± 0.09 CON vs. 0.7 ± 0.04 INT, $t = -2.64$, 95% CI -0.56 to -0.07, $P = 0.02$) with no difference between CON vs. INT at 24 hrs (1.03 ± 0.13 CON vs. 0.86 ± 0.04 INT, $t = -1.43$, 95% CI -0.42 to 0.08, $P = 0.17$; see Figure 5.4).

IL-6 Signalling

There was no significant main effect for loading ($F_{1,21} = 0.02$, $P = 0.89$) on STAT3 mRNA expression, albeit, there was a significant main effect for time ($F_{1,21} = 11.95$, $P < 0.001$) with no significant interaction ($F_{2,21} = 2.24$, $P = 0.13$). Mean expression at 3 hrs (1.34 ± 0.07) was significantly greater than that at 30 mins (0.91 ± 0.06 , $t = -4.85$, 95% CI -0.64 to -0.51, $P < 0.001$) and 24 hrs (1.06 ± 0.06 , $t = -3.16$, 95% CI -0.47 to -0.1, $P = 0.01$) with no difference between 30 mins and 24 hrs ($t = -1.88$, 95% CI -0.34 to 0.02, $P = 0.08$). Transcript expression was not significantly different between CON and INT at 30 mins (1.01 ± 0.07 CON vs. 0.78 ± 0.07 INT, $t = -1.8$, 95% CI -0.49 to 0.04, $P = 0.09$), 3 hrs (1.29 ± 0.13 CON vs. 1.39 ± 0.06 INT, $t =$

0.73, 95% CI -0.18 to 0.38, $P = 0.48$) or 24 hrs post-loading ($1.01 \pm 0.06_{\text{CON}}$ vs. $1.11 \pm 0.11_{\text{INT}}$, $t = 0.84$, 95% CI -0.15 to 0.35, $P = 0.41$; see Figure 5.4).

Retinoic Signalling

There was no significant main effect for condition ($F_{1,23} = 1.69$, $P = 0.21$), nor time ($F_{2,23} = 1.35$, $P = 0.28$) on RARA mRNA expression with no significant interaction ($F_{2,23} = 1.43$, $P = 0.26$). There was no statistical difference in mean expression at 30 mins (0.92 ± 0.08) vs. 3 hrs (1.05 ± 0.06 , $t = -1.61$, 95% CI -0.32 to 0.04, $P = 0.12$) and 24 hrs (0.96 ± 0.04 , $t = -0.6$, 95% CI -0.24 to 0.13, $P = 0.55$) with no further difference between 3 and 24 hrs ($t = -1.04$, 95% CI -0.27 to 0.09, $P = 0.31$). Furthermore, transcript expression was not statistically different between CON and INT at 30 mins ($1.03 \pm 0.12_{\text{CON}}$ vs. $0.79 \pm 0.09_{\text{INT}}$, $t = -1.83$, 95% CI -0.5 to 0.03, $P = 0.08$), 3 hrs ($1.02 \pm 0.1_{\text{CON}}$ vs. $1.08 \pm 0.08_{\text{INT}}$, $t = 0.51$, 95% CI -0.19 to 0.31, $P = 0.61$) and 24 hrs post-loading ($1.01 \pm 0.08_{\text{CON}}$ vs. $0.91 \pm 0.04_{\text{INT}}$, $t = -0.87$, 95% CI -0.36 to 0.15, $P = 0.39$; see Figure 5.4).

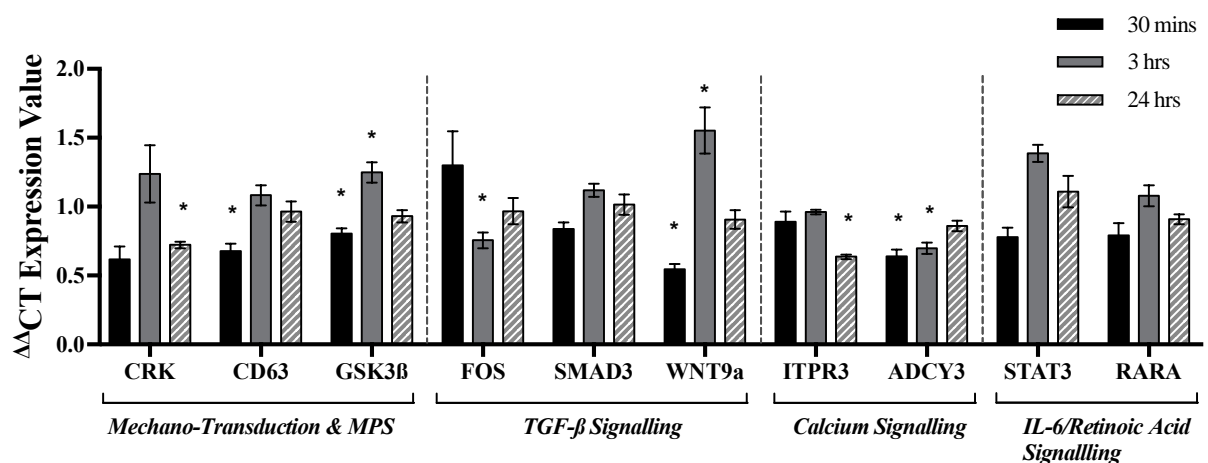


Figure 5.4. mRNA expression of genes associated with mechano-transduction, MPS and TGF-β/calcium/IL-6/retinoic acid signalling after loading in bioengineered SkM.

Gene expression of genes associated with mechano-transduction (CRK, CD63), MPS (GSK3β) and TGF-β (FOS, SMAD3, WNT9a) / calcium (ITPR3, ADCY3) / IL-6 (STAT3) / retinoic acid (RARA) signalling was assessed at 30 mins, 3 hrs and 24 hrs post-loading in loaded (INT) and non-loaded (CON) bioengineered SkM ($n = 5$ replicate cultures/muscles per condition [CON

and INT] and time point [30 mins, 3 and 24 hrs]). (*) depicts significant mRNA expression fold-change after INT relative to CON at the same relative timepoint ($P \leq 0.05$). Data is presented as mean \pm standard error of mean (SEM).

Other

There was no significant main effect for loading ($F_{1,22} = 1.6$, $P = 0.22$) nor time ($F_{2,22} = 0.54$, $P = 0.59$) on RASSF5 transcript expression with no significant interaction ($F_{2,22} = 0.62$, $P = 0.55$). Furthermore, there was no significant difference in mean expression at 30 mins (0.96 ± 0.06) versus 3 (0.95 ± 0.08 ; $t = 0.02$, 95% CI -0.2 to 0.2, $P = 0.98$) and 24 hrs (1.03 ± 0.06 , $t = -0.88$, 95% CI -0.28 to 0.11, $P = 0.39$) with no statistical difference between 3 and 24 hrs ($t = 0.9$, 95% CI -0.11 to 0.28, $P = 0.38$). Additionally, there was no significant difference in mRNA expression post-loading at 30 mins (1.02 ± 0.1 CON vs. 0.88 ± 0.06 INT, $t = -1.04$, 95% CI -0.43 to 0.14, $P = 0.87$), 3 hrs (1.03 ± 0.13 CON vs. 0.86 ± 0.09 INT, $t = -1.26$, 95% CI -0.46 to 0.11, $P = 0.22$) and 24 hrs (1.02 ± 0.1 CON vs. 1.04 ± 0.06 INT, $t = 0.16$, 95% CI -0.25 to 0.29, $P = 0.88$; see Figure 5.5).

There was no significant main effect for condition ($F_{1,22} = 1.69$, $P = 0.21$), nor time ($F_{2,22} = 2.59$, $P = 1$) on F2LR3 mRNA expression with no significant interaction ($F_{2,22} = 3.1$, $P = 0.07$). There was no statistical difference in mean expression at 30 mins (0.96 ± 0.07) vs. 3 hrs (1.06 ± 0.05 , $t = -1.34$, 95% CI -0.29 to 0.06, $P = 0.19$) and 24 hrs (0.88 ± 0.07 , $t = 0.88$, 95% CI -0.1 to 0.25, $P = 0.39$). However mRNA was significantly lower at 24 vs. 3 hrs ($t = -1.34$, 95% CI -0.29 to 0.06, $P = 0.19$) post-loading. Furthermore, transcript expression was not statistically different between CON and INT at 30 mins (1.02 ± 0.09 CON vs. 0.89 ± 0.13 INT, $t = -1.02$, 95% CI -0.38 to 0.13, $P = 0.32$) and 3 hrs (1 ± 0.03 CON vs. 1.13 ± 0.1 INT, $t = 1.1$, 95% CI -0.12 to 0.39, $P = 0.29$), albeit, expression significantly reduced at 24 hrs post-loading (1.02 ± 0.1 CON vs. 0.74 ± 0.04 INT, $t = -2.42$, 95% CI -0.51 to -0.04, $P = 0.02$; see Figure 5.5).

There was no significant main effect for condition ($F_{1,22} = 1.05$, $P = 0.32$), nor time ($F_{2,22} = 1.08$, $P = 0.36$) on DOT1L mRNA expression with no significant interaction ($F_{2,22} = 0.92$, $P = 0.41$). There was no statistical difference in mean expression at 30 mins (1.01 ± 0.06) vs. 3 hrs (1.12 ± 0.07 , $t = -1.26$, 95% CI -0.28 to 0.07, $P = 0.22$) and 24 hrs (1.01 ± 0.04 , $t = -0$, 95% CI -0.18 to 0.18, $P = 1$) with no difference between 3 and 24 hrs ($t = -1.26$, 95% CI -0.28 to 0.07, $P = 0.22$) post-loading. Furthermore, transcript expression was not statistically different between CON and INT at 30 mins (1.02 ± 0.09 CON vs. 0.89 ± 0.13 INT, $t = -1.04$, 95% CI -0.43 to 0.14, $P = 0.31$), 3 (1 ± 0.03 CON vs. 1.13 ± 0.1 INT, $t = -1.26$, 95% CI -0.46 to 0.11, $P = 0.22$) and 24 hrs post-loading (1.02 ± 0.1 CON vs. 0.74 ± 0.04 INT, $t = 0.16$, 95% CI -0.25 to 0.29, $P = 0.88$; see Figure 5.5).

There was no significant main effect for condition ($F_{1,15} = 0.5$, $P = 0.49$) on KDR mRNA expression, however there was for time ($F_{2,15} = 4.27$, $P = 0.03$) with no significant interaction ($F_{2,15} = 3.41$, $P = 0.06$). Mean expression at 30 mins (0.94 ± 0.04) was significantly lower vs. 3 hrs (1.19 ± 0.1 , $t = -2.82$, 95% CI -0.43 to -0.06, $P = 0.01$) and 24 hrs (1.11 ± 0.04 , $t = -2.19$, 95% CI -0.34 to -0, $P = 0.05$) with no difference between 3 and 24 hrs post-loading ($t = -0.89$, 95% CI -0.24 to 0.1, $P = 0.39$). Furthermore, transcript expression significantly increased in INT vs. CON at 3 hrs (1.04 ± 0.04 CON vs. 1.34 ± 0.16 INT, $t = 2.45$, 95% CI 0.04 to 0.56, $P = 0.03$) with no difference between CON and INT at 30 mins (0.98 ± 0.04 CON vs. 0.9 ± 0.08 INT, $t = -0.63$, 95% CI -0.34 to 0.18, $P = 0.54$) and 24 hrs post-loading (1.16 ± 0.1 CON vs. 1.08 ± 0.03 INT, $t = -0.8$, 95% CI -0.3 to 0.14, $P = 0.44$; see Figure 5.5).

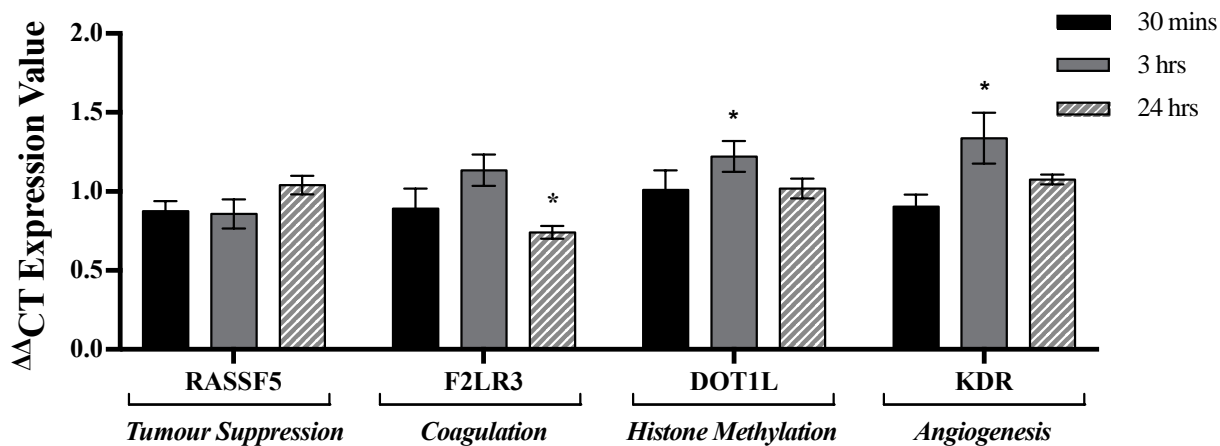


Figure 5.5. mRNA expression of upregulated/hypomethylated genes associated with DNA methylation, angiogenesis and tumour suppression after loading in bioengineered SkM.

Gene expression of genes associated with DNA methylation (DOT1L), angiogenesis (KDR) and tumour suppression (RASSF5) was assessed at 30 mins, 3 hrs and 24 hrs post-loading in loaded (INT) and non-loaded (CON) bioengineered SkM ($n = 5$ replicate cultures/muscles per condition [CON and INT] and time point [30 mins, 3 and 24 hrs]). (*) depicts significant mRNA expression fold-change after INT relative to CON at the same relative timepoint ($P \leq 0.05$).

Data is presented as mean \pm standard error of mean (SEM).

After analysing mRNA expression of upregulated/hypomethylated genes identified in chapter 4) at 30 mins, 3 hrs and 24 hrs post mechanical loading in bioengineered SkM alone, gene expression at 3 hrs post-loading was compared to that following acute and chronic loading/RE in human and rat SkM, respectively (see Figure 5.6). Interestingly, there was a significant main effect for model on F2LR3 ($F_{2,9} = 5.98$, $P = 0.03$), THBS1 ($F_{2,9} = 28.23$, $P < 0.01$) and FOS ($F_{2,10} = 60.12$, $P < 0.01$). However, there no significant main effect for model/species of loading for genes; WNT9a ($F_{2,10} = 1.16$, $P = 0.84$), MSN ($F_{2,10} = 0.29$, $P = 0.76$), ITGB3 ($F_{2,10} = 0.89$, $P = 0.45$), STAT3 ($F_{2,9} = 0.5$, $P = 0.63$), TIMP3 ($F_{2,10} = 0.26$, $P = 0.78$), CTTN ($F_{2,9} = 0.31$, $P = 0.72$), DOT1L ($F_{2,10} = 0.41$, $P = 0.68$), GSK3 β ($F_{2,10} = 0.06$, $P = 0.94$), UBR5 ($F_{2,9} = 0.43$, $P = 0.67$), LAMA5 ($F_{2,10} = 0.07$, $P = 0.93$), SMAD3 ($F_{2,10} = 0.21$, $P = 0.82$), COL4A1 ($F_{2,9} = 1.53$, $P = 0.28$), FLNB ($F_{2,9} = 1.11$, $P = 0.89$), CD63 ($F_{2,10} = 1.91$, $P = 0.21$), RARA ($F_{2,10} = 0.73$, $P = 0.51$), CRK ($F_{2,8} = 1.44$, $P = 0.31$), RASSF5 ($F_{2,9} = 1.13$, $P = 0.38$), ITPR3 ($F_{2,9} =$

1.76, $P = 0.24$), ADCY3 ($F_{2,10} = 1.67$, $P = 0.25$) and KDR ($F_{2,8} = 1.06$, $P = 0.4$; see Figure 5.6). After detecting main effects for condition, unpaired *t*-tests were then performed for genes which were differentially regulated between models/species (i.e. F2LR3, THBS1 and FOS) to identify where main effects occurred.

F2LR3

For F2LR3, there was a significant difference in mean expression for bioengineered (1.13 ± 0.1) and rat (2.35 ± 0.72 ; $t_7 = -3.23$, 95% CI -2.11 to -0.33, $P = 0.01$) SkM, however, there was no statistical difference between bioengineered and human SkM (1.08 ± 0 ; $t_3 = 0.24$, 95% CI -0.65 to 0.76, $P = 0.82$). Furthermore, there was no significant difference rat and human SkM ($t_4 = 1.61$, 95% CI -0.93 to 3.48, $P = 0.18$; see Figure 5.6)

THBS1

For THBS1, mean expression was significantly lower in bioengineered (0.72 ± 0.07) versus rat (1.54 ± 0.12 ; $t_7 = -5.53$, 95% CI -1.17 to -0.47, $P = 0.001$) and human (2.36 ± 0 ; $t_3 = -10.19$, 95% CI -2.16 to -1.13, $P = 0.002$) SkM. There was also a significant difference in THBS1 mRNA between rat and human SKM ($t_4 = -2.83$, 95% CI -1.63 to -0.02, $P = 0.05$; see Figure 5.6).

FOS

FOS mRNA expression did not significantly differ between bioengineered (0.76 ± 0.06) and rat (0.58 ± 0.11 ; $t_7 = 1.35$, 95% CI -0.13 to -0.48, $P = 0.22$). However, transcript expression was significantly greater in human SkM (2.89 ± 0) versus bioengineered ($t_3 = -16.98$, 95% CI -2.53 to -1.73, $P < 0.001$) and rat SkM ($t_3 = -8.85$, 95% CI -3.03 to -1.58, $P = 0.001$; see Figure 5.6).

The current section demonstrates that out of the 22 upregulated/hypomethylated genes identified in chapter 4 that were also assessed after loading in bioengineered SkM in the present chapter, no genes were upregulated at 30 mins post-loading, however, 22% (5; THBS1, CD63, GSK3 β , WNT9a, ADCY3) showed a reduction in mRNA expression. At 3 hrs, 33% (7; MSN, TIMP3, ITGB3, GSK3 β , WNT9a, DOT1L, KDR) showed an increase in mRNA expression whereas 14% (3; THBS1, FOS, ADCY3) decreased with the remaining genes demonstrating no statistical significant change. Finally, 1 gene (TIMP3) showed an increase at 24 hrs post-loading whereas 19% (4; MSN, CRK, ITPR3 F2LR3) of genes showed a decrease in mRNA expression. Overall, the present section suggests that gene expression is reduced immediately post-loading whereas the most abundant increase is observed at 3 hrs with expression decreasing again by 24 hrs.

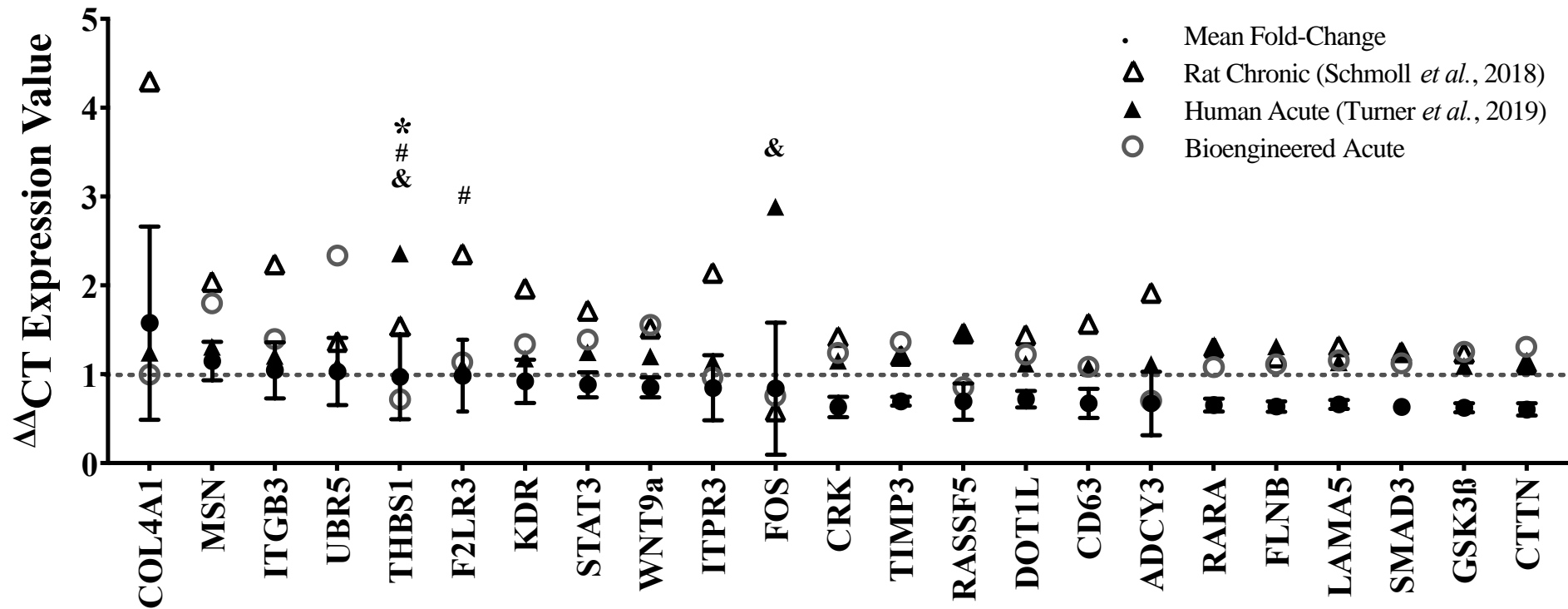


Figure 5.6. Comparison of upregulated/hypomethylated genes after mechanical loading/RE in bioengineered, rodent and human SkM.

As described in section 5.3.1 above, mRNA expression of upregulated/hypomethylated genes identified in chapter 4 were compared across various models of loading/RE - bioengineered SkM (clear circles) versus acute RE in humans (bold triangles) and chronic electrical stimulation/RE in rats (clear triangles). Bold circles with errors represent mean \pm SEM for all models of exercise pooled. (*) represents statistical significance ($P \leq 0.05$) between loaded bioengineered SkM versus exercised human SkM; (#) = bioengineered versus stimulated rat SkM; (&) = human versus rat SkM.

5.3.2 Epigenetic Regulation of Upregulated/Hypomethylated Genes were Assessed After Loading in Bioengineered Skeletal Muscle

After detection of the most significantly regulated genes at 3 hrs post mechanical loading in section 5.3.1 that were also upregulated/hypomethylated after acute RE *in-vivo* (identified in chapter 4), DNA methylation of a selection of these genes was also assessed to determine whether changes in mRNA corresponded to epigenetic modifications of the same gene. Specifically, the DNA methylation status of various regulatory regions of mouse genes; MSN, TIMP3, WNT9a, CTTN, GSK3 β , TIMP3 was assessed at 3 hrs post-loading via tNGBS (see sections 5.2.8 and 2.10.6). Transcripts analysed for DNA methylation were carefully considered based on changes in gene expression after 3D loading or their well-characterised regulatory role(s) in SkM after exercise *in-vivo*. For example, MSN and WNT9a displayed the greatest increase in mRNA at 3 hrs post-loading and are important genes involved in actin crosslinking and TGF β signalling, respectively. Furthermore, GSK3 β and TIMP3 (which were also significantly increased at 3 hrs post-loading). Despite a non-significant increase in CTTN observed in the present chapter (see Figure 5.3), this gene is important for actin cytoskeleton remodelling and together with FLNB, was 1 of 23 genes highlighted in chapter 4 that was significantly upregulated and hypomethylated after both acute and chronic RE in humans (Turner *et al.*, 2019b). CTTN and not FLNB, was therefore selected for methylation analysis given CTTN demonstrated a non-significant increase whereas FLNB did not change after loading (see Figure 5.3).

MSN

There was no significant difference in MSN intron 2 (1 ± 0.02 CON vs. 1.04 ± 0.02 INT, $t_{25} = 1.76$, 95% CI -0.09 to -0.01, $P = 0.09$) or 5-upstream (1 ± 0.03 CON vs. 1.1 ± 0.04 INT, $t_{34} = 1.93$, 95% CI -0.2 to -0.01, $P = 0.06$) region-specific DNA methylation after INT loading. Interestingly however, intron 1 (1 ± 0.02 CON vs. 1.04 ± 0.02 INT, $t_{25} = 1.76$, 95% CI -0.09 to -0.01, $P = 0.09$) and pooled (intron 1/2 and 5-upstream combined) methylation (1 ± 0.01 CON vs.

1.1 ± 0.02 INT, $t_{142} = 4.213$, 95% CI -0.14 to -0.05, $P < 0.001$) significantly increased after INT loading (see Figure 5.7A).

WNT9a

There was no significant change in WNT9a intron 1 (1 ± 0.1 CON vs. 1.22 ± 0.14 INT, $t_{160} = 1.26$, 95% CI -0.57 to 0.13, $P = 0.21$) nor 5-upstream (1 ± 0.07 CON vs. 1.13 ± 0.08 INT, $t_{124} = 1.23$, 95% CI -0.34 to 0.08, $P = 0.22$) region-specific DNA methylation after loading. Furthermore, no changes were observed when both intron 1 and 5-upstream regions were pooled (1 ± 0.06 CON vs. 1.18 ± 0.08 INT, $t_{286} = 1.66$, 95% CI -0.4 to 0.03, $P = 0.1$; see Figure 5.7B).

GSK3 β

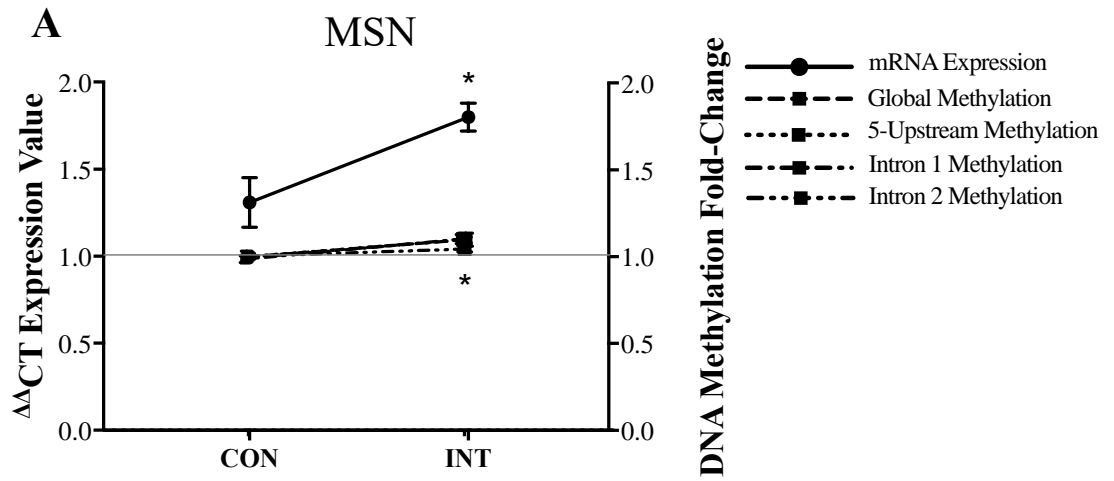
Despite a reduction in GSK3 β intron 1 (1 ± 0.2 CON vs. 0.7 ± 0.18 INT, $t_{52} = 1.11$, 95% CI -0.24 to 0.84, $P = 0.27$) methylation, changes failed to reach statistical significance. Furthermore, there was no significant changes in exon 1 (1 ± 0.06 CON vs. 1.13 ± 0.14 INT, $t_{34} = 0.81$, 95% CI -0.47 to 0.2, $P = 0.42$) and 5-upstream (1 ± 0.16 CON vs. 1.34 ± 0.26 INT, $t_{88} = 1.05$, 95% CI -1 to 0.31, $P = 0.42$) region-specific DNA methylation, nor when pooling all regions (intron 1, exon 1 and 5-upstream) analysed (1 ± 0.1 CON vs. 1.11 ± 0.15 INT, $t_{178} = 0.58$, 95% CI -0.48 to 0.26, $P = 0.56$; see Figure 5.7C).

TIMP3

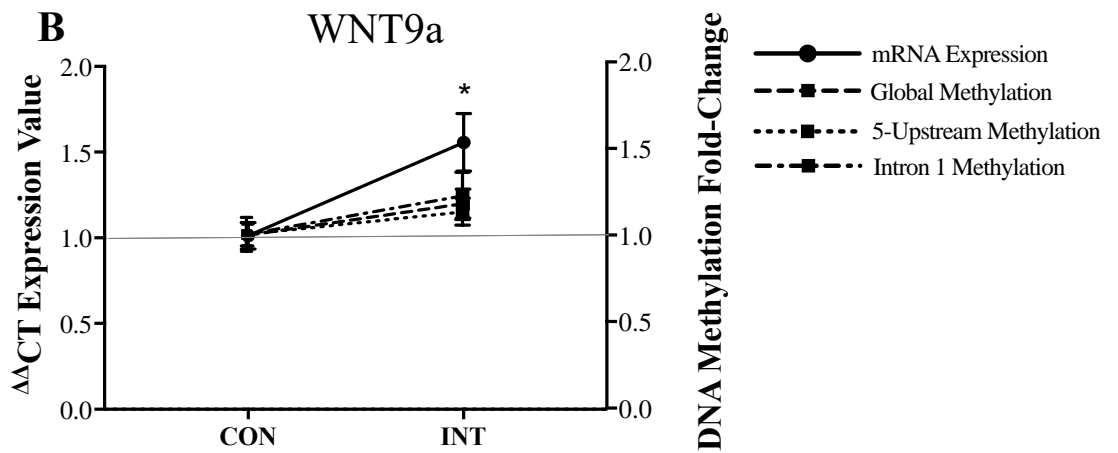
There was no significant different in TIMP3 intron 1 (1 ± 0.18 CON vs. 1.22 ± 0.3 INT, $t_{16} = 0.59$, 95% CI -0.22 to 0.37, $P = 0.56$), exon 1 (1 ± 0.11 CON vs. 1.05 ± 0.12 INT, $t_{43} = 0.32$, 95% CI -0.37 to 0.27, $P = 0.75$) nor 5-upstream (1 ± 0.04 CON vs. 1.04 ± 0.05 INT, $t_{97} = 0.6$, 95% CI -0.17 to 0.09, $P = 0.55$) region-specific DNA methylation after loading. Furthermore, no changes were observed for DNA methylation when all regions assessed (intron 1, exon 1 and 5-upstream) were pooled (1 ± 0.05 CON vs. 1.06 ± 0.05 INT, $t_{160} = 0.87$, 95% CI -0.2 to 0.08, $P = 0.38$; see Figure 5.7D).

CTTN

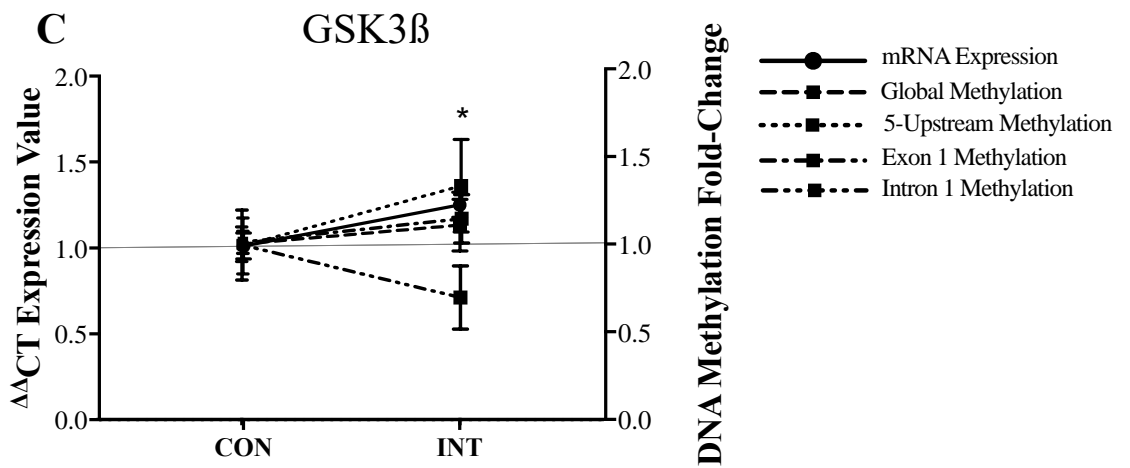
Interestingly, *CTTN* intron 1 specific DNA methylation significantly increased after INT loading in engineered SkM (1 ± 0.05 CON vs. 1.32 ± 0.1 INT, $t_{171} = 2.64$, 95% CI -0.56 to -0.08, $P = 0.01$). However, there was no significant difference in intron 2 (1 ± 0.01 CON vs. 1.01 ± 0.01 INT, $t_{16} = 0.62$, 95% CI -0.03 to 0.02, $P = 0.54$) nor 5-UTR (1 ± 0.14 CON vs. 0.79 ± 0.17 INT, $t_{159} = 0.95$, 95% CI -0.23 to 0.66, $P = 0.34$), despite a reduction in 5-UTR methylation after loading. Furthermore, no changes were observed when all regions assessed (intron 1/2 and 5-UTR) were pooled (1 ± 0.07 CON vs. 1.06 ± 0.1 INT, $t_{332} = 0.49$, 95% CI -0.31 to 0.19, $P = 0.62$; see Figure 5.7E).



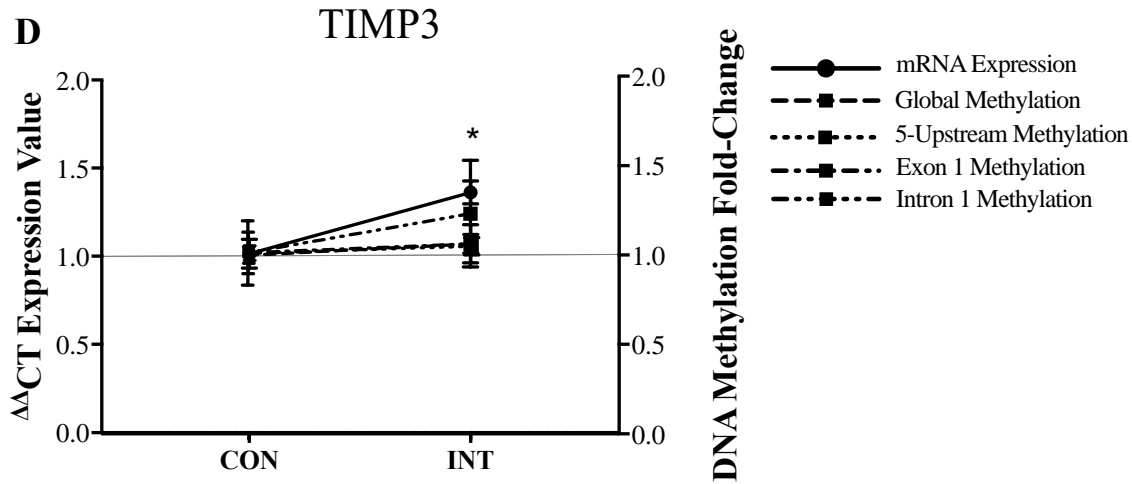
(*) Depicts significantly increased mRNA expression and global and intron 1 hypermethylation after loading (INT)



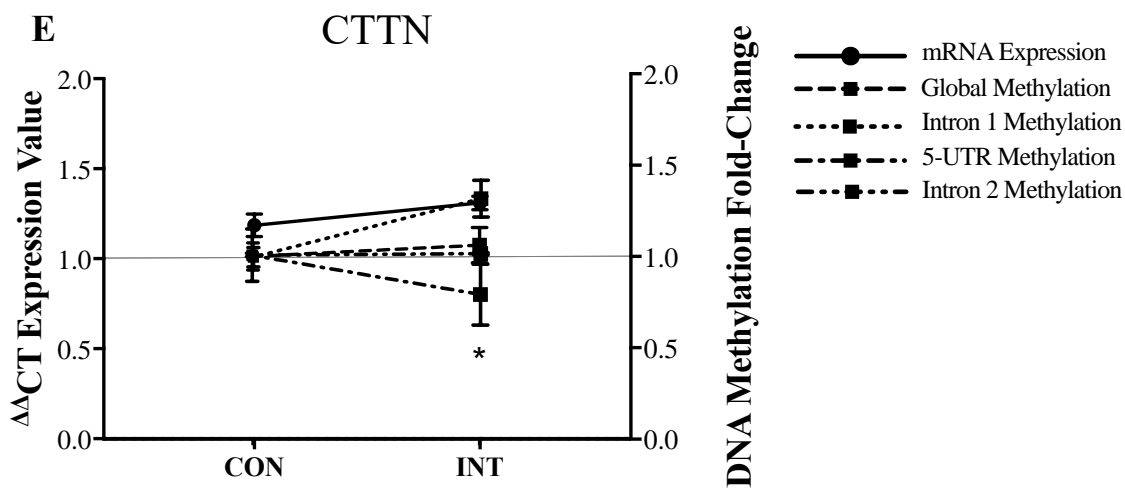
(*) Depicts significantly increased mRNA expression after loading (INT)



(*) Depicts significantly increased mRNA expression after loading (INT)



(*) Depicts significantly increased mRNA expression after loading (INT)



(*) Depicts significant hypermethylation in intron 1 region after loading (INT)

Figure 5.7. mRNA expression and DNA methylation of upregulated/hypomethylated genes identified in chapter 4 following mechanical loading in bioengineered SkM.

mRNA expression and DNA methylation of upregulated/hypomethylated genes, (A) MSN, (B) WNT9a, (C) GSK3 β , (D) TIMP3 and (E) CTTN in loaded (INT) and non-loaded (CON) bioengineered SkM ($n = 5$ replicate cultures/muscles per condition [CON and INT]) at 3 hrs post-loading. (*) Depicts significant difference ($P \leq 0.05$) in mRNA expression and/or region-specific DNA methylation after INT versus CON with specific changes described in each figure section (A-E). Data is presented as mean \pm standard error of mean (SEM).

5.3.3 mRNA Expression of Genes that are Downregulated/Hypermethylated after Exercise in Human Skeletal Muscle were Assessed After Loading in Bioengineered Muscle

After analysing the mechano-responses of upregulated/hypomethylated genes identified in chapter 4 following loading in bioengineered SkM (see section 5.3.1), mRNA expression of genes that were downregulated and hypermethylated in the previous chapter were also assessed at 30 mins, 3 hrs and 24 hrs post-acute loading (INT) in engineered SkM. This included genes; AGTR1, PAX3, NOS2, ESR1, NANOG, LAMA3, ATM, GADD45G, ANK3, DROSHA, SMO and APAF1 (see Figure 5.8). Collective mRNA expression of all downregulated/hypermethylated genes assessed all three time points after 3D loading is presented in Figure 5.2.

AGTR1a

There was a significant main effect for condition/loading ($F_{1,20} = 12.75$, $P = 0.002$) and time ($F_{2,20} = 5.12$, $P = 0.02$) on AGTR1a mRNA expression with no significant interaction ($F_{2,20} = 1.15$, $P = 0.34$). Mean transcript expression at 3 hrs (0.67 ± 0.12) post-loading significantly reduced compared to 30 mins (1.06 ± 0.07 , $t = 3.2$, 95% CI 0.14 to 0.64, $P = 0.01$) with no difference between 3 and 24 hrs (0.87 ± 0.1 , $t = 1.7$, 95% CI -0.05 to 0.44, $P = 0.11$) and 30 mins vs. 24 hrs post-loading ($t = 1.68$, 95% CI -0.05 to 0.43, $P = 0.11$). There was no statistical difference in mRNA after loading at 30 mins ($1.14 \pm 0.09_{\text{CON}}$ vs. $0.98 \pm 0.11_{\text{INT}}$, $t = -0.97$, 95% CI -0.52 to 0.19, $P = 0.35$), however expression significantly reduced after 3 hrs ($0.94 \pm 0.14_{\text{CON}}$ vs. $0.46 \pm 0.07_{\text{INT}}$, $t = -3.10$, 95% CI -0.89 to -0.17, $P = 0.01$) and remained suppressed after 24 hrs post-loading ($1.03 \pm 0.14_{\text{CON}}$ vs. $0.7 \pm 0.12_{\text{INT}}$, $t = -2.13$, 95% CI -0.65 to -0.01, $P = 0.05$).

PAX3

There was a significant main effect for condition/loading ($F_{1,20} = 30.82$, $P < 0.001$) and time ($F_{2,20} = 17.66$, $P < 0.001$) on PAX3 mRNA expression with a significant interaction ($F_{2,20} = 14.60$, $P < 0.001$). Mean transcript expression at 3 hrs (0.54 ± 0.08) significantly lower after loading compared to 30 mins (1.03 ± 0.06 , $t = 5.9$, 95% CI 0.29 to 0.61, $P < 0.001$) and 24 hrs (0.74 ± 0.14 , $t = 2.59$, 95% CI 0.04 to 0.36, $P = 0.02$). Expression was also significantly lower at 24 hrs vs. 30 mins ($t = 3.45$, 95% CI 0.1 to 0.41, $P = 0.003$). There was no statistical difference in mRNA in CON vs. INT at 30 mins (1.01 ± 0.05 CON vs. 1.06 ± 0.12 INT, $t = 0.55$, 95% CI -0.16 to 0.27, $P = 0.59$), however expression significantly reduced at 3 hrs (0.76 ± 0.14 CON vs. 0.41 ± 0.03 INT, $t = -3.08$, 95% CI -0.59 to -0.11, $P = 0.01$) and remained suppressed at 24 hrs post INT loading (1.15 ± 0.08 CON vs. 0.41 ± 0.04 INT, $t = -7.1$, 95% CI -0.96 to -0.52, $P < 0.001$; see Figure 5.8).

NOS2

There was a significant main effect for condition/loading ($F_{1,18} = 12.60$, $P = 0.002$) and time ($F_{2,18} = 39.23$, $P < 0.001$) on NOS2 mRNA expression with a significant interaction ($F_{2,18} = 34.72$, $P < 0.001$). Mean transcript expression at 24 hrs (1.95 ± 0.43) post-loading was significantly greater than that at 30 mins (0.81 ± 0.07 , $t = -7.86$, 95% CI -1.45 to -0.84, $P < 0.001$) and 3 hrs (0.84 ± 0.1 , $t = 7.97$, 95% CI 0.82 to 1.4, $P < 0.001$) with no significant difference between 30 mins and 3 hrs ($t = -0.28$, 95% CI -0.3 to 0.23, $P = 0.78$). Despite a reduction in transcript expression after loading at 30 mins, changes did not reach statistical significance (0.92 ± 0.07 CON vs. 0.74 ± 0.1 INT, $t = -1.23$, 95% CI -0.63 to 0.17, $P = 0.24$). Interestingly however, mRNA was statistically lower in INT vs. CON at 3 hrs (1.02 ± 0.12 CON vs. 0.66 ± 0.1 INT, $t = -2.18$, 95% CI -0.73 to -0.01, $P = 0.04$), but increased after loading at 24 hrs post (1.05 ± 0.14 CON vs. 2.85 ± 0.30 INT, $t = 8.19$, 95% CI 1.34 to 2.26, $P < 0.001$; see Figure 5.8).

ESR1

There was no significant main effect for loading ($F_{1,23} = 1.63$, $P = 0.21$) nor time ($F_{2,23} = 1.67$, $P = 0.21$) on ESR1 mRNA expression with no significant interaction ($F_{2,23} = 1.66$, $P = 0.21$). There was no significant difference in mean mRNA expression at 30 mins (0.9 ± 0.08) vs. 3 hrs (1.01 ± 0.06 , $t = -1.44$, 95% CI -0.31 to 0.06, $P = 0.16$) and 24 hrs (1.03 ± 0.06 , $t = -1.72$, 95% CI 0.33 to 0.03, $P = 0.1$) with no difference between 3 and 24 hrs post-loading ($t = 0.29$, 95% CI -0.15 to 0.2, $P = 0.77$). Interestingly, gene expression reduced at 30 mins post-loading (1.02 ± 0.1 CON vs. 0.74 ± 0.05 INT, $t = -2.15$, 95% CI -0.54 to -0.01, $P = 0.04$) with no difference between CON vs. INT at 3 hrs (1.02 ± 0.09 CON vs. 1 ± 0.09 INT, $t = -0.18$, 95% CI -0.27 to 0.23, $P = 0.86$) and 24 hrs post-loading (1.02 ± 0.11 CON vs. 1.05 ± 0.05 INT, $t = 0.21$, 95% CI -0.23 to 0.28, $P = 0.84$; see Figure 5.8).

NANOG

There was no significant main effect for loading ($F_{1,21} = 2.28$, $P = 0.15$) nor time ($F_{2,21} = 2.26$, $P = 0.13$) on NANOG mRNA expression with no significant interaction ($F_{2,21} = 1.08$, $P = 0.36$). There was no significant difference in mean mRNA expression at 30 mins (1.01 ± 0.06) vs. 3 hrs (1.01 ± 0.05 , $t = 0.09$, 95% CI -0.15 to 0.17, $P = 0.93$) and 24 hrs (0.87 ± 0.05 , $t = 1.83$, 95% CI -0.02 to 0.31, $P = 0.08$) with no difference between 3 and 24 hrs post-loading ($t = -1.85$, 95% CI -0.29 to 0.02, $P = 0.08$). Despite a reduction in gene expression following INT vs. CON at 30 mins post-loading (1.13 ± 0.06 CON vs. 0.9 ± 0.08 INT), such changes failed to reach statistical significance ($t = -1.99$, 95% CI -0.47 to 0.01, $P = 0.06$). Furthermore, there was no difference between CON vs. INT at 3 hrs (1.02 ± 0.11 CON vs. 1 ± 0.03 INT, $t = -0.23$, 95% CI -0.24 to 0.19, $P = 0.82$) and 24 hrs post-loading (0.89 ± 0.06 CON vs. 0.86 ± 0.09 INT, $t = -0.31$, 95% CI -0.26 to 0.19, $P = 0.76$; see Figure 5.8).

LAMA3

There was no significant main effect for loading ($F_{1,23} = 0.17$, $P = 0.68$), however there was for time ($F_{2,23} = 3.67$, $P = 0.04$) on LAMA3 mRNA expression with a significant interaction ($F_{2,23}$

= 3.27, $P = 0.05$). Mean mRNA expression at 30 mins (0.89 ± 0.06) was significantly lower than that at 3 hrs (1.17 ± 0.11 , $t = -2.56$, 95% CI -0.53 to -0.6, $P = 0.02$) with no difference between 30 mins vs. 24 hrs (0.95 ± 0.07 , $t = -0.61$, 95% CI -0.31 to 0.17, $P = 0.55$). Expression was also significantly lower at 3 hrs compared to 24 hrs ($t = -2.01$, 95% CI -0.46 to 0.01, $P = 0.05$) post-loading. There was no significant difference between CON vs. INT at 30 mins (1 ± 0.05 CON vs. 0.75 ± 0.07 INT, $t = -1.53$, 95% CI -0.6 to 0.09, $P = 0.14$) 3 hrs (1.03 ± 0.12 CON vs. 1.32 ± 0.18 INT, $t = 1.84$, 95% CI -0.04 to 0.62, $P = 0.08$) and 24 hrs post-loading (1.02 ± 0.11 CON vs. 0.87 ± 0.09 INT, $t = -0.96$, 95% CI -0.48 to 0.18, $P = 0.35$; see Figure 5.8).

GADD45G

There was no significant main effect for loading ($F_{1,22} = 0.61$, $P = 0.44$) nor time ($F_{2,22} = 1.59$, $P = 0.23$) on GADD45G mRNA expression with no significant interaction ($F_{2,22} = 0.37$, $P = 0.69$). There was no significant difference in mean mRNA expression at 30 mins (1.17 ± 0.05) vs. 3 hrs (1.06 ± 0.04 , $t = 1.28$, 95% CI -0.07 to 0.28, $P = 0.22$) and 24 hrs (1.02 ± 0.07 , $t = 1.74$, 95% CI -0.03 to 0.32, $P = 0.1$) with no difference between 3 and 24 hrs post-loading ($t = -0.5$, 95% CI -0.2 to 0.12, $P = 0.63$). Furthermore, expression did not statistically differ between CON vs. INT at 30 mins (1.14 ± 0.09 CON vs. 1.19 ± 0.06 INT, $t = 0.44$, 95% CI -0.2 to 0.31, $P = 0.67$), 3 hrs (1 ± 0.04 CON vs. 1.12 ± 0.06 INT, $t = 1.07$, 95% CI -0.11 to 0.35, $P = 0.3$) or 24 hrs post-loading (1.03 ± 0.13 CON vs. 1.02 ± 0.07 INT, $t = -0.15$, 95% CI -0.25 to 0.21, $P = 0.88$; see Figure 5.8).

DROSHA

There was a significant main effect for loading ($F_{1,21} = 43.44$, $P < 0.001$) on DROSHA mRNA expression, however, there was no significant main effect for time ($F_{2,21} = 0.81$, $P = 0.46$) with no significant interaction ($F_{2,21} = 0.91$, $P = 0.42$). There was no significant difference in mean mRNA expression at 30 mins (0.81 ± 0.1) vs. 3 hrs (0.83 ± 0.08 , $t = -1.19$, 95% CI -0.25 to 0.07, $P = 0.25$) and 24 hrs (0.74 ± 0.08 , $t = -0.3$, 95% CI -0.19 to 0.14, $P = 0.77$) with no

difference between 3 and 24 hrs post-loading ($t = -0.9$, 95% CI -0.22 to 0.08, $P = 0.36$). Interestingly, transcript expression significantly reduced after INT at 30 mins (1 ± 0.5 CON vs. 0.47 ± 0.08 INT, $t = -4.57$, 95% CI -0.77 to -0.29, $P < 0.001$), 3 hrs (1.02 ± 0.1 CON vs. 0.64 ± 0.04 INT, $t = -3.77$, 95% CI -0.59 to -0.17, $P = 0.001$) and 24 hrs post-loading (0.92 ± 0.11 CON vs. 0.6 ± 0.06 INT, $t = -3.03$, 95% CI -0.55 to -1, $P = 0.01$; see Figure 5.8).

ANK3

There was no significant main effect for loading ($F_{1,23} = 0.32$, $P = 0.58$) nor time ($F_{2,23} = 0.31$, $P = 0.74$) on ANK3 mRNA expression with no significant interaction ($F_{2,23} = 0.13$, $P = 0.88$). There was no significant difference in mean mRNA expression at 30 mins (1.07 ± 0.08) vs. 3 hrs (1.11 ± 0.12 , $t = -0.24$, 95% CI -0.32 to 0.25, $P = 0.81$) and 24 hrs (1 ± 0.07 , $t = 0.51$, 95% CI -0.21 to 0.35, $P = 0.62$) with no difference between 3 and 24 hrs post-loading ($t = -0.77$, 95% CI -0.38 to 0.17, $P = 0.45$). Furthermore, expression was not statistically different between CON vs. INT at 30 mins (1.02 ± 0.11 CON vs. 1.12 ± 0.14 INT, $t = 0.52$, 95% CI -0.31 to 0.52, $P = 0.61$), 3 hrs (1.05 ± 0.17 CON vs. 1.16 ± 0.17 INT, $t = 0.54$, 95% CI -0.29 to 0.49, $P = 0.59$) or 24 hrs post-loading (1.01 ± 0.09 CON vs. 1 ± 0.11 INT, $t = -0.1$, 95% CI -0.41 to 0.37, $P = 0.92$; see Figure 5.8).

SMO

There was a significant main effect for condition/loading ($F_{1,16} = 8.6$, $P = 0.01$) and time ($F_{2,16} = 10.59$, $P = 0.001$) on SMO mRNA expression with a significant interaction ($F_{2,16} = 4.56$, $P = 0.03$). Mean transcript expression at 30 mins (0.81 ± 0.11) post-loading was significantly lower than that at 3 hrs (1.09 ± 0.07 , $t = -2.70$, 95% CI -0.49 to -0.06, $P = 0.02$) and 24 hrs (1.24 ± 0.11 , $t = -4.55$, 95% CI -0.67 to -0.25, $P < 0.001$) with no significant difference between 3 hrs and 24 hrs ($t = 1.78$, 95% CI -0.04 to 0.41, $P = 0.09$). Interestingly, transcript expression was lower after 30 mins (1.01 ± 0.09 CON vs. 0.65 ± 0.16 INT, $t = -2.96$, 95% CI -0.7 to -0.12, $P = 0.01$) and 24 hrs (1.5 ± 0.08 CON vs. 1.05 ± 0.09 INT, $t = -3$, 95% CI -0.76 to -0.13, $P = 0.01$)

post-loading with no difference at 3 hrs (1.03 ± 0.17 CON vs. 1.14 ± 0.03 INT, $t = 0.78$, 95% CI -0.2 to 0.43, $P = 0.45$; see Figure 5.8).

APAF1

There was no significant main effect for condition ($F_{1,18} = 0.58$, $P = 0.46$) nor time ($F_{2,18} = 0.58$, $P = 0.57$) on SMO mRNA expression with no significant interaction ($F_{2,18} = 0.47$, $P = 0.63$). There was no significant difference in mean mRNA at 30 mins (0.98 ± 0.08) vs. 3 hrs (1.04 ± 0.05 , $t = -0.7$, 95% CI -0.27 to 0.13, $P = 0.49$) and 24 hrs (0.94 ± 0.05 , $t = 0.31$, 95% CI -0.16 to 0.2, $P = 0.76$) with no further significant difference between 3 hrs and 24 hrs ($t = -1.07$, 95% CI -0.28 to 0.09, $P = 0.30$). Furthermore, transcript expression did not significantly change after loading at 30 mins (1.02 ± 0.1 CON vs. 1.06 ± 0 INT, $t = -0.65$, 95% CI -0.37 to -0.2, $P = 0.52$), 3 hrs (1.02 ± 0.14 CON vs. 1.06 ± 0.02 INT, $t = 0.32$, 95% CI -0.24 to 0.33, $P = 0.75$) and 24 hrs post-loading (1.01 ± 0.06 CON vs. 0.88 ± 0.08 INT, $t = -1.1$, 95% CI -0.36 to 0.11, $P = 0.28$; see Figure 5.8).

ATM

There was no significant main effect for condition ($F_{1,17} = 0.48$, $P = 0.5$) nor time ($F_{2,17} = 0.43$, $P = 0.66$) on ATM mRNA expression with no significant interaction ($F_{2,17} = 0.49$, $P = 0.62$). There was no significant difference in mean mRNA at 30 mins (0.96 ± 0.04) vs. 3 hrs (1.03 ± 0.04 , $t = -0.91$, 95% CI -0.28 to 0.11, $P = 0.38$) and 24 hrs (0.97 ± 0.06 , $t = -0.31$, 95% CI -0.2 to 0.15, $P = 0.76$) with no further significant difference between 3 hrs and 24 hrs ($t = -0.68$, 95% CI -0.24 to 0.12, $P = 0.51$). Furthermore, transcript expression did not significantly change after INT loading at 30 mins (1.01 ± 0.7 CON vs. 0.89 ± 0.01 INT, $t = -0.94$, 95% CI -0.38 to 0.15, $P = 0.36$), 3 hrs (1 ± 0.06 CON vs. 1.06 ± 0.08 INT, $t = 0.41$, 95% CI -0.23 to 0.34, $P = 0.69$) and 24 hrs post-loading (1.01 ± 0.09 CON vs. 0.93 ± 0.1 INT, $t = -0.79$, 95% CI -0.3 to 0.14, $P = 0.44$; see Figure 5.8).

The current section demonstrates that out of the 12 downregulated/hypermethylated genes identified in chapter 4 that were also assessed after loading in bioengineered SkM, 25% (3; DROSHA, ESR1, SMO) of genes at 30 mins and 33% (4) of genes at 3 (PAX3, AGTR1, DROSHA, NOS2) and 24 hrs (PAX3, AGTR1, DROSHA, SMO) post-loading showed a reduction in mRNA expression, whereas only 1 gene (NOS2) increased at 24 hrs. As with the upregulated/hypomethylated genes assessed after loading in section 5.3.1, data reported herein suggests that gene expression demonstrates the greatest change at 3 hrs post loading with genes showing continuous downregulation at 24 hrs.

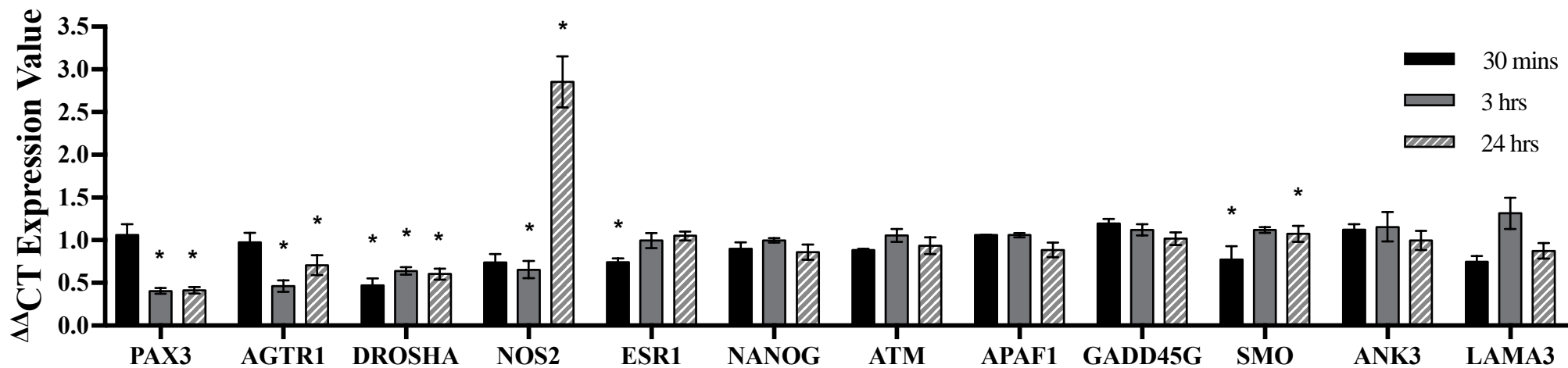


Figure 5.8. mRNA expression of downregulated/hypermethylated genes after loading in bioengineered SkM.

As described in section 5.3.3 above, gene expression of downregulated/hypermethylated genes identified in chapter 4 were assessed at 30 mins, 3 hrs and 24 hrs post mechanical loading in loaded (INT) and non-loaded (CON) bioengineered SkM ($n = 5$ replicate cultures/muscles per condition [CON and INT] and time point [30 mins, 3 and 24 hrs]). (*) depicts significant change in mRNA expression after INT versus CON at the same relative timepoint ($P \leq 0.05$). Data is presented as mean \pm standard error of mean (SEM).

After analysing mRNA expression of downregulated/hypermethylated genes (identified in chapter 4) after mechanical loading in bioengineered SkM alone across all time points (30 mins, 3 and 24 hrs), gene expression at 3 hrs post-loading only was compared to that following acute and chronic loading/RE in human (see section 4.3; Turner *et al.*, 2019b) and rat (Schmoll *et al.*, 2018; Seaborne *et al.*, 2019) SkM, respectively (see Figure 5.9). Interestingly, the majority of downregulated/hypermethylated genes demonstrated significant main effects for the model/species of loading employed. These included; PAX3 ($F_{2,10} = 4.85$, $P = 0.04$), NOS2 ($F_{2,10} = 15$, $P = 0.002$), ESR1 ($F_{2,10} = 8.99$, $P = 0.01$), LAMA3 ($F_{2,10} = 22.12$, $P = 0.001$), GADD45G ($F_{2,10} = 6.32$, $P = 0.02$), DROSHA ($F_{2,10} = 7.65$, $P = 0.01$), ANK3 ($F_{2,10} = 7.04$, $P = 0.02$) and ATM ($F_{2,9} = 14.12$, $P = 0.003$). Therefore AGTR1 ($F_{2,10} = 4.24$, $P = 0.06$) and NANOG ($F_{2,10} = 2.29$, $P = 0.16$) were the only two downregulated/hypermethylated genes that did not display differential gene expression across models of loading (see Figure. 2.9). After main effects were detected, unpaired *t-tests* were performed to determine where main effects occurred for genes; PAX3, NOS2, LAMA3, GADD45G, DROSHA, ANK3 and ATM.

PAX3

There was a significant difference in PAX3 mean expression between bioengineered (0.41 ± 0.03) versus rat (2.27 ± 0.76 ; $t_8 = -2.46$, 95% CI -3.61 to -0.12, $P = 0.04$) and human SkM (-1.06 ± 0 ; $t_4 = -18.24$, 95% CI 1.24 to 1.69, $P < 0.001$). Interestingly however, there was no statistical difference between rat and human SkM (-1.06 ± 0 ; $t_4 = 1.8$, 95% CI -1.81 to 8.47, $P = 0.15$; see Figure 5.9),

NOS2

For NOS2, there was a significant difference in mean gene expression between bioengineered (0.66 ± 0.1) versus rat (1.97 ± 0.34 ; $t_8 = -3.73$, 95% CI -2.13 to -0.5, $P = 0.04$) and human SkM (-1.03 ± 0 ; $t_4 = 6.98$, 95% CI 1.02 to 2.36, $P = 0.002$). Furthermore, NOS2 expression was

significantly lower in human versus rat SkM ($t_4 = 3.62$, 95% CI 0.7 to 5.3, $P = 0.02$; see Figure 5.9).

ESR1

There was no significant difference in ESR1 transcript expression between bioengineered (1 ± 0.09) and rat SkM (1.57 ± 0.37 ; $t_8 = -1.53$, 95% CI -2 to -0.5, $P = 0.04$). However, expression was significantly lower in human (-1.18 ± 0) versus bioengineered ($t_4 = 10.29$, 95% CI 1.59 to 2.77, $P = 0.001$) and rat SkM ($t_4 = 3.07$, 95% CI 0.27 to 5.24, $P = 0.04$) following loading/RE (see Figure 5.9).

LAMA3

There was a significant difference in LAMA3 mRNA expression between bioengineered (1.32 ± 0.18) and rat SkM (0.78 ± 0.11 ; $t_8 = 2.51$, 95% CI 0.04 to 1.03, $P = 0.05$). Transcript expression was also significantly lower in human (-1.13 ± 0) versus bioengineered ($t_4 = 5.47$, 95% CI 1.21 to 3.69, $P = 0.01$) and rat SkM ($t_4 = 7.08$, 95% CI 1.16 to 2.66, $P = 0.002$; see Figure 5.9).

GADD45G

There was a significant difference in GADD45G transcript expression after loading in bioengineered (1.12 ± 0.06) versus rat (1.99 ± 0.56 ; $t_8 = -1.54$, 95% CI -2.16 to 0.43, $P = 0.01$) and human SkM (-1.42 ± 0 ; $t_4 = 16.32$, 95% CI 2.11 to 2.97, $P < 0.001$). However, there was no statistical significance in the loading response for rat versus human SkM ($t_4 = 2.5$, 95% CI -0.38 to 7.19, $P = 0.07$; see Figure 5.9).

DROSHA

There was a significant difference in DROSHA mRNA expression between bioengineered (0.64 ± 0.04) and rat (1.71 ± 0.44 ; $t_8 = -2.42$, 95% CI -2.08 to -0.05, $P < 0.001$) and human

SkM (-1.07 ± 0 ; $t_4 = 15.92$, 95% CI 1.41 to 2.01, $P < 0.001$). Interestingly however, there no statistical difference between rat versus human SkM ($t_4 = 2.59$, 95% CI -0.2 to 5.75, $P = 0.06$; see Figure 5.9).

ANK3

For the ANK3 gene, there was no significant difference in transcript expression between bioengineered (1.16 ± 0.17) and rat SkM (1.41 ± 0.36 ; $t_8 = -0.63$, 95% CI -1.17 to 0.67, $P = 0.15$). Interestingly however, transcript expression was significantly lower in human (-1.17 ± 0) versus bioengineered ($t_4 = 5.49$, 95% CI 1.15 to 3.5, $P = 0.01$) and rat SkM ($t_4 = 2.91$, 95% CI 0.13 to 5, $P = 0.04$) following loading/RE (see Figure 5.9).

ATM

Finally, there was no significant difference in ATM mRNA expression between bioengineered (1.11 ± 0.04) and rat SkM (1.5 ± 0.26 ; $t_7 = -1.29$, 95% CI -1.09 to 0.32, $P = 0.15$). However, transcript expression was significantly lower in human (-1.09 ± 0) versus bioengineered ($t_3 = 23.16$, 95% CI 1.9 to 2.5, $P < 0.01$) and rat SkM ($t_4 = 4.05$, 95% CI 0.81 to 4.36, $P = 0.02$) following loading/RE (see Figure 5.9).

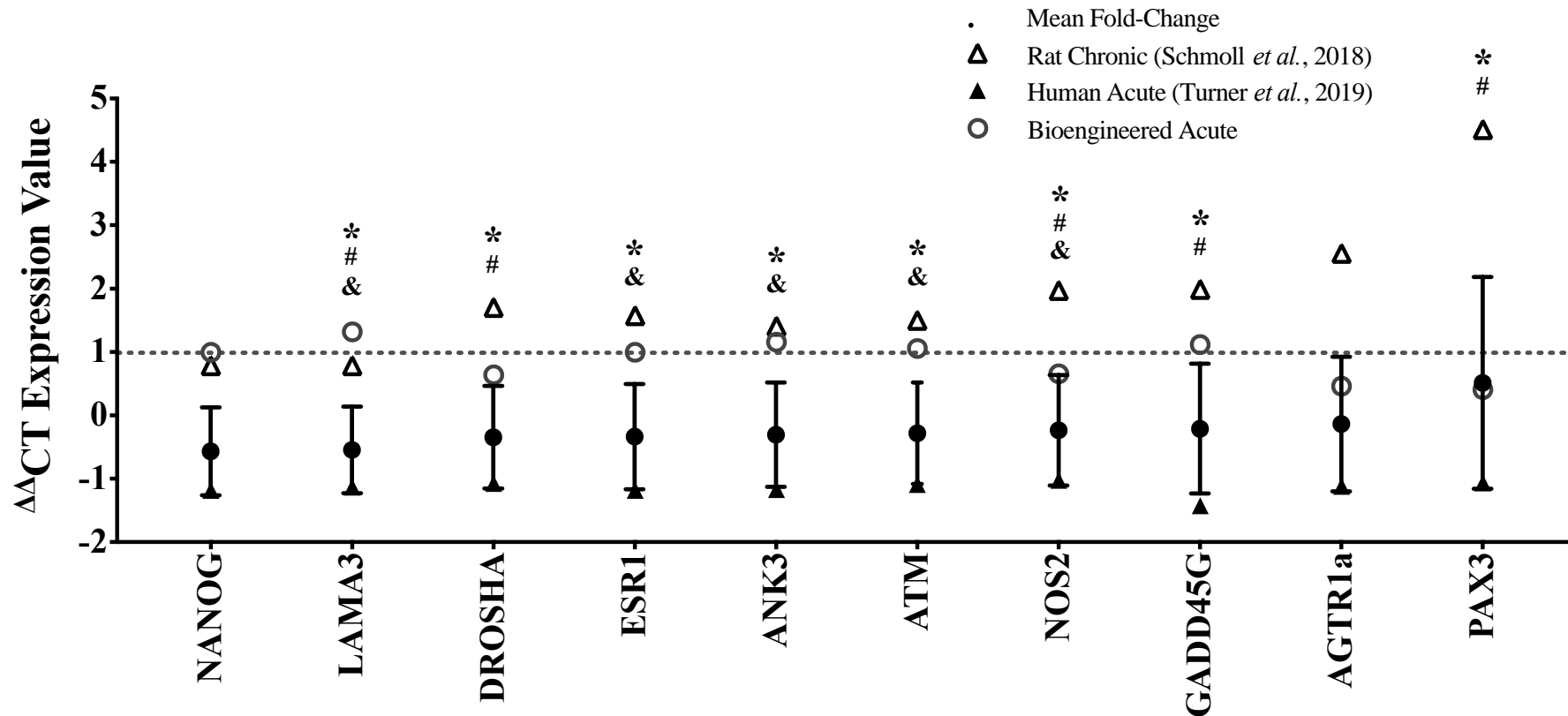


Figure 5.9. Comparison of downregulated/hypermethylated genes identified in chapter 4 after loading/RE in bioengineered, rodent and human SkM.

As described in section 5.3.3 above, mRNA expression of downregulated/hypermethylated genes identified in chapter 4 were compared across various models of loading/RE - bioengineered SkM (clear circles) versus acute RE in humans (bold triangles) and chronic electrical stimulation/RE in rats (clear triangles). Bold circles with errors represent mean \pm SEM for all models of exercise pooled. (*) represents statistical significance ($P \leq 0.05$) between loaded bioengineered SkM versus exercised human SkM; (#) = bioengineered versus stimulated rat SkM; (&) = human versus rat SkM.

5.3.4 Epigenetic Regulation of Downregulated/Hypermethylated Genes After Loading in Bioengineered Skeletal Muscle

After detection of which downregulated/hypomethylated genes (identified in chapter 4) were significantly downregulated at the mRNA level 3 hrs post-acute mechanical loading in bioengineered SkM (see section 5.3.3), the present chapter next wished to determine whether such genes were also epigenetically modified at the DNA methylation level. Transcripts which were most significantly downregulated at the mRNA level at 3 hrs post-loading (see section 5.3.1) were analysed at the methylation level. Specifically, numerous regions of the mouse *AGTR1a* and *PAX3* genes were assessed at 3 hrs post-loading.

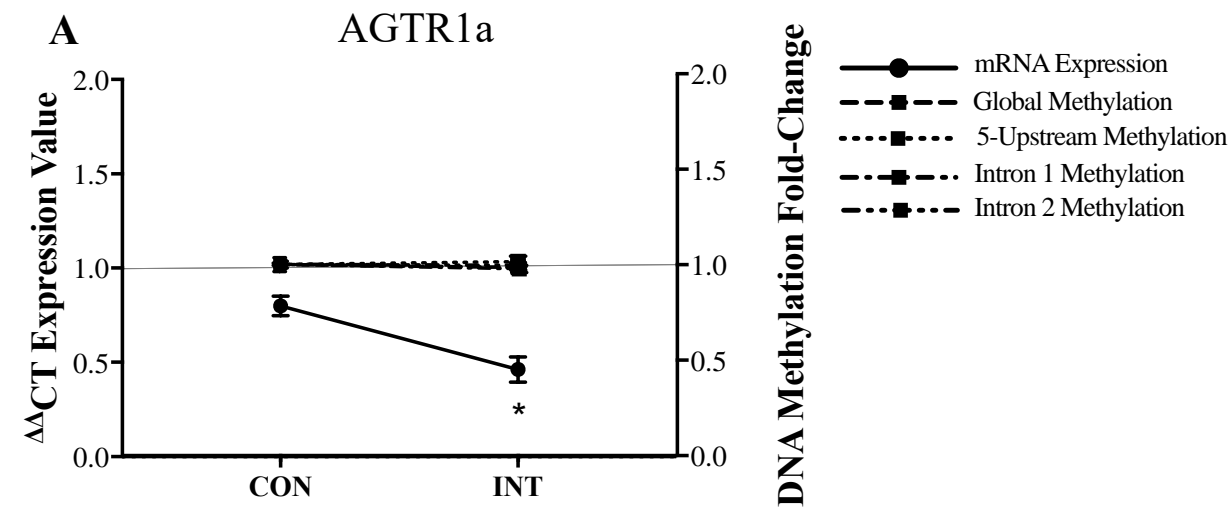
AGTR1a

There was no significant alterations in *AGTR1a* intron 1 (1 ± 0.02 CON vs. 0.98 ± 0.02 INT, $t_{219} = 0.84$, 95% CI -0.03 to 0.08, $P = 0.39$), intron 2 (1 ± 0.01 CON vs. 1 ± 0.01 INT, $t_{76} = 0.31$, 95% CI -0.03 to 0.04, $P = 0.76$) nor 5-upstream (1 ± 0.04 CON vs. 1.02 ± 0.03 INT, $t_{34} = 0.35$, 95% CI -0.11 to 0.08, $P = 0.73$) region-specific DNA methylation after loading. Furthermore, no changes were observed for DNA methylation when all regions assessed (intron 1, intron 2 and 5-upstream) were pooled (1 ± 0.01 CON vs. 0.99 ± 0.01 INT, $t_{333} = 0.78$, 95% CI -0.02 to 0.05, $P = 0.44$; see Figure 5.10A).

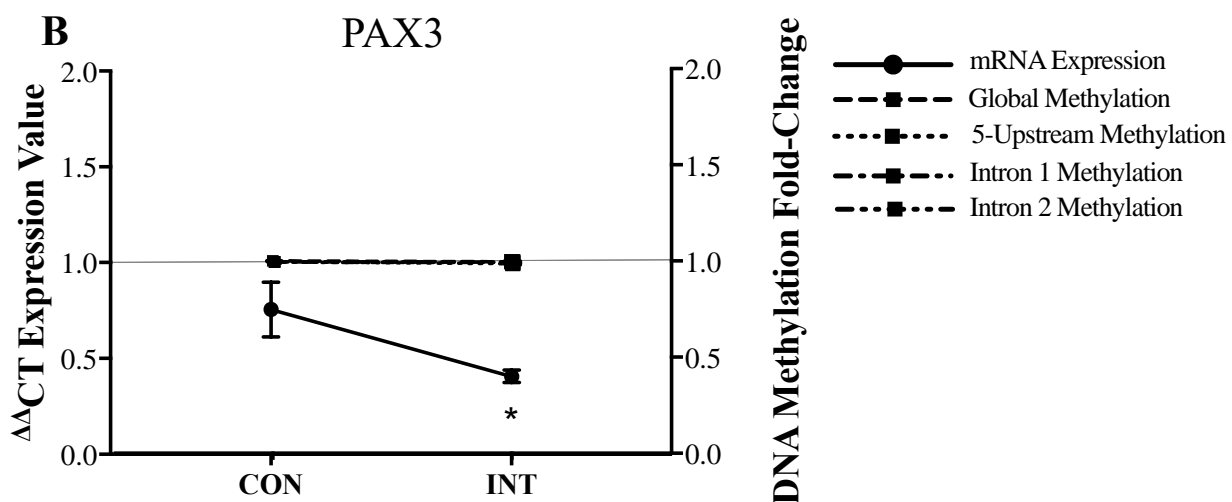
PAX3

There was no significant change in *PAX3* intron 1 (1 ± 0 CON vs. 1 ± 0.01 INT, $t_{178} = 0.15$, 95% CI -0.01 to 0.01, $P = 0.88$), exon 2 (1 ± 0 CON vs. 1 ± 0 INT, $t_{52} = 0.3$, 95% CI -0.01 to 0.01, $P = 0.77$) nor 5-upstream (1 ± 0.01 CON vs. 1 ± 0.01 INT, $t_{250} = 1.06$, 95% CI -0.01 to 0.02, $P = 0.29$) region-specific DNA methylation after loading. Furthermore, no changes were observed for

DNA methylation when all regions assessed (intron 1, exon 2 and 5-upstream) were pooled ($1 \pm 0_{\text{CON}}$ vs. $1 \pm 0_{\text{INT}}$, $t_{484} = 1.01$, 95% CI -0 to 0.01, $P = 0.31$; see Figure 5.10B).



(*) Depicts significantly reduced mRNA expression after loading (INT)



(*) Depicts significantly reduced mRNA expression after loading (INT)

Figure 5.10. mRNA expression and DNA methylation of the most significantly downregulated genes after loading in bioengineered SkM.

mRNA expression and DNA methylation of the most significantly downregulated, (A) AGTR1 and (B) PAX3 in loaded (INT) and non-loaded (CON) bioengineered SkM ($n = 5$ replicate cultures/muscles per condition [CON and INT]) at 3 hrs post-loading. (*) Depicts significant difference ($P \leq 0.05$) in mRNA expression and/or region-specific DNA methylation after INT versus CON with specific changes described in each figure section (A-B). Data is presented as mean \pm standard error of the mean (SEM).

5.3.5 mRNA Expression of Genes that are Significantly Altered After Acute and Chronic Resistance Exercise in Human Skeletal Muscle were Assessed After Mechanical Loading in Bioengineered Muscle

Following mRNA and DNA methylation analysis of regulated genes identified in chapter 4, another subset of genes that were upregulated immediately after acute RE in humans in previous published work by our group (Seaborne *et al.*, 2018a) were also analysed at 30 mins post-loading in engineered muscle. After MANOVA analysis, there was a significant main effect for loading on mRNA expression for all genes combined ($P = 0.01$). Unpaired *t*-tests were then conducted to determine which genes were significantly regulated after loading in engineered SkM.

After just 30 mins post-loading, there was a significant increase in UBR5 ($1 \pm 0.02_{CON}$ vs. $1.77 \pm 0.23_{INT}$; $t_5 = -3.90$, 95% CI -1.28 to -0.26, $P = 0.01$), ODF2 ($1.01 \pm 0.08_{CON}$ vs. $1.93 \pm 0.10_{INT}$, $t_5 = -7.55$, 95% CI -1.24 to -0.61, $P = 0.001$), RSU1 ($0.88 \pm 0.13_{CON}$ vs. $1.65 \pm 0.09_{INT}$, $t_4 = -4.93$, 95% CI -1.2 to -0.34, $P = 0.01$), SETD3 ($0.88 \pm 0.14_{CON}$ vs. $1.48 \pm 0.17_{INT}$, $t_4 = -2.76$, 95% CI -1.2 to 0, $P = 0.05$), GRIK2 ($0.91 \pm 0.03_{CON}$ vs. $1.40 \pm 0.1_{INT}$, $t_4 = -3.56$, 95% CI -0.87 to -0.11, $P = 0.02$), RPL35a ($0.91 \pm 0.05_{CON}$ vs. $1.38 \pm 0.22_{INT}$, $t_4 = -2.12$, 95% CI -1.1 to 0.15, $P = 0.05$) and AXIN1 ($1 \pm 0.05_{CON}$ vs. $1.41 \pm 0.03_{INT}$, $t_5 = -6.5$, 95% CI -0.57 to -0.24, $P = 0.001$) transcript expression at 30 mins post-loading (see Figure 5.11). Although non-significant, there was also an increase in TRAF1 ($1.38 \pm 0.73_{CON}$ vs. $1.74 \pm 1.07_{INT}$, $t_5 = -0.29$, 95% CI -3.55 to 2.83, $P = 0.78$), and STAG1 ($1.04 \pm 0.16_{CON}$ vs. $1.24 \pm 0.2_{INT}$, $t_5 = -0.8$, 95% CI -0.85 to 0.45, $P = 0.46$) with a non-significant reduction in PLA2G16 ($1 \pm 0.05_{CON}$ vs. $0.89 \pm 0.06_{INT}$, $t_5 = 1.47$, 95% CI -0.09 to 0.32, $P = 0.2$) and KLHDC1 ($0.87 \pm 0.1_{CON}$ vs. $0.62 \pm 0.07_{INT}$, $t_4 = 2.03$, 95% CI -0.09 to 0.59, $P = 0.11$) mRNA expression (see Figure 5.11). Furthermore, there was no statistical difference in HEG1 ($1.22 \pm 0.18_{CON}$ vs. $1.38 \pm 0.08_{INT}$, $t_4 = -0.78$, 95% CI -0.7 to 0.39, $P = 0.48$), AFF3 ($1.05 \pm 0.21_{CON}$ vs. $1.19 \pm 0.57_{INT}$, $t_5 = -0.25$, $P = 0.81$, 95% CI -1.52 to 1.25), ZFP2 ($1.03 \pm 0.13_{CON}$ vs. $1.13 \pm 0.07_{INT}$, $t_5 = -0.64$, 95% CI -

0.53 to 0.32, $P = 0.55$) and BICC1 ($1.02 \pm 0.13_{\text{CON}}$ vs. $1 \pm 0.04_{\text{INT}}$, $t_5 = 0.15$, 95% CI -0.38 to 0.42, $P = 0.89$) mRNA expression 30 mins post-loading (see Figure 5.11).

After analysing gene expression in response to acute loading in bioengineered SkM alone, such changes were compared to mRNA expression following acute and chronic RE in humans (Seaborne *et al.*, 2018a) and chronic high-frequency electrical stimulation in rats (Schmoll *et al.*, 2018; Seaborne *et al.*, 2019). Interestingly, there was no significant differences in mRNA across all models of exercise for UBR5 ($F_{3,16} = 0.22$, $P = 0.88$), ODF2 ($F_{3,17} = 1.38$, $P = 0.28$), AXIN1 ($F_{3,18} = 0.5$, $P = 0.69$), RSU1 ($F_{3,14} = 0.46$, $P = 0.72$), HEG1 ($F_{3,12} = 1.24$, $P = 0.32$), TRAF1 ($F_{3,18} = 0.57$, $P = 0.64$), RPL35a ($F_{3,16} = 0.91$, $P = 0.46$), SETD3 ($F_{3,18} = 0.36$, $P = 0.79$), GRIK2 ($F_{3,18} = 0.08$, $P = 0.97$), STAG1 ($F_{3,18} = 0.34$, $P = 0.8$), PLA2G16 ($F_{3,14} = 1.16$, $P = 0.36$), KLHDC1 ($F_{3,13} = 1.41$, $P = 0.29$), AFF3 ($F_{3,19} = 0.42$, $P = 0.74$), BICC1 ($F_{3,15} = 0.04$, $P = 0.99$) and ZFP2 ($F_{3,19} = 0.77$, $P = 0.53$; see Figure 5.11).

The present section demonstrates that almost half (47%; UBR5, ODF2, RSU1, SETD3, GRIK2, RPL35a and AXIN1) of the genes analysed herein displayed a significant increase in mRNA expression at 30 mins post-loading. Interestingly, there was no significant difference in mRNA expression between models of loading/RE, suggestive that mechanical loading of murine bioengineered SkM *in-vitro* demonstrates similar transcriptional responses to loading/RE *in-vivo*.

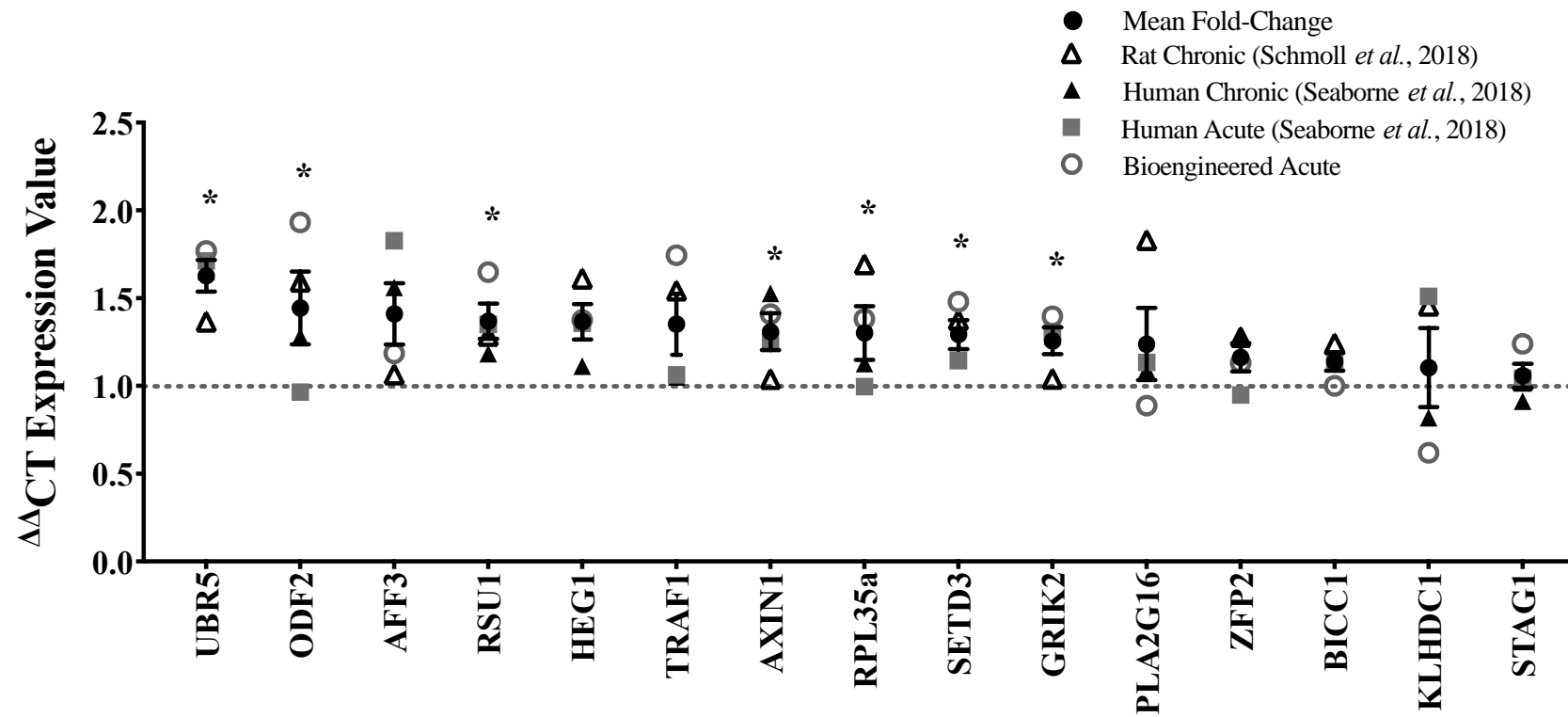


Figure 5.11. Comparison of mRNA expression for genes identified in Seaborne *et al.*, (2018a) after loading/RE in bioengineered, rodent and human SkM

As described in section 5.3.5 above, mRNA expression of regulated genes identified in Seaborne *et al.*, (2018a) after acute and chronic RE in human SkM were compared across various models of loading/RE - bioengineered SkM (clear circles) versus acute (shaded squares) and chronic (bold triangles) RE in humans (Seaborne *et al.*, 2018a) and chronic electrical stimulation/RE in rats (clear triangles; Schmoll *et al.*, 2018). Bold circles with errors represent mean \pm SEM for all models of loading/exercise pooled. (*) Depicts significant increase ($P \leq 0.05$) in transcript expression at 30 mins post-loading in bioengineered SkM alone. There was no significant difference in mRNA expression across all models of loading/RE for any of the genes analysed.

5.3.6 DNA Methylation of Upregulated/Hypomethylated Genes in Bioengineered and Human Skeletal Muscle were Assessed After Loading *In-Vitro*

Given ODF2 (together with UBR5 as discussed in section 5.3.7) was one of the most significantly regulated genes across all models of mechanical loading assessed throughout the present chapter (acute loading/RE in engineered and human SkM, chronic RE in human and rat SkM, see Figure 5.11), the DNA methylation status of this gene was also assessed. Despite no significant change in mRNA expression observed for genes; BICC1, GRIK2, STAG1 and TRAF1 after loading in bioengineered muscle, the DNA methylation was also assessed given these genes were hypomethylated after just one single bout of RE in human SkM, which preceded significant upregulation of mRNA and subsequent muscle hypertrophy after chronic loading in human SkM (Seaborne *et al.*, 2018a).

ODF2

There was no significant difference in ODF2 5-upstream (1 ± 0.01 CON vs. 0.95 ± 0.03 INT, $t_{38} = 1.58$, 95% CI -0.01 to 0.11, $P = 0.12$), 5-UTR (1 ± 0.11 CON vs. 0.83 ± 0.16 INT, $t_{22} = 0.85$, 95% CI -0.24 to 0.57, $P = 0.41$), intron 2 (1 ± 0.02 CON vs. 1 ± 0 INT, $t_{54} = 0.75$, 95% CI -0.07 to 0.06, $P = 0.94$), intron 3 (1 ± 0.01 CON vs. 1 ± 0.01 INT, $t_{30} = 0.81$, 95% CI -0.05 to 0.02, $P = 0.43$) and exon 5 (1 ± 0.01 CON vs. 1 ± 0.01 INT, $t_{30} = 0.81$, 95% CI -0.05 to 0.02, $P = 0.43$) region-specific DNA methylation after loading. Furthermore, there was no statistical difference in DNA methylation when all regions assessed (5-upstream, 5-UTR, intron 2, intron 3 and exon 5) were pooled (1 ± 0.01 CON vs. 0.98 ± 0.02 INT, $t_{222} = 0.94$, 95% CI -0.02 to 0.07, $P = 0.35$; see Figure 5.12A).

BICC1

There was no significant difference in BICC1 intron 1 (1 ± 0.01 CON vs. 0.97 ± 0.01 INT, $t_{86} = 1.74$, 95% CI -0 to 0.06, $P = 0.09$) or 5-upstream (1 ± 0.01 CON vs. 0.98 ± 0.01 INT, $t_{64} = 0.99$, 95% CI -0.02 to 0.06, $P = 0.33$) region-specific DNA methylation after loading. Interestingly

however, *BICC1* was hypomethylated when all regions assessed (intron 1 and 5-upstream) were pooled (1 ± 0.01 CON vs. 0.98 ± 0.01 INT, $t_{152} = 1.96$, 95% CI 0 to 0.05, $P = 0.05$; see Figure 5.12B).

GRIK2

There was no significant difference in *GRIK2* 5-upstream (1 ± 0.09 CON vs. 1.35 ± 0.44 INT, $t_{171} = 0.77$, 95% CI -1.26 to 0.55, $P = 0.44$) or 5-UTR (1 ± 0.19 CON vs. 1.94 ± 0.59 INT, $t_{54} = 1.33$, 95% CI -2.35 to 0.48, $P = 0.19$) region-specific DNA methylation after loading. Interestingly however, *GRIK2* intron 2 was hypomethylated after loading (1 ± 0.17 CON vs. 0.42 ± 0.09 INT, $t_{29} = 2.93$, 95% CI 0.17 to 0.98, $P = 0.01$). Finally, there was no statistical difference in DNA methylation when all regions assessed (5-upstream, 5-UTR and intron 2) were pooled (1 ± 0.07 CON vs. 1.39 ± 0.32 INT, $t_{258} = 1.13$, 95% CI -1.06 to 0.29, $P = 0.26$; see Figure 5.12C).

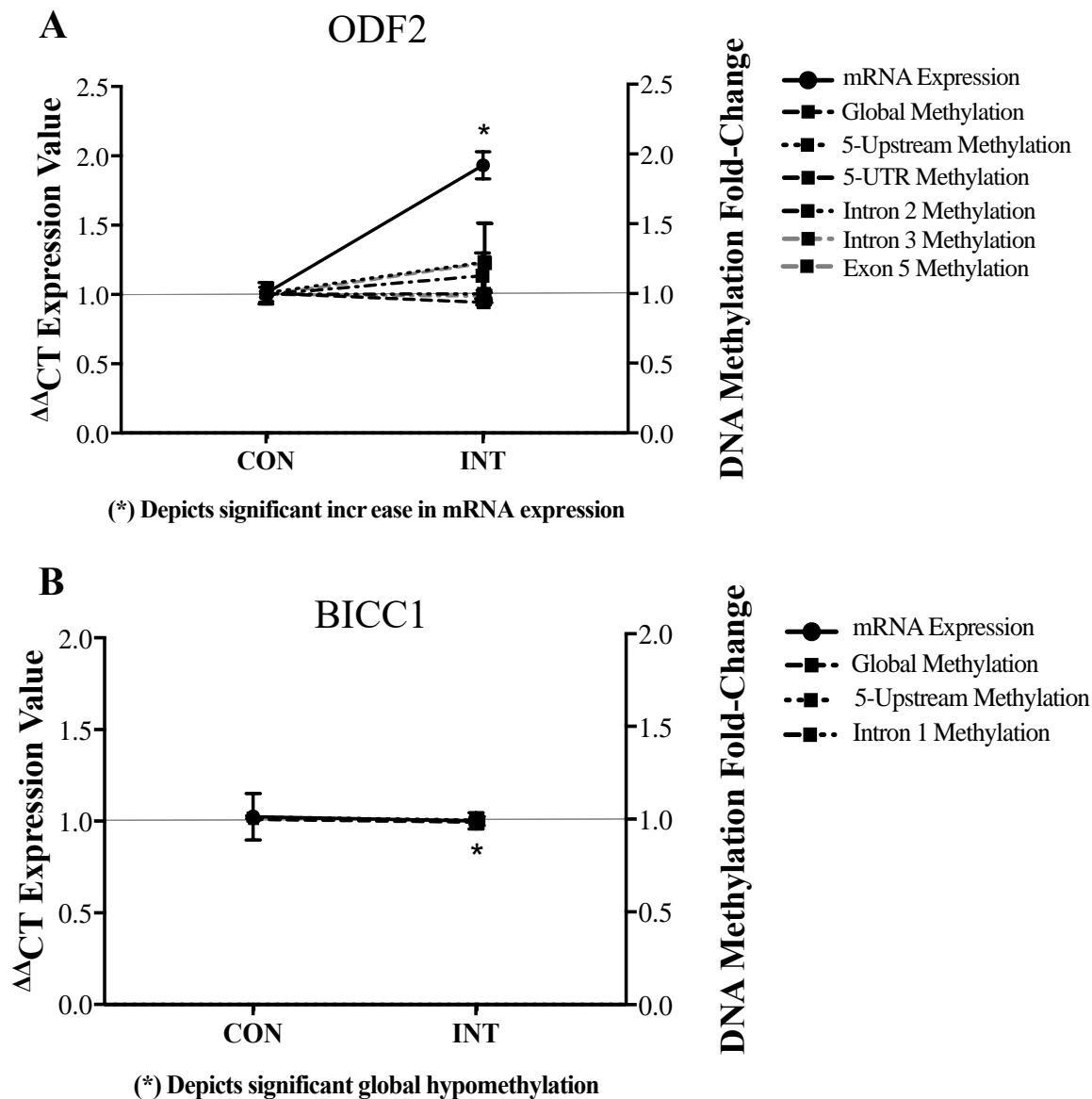
STAG1

There was no significant difference in *STAG1* 5-upstream (1 ± 0.63 CON vs. 2.32 ± 1.52 INT, $t_{11} = 0.65$, 95% CI -5.75 to 3.11, $P = 0.53$), 5-UTR (1 ± 0.26 CON vs. 1.05 ± 0.32 INT, $t_{62} = 0.11$, 95% CI -0.87 to 0.77, $P = 0.91$), intron 1 (1 ± 0.2 CON vs. 1.39 ± 0.76 INT, $t_{104} = 0.46$, 95% CI -2.03 to 1.26, $P = 0.64$), region-specific DNA methylation after loading. Furthermore, there was no statistical difference in DNA methylation when all regions assessed (5-upstream, 5-UTR and intron 1) were pooled (1 ± 0.2 CON vs. 1.35 ± 0.47 INT, $t_{181} = 0.68$, 95% CI -1.37 to 0.67, $P = 0.5$; see Figure 5.12D).

TRAF1

There was no significant difference in *TRAF1* intron 2 (1 ± 0.24 CON vs. 0.83 ± 0.15 INT, $t_{22} = 0.58$, 95% CI -0.43 to 0.76, $P = 0.57$) nor intron 3 (1 ± 0.03 CON vs. 0.96 ± 0.04 INT, $t_{62} = 0.74$, 95% CI -0.06 to 0.14, $P = 0.46$) region-specific DNA methylation after loading. Interestingly however, *TRAF1* 5-upstream was hypermethylated after loading (1 ± 0.04 CON vs. 1.14 ± 0.04

INT, $t_{62} = 2.48$, 95% CI -0.26 to -0.03, $P = 0.02$). Finally, there was no statistical difference in DNA methylation when all regions assessed (5-upstream, 5-UTR and intron 2) were pooled (1 ± 0.04 CON vs. 1.02 ± 0.04 INT, $t_{150} = 0.33$, 95% CI -0.13 to 0.09, $P = 0.74$; see Figure 5.12E).



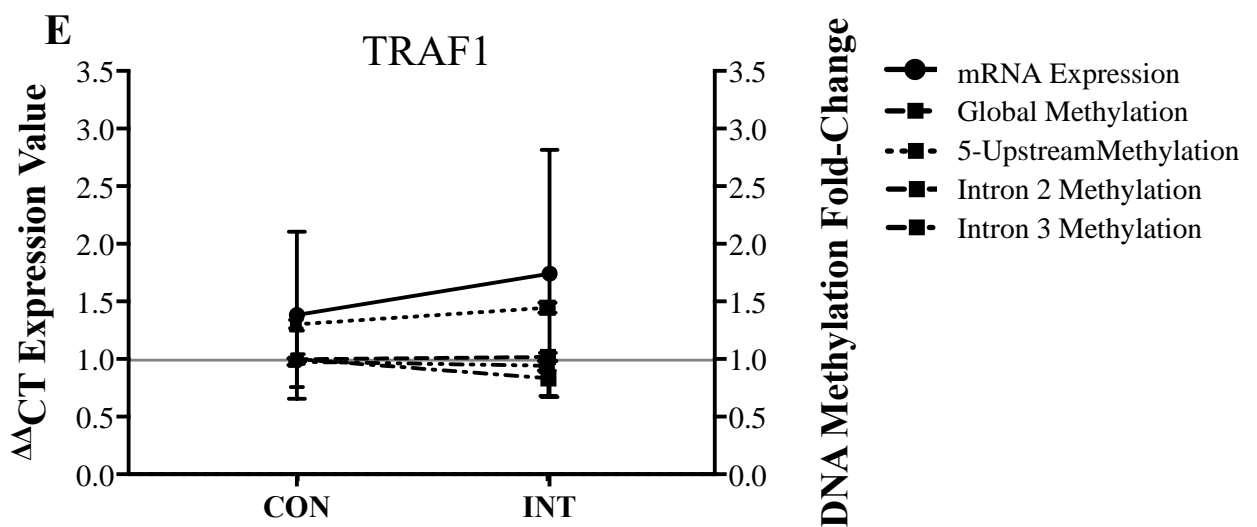
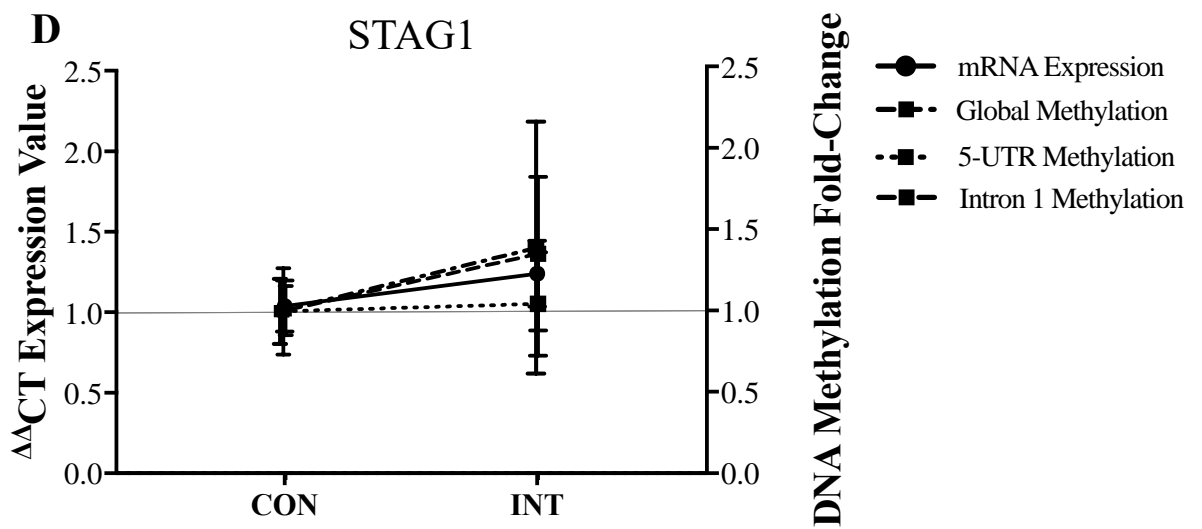
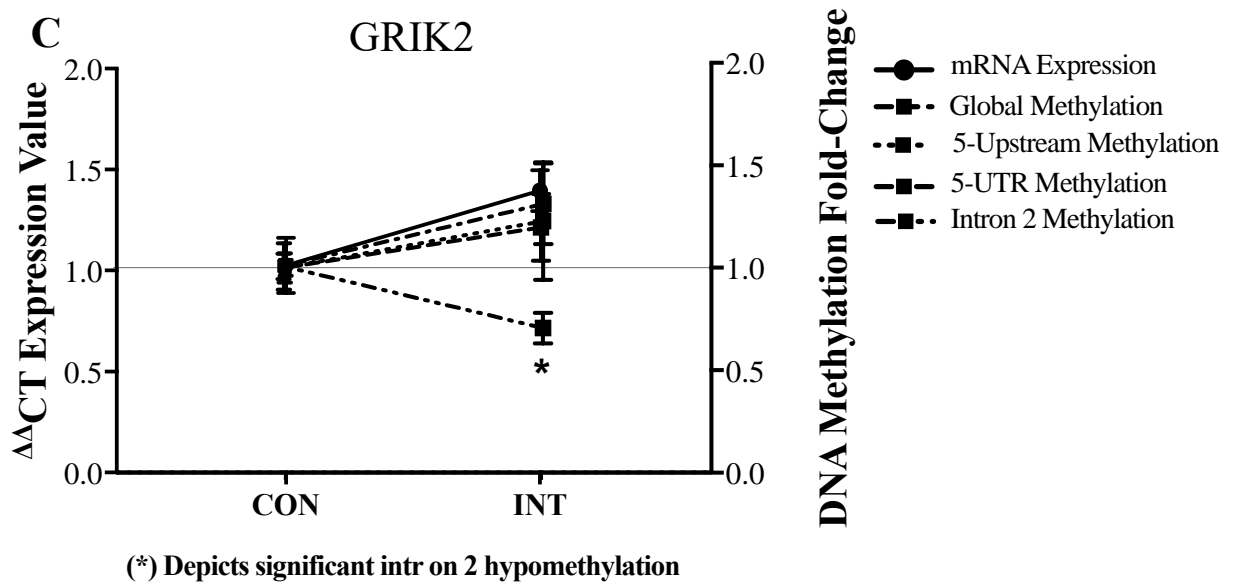


Figure 5.12. mRNA expression and DNA methylation of regulated genes after RE in human SkM were assessed after loading in bioengineered SkM

mRNA expression and DNA methylation of genes identified in (Seaborne *et al.*, 2018a) - (A) ODF2, (B) BICC1, (C) GRIK2, (D) STAG1 and (E) TRAF1 in loaded (INT) and non-loaded (CON) bioengineered SkM ($n = 5$ replicate cultures/muscles per condition [CON and INT]) at 30 mins post-loading. (*) Depicts significant difference ($P \leq 0.05$) in mRNA expression and/or region-specific DNA methylation after INT versus CON with specific changes described in each figure section (A-E). Data is presented as mean \pm standard error of mean (SEM).

5.3.7 mRNA Expression and DNA Methylation of the Most Significantly Upregulated Gene Across All Models of Loading

As discussed in section 5.3.5, UBR5 was the most significantly upregulated transcript across all models of loading/exercise (see Figure 5.11). Specifically at 30 mins post-acute loading in human and bioengineered SkM and also following chronic RE/high-frequency electrical stimulation in human and rat SkM (Schmoll *et al.*, 2018; Seaborne *et al.*, 2018a, 2019). Therefore, UBR5 mRNA expression was further assessed at 3 and 24 hrs post-loading.

UBR5 mRNA Expression

There was a significant main effect for loading ($F_{1,17} = 33.14$, $P < 0.001$) and time ($F_{2,17} = 12.57$, $P < 0.001$) on UBR5 expression with a significant interaction ($F_{2,17} = 12.11$, $P = 0.001$). Mean mRNA expression at 30 mins (1.33 ± 0.18) was significantly greater than that at 24 hrs (1 ± 0.05 , $t = 2.85$, 95% CI 0.1 to 0.67, $P = 0.01$) post-loading with no significant difference between 30 mins vs. 3 hrs (1.69 ± 0.33 ; $t = -2$, 95% CI -0.63 to 0.02, $P = 0.06$). Furthermore, mean expression was significantly greater at 3 vs. 24 hrs ($t = -4.91$, 95% CI -0.99 to -0.39, $P < 0.001$). Mechanical loading elicited a significant increase in UBR5 expression at 30 mins (1 ± 0.02 CON vs. 1.77 ± 0.23 INT, $t = 3.70$, 95% CI 0.33 to 1.21, $P = 0.002$) and 3 hrs (1.05 ± 0.22 CON vs. 2.34 ± 0.26 INT, $t = 5.81$, 95% CI 0.82 to 1.76, $P < 0.001$) with no change at 24 hrs post-

loading (1.02 ± 0.1 CON vs. 0.98 ± 0.03 INT, $t = -0.27$, 95% CI -0.41 to 0.32, $P = 0.79$; see Figure 5.13).

UBR5 DNA Methylation 30 mins Post-loading

Given UBR5 exponentially increased at the mRNA level at 30 mins and 3 hrs with no change at 24 hrs post-loading (see Figure 5.2 and data above in section 5.3.7), the DNA methylation status at 30 mins and 3 hrs post-loading was assessed. At 30 mins post-loading, there was no significant difference in UBR5 5-upstream (1 ± 0.19 CON vs. 1.18 ± 0.36 INT, $t = 0.44$, 95% CI -0.99 to 0.63, $P = 0.66$) or intron 1 (1 ± 0.01 CON vs. 1.01 ± 0.02 INT, $t = 0.41$, 95% CI -0.05 to 0.03, $P = 0.68$) region-specific DNA methylation or when regions assessed (5-upstream and intron 1) were pooled (1 ± 0.04 CON vs. 1.05 ± 0.08 INT, $t = 0.51$, 95% CI -0.22 to 0.13, $P = 0.61$; see Figure 5.13).

UBR5 DNA Methylation 3 hrs Post-loading

There was no significant difference in UBR5 5-upstream (1 ± 0.09 CON vs. 1.12 ± 0.13 INT, $t = 0.68$, 95% CI -0.46 to 0.22, $P = 0.50$) or intron 1 (1 ± 0.03 CON vs. 1.04 ± 0.03 INT, $t = 0.95$, 95% CI -0.12 to 0.04, $P = 0.34$) region-specific DNA methylation after loading with also no statistical difference in DNA methylation when regions 5-upstream and intron 1 were pooled (1 ± 0.03 CON vs. 1.05 ± 0.03 INT, $t = 1.16$, 95% CI -0.14 to 0.04, $P = 0.25$; see Figure 5.13).

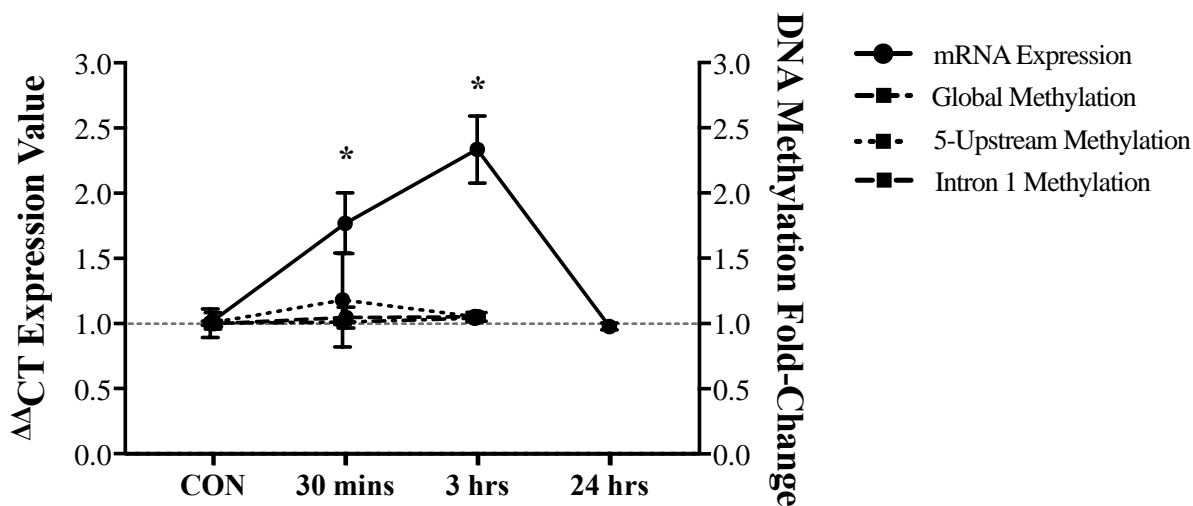


Figure 5.13. UBR5 mRNA expression and DNA methylation after mechanical loading in bioengineered SkM

UBR5 was the most significantly upregulated transcript after loading in bioengineered SkM alone (see Figure 5.2) and across all models of RE (see Figure 5.11). Therefore, region specific DNA methylation was assessed at 30 mins and 3 hrs post-loading in bioengineered SkM which was then mapped against changes in mRNA expression at 30 mins, 3 and 24 hrs post-loading ($n = 5$ replicate cultures/muscles per condition [CON and INT] and timepoint). (*) Depicts significant upregulation of UBR5 at 30 mins and 3 hrs post-loading ($P \leq 0.05$). Data is presented as mean \pm standard error of mean (SEM).

After analysing region-specific DNA methylation, $6 \times$ CpG sites in the intron 1 region of the were also assessed in order to investigate CpG-specific DNA methylation. There was a non-significant increase in CpG-7 (1 ± 0.08 CON vs. 2.42 ± 0.88 INT, $t_5 = 1.91$, 95% CI -3.33 to 0.49, $P = 0.12$), -8 (1 ± 0.12 CON vs. 1.79 ± 0.55 INT, $t_5 = 1.63$, 95% CI -2.04 to 0.46, $P = 0.16$), -9 (1 ± 0.34 CON vs. 2.67 ± 0.94 INT, $t_5 = 1.88$, 95% CI -3.94 to 0.61, $P = 0.12$) and -11 (1 ± 0.04 CON vs. 1.82 ± 0.44 INT, $t_5 = 2.17$, 95% CI -1.79 to 0.15, $P = 0.08$) intron 1 methylation (see Figure 14). Despite a reduction in methylation at CpG-10, such changes did not reach statistical significance (1 ± 0.14 CON vs. 0.61 ± 0.32 INT, $t_5 = 1.26$, 95% CI -0.41 to 0.18, $P = 0.27$). Interestingly however, CpG-6 (1 ± 0.1 CON vs. 2.04 ± 0.33 INT, $t_5 = 3.48$, 95% CI -1.8 to -0.27,

$P = 0.02$) was significantly hypermethylated, alongside all CpG sites (6-11) combined (1 ± 0.1 CON vs. 1.89 ± 0.24 INT, $t_{47} = 4.16$, 95% CI -1.32 to -0.46, $P < 0.001$) at 30 mins post-loading (see Figure 5.14).

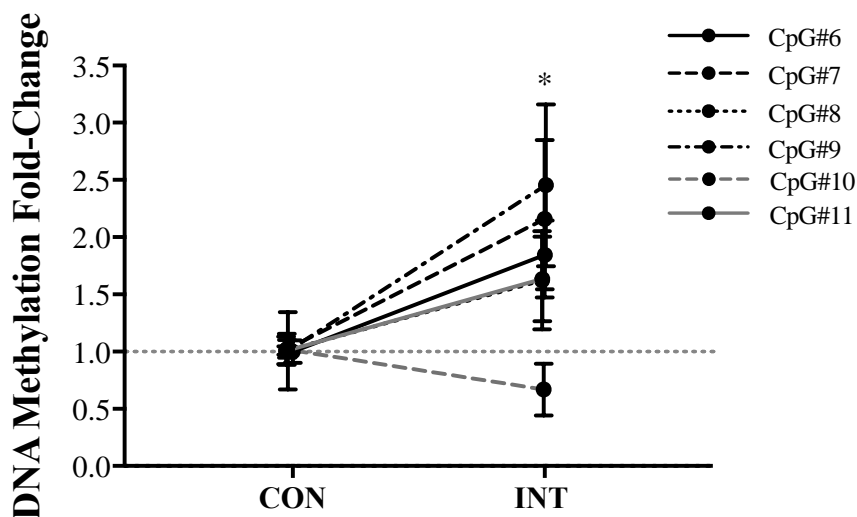


Figure 5.14. CpG-specific DNA methylation of UBR5 after loading in bioengineered SkM
CpG-specific DNA methylation (pyrosequencing) in the intron 1 region of UBR5 at 30 mins post mechanical loading in bioengineered SkM ($n = 5$ replicate cultures/muscle per condition [CON and INT]). (*) Depicts significant hypermethylation on CpG-6 and when all CpG's assessed (6-11) were pooled ($P \leq 0.05$). Date published in Seaborne *et al.*, (2019).

5.4 Discussion

In the present chapter, mRNA expression and DNA methylation of a number of frequently regulated genes across the human transcriptome and methylome after acute RE identified in chapter 4 and previous work by our group (Seaborne *et al.*, 2018a) were analysed in response to acute mechanical loading in murine bioengineered fibrin SkM to determine whether mechanical loading of bioengineered SkM somewhat mimics the molecular responses after loading/RE *in-vivo*. Similar observations would subsequently validate the use of the bioengineered SkM model described throughout this thesis when attempting to delineate novel transcript and epigenetic mechanisms involved in SkM adaptation after RE in future studies.

5.4.1 mRNA Expression of Upregulated/Hypomethylated Genes After Acute Resistance Exercise in Humans were Assessed Following Mechanical Loading in Bioengineered Skeletal Muscle

Transcript expression of a number of genes that were upregulated and hypomethylated across the pooled transcriptome after acute RE in humans (as described in chapter 4) were assessed in response to mechanical loading in bioengineered SkM. Specifically, expression of genes involved in ECM/actin structure/remodelling, mechano-transduction, protein synthesis, TGF- β /calcium/retinoic/IL-6 signalling, methylation and tumour suppression were examined.

Out of the 22 genes that were upregulated and hypomethylated across the human transcriptome and methylome in chapter 4 and were analysed after mechanical loading in the present chapter, 22% (5; THBS1, CD63, GSK3 β , WNT9a, ADCY3) of genes displayed a reduction in mRNA expression at 30 mins post-loading. At 3 hrs post-acute loading, 33% (7; MSN, TIMP3, ITGB3, GSK3 β , WNT9a, DOT1L, KDR) of genes increased whereas 14% (3; THBS1, FOS, ADCY3) decreased with the remaining genes showing no statistical change. Finally, 1 gene (TIMP3) increased at 24 hrs post-loading, however 19% (4; MSN, CRK, ITPR3 F2LR3) decreased with the remainder of genes showing no significant change in transcript expression. As described in section 4.4.1 of this thesis, ITGB3 (integrin subunit beta-3) is an ECM protein binding receptor and is involved in migration of craniofacial muscle cells (Sinanan *et al.*, 2008) and is also increased after acute RE (3 \times 12 reps at 70% 1-RM on leg press and extension exercises) in young but not old human SkM (Wessner *et al.*, 2019). KDR (also known as kinase insert domain receptor) is a major VEGF receptor (specifically VEGFR-2) involved in angiogenesis and has been shown to increase following submaximal aerobic exercise (45 min of cycling at 50% VO_{2max}) in both young and aged individuals (Ryan *et al.*, 2006) and also in lengthening TA muscle post osteotomy in mice (Nishisho *et al.*, 2012). MSN (or moesin) is a member of the ezrin-radixin-moesin (ERM) protein family and is an important actin-plasma membrane crosslinker, associated with dystrophy myopathies (Pines *et al.*, 2017). Furthermore, the

methylation status of moesin has also been reported in active and sedentary aged individuals whereby those whom participated in frequent exercise throughout their life span displayed hypomethylation relative to those who were less active (Sailani *et al.*, 2019). As discussed in chapter 4 of this thesis, TIMP3 (tissue inhibitor of metalloproteinase 3) is part of the TIMP protein family which contributes to ECM turnover and is downregulated during C₂C₁₂ muscle differentiation and also in regenerating CTX-injured and overloaded soleus mouse muscle (Liu *et al.*, 2010b). Such findings are interesting given TIMP3 was significantly upregulated and hypomethylated after acute RE in humans (see chapter 4 of this thesis) and also increased at the transcript level expression after acute mechanical loading in C₂C₁₂ engineered SkM in the present chapter. Discrepancies observed in TIMP3 expression between models of loading therefore suggests that following the initial increase immediately post-loading, TIMP3 is subsequently reduced to enable MMP activity to assist in initiating the ECM remodelling and hypertrophic response observed after functional overload (Zhang *et al.*, 2014). GSK3 β (Glycogen synthase kinase-3 beta) is an important MPS regulator, downstream of Akt (Glass, 2003) and is key for muscle (C₂C₁₂) differentiation (Litwiniuk *et al.*, 2016). Furthermore, GSK3 β protein phosphorylation is increased and decreased during hypertrophy and atrophy, respectively in human SkM (Léger *et al.*, 2006). Moreover, basal GSK3 β protein content is greater in lifelong aged physically active versus physically inactive aged human SkM, although no difference was observed in promoter-related DNA methylation (Sailani *et al.*, 2019). As described in section 4.4.2 of this thesis, WNT9a which functions via the canonical Wnt/beta-catenin signalling pathway has been demonstrated to be key during SkM development both at the transcript (Zhang *et al.*, 2018) and DNA methylation level (Zhang *et al.*, 2019a).

5.4.2 DNA Methylation of Upregulated/Hypomethylated Genes After Acute Resistance Exercise in Humans were Assessed Following Mechanical Loading in Bioengineered Skeletal Muscle

The genes analysed for DNA methylation were carefully considered according to the reported changes in gene expression after loading or due to their well-characterised regulatory role in SkM after RE *in-vivo*. Firstly, the methylation status of genes, MSN and WNT9a, at 3 hrs post-loading were analysed given the mRNA expression of these genes displayed the greatest increase relative to all other upregulated/hypomethylated genes (identified in chapter 4) after loading (see section 5.3.1). Whilst DNA methylation of the actin crosslinker MSN is altered in SkM of lifelong active individuals and WNT9a changes during muscle development (see section 4.4.1 and 5.4.2), the present chapter is the first to report the epigenetic response of these genes after mechanical loading. Interestingly, no change was observed in methylation for WNT9a, however, MSN global (5-upstream and intron 1/2 combined) and intron 1 methylation increased 3 hrs post-loading (see Figure 5.7). DNA methylation of TIMP3 and GSK3 β was also analysed on the basis that these genes are important for SkM ECM remodelling and protein synthesis, respectively (see section 4.4.1 and 5.4.2). As with WNT9a, there were no significant changes in DNA methylation for TIMP3 and GSK3 β (see Figure 5.7). Despite the non-significant increase in CTTN observed after loading in the present chapter, this gene is important for actin cytoskeleton remodelling and together with FLNB, was 1 of 23 genes highlighted in chapter 4 that was significantly upregulated and hypomethylated after both acute and chronic RE (Turner *et al.*, 2019b). Similarly, to MSN, the CTTN intron 1 region was significantly hypermethylated after loading with no change in 5-UTR or intron 2 region-specific methylation nor when all regions assessed were pooled (see Figure 5.7).

5.4.3 mRNA Expression of Downregulated/Hypermethylated Genes After Acute Resistance Exercise in Humans were Assessed Following Mechanical Loading in Bioengineered Skeletal Muscle

Out of the 12 genes that were downregulated and hypermethylated across the human transcriptome and methylome in chapter 4 and were also assessed after mechanical loading in the present chapter, 25% (3; DROSHA, ESR1, SMO) significantly reduced at 30 mins whereas mRNA expression in 33% (4) of genes decreased at both 3 (PAX3, AGTR1, DROSHA, NOS2) and 24 hrs (PAX3, AGTR1, DROSHA, SMO) post-loading in bioengineered SkM. No genes significantly increased at 30 mins and 3 hrs post-loading. However, only 1 gene (NOS2) significantly increased at 24 hrs post-loading (see Figure 5.8). Genes which significantly reduced after loading included; AGTR1a, PAX3, NOS2, ESR1, DROSHA and SMO. Their roles (or lack of) in SkM are described in section 4.4.3 of this thesis. Briefly, AGTR1 is an angiotensin receptor (angiotensin II receptor type I) displaying mechano-sensitive properties in various cells types (Zou *et al.*, 2004; Yasuda *et al.*, 2008). In SkM, AGTR1 knock-down prolonged life-span and improved repair and regeneration after injury in rodents (Yabumoto *et al.*, 2015). Therefore, reduced AGTR1 mRNA expression during regeneration and across the human transcriptome after acute RE in chapter 4 and after acute loading in bioengineered muscle in the present chapter suggests an important role for this gene in anabolism and regeneration in human and rodent SkM. PAX3 (paired box 3) is highly expressed in SkM satellite cells and determines myogenic stem cell fate via activation of the MRF, myoD (Relaix *et al.*, 2005, 2006). NOS2 (nitric oxide synthase 2 or inducible nitric oxide) produces nitric oxide and is expressed during SkM development and in adult SkM tissue subject to inflammation (Rigamonti *et al.*, 2013). Indeed, it has been demonstrated that NOS2 is exclusively expressed in macrophages infiltrating regenerating SkM following CTX-induced muscle damage in mice (Rigamonti *et al.*, 2013). Furthermore, basal NOS2 protein expression is significantly greater in old vs. young sedentary rat gastrocnemius muscle which also supports the notion that NOS2 is abundant in inflamed tissue (Song *et al.*, 2009). Interestingly however,

NOS2 expression was significantly reduced after chronic exercise (treadmill running at 75% VO_{2max} , 1 hr/day, 5 days/week for 12 weeks) in aged, as well as young rats (Song *et al.*, 2009), supporting findings observed in the present study that NOS2 is reduced after exercise. ESR1 is an estrogen receptor 1 and is associated with muscle weakness in female mice with ESR1 deletion (Collins *et al.*, 2018), yet, overexpression results in a slow muscle phenotype (Chen *et al.*, 2016). Given RE typically increases size and abundance of type II fibres, it seems logical that a reduction was observed after RE in humans (see chapter 4) and loading in engineered SkM. SMO (Smoothed, Frizzled Class Receptor), a G-protein receptor involved in signal transduction is highly expressed in developing SkM tissue and myotubes (Elia *et al.*, 2007). DROSHA (also known as Drosha Ribonuclease III) is important for formation of miRNA's (Lee *et al.*, 2003) and is increased at the mRNA level after acute aerobic exercise (Russell *et al.*, 2013). Given DROSHA was increased after RE/loading in human and bioengineered SkM suggests that regulation of this gene may be dependent on the specific stimulus the muscle is subjected to (i.e. mode of exercise performed).

5.4.4 DNA Methylation of Downregulated/Hypermethylated Genes After Acute Resistance Exercise in Humans were Assessed Following Mechanical Loading in Bioengineered Skeletal Muscle

After detection of which downregulated/hypomethylated genes (identified in chapter 4) were also downregulated at the mRNA level 3 hrs post-acute mechanical loading in bioengineered SkM (see section 5.4.3), the DNA methylation status of the most significantly downregulated genes at the mRNA level at 3 hrs post-loading were assessed. Specifically, PAX3 and AGTR1a were analysed at the DNA methylation level. Interestingly, previous studies demonstrated increased methylation of PAX3 in human rhabdomyosarcoma muscle tissue (Kurmasheva *et al.*, 2005) and SkM myoblasts (Tsumagari *et al.*, 2013). Additionally, promoter-associated DNA hypermethylation of AGTR1 has also been reported in lung tumour, but not healthy tissue (Chen *et al.*, 2017). With the exception of the work conducted in chapter 4 of this thesis, nobody

has yet reported the methylation patterns of both PAX3 and AGTR1 in response to RE/mechanical loading. The present chapter is therefore the first to determine DNA methylation after loading, specifically in engineered SkM. Despite PAX3 and AGTR1 displaying the greatest differential transcript expression after loading in the present chapter and their known hypermethylated profiles in malignant tissue, no changes in region-specific (5'-upstream, intron 1/2) or global (all regions assessed pooled) DNA methylation was observed for both genes.

5.4.5 mRNA Expression of Genes that are Significantly Altered After Acute and Chronic Resistance Exercise in Humans were Assessed After Mechanical Loading in Bioengineered Muscle

After analysing genes that were both upregulated/hypomethylated and downregulated/hypermethylated across the human transcriptome and methylome after acute RE (see chapter 4), genes that were significantly regulated in previous work by our group after RE (Seaborne *et al.*, 2018a) were also analysed following mechanical loading in bioengineered SkM. Specifically, mRNA expression of genes including; UBR5, ODF2, AFF3, RSU1, HEG1, TRAF1, AXIN1, RPL35a, SETD3, GRIK2, PLA2G16, ZFP2, BICC1, KLHDC1 and STAG1 were assessed at 30 mins post-loading in engineered SkM. This timepoint was selected due to muscle biopsies being taken immediately post (~30 mins) RE in human SkM (Seaborne *et al.*, 2018a). Interestingly, almost half (47%) of these genes were significantly upregulated at 30 mins post-loading in bioengineered SkM with the remaining 53% showing no statistical change in transcript expression. Specifically, genes UBR5, ODF2, RSU1, SETD3, GRIK2, RPL35a and AXIN1 displayed differential mRNA expression 30 mins post-loading.

ODF2 (also known as outer dense fibre of sperm tails 2) is a major component of the sperm tail cytoskeletal structure and is important for embryonic development (Salmon *et al.*, 2006). Furthermore, ODF2 mRNA expression was highest in quiescent (G0 phase) mouse NIH3T3

fibroblast cells with minimal expression during the G1/G2 phase of the cell cycle (Pletz *et al.*, 2013). However, to the authors knowledge, no previous research has reported ODF2 expression during myogenesis, nor in SkM tissue after RE (with the exception of previous work by our group which identified ODF2 as upregulated and hypomethylated after RE Seaborne *et al.*, 2018a). RSU1 (ras suppressor protein 1) is involved in ras-specific signal transduction and integrin adhesion complexes. In SkM, overexpression of ras has been shown to inhibit myotube formation and MHC protein expression in 10TI/2 cells whereas treatment with MyoD expression vector displayed distinct myotubes after 48 hrs of treatment (Mitin *et al.*, 2001). Therefore, an increase in RSU1 observed after acute loading in bioengineered SkM and RE in humans (Seaborne *et al.*, 2018a) may suggest that a reduction in Ras1 signalling may subsequently permit regeneration of myotubes/SkM tissue after loading. Interestingly, recent work has demonstrated that RSU1 knockdown in the drosophila/fruit fly results in a reduction and an increase myofibre diameter and sarcomere length, respectively and regulates PINCH activity which is important for integrin adhesion in the myotendinous junction of flight muscles. Furthermore, recent work has also shown that RSU1 is downregulated in atherosclerotic human VSMCs (Fasehee *et al.*, 2019) and that RSU1 regulates AChR distribution in *C. elegans* muscle cells (Pierron *et al.*, 2016). Previous work by our group demonstrated that SETD3 (SET Domain Containing 3) gene expression correlated with changes in SkM hypertrophy in human muscle after RE (Seaborne *et al.*, 2018a). Indeed, mRNA increased after load-induced hypertrophy which reduced to basal levels after 7 weeks unloading (Seaborne *et al.*, 2018a). Furthermore, mRNA increased to a greater extent after chronic reloading (where the greatest increase in hypertrophy was observed) which coincided with a reduction in DNA methylation. SETD3 is a H3K4/H3K36 methyltransferase and is expressed in high abundance in SkM (Eom *et al.*, 2011). Overexpressing SETD3 has been shown to enhance C₂C₁₂ muscle differentiation via activation of muscle creatine kinase and the MRF, myogenin and Myf6 (or MRF4; Eom *et al.*, 2011). Conversely, shRNA-induced inhibition of SETD3 negatively affected myoblast differentiation (Eom *et al.*, 2011) which may be regulated by two specific miRNA's, miR-15b

and miR-322, shown to target the 3-UTR of SETD3 and subsequently repress its mRNA expression (Zhao *et al.*, 2019). Collectively, these results suggest that SETD3 is important for SkM regeneration which may explain the increase in expression observed post mechanical loading in the present chapter. As with SETD3, RPL35a (ribosomal protein L35a) was also associated with SkM hypertrophy following RE exercise in humans whereby mRNA expression and DNA methylation somewhat increased and decreased, respectively to the greatest level after 7 weeks of retraining (Seaborne *et al.*, 2018a). RPL35a is part of the ribosomal 60S large subunit, essential for the translation of proteins. Two-hybrid yeast screening revealed a protein-protein interaction between RPL35a and CMYA1 (aka Xin) in bovine SkM (Xin *et al.*, 2017). XIN is an actin binding protein involved in SkM development. Under normal conditions, this gene is expressed in the myotendinous junction, albeit, was localised in SkM satellite cells of damaged single EDL myofibres with significant increase in mRNA expression ~2 days post CTX (Hawke *et al.*, 2007). These findings therefore suggest the importance of XIN in muscle regeneration, which was later confirmed by the same group whereby shRNA-induced silencing in mouse TA muscle ablated muscle regeneration post CTX injury, evidenced by expression of the embryonic MYHC (MYHC-3) and reduced myofibre size (Nissar *et al.*, 2012). In regards to exercise, work from the same lab also reported significantly increased XIN expression 24 hrs post eccentric exercise (300 × maximal eccentric quadriceps lengthening contractions) in healthy human VL muscle (Nilsson *et al.*, 2013). Taken together, the increase in RPL35a mRNA expression observed within the present chapter suggests a potential role in regeneration via interacting with CMYA1/XIN post-loading in bioengineered mouse SkM. However, future studies investigating the expression of CMYA1/XIN and other interacting proteins post-loading is warranted. GRIK2 (glutamate ionotropic receptor kainate type subunit 2) is a member of the glutamate receptor kainate family, composed of four subunits which function as ligand-activated ion channels (Han *et al.*, 2010). Previous work by our group demonstrated that GRIK2 was one of four genes which was hypomethylated after just one single bout of RE in humans and that changes in DNA methylation preceded upregulation of gene transcription after the first

and second periods of chronic RE (Seaborne *et al.*, 2018a). Suggestive that acutely regulated DNA methylation changes determined subsequent transcript expression after repeated RE. Finally, AXIN1 was also significantly upregulated after acute loading in the present chapter (see Figure 5.11) and was also upregulated and hypomethylated after training and later retraining in human SkM (Seaborne *et al.*, 2018a). AXIN1 (together with AXIN2) is a major component of the β -catenin destruction complex and inhibits WNT signalling (Figeac & Zammit, 2015). Furthermore, AXIN1 is abundantly expressed in proliferating primary and C₂C₁₂ muscle cells compared to differentiated cells whereby siRNA AXIN1 knockdown significantly inhibited cell proliferation (Figeac & Zammit, 2015; Huraskin *et al.*, 2016). Previous and current data within the present chapter therefore suggests that upregulation of AXIN1 may assist in initiating the SkM regeneration process after mechanical loading/RE.

5.4.6 DNA methylation of Upregulated/Hypomethylated Genes in Bioengineered and Human Skeletal Muscle were Assessed After Loading *In-Vitro*

After assessing the mRNA expression of significantly regulated genes after acute and chronic RE in humans as described in section 5.4.3, the DNA methylation status of the most significantly upregulated genes were assessed. Specifically, this included genes UBR5 and ODF2 which were not only the most significantly upregulated genes after loading in bioengineered SkM but also displayed the greatest mean increase in expression across all models of loading (i.e. acute/chronic RE in humans and rats). Interestingly however, no changes in DNA methylation was observed for both ODF2 (see Figure 5.12) or UBR5 (see section 4.5.7). It is important to note that UBR5 methylation was not significantly altered after acute RE in humans, albeit was significantly hypomethylated after chronic RE (Seaborne *et al.*, 2018a, 2019), suggestive that repetitive loading stimuli may be required for inducing significant changes in UBR5 DNA methylation. However, further work is required to determine UBR5 DNA methylation after chronic loading in bioengineered SkM.

Despite a non-significant change in mRNA expression of genes, STAG1, TRAF1 and BICC1 in engineered SkM after acute loading in the present chapter (see section 5.4.5), previous work demonstrated similar non-significant changes in mRNA after acute RE *in-vivo* (Seaborne *et al.*, 2018a). Interestingly however, these genes (together with GRIK2) were hypomethylated after just one single bout of exercise which preceded increased transcript expression after chronic RE (Seaborne *et al.*, 2018a). The DNA methylation status of TRAF1, STAG1, BICC1 and GRIK2 after loading in bioengineered SkM was therefore determined. TRAF1 (TNF receptor associated factor 1) encodes a member of the inflammatory cytokine TNF- α receptor family which together with TRAF2, regulates MAPK, JNK and NF- κ B activation (Pomerantz, 1999). *In-vivo*, TNF- α significantly increased following exercise-induced muscle damage (2 \times 5 min bouts of downhill running at 10% decline, 85% VO_{2max}) which correlated with increased Pax7⁺ cell number (Van De Vyver & Myburgh, 2012). Furthermore, the associated increase in satellite cell number after exercise was ablated in response to NSAID administration following a 36-km run in male endurance athletes (Mackey *et al.*, 2007), suggestive that the acute TNF- α inflammatory cytokine response after exercise is crucial for initiating the myogenic regeneration process. Indeed, administration of TNF- α in cultured primary and C₂C₁₂ SkM cells increases myoblast proliferation via ERK, JNK and P38 MAPK signalling (Foulstone *et al.*, 2004; Li *et al.*, 2005), however chronic exposure inhibits myoblast differentiation and promotes myotube atrophy in C₂C₁₂ myoblasts, due to a reduction in IGF1 and myogenin expression and increased FoxO3 (Girven *et al.*, 2016) and Atrogin 1/MAFbx (Li *et al.*, 2005) mRNA expression. Furthermore, previous work by our group also demonstrated that early TNF- α administration in low passaged C₂C₁₂ cells exacerbated the reduction in myotube formation when cells having undergone 30 population doubling cells were retreated with TNF- α , which coincided with increased and decreased MyoD DNA methylation and mRNA expression, respectively (Sharples *et al.*, 2016a). Suggestive that gene expression and morphology may be determined by early changes observed in DNA methylation. Interestingly however, TRAF1, specifically the 5-upstream region was hypermethylated in the present chapter after acute

loading in engineered muscle (see Figure 5.12). Suggestive that TRAF1 may not change or even decrease at the mRNA level if engineered muscle was subject to chronic loading given promoter-specific methylation is able to suppress corresponding mRNA expression of the same gene after exercise (Barrès *et al.*, 2012; Seaborne *et al.*, 2018a). STAG1 (aka stromal antigen 1) DNA methylation was also assessed after mechanical loading in bioengineered SkM and displayed no statistically significant change in region-specific (5-upstream, 5-UTR and intron 1) or pooled methylation (see Figure 5.12). STAG1 is part of the cohesin complex, critical for the cohesion of sister chromatids and segregation of chromosomes during mitosis, and is responsive to DNA damage in HeLa cells (Kong *et al.*, 2014). With the exception of previous work by our group following RE in humans (Seaborne *et al.*, 2018a), there is limited research suggesting a role for STAG1 in SkM regulation at the cellular and tissue level. Finally, the DNA methylation status of BICC1 and GRIK2 was also reported in the present chapter. BICC1 (bicaudal C homolog 1) is an RNA-binding protein and is involved in embryonic development, specifically during the formation of the mesoderm of which SkM is derived (Zhang *et al.*, 2005). Moreover, BICC1 transcript expression was reported in prenatal developing muscle in two different pig breeds (Muráni *et al.*, 2007). Interestingly, BICC1 displayed hypomethylation after mechanical loading when 5-upstream and intron 1 regions were pooled (see Figure 5.12). Such findings observed in the present chapter, together with those following RE *in-vivo* (Seaborne *et al.*, 2018a) suggests DNA methylation may precede changes in mRNA, and that upregulation in transcript expression may occur if engineered muscle was subjected to chronic intermittent loading, particularly if the gene remained hypomethylated. However, mRNA expression and DNA methylation patterns after repeated loading in bioengineered SkM requires further investigation. Finally, GRIK2, specifically the intron 2 region was hypomethylated after loading in bioengineered SkM which coincided with upregulation of transcript expression (see Figure 5.12). As discussed in section 5.4.5, GRIK2 is a member of the glutamate receptor family with no defined role in SkM. However, upregulation and hypomethylation of GRIK2 after 3D loading in the present chapter and in response to acute and chronic RE in humans

(Seaborne *et al.*, 2018a) suggests an important mechano-sensory role of this gene in murine engineered and human SkM *in-situ*.

5.4.7 mRNA Expression and DNA Methylation of the Most Significantly Upregulated Gene Across All Models of Loading

In the present chapter, UBR5 was the most significantly upregulated transcript across all models of RE (see Figure 5.10), displaying an exponential increase in mRNA at 30 mins and 3 hrs post-loading (see Figure 5.13). Specifically, at 30 mins post-acute loading in human and bioengineered SkM and also following chronic RE/high-frequency electrical stimulation in human and rat SkM (Schmoll *et al.*, 2018; Seaborne *et al.*, 2018a). Together with ODF2, UBR5 was the most significantly upregulated transcript at 30 mins post-loading and also demonstrated the greatest increase at 3 hrs post (see Figure 5.14). As with MuRF-1 and MAFbx, UBR5 is also an E3 ubiquitin ligase. However, MuRF-1 and MAFbx contain a RING domain while UBR5 contains a HECT domain, both of which differ in how they catalyse ubiquitin to their protein substrates. Indeed, E3 RING finger proteins act as a scaffold to bring E2 ubiquitin-conjugating enzymes to the protein substrates together whereas E3 HECT domain ligases directly catalyses attachment of ubiquitin to the protein substrate (Bodine & Baehr, 2014). Unlike RING domain E3 proteins, the roles of HECT E3 ligases in SkM adaptation have only recently begun to emerge (Seaborne *et al.*, 2018a, 2019). Indeed, previous work by our group demonstrated a significant increase in UBR5 mRNA expression after exercise-induced hypertrophy and anabolism in humans (Seaborne *et al.*, 2018a) and rodents (Seaborne *et al.*, 2019). Furthermore, recent work by our group demonstrated a reduction and an increase in UBR5 expression during periods of muscle atrophy and recovery from atrophy, respectively (Seaborne *et al.*, 2019), suggesting an opposing role to the atrophy associated E3 ligases, MuRF1 and MAFbx which increased with atrophy but did not change during recovery from atrophy. The increase in mRNA expression observed in the present chapter after 3D loading further supports the notion that UBR5 may indeed be an important anabolic regulator of SkM

after RE/loading. It is also worth noting that despite no change observed in DNA methylation (see Figures 5.13 and 5.14) after loading in the present chapter, methylation also did not significantly change after acute RE in human SkM (Seaborne *et al.*, 2018a, 2019). Indeed, DNA methylation significantly increased after chronic RE only (Seaborne *et al.*, 2018a), suggestive that continuous loading in engineered muscle may be required to potentially evoke changes in UBR5 methylation. However, DNA methylation after chronic mechanical loading chronic in bioengineered SkM warrants future investigation.

5.5 Limitations

It is worth acknowledging the limitations of the present chapter. Firstly, mRNA expression of regulated genes across the human transcriptome and methylome identified in chapter 4 were assessed at 30 mins, 3 hrs and 24 hrs post-loading in bioengineered muscle whereas pooled expression from the myriad of transcriptome studies was derived from biopsy samples taken immediately post *in-vivo* exercise to ~24 hrs post exercise making direct comparisons between loaded engineered muscle and RE *in-vivo* more complex. Furthermore, engineered SkM in the present chapter was subjected to mechanical loading alone and therefore represents a model of intermittent eccentric lengthening contraction only, with no concentric portion induced via electrical stimulation, therefore neglecting the importance of a replicative neural input which has been shown to elicit an anabolic and hypertrophic response in human fibrin bioengineered SkM (Khodabukus *et al.*, 2018a). This may somewhat explain the limited alterations observed in DNA methylation. Future studies should therefore ascertain transcript expression and DNA methylation of genes described herein after electrical stimulation alone, alongside simultaneous mechanical loading to more closely mimic a muscle contraction *in-vivo*. Moreover, future studies should wish to assess the transcriptional and epigenetic status of genes known to be regulated after chronic RE in humans (Seaborne *et al.*, 2018a; Turner *et al.*, 2019b) following chronic loading in engineered SkM. This would enable the identification of whether changes in

DNA methylation precede alterations in mRNA in engineered SkM that ultimately leads to hypertrophy as seen following chronic RE in humans (Seaborne *et al.*, 2018a).

5.6 Conclusion

Data obtained within the present chapter suggests that mechanical loading of bioengineered SkM alone is sufficient for inducing changes in mRNA expression of genes which were significantly regulated at the mRNA and/or DNA level after acute RE in human SkM (Seaborne *et al.*, 2018a). However, acute loading alone displayed limited changes in DNA methylation, potentially suggesting a need for chronic repetitive loading and/or an electrical input as described in section 5.5. Interestingly, UBR5 presented the greatest increase in mRNA expression after mechanical loading alone and across all additional models of exercise employed, indicative that mechanical loading of bioengineered SkM alone may be a useful *in-vitro* model for characterising potential novel anabolic mechano-responsive genes at the mRNA level.

CHAPTER 6

The Mechanistic Role of UBR5 in Response to Mechanical Loading in Human Myotubes

6.1 Introduction

In chapter 5, the ubiquitin protein ligase E3 component n-recognin 5 (UBR5 aka EDD1) gene displayed the greatest change in mRNA expression after mechanical loading in fibrin bioengineered SkM alone and also when all models of loading/resistance exercise (RE) across species were compared (i.e. acute and chronic loading/RE in humans and chronic high frequency electrical stimulation/RE in rats; Schmoll *et al.*, 2018; Seaborne *et al.*, 2018a, 2019). As discussed extensively in section 5.4.7 of this thesis, UBR5 is an E3 ubiquitin ligase containing a HECT domain which directly catalyses ubiquitin to the target protein substrate. UBR5 therefore functionally differs from RING-finger domain E3 ubiquitin ligases which act as a scaffold to bring E2-conjugating enzymes and the protein substrate together for recognition and subsequent degradation within the 26S proteasome system.

In SkM, UBR5 mRNA expression increased after just one bout of acute RE, which exponentially increased to a greater extent following several weeks of training and retraining in human SkM (Seaborne *et al.*, 2018a), suggestive that UBR5 may have opposing roles in SkM to the well-characterised RING finger E3-ubiquitin ligases, MuRF1 (Trim63) and MAFbx/Atrogin 1 (Fbxo32) which are associated with SkM atrophy (Bodine *et al.*, 2001a; Bodine & Baehr, 2014). Furthermore, recent work by our group supported this hypothesis demonstrating that UBR5 significantly increased after acute loading in bioengineered SkM and in response to synergistic ablation or chronic electrical stimulation-induced hypertrophy in rodent muscle with no change in MuRF-1 and MAFbx expression (Seaborne *et al.*, 2019). Moreover, UBR5 also increased during recovery from hindlimb unloading (HU) and tetrodotoxin (TTX)-induced atrophy, with no increase in MuRF1 and MAFbx during recovery from atrophy (Seaborne *et al.*, 2019), further supporting the notion that UBR5 may contribute to the fundamental hypertrophic processes following anabolic stimuli and recovery following catabolic stimuli. Despite previous work demonstrating significant upregulation of UBR5 in human, rodent and murine bioengineered SkM after mechanical loading/RE, the loading

response in human myotubes has not been characterised. Furthermore, the manipulation of UBR5 using gene silencing technology in the presence and/or absence of mechanical loading is required to further investigate and confirm its mechanistic role both *in-vivo* and *in-vitro*.

6.1.1 Aims and Objectives

As UBR5 increased to the greatest extent at the transcriptional level across human, rodent tissue and in murine bioengineered SkM models of loading/RE in chapter 5, the present chapter first aimed to ascertain UBR5 gene expression after loading in human myotubes. The present chapter then aimed to induce gene-specific knockdown (via siRNA) of UBR5 during mechanical loading in attempt to further confirm its mechanistic role in response to acute loading *in-vitro*. In previous chapters, a murine self-assembling fibrin engineered SkM models was employed to investigate the transcriptional and epigenetic responses to loading in C₂C₁₂ cells. In the present chapter however, myotubes were differentiated and loaded in monolayer to overcome many of the technical challenges (i.e. high seeding densities and inter-individual maturation capacity/rates) of producing human self-assembled fibrin bioengineered SkM and transfecting myotubes embedded within a surrounding fibrin matrix. Given UBR5 significantly increased in various models of loading/RE in chapter 5, it was hypothesised that mechanical loading of human myotubes would upregulate UBR5 gene expression, and that silencing of UBR5 would prevent the load-induced increase in mRNA, ultimately impairing the anabolic response to loading in human myotubes (assessed by global protein synthesis measures via puromycin incorporation).

6.2 Materials and Methods

6.2.1 Cell Culture

HMDCs were derived from SkM biopsies obtained from the vastus lateralis (VL) muscle of consenting young males as described in section 2.2.2. Donor information is also detailed in

Table 2.1. After collection of SkM tissue, samples were transported to the cell culture laboratory for subsequent cell isolations (see section 2.2.2) and serial passaging (see section 2.2.3) to increase cell yield. Once expanded, cells were trypsinised (see section 2.2.3), counted (see section 2.2.4) and reseeded onto fibronectin (10 µg/ml in 1× PBS) coated 6-well plastic (for the 0 hr time point) or flexible-bottomed BioFlex[®] (for the 3 hr +/- loading timepoint/condition) culture plates at a concentration of 9×10^4 cells/ml in 2 ml of HGM as described in section 6.2.3. Once ~80% confluency was attained (typically ~48 hrs), cells were rinsed 2 × with PBS and switched to low serum HDM to promote differentiation of HMDCs into multinucleated myotubes over the ensuing 10 days (see section 2.2.7 and Figure 2.2). HDM was topped up with 1 ml at 72 hrs and 7 days. Once mature, myotubes were dosed with either siRNA or fresh HDM (see section 6.2.2).

6.2.2 Dosing of Human Myotubes

As described in section 2.3.2, myotubes were dosed with 4 × synthetic siRNAs (see Table 2) targeting various regions of the UBR5 human gene to maximise transcriptional gene silencing (see Figure 2.5). For the initial validation experiment, myotubes were subjected to 1 of 4 conditions. Specifically, myotubes were dosed with 2 ml HDM containing either; 10 nmol Flexitube GeneSolutions[™] (siUBR5) and 12 µl HiPerFectTransfection[™] (transfection reagent), 10 nmol AllStars Negative Control siRNA[™] (siScram) and 12 µl transfection reagent, transfection reagent alone or HDM alone for the non-treated group (see Section 2.3.2 and Figure 6.1). Myotubes were then incubated for 3 hrs before lysing for subsequent RNA isolation and qRT-PCR to quantify UBR5 gene expression (see section 6.2.4). Due to the low knockdown efficiency after dosing with 10 nmol within the validation experiments ($-25.72 \pm 4.72\%$), siRNA concentrations were increased to 20 nmol during subsequent experiments which enabled a reduction in UBR5 gene expression by $77.39 \pm 0.74\%$ after 3 hrs incubation (see Figure 6.1).

6.2.3 Mechanical Loading of Human Myotubes

BioFlex[®] culture plates containing treated/non-treated myotubes were assembled to the Flexcell[®] FX-5000[™] system housed in a humidified incubator at 37°C, 5% CO₂ for subsequent loading as described in section 2.6.3. Once assembled, myotubes were subjected to a low frequency (0.15 Hz with sine wave; see Figure 2.11) intermittent loading (10%) regime (INT) similar to that employed when loading bioengineered SkM in chapters 3 and 5. Specifically, the loading protocol consisted of 4 × 10 reps which represented 1 of 5 ‘exercises’. Each set was interspersed with a 90 s rest whereas each exercise was separated with 3.5 mins rest where myotubes were kept at resting length. Non-loaded cells acting as controls (CON) were also assembled to the Flexcell[®] base plate, however, the vacuum entry was sealed with tape to avoid any unwanted loading. Cells cultured on BioFlex[®] culture plates were incubated for a further 3 hrs post-loading. Cells grown on 6-well plastic culture plates were incubated during the stretch regime (37°C, 5% CO₂) and were lysed for RNA (see section 6.2.4) and protein (see section 6.2.5) at 30 mins (0 hrs) post-loading.

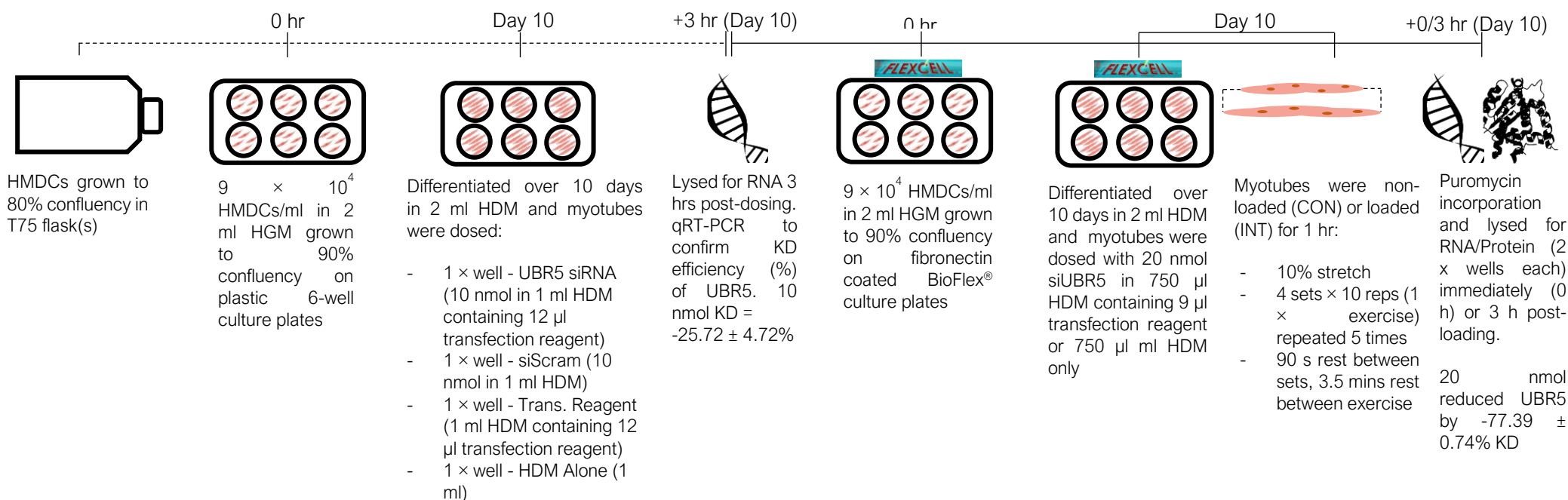


Figure 6.1. Schematic representation of siUBR5 experimental procedures

The dotted timeline depicts initial siRNA validation experiment whereby dosing with 10 nmol siUBR5 resulted in $-25.72 \pm 4.72\%$ KD at 3 hrs post-treatment ($n = 3$ per condition [CON/INT] and treatment [HDM/siUBR5] at each timepoint [0/3 hrs]). The solid line indicates repetition of experiments with higher 20 nmol siUBR5 dose +(INT) / -(CON) loading and RNA and protein was isolated at 0 and 3 hrs post resulting in a $-77.39 \pm 0.74\%$ reduction of UBR5 mRNA expression at 3 hrs.

6.2.4 RNA Extraction and Quantitative Real-Time Polymerase Chain Reaction

(qRT-PCR)

Following the relevant incubation period post-loading (0/3 hrs), existing media was aspirated and myotubes were washed $2 \times$ in PBS before lysing with 300 μ l TRIzol (section 2.8.1) for subsequent RNA extraction (see section 3.2.5). RNA concentrations (76.64 ± 57.94 ng/ μ l) and purities (A_{260}/A_{280} ratio, 1.91 ± 0.22) were then quantified using a spectrophotometer (see section 2.9.3). After RNA quantification, samples were diluted in nuclease-free H₂O to ensure a concentration of 35 ng in 10 μ l reactions, made up of: 4.75 μ l (7.37 ng/ μ l) RNA sample, 5.25 μ l of master mix (MM), composed of 5 μ l SYBR green, 0.1 μ l of reverse transcriptase (RT) mix and 0.075 μ l of both forward and reverse primers. Alternatively, sample '003' was diluted in nuclease-free H₂O to ensure a total 35 ng RNA reaction, however due to a lower concentration:volume ratio for this sample, reactions were prepared in a total volume of 20 μ l: 9.5 μ l (3.68 ng/ μ l) RNA, mixed with 10.5 μ l of MM with components adjusted accordingly (10 μ l SYBR green, 0.2 μ l RT mix and 0.15 μ l of both forward/reverse primers for 10.5 μ l total MM). All primer sequences and location information for the genes analysed are described in Table 6.1. PCR reactions were then transferred to a thermal cycler for amplification (see section 2.9.4.2) and subsequent quantification of gene expression using the DDCT ($\Delta\Delta C_T$) equation (Schmittgen & Livak, 2008) against the mean of 2 reference genes (B2M and RPL13a, 15.33 ± 0.7 with low variation of 4.56%) and the mean C_T value derived from the HDM non-treated group for each time point (0/3 hrs) and condition (CON/INT; see section 2.9.4.3). Alternatively, all samples were relativised to the mean of the 2 reference genes and non-treated HDM cells at 0 hrs post-loading only. The PCR efficiencies were similar for reference genes, RPL13a ($97.4 \pm 7.75\%$, with 7.96% variation) and B2M ($92.08 \pm 3.18\%$, with 3.46% variation), and UBR5 ($90.93 \pm 4.94\%$, with 5.43% variation).

Table 6.1. Human primer sequences for genes analysed

UBR5 mRNA expression was relativised to the mean C_T value for reference genes, RPL13a and B2M

Target Gene	Primer Sequence (5'-3')	Product Length (bp)	Reference Seq. Number
UBR5	F: AGGCAACACCTTAGGAAGC	81	NM_015902.6
	R: GCTCCAGCTGATGACCTAC		XM_024447179.1
			XM_024447178.1
			XM_011517106.3
			XM_017013534.2
			XM_017013533.2
			XM_011517105.3
			XM_011517104.3
			NM_001282873.1
RPL13a	F: GGCTAAACAGGTACTGCTGGG	104	NM_012423.4
	R: GGAAAGCCAGGTACTTCAACTT		
B2M	F: CCGTGTGAACCATGTGACT	91	NM_004048.3
	R: TGCGGCATCTTCAAACCT		

6.2.5 Puromycin Incorporation and SDS-PAGE

After 0 and 3 hrs incubation post-loading, myotubes were thoroughly washed 3 × in PBS prior to incubating cells for 15-30 mins in 2 ml of fresh HDM containing 10 µg/ml of puromycin (see section 2.11), as a measure of global protein synthesis. After incubation, media containing puromycin was aspirated and 100 µl ice-cold RIPA buffer (1×) containing protease and phosphatase inhibitors was then added to myotubes and placed on ice for 10 mins. Lysed cells were then scraped and centrifuged (16,000 × g for 10 mins, 4°C) in fresh 2 ml Eppendorf's (see section 2.11). The supernatant was then transferred to a new Eppendorf tube which was sonicated for 1 min prior to protein quantification using the BCA assay (see section 2.12) and precipitated using the acetone method (see section 2.13).

Given that protein concentrations were considerably low and variable for each sample, even after acetone precipitation procedures ($0.38 \pm 0.37 \mu\text{g}/\mu\text{l}$ in $20 \mu\text{l}$), $4 \times$ laemmli buffer was added directly to the samples as described in sections 2.13 and 2.14. Samples were placed on a heat block for 10 mins at 95°C and then on ice for a further 10 mins. All samples were then vortexed, ready for separation (see section 2.13.2). Once separated and imaged for total protein using stain-free technology (see section 2.15.2), membranes were blocked (1 hr at RT in 5% non-fat dry milk in TBST) and incubated overnight on a rocker at 4°C in anti-puromycin antibody (1:10000 in blocking buffer) as described in section 2.13.2. After overnight incubation, membranes underwent 3×5 min TBST washes prior to incubating in secondary antibody (rabbit anti-mouse IgG, 1:1000 in blocking buffer) at RT for 2 hrs (see section 2.15.2).

6.2.6 Statistical Analysis

A paired *t-test* was first conducted using GraphPad Software (Prism, Version 7.0a, San Diego, CA) to determine UBR5 mRNA fold-change in non-loaded (CON) vs. loaded (INT) myotubes dosed with HDM alone. Unpaired *t-tests* were then carried out to assess knockdown efficiency (%) in siUBR5 treated vs. HDM non-treated cells at 0 and 3 hrs in loaded and non-loaded cells. Finally, unpaired *t-tests* were performed when normalising all samples to HDM non-treated cells at 0 hrs only. Data is present as mean \pm standard error of the mean (SEM). $P \leq 0.05$ represents statistical significance.

6.3 Results

6.3.1 UBR5 mRNA Expression After Mechanical Loading in Non-Treated Myotubes

In chapter 5, UBR5 significantly increased after loading in bioengineered SkM and after RE in humans and rats. Therefore, the aim of the present chapter was to first ascertain UBR5 mRNA expression in response to mechanical loading (INT) in non-treated myotubes. Despite an increased mean fold-change in UBR5 expression after INT (1.58 ± 0.65) vs. CON (1 ± 0), such changes failed to reach statistical significance ($t_2 = 0.89$, 95% CI -3.36 to 2.21, $P = 0.47$; see Figure 6.2 and Table 6.2).

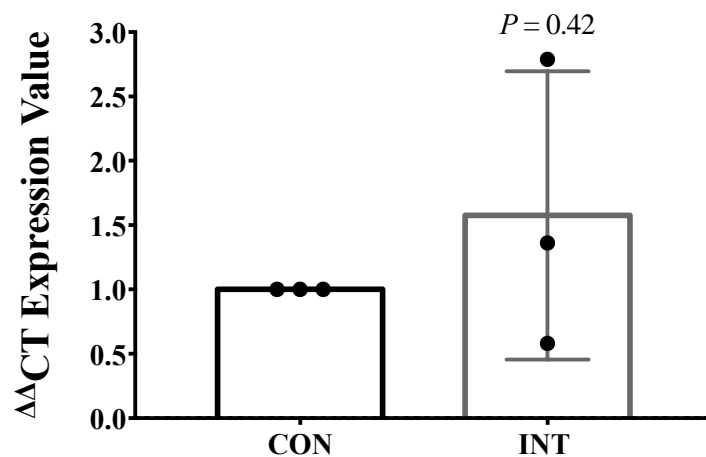


Figure 6.2. UBR5 mRNA expression following mechanical loading in non-treated human myotubes

UBR5 mRNA expression was assessed in loaded (INT, $n = 3$) and non-loaded (CON, $n = 3$) human myotubes that were dosed with HDM alone to determine gene expression fold-change due to loading alone. Data is present as mean \pm standard error of mean (SEM).

Table 6.2. Raw C_T values for each timepoint and condition

Raw C_T values obtained in treated (siUBR5) / non-treatment (HDM) and loaded (INT) / non-loaded (CON) myotubes at each timepoint (0 and 3 hrs) after qRT-PCR analysis (*n* = 3). C_T values are presented as mean ± standard error of mean (SEM). HDM = human differentiation medium only; siUBR5 = siRNA targeting UBR5; CON = non-loaded; INT = loaded.

Gene	0 hr HDM CON C_T Values	0 hr siUBR5 CON C_T Values	3 hr HDM CON C_T Values	3 hr siUBR5 CON C_T Values	3 hr HDM INT C_T Values	3 hr siUBR5 INT C_T Values
RPL13a	15.84 ± 0.5	16.33 ± 0.66	15.66 ± 0.72	15.33 ± 0.36	15.46 ± 0.19	15.8 ± 0.63
B2M	15.46 ± 0.07	15.62 ± 0.57	14.43 ± 0.24	15.21 ± 0.75	14.56 ± 0.06	14.57 ± 0.25
UBR5	26.56 ± 3.25	26.72 ± 3.39	25.08 ± 3.38	27.22 ± 3.29	24.76 ± 4.3	25.1 ± 4.13

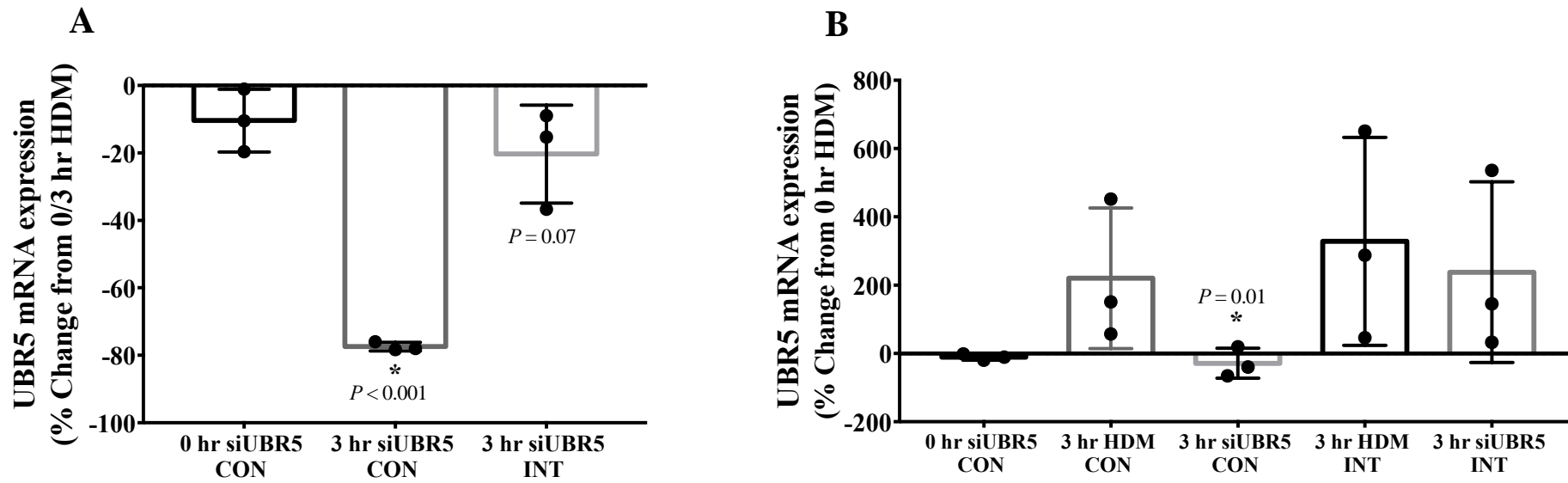


Figure 6.3. UBR5 mRNA expression in human myotubes after loading

(A) UBR5 mRNA expression (%) when all treated (siUBR5) myotubes were relativised to non-treated (HDM) myotubes at the same timepoint (0/3 hrs) within the same condition (CON/INT). (B) UBR5 gene expression when all samples were relativised to 0 hr HDM myotubes only ($n = 3$ per condition [CON/INT] and treatment [HDM/siUBR5] at each timepoint [0/3 hrs]). (*) Depicts statistical significant ($P \leq 0.05$) reduction in mRNA expression in non-loaded (CON), treated (siUBR5) myotubes at 3 hrs (HDM = human differentiation medium only; siUBR5 = siRNA targeting UBR5; CON = non-loaded ; INT = loaded).

6.3.2 UBR5 mRNA Expression in Loaded and Non-Loaded Myotubes After siUBR5 Treatment

After determining UBR5 mRNA expression in non-treated (HDM) myotubes after loading, the present chapter next wished to ascertain UBR5 expression after dosing with siUBR5 at 0 hrs and 3 hrs post-loading. Despite a non-significant change in mean UBR5 mRNA expression at 0 hrs post-loading ($100 \pm 0\%$ HDM vs. $90.14 \pm 5.38\%$ siUBR5, $t_4 = 1.83$, -95% CI -5.09 to 24.81, $P = 0.14$), treatment of siUBR5 significantly reduced UBR5 expression at 3 hrs by an average ~78% in non-loaded myotubes ($100 \pm 0\%$ HDM vs. $22.61 \pm 0.74\%$ siUBR5, $t_4 = 105$, -95% CI 75.35 to 79.44, $P < 0.001$; see Figure 6.3A). Interestingly however, mechanical loading partially rescued UBR5 mRNA expression back towards baseline levels at 3 hrs post-loading, evidenced by a non-significant difference between non-treated ($100 \pm 0\%$ HDM) and treated ($79.68 \pm 8.4\%$ siUBR5, $t_4 = 2.42$, 95% CI -3 to 43.64, $P = 0.07$) myotubes after loading.

6.3.3 UBR5 mRNA Expression when All Samples were Relativised to Non-Treated Myotubes at 0 hrs

After comparing treated (siUBR5) and non-treated (HDM) myotubes for each time point (0 /3 hr) and condition (CON/INT), the present chapter next wished to ascertain UBR5 mRNA expression when the mean expression from each group was relativised to 0 hr HDM cells only. Despite an increase in mean UBR5 expression in non-loaded (CON) and non-treated (HDM) myotubes at 3 hrs post ($220 \pm 119\%$), such changes failed to reach statistical significance ($t_4 = 1.01$, 95% CI -450.8 to 210.1, $P = 0.37$; see Figure 6.3B). Interestingly however, mRNA significantly reduced at 3 hrs post treatment with siUBR5 ($-28.33 \pm 25.16\%$) versus 0 hr HDM cells ($t_4 = 5.1$, 95% CI 58.47 to 198.2, $P = 0.01$). As with non-loaded/non-treated myotubes at 3 hrs, mean expression in HDM ($100 \pm 0\%$ 0 hr HDM CON vs. $328.4 \pm 176\%$ 3 hr HDM INT, $t_4 = 1.3$, 95% CI -717.2 to 260.3, $P = 0.26$) and siUBR5 ($100 \pm 0\%$ 0 hr HDM CON vs. $238.2 \pm 152.6\%$ 3 hr

siUBR5 INT, $t_4 = 0.91$, 95% CI -561.9 to 285.5, $P = 0.26$) treated myotubes displayed a non-significant increase after loading (see Figure 6.3B).

6.3.4 Global Muscle Protein Synthesis After Mechanical Loading in Human Myotubes

After reporting UBR5 mRNA expression in response to loading and transfection of myotubes, the present chapter next wished to determine changes in global MPS after loading/transfection via incorporating puromycin into human myotubes. Unfortunately, however, quantification of changes of MPS was not possible, potentially due to the very low total amount of protein loaded for each sample (see Figure 6.4).

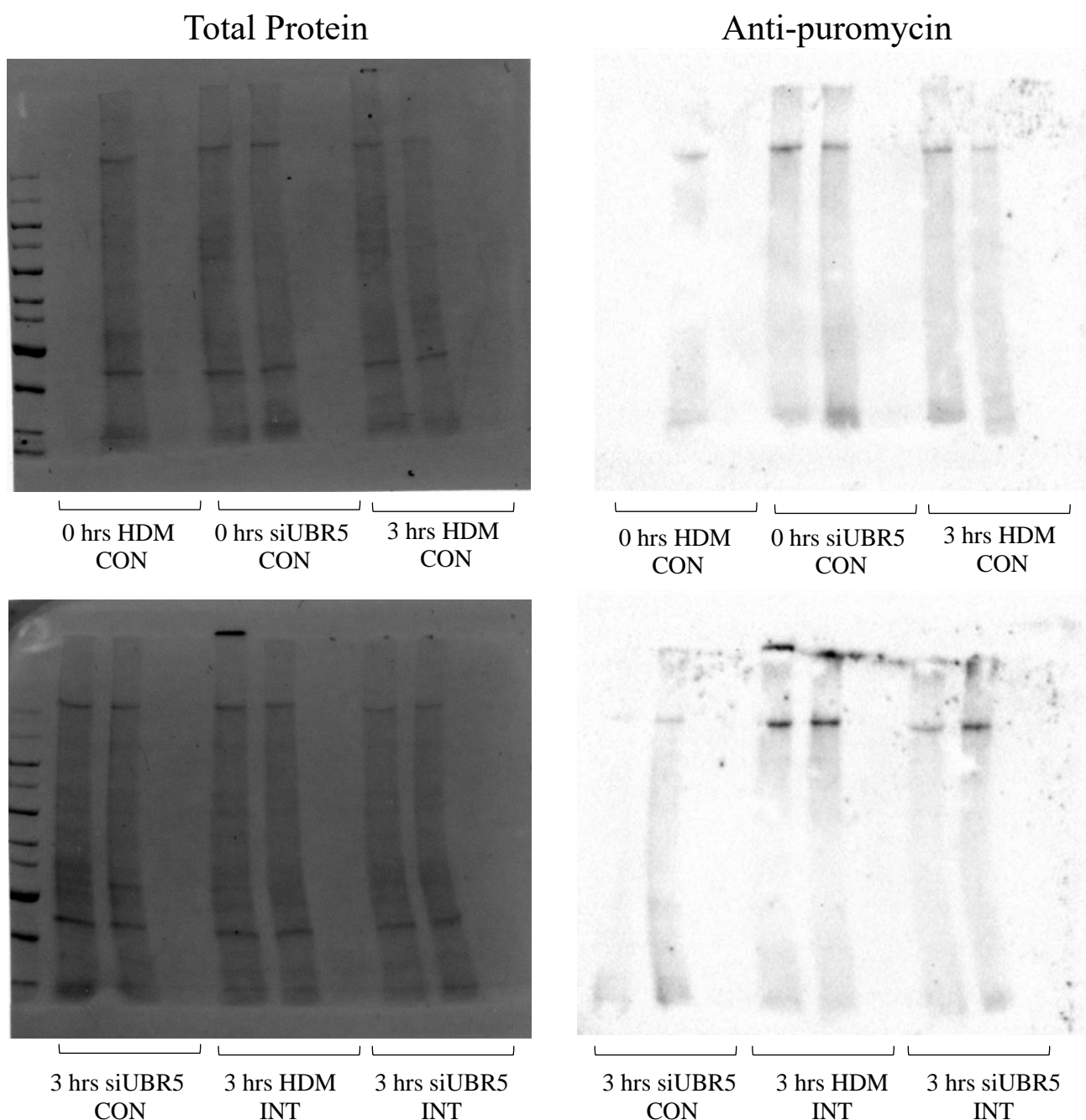


Figure 6.4. Puromycin western blots for assessment of total muscle protein synthesis

Western blots demonstrating that very limited protein is present in the ‘total protein’ blots (left) prior to incubating with puromycin targeting antibodies shown in the ‘anti-puromycin’ blots (right), therefore preventing quantification of MPS. Total protein was detected using stain-free technology (ChemiDoc system, Bio-Rad Laboratories) whereas puromycin was detected using anti-puromycin (1:10000, Merck Millipore) and rabbit anti-mouse IgG (1:1000, Abcam) antibodies (HDM = human differentiation medium only; siUBR5 = siRNA targeting UBR5; CON = non-loaded ; INT = loaded).

6.4 Discussion

The present chapter aimed to determine the mechanistic role of UBR5 in response to mechanical loading in human myotubes. To achieve this, synthetic siRNAs were transfected into differentiated human myotubes cultured in monolayer which were subsequently loaded using the Flexcell® FX-5000™ Tension system.

6.4.1 Transfection of Human Myotubes Induces Sufficient UBR5-Specific Knockdown at 3 hrs Post-Loading

In previous chapters of this thesis, C₂C₁₂ self-assembling fibrin muscle was loaded in attempt to mimic the transcriptional and epigenetic responses to mechanical loading/RE *in-vivo*. In the present chapter however, HMDCs were cultured in traditional monolayer to permit sufficient differentiation and transfection of human myotubes, therefore enabling the mechanistic role of UBR5 to be determined following mechanical loading *in-vitro*. Using the self-assembling model employed within previous chapters, fabrication of a mature human fibrin muscle requires extensive optimisation, alongside the need for high seeding densities (with cell quantity originally being limited). Indeed, $\sim 4 \times 10^5$ cells are required to produce just one mature human self-assembling bioengineered fibrin muscle (Martin *et al.*, 2013) which would have proven difficult to conduct the work presented herein given the number of timepoints/conditions required and the limited stock of HMDCs available prior to experimentation. Despite the simplicity of increasing cell yield via serial passaging, primary cells are also restricted to the number of passages they may undergo before experiencing diminished proliferative capacity and DNA damage (i.e. cellular senescence). Moreover, separation of myoblasts from mixed myoblast:fibroblast populations via pre-plating (Khodabukus *et al.*, 2018a) or fluorescence/magnetic cell sorting (Martin *et al.*, 2013) is typically a necessity to improve myotube maturation. Taken together, culturing of HMDCs in monolayer within the present chapter required less than half the number of cells (1.8×10^5 cells/well) versus self-assembling fibrin muscle, making the present experiment more achievable with the resources available.

Indeed, a total number of $\sim 4.5 \times 10^6$ cells for each participant were required in the present chapter which would have increased to an approximate 9.6×10^6 cells if using the fibrin bioengineered SkM model (this is assuming a 100% success rate when culturing the engineered muscles which is also unlikely to occur). The use of the flexcell/monolayer culture system in the present chapter also permitted sufficient knockdown in human myotubes across all samples (see Figure 6.3) which may have proven difficult if attempting to transfect cells embedded within a surrounding ECM as with bioengineered SkM. Furthermore, previous work by our group also demonstrated the efficacy of transfecting SkM cells cultured in monolayer with similar commercially available synthetic siRNAs used herein to determine the role of a specific gene during myoblast differentiation and hypertrophy (Sharples *et al.*, 2013). Indeed, targeted knockdown of the phosphatase and tensin homologue (PTEN) was shown to promote myotube hypertrophy, particularly in the absence of IGFBP-2 expression (Sharples *et al.*, 2013). In regards to transfection in bioengineered SkM, previous research demonstrated sufficient lentivirus-induced overexpression of NANOG in collagen type 1 C₂C₁₂ bioengineered SkM (Shahini *et al.*, 2018). To the authors knowledge however, no previous research has yet reported sufficient gene-specific knockdown in fibrin bioengineered SkM. In the present chapter, human myotubes were treated with HiPerFectTransfection™ reagent containing cationic and natural lipids to facilitate uptake of siRNAs into the cell. However, physical methods such as low frequency electrical stimulation (i.e. electroporation) may be necessary to effectively deliver siRNAs into cells cultured in bioengineered muscle which may in itself induce gene regulatory and morphological alterations, therefore suggesting that any changes in UBR5 mRNA expression observed would not necessarily be extrapolated to the loading stimulus alone. However, gene-specific knockdown in fibrin engineered SkM warrants future investigation before the present experiments can be carried out in such systems. At present however, the current chapter demonstrates an easy and repeatable (evidenced by consistent KD efficiencies between all human samples) *in-vitro* human SkM model for investigating the mechanistic role of a gene of interest in response to mechanical loading.

6.4.2 UBR5 mRNA Expression After Mechanical Loading in Non-Treated Human Myotubes

As discussed extensively in chapter 5, UBR5 is an E3 ubiquitin ligase with a suggested opposing role to the well-known SkM atrophy-associated E3 ligases, MuRF-1 and MAFbx. Indeed, previous work by our group reported increases in UBR5 following acute and chronic loading/RE in human and rodent muscle tissue and C₂C₁₂ bioengineered SkM (Seaborne *et al.*, 2018a, 2019) and also during recovery from atrophy, where MuRF1 and MAFbx did not show similar trends during recovery. Furthermore, UBR5 gene expression significantly increased to the greatest extent across all models of loading/RE (acute loading/RE in human/bioengineered SkM and chronic exercise in humans/rats) and in loaded bioengineered SkM alone in chapter 5. Therefore, the present chapter first wished to ascertain UBR5 gene expression in loaded, non-treated myotubes using the flexcell system. Interestingly, the present chapter demonstrated a non-significant increase in UBR5 mRNA expression after loading, which is in contrast to that identified in loaded C₂C₁₂ bioengineered SkM in chapter 5, demonstrating a significant increase (see Figure 6.2). However, it is important to note the disparities between models employed within the present and previous chapters. Firstly, bioengineered SkM constructs in previous chapters were fabricated using C₂C₁₂ cell line cells where gene expression demonstrated greater consistency within groups (CON vs. INT) given these cells are 100% myogenic cells from the same source. In contrast, the present chapter investigated the effects of loading in human muscle cells which contain additional cell sources (i.e. predominantly fibroblasts and others such as a small proportion of mesenchymal stem cells) and display greater inter-individual variation in mRNA expression compared to C₂C₁₂ cells. *In-vivo*, the morphological and functional responses to RE in SkM also demonstrate inter-variability between human individuals after chronic training (Erskine *et al.*, 2010). Furthermore, UBR5 also displayed a non-significant increase in human SkM after acute loading/RE which reached statistical significance following chronic exercise (Seaborne *et al.*, 2018a). Present and previous findings therefore suggest that

repeated loading may be required to induce significant changes in UBR5 mRNA expression in human SkM cells and tissue and/or that a larger sample size ($n > 3$) may achieve statistical significance.

Although myotubes were subjected to a replicative loading regime which was applied to bioengineered SkM (10% loading, 4 sets \times 10 reps \times 5 exercise, 90s between sets, 3.5 mins rest between exercises), differences in the direction and mode of strain applied to myotubes may also explain the inconsistencies in UBR5 mRNA expression observed between models of loading. Indeed, the flexcell system utilises vacuum pressure to apply equiaxial strain whereas the bioreactor system induced physical uniaxial strain to engineered SkM. Moreover, previous research demonstrated that intracellular signalling somewhat differs following 15% equiaxial/multiaxial vs. uniaxial stretch/loading in C₂C₁₂ cells cultured in monolayer (Hornberger *et al.*, 2005). Finally, the Bioflex culture membrane stiffness (~900 kPa) is significantly greater versus the surrounding fibrin matrix (~12 kPa) in which SkM cells are cultured in in bioengineered muscle systems. Indeed, substrate stiffness has been shown to affect muscle structure and function (Romanazzo *et al.*, 2012) whilst myotubes cultured on fibrin substrates which resemble native muscle stiffness (~12 kPa) show improved differentiation capacity in engineered SkM (Chiron *et al.*, 2012). Taken together, the lack of significance in UBR5 gene expression in human myotubes versus the significant increase observed in loaded C₂C₁₂ bioengineered SkM may be a consequence of the different cell sources, culture conditions/environment and direction/mode of strain employed between both models.

6.4.3 Mechanical Loading of Human Myotubes Post-Transfection Partially Rescues UBR5 mRNA Expression

As discussed in section 6.4.1, dosing of myotubes with siUBR5 induced sufficient (~77%) gene-specific knockdown at 3 hrs post-loading (see Figure 6.3 and Table 6.2). Interestingly

however, mechanical loading seemed to negate the reduction in UBR5 mRNA expression following transfection-induced knockdown, evidenced by a non-significant difference in gene expression between treated and non-treated myotubes at 3 hrs post-loading (see Figure 6.3A). Therefore, this suggests that mechanical loading rescued the siRNA induced reductions in UBR5. Such findings therefore support the notion that UBR5 plays a critical role in the adaptive response to acute anabolic stimuli/loading in SkM cells as well as SkM tissue *in-vivo* (Seaborne *et al.*, 2018a, 2019). The data presented herein also suggests that UBR5 is likely a downstream target of ERK/p90RSK signalling, a pathway that is responsive to mechanical loading and important for translation initiation. Indeed, previous work demonstrated that UBR5 is a target substrate for ERK2 in COS-1 fibroblast kidney cell line cells after treatment with epidermal growth factor (EGF; Eblen *et al.*, 2003) whilst others have shown that the ribosomal S6 kinase, p90RSK phosphorylates UBR5 in HeLa cancer cells at numerous sites, specifically at Thr⁶³⁷, Ser¹²²⁷ and Ser²⁴⁸³ (Cho *et al.*, 2017). Interestingly, ERK/p90RSK activity is considerably increased after acute aerobic exercise (60 mins cycling at 70% VO_{2max}) in humans (Aronson *et al.*, 1997) and chronic aerobic exercise (5 days/week of treadmill running for 7 weeks) in rodent SkM (Osman *et al.*, 2001). Furthermore, ERK/MEK/RSK signalling is exponentially increased acute loading in humans (after both 8-10 reps at 80-85% 1RM and 18-20 reps at 60-65% 1RM; Taylor *et al.*, 2012) and mice (post mechanical overload; (Miyazaki *et al.*, 2011) and also after acute (10 and 60 mins) uniaxial and multiaxial loading/stretch (15%) in C₂C₁₂ SkM cells using the same flexcell system employed herein (Hornberger *et al.*, 2005). In the present chapter, the mechanism by which transfected siRNAs, and the resulting RNA-induced silencing complex (RISC) degrade targeted complimentary DNA sequences may suggest that more sustained gene transcription of UBR5 after loading may counteract siUBR5 induced-silencing and that the extent to which enhanced UBR5 transcription may override transfection-induced degradation of the target sequence(s). However, future studies should wish to determine the definitive mechanisms of increased UBR5 expression via assessing the activity of potential upstream

signalling (i.e. ERK/p90RSK) and downstream targets in response to loading with and without muscle-specific knockdown of UBR5.

6.4.4 The Reduction in UBR5 mRNA Expression Post-Treatment is Negated Following Mechanical Loading

In the present chapter, alternative analysis was carried out to determine the temporal change in UBR5 mRNA expression when all loaded/non-loaded and treated/non-treated myotubes were relativised to non-treated myotubes at 0 hrs as opposed to relativising mRNA expression to non-treated myotubes at the same timepoint and condition as described in section 6.3.2. Consistent with previous analysis, treatment of siUBR5 in non-loaded myotubes displayed a significant reduction in UBR5 mRNA expression at 3 hrs post-loading (see Figure 6.3B). Furthermore, UBR5 gene expression displayed a non-significant increase in non-loaded, HDM non-treated cells at 3 hrs which was similar to levels of mRNA expression in siUBR5 treated cells at 3 hrs post-loading, further suggesting that siRNA-induced silencing of UBR5 is negated following mechanical loading in human myotubes (see Figure 6.3B). In summary, the present data suggests that UBR5 is sufficiently silenced in siUBR5 treated myotubes, however, upregulation of UBR5 after mechanical loading is able to negate the reduction in UBR5 observed in non-loaded cells.

6.5 Limitations

It is worth also noting the limitations of the present chapter. As described in section 6.4.2, myotubes were cultured and loaded in Bioflex plates which have stiffer substrates (~900 kPa) to those observed in fibrin bioengineered SkM (~12 kPa) which may therefore affect subsequent myotube maturation and mRNA expression. In attempt to overcome this issue, SkM cells derived from biopsies with the highest myogenic population ($72 \pm 2.36\%$; see Table 2.1) were carefully considered and were differentiated over 10 days (rather than the typical 5-7 day period

when differentiating C₂C₁₂ cells) to ensure formation of mature myotubes (see Figure 2.2). The non-uniform directionality of myotubes due to the absence of tension applied to the cells imposes another limitation to the model employed within the present chapter. Indeed, the random, swirling formation of myotubes observed in monolayer do not resemble the uniaxial alignment of SkM fibres *in-vivo*, suggesting that only a sub-population of myotubes may have actually been subjected to the maximal strain applied (10%). Furthermore, the flexcell system induces multiaxial strain to cells suggesting that such findings observed in the present chapter may not translate to native and/or bioengineered SkM muscle which mainly undergo uniaxial strain given previous research demonstrating differences in anabolic signalling according to the direction of loading (Hornberger *et al.*, 2005). Given the methodological issues encountered during total MPS procedures, the present chapter was not able to conclude whether silencing of UBR5 affected the anabolic response to mechanical loading. The inability to measure MPS in the present chapter was most likely due to the low initial protein concentrations and therefore the subsequent total amount of protein loaded for puromycin western blotting (despite attempting to precipitate using the acetone method). If initial primary cell quantities are sufficient, future studies should consider experimenting with a greater cell number or possibly trypsinise and centrifuge cells (rather than mechanical dissociation as employed herein) in attempt to maximise cell dissociation and therefore increase protein concentrations. Furthermore, future studies should investigate the activity of key anabolic signalling proteins such as ERK and p90RSK (that have previously been associated with UBR5 as described in section 6.4.3) in the presence and absence of siRNA to determine UBR5s mechanistic role in SkM anabolism after loading. Despite these limitations, the present chapter demonstrates that mechanical loading of UBR5-specific knockdown in human myotubes is able to rescue its expression, providing novel mechanistic findings regarding the role of UBR5 in response to mechanical loading/RE, adding to exciting recent data suggesting an importance of this gene during SkM anabolism/hypertrophy and remodelling.

6.6 Conclusion

Data reported in the present chapter suggests that muscle-specific knockdown of UBR5 in human myotubes is rescued in the presence of mechanical loading, further supporting present (see chapter 5) and previous (Seaborne *et al.*, 2018a, 2019) work by our group, suggesting an important role for UBR5 in SkM anabolism/hypertrophy and remodelling after loading/RE. Despite the aforementioned limitations described in section 6.5, the present chapter proves a cost effective and repeatable model for determining the load-induced mechanistic role of a specific gene of interest in human SkM cells.

CHAPTER 7

Thesis Conclusion

7.1 Summary of Thesis Aims and Main Findings

The work conducted in the present thesis aimed to develop and characterise the use of a murine fibrin bioengineered SkM model to study the transcriptional and epigenetic regulation following mechanical loading *in-vitro*. Moreover, to determine whether mechanical loading of bioengineered fibrin muscle mimics the transcriptional and epigenetic responses after loading/RE *in-vivo*.

The first experimental chapter (chapter 3) demonstrated that intermittently loading fibrin C₂C₁₂ engineered muscle using a novel bioreactor system induced similar changes in gene expression of well-characterised mechano-sensitive genes that have previously been shown to be regulated after RE *in-vivo* and in response to loading in collagen bioengineered muscle using previously published bioreactors (Cheema *et al.*, 2005; Mudera *et al.*, 2010; Player *et al.*, 2014; Aguilar-Agon *et al.*, 2019). Indeed, gene expression profiles following intermittent loading using the TC-3 bioreactor suggested a greater anabolic response (i.e. increases in IGF-1, IGF-IEa, MGF and reductions in IGFBP-2/5) and acute SkM remodelling (increases in MMP-9, MuRF-1 and MAFbx) versus static loading.

After characterising the culture methods, loading regime and transcriptional response of known ‘mechano-sensitive’ genes after loading in fibrin bioengineered muscle, the following experimental chapter (chapter 4) carried out extensive bioinformatics analysis to determine the most frequently regulated genes across the human transcriptome and methylome after acute loading/RE in human SkM, and therefore identify an appropriate subset of genes to analyse at the mRNA and DNA methylation level after loading in fibrin muscle using the system characterised in chapter 3. Interestingly, a number of genes that were frequently regulated across the human transcriptome were also epigenetically altered at the DNA level after acute RE in humans. This included genes enriched in ‘cancer’ pathways which in SkM, are associated

with ECM/actin structure and remodelling, TGF- β , calcium, IL-6 and retinoic acid signalling as well as mechano-transduction.

After identifying regulated genes across the human transcriptome and methylome after acute RE in chapter 4, chapter 5 then sought to determine mRNA expression and DNA methylation of these genes after loading in fibrin bioengineered using the model characterised in chapter 3. Data derived from this work suggests that mechanical loading alone is sufficient for inducing changes in mRNA expression in engineered fibrin muscle, albeit, the few changes observed in DNA methylation suggested a potential need for chronic/repeated loading and/or an electrical input to induce concentric shortening contraction and perhaps subsequent epigenetic changes. However, this requires future investigation. In regards to chronic loading, whilst it has been shown that the rates of fibrinolysis in C₂C₁₂ bioengineered muscle can be regulated via the use of plasminogen inhibitors (Khodabukus & Baar, 2009), incubation of fibrin SkM for >24 hrs post-loading in our lab has proven difficult, even when kept at resting length without the application of additional loading. Furthermore, despite the TC-3 permitting simultaneous mechanical loading and electrical stimulation, this method is yet to be fully optimised and future work should therefore continue to characterise these methods to explore whether chronic loading with and without electrical stimulation is indeed imperative for inducing changes in DNA methylation in murine fibrin engineered muscle. Interestingly, the E3-ubiquitin ligase, UBR5, demonstrated the greatest increase in mRNA expression after loading in bioengineered SkM alone and across all additional models of exercise/loading such as acute and chronic RE/loading in human and rodent SkM *in-vivo*.

The final experimental chapter of this thesis (chapter 6) therefore wished to ascertain the mechanistic role of UBR5 in response to mechanical loading in human myotubes cultured in monolayer using the flexcell system. Interestingly, the results demonstrated that mechanical loading was able to rescue siRNA-induced knockdown of UBR5 gene expression in human

myotubes, further supporting the notion that UBR5 may indeed be an important mechano-responsive regulator of SkM anabolism/hypertrophy and remodelling after loading/RE. However, as discussed extensively in chapter 6 (section 6.5), we were unable to conclude whether UBR5-specific knockdown in human myotubes was able to affect the anabolic responses to loading due to methodological issues with total MPS procedures. Despite this, the results presented herein add to the recent body of work suggesting an importance for UBR5 in SkM anabolism and hypertrophy (Seaborne *et al.*, 2018a, 2019).

7.2 Thesis Conclusion

Overall, the work carried out within the thesis has proven an effective bioengineered SkM *in-vitro* model for studying the mechano-transcriptional responses to loading *in-vivo*. Furthermore, the present thesis demonstrates a cost effective, simple and repeatable model for inducing gene-specific knockdown in human myotubes during mechanical loading to investigate the mechanistic role of a gene of interest in response to loading.

CHAPTER 8

References

- Abe S, Rhee S, Iwanuma O, Hiroki E, Yanagisawa N, Sakiyama K & Ide Y (2009). Effect of mechanical stretching on expressions of muscle specific transcription factors myod, Myf-5, myogenin and MRF4 in proliferated myoblasts. *J Vet Med Ser C Anat Histol Embryol* **38**, 305–310.
- Adams G. & McCue S. (1998). Localized infusion of IGF-I results in skeletal muscle hypertrophy in rats GREGORY. *J Appl Physiol* **84**, 1716–1722.
- Aguilar-Agon KW, Capel AJ, Martin NRW, Player DJ & Lewis MP (2019). Mechanical loading stimulates hypertrophy in tissue-engineered skeletal muscle: Molecular and phenotypic responses. *J Cell Physiol* **234**, 23547–23558.
- Allis CD & Jenuwein T (2016). The molecular hallmarks of epigenetic control. *Nat Rev Genet* **17**, 487–500.
- Aronson D, Violan MA, Dufresne SD, Zangen D, Fielding RA & Goodyear LJ (1997). Exercise stimulates the mitogen-activated protein kinase pathway in human skeletal muscle. *J Clin Invest* **99**, 1251–1257.
- Audet GN, Fulks D, Stricker JC & Olfert IM (2013). Chronic Delivery of a Thrombospondin-1 Mimetic Decreases Skeletal Muscle Capillarity in Mice. *PLoS One* **8**, 1–9.
- Auluck A, Mudera V, Hunt NP & Lewis MP (2005). A three-dimensional in vitro model system to study the adaptation of craniofacial skeletal muscle following mechanostimulation. *Eur J Oral Sci* **113**, 218–224.
- Awede B, Thissen JP, Gailly P & Lebacqz J (1999). Regulation of IGF-I, IGFBP-4 and IGFBP-5 gene expression by loading in mouse skeletal muscle. *FEBS Lett* **461**, 263–267.
- Baar K (2005). New dimensions in tissue engineering: Possible models for human physiology. *Exp Physiol* **90**, 799–806.
- Baar K & Esser K (1999). Phosphorylation of p70S6k correlates with increased skeletal muscle mass following resistance exercise. *Am J Physiol Cell Physiol* **C120–C127**.
- Baar K, Torgan CE, Kraus WE & Esser K (2000). Autocrine Phosphorylation of p70 S6k in Response to Acute Stretch in Myotubes. **80**, 76–80.

- Baehr LM, Tunzi M & Bodine SC (2014). Muscle hypertrophy is associated with increases in proteasome activity that is independent of MuRF1 and MAFbx expression. *Front Physiol* **5 FEB**, 1–8.
- Bannister AJ & Kouzarides T (2011). Regulation of chromatin by histone modifications. *Cell Res* **21**, 381–395.
- Barrès R, Yan J, Egan B, Treebak JT, Rasmussen M, Fritz T, Caidahl K, Krook A, O’Gorman DJ & Zierath JR (2012). Acute exercise remodels promoter methylation in human skeletal muscle. *Cell Metab* **15**, 405–411.
- Begue G, Douillard A, Galbes O, Rossano B, Vernus B, Candau R & Py G (2013). Early Activation of Rat Skeletal Muscle IL-6/STAT1/STAT3 Dependent Gene Expression in Resistance Exercise Linked to Hypertrophy. *PLoS One* **8**, 1–12.
- van den Beld AW, Blum WF, Pols HAP, Grobbee DE & Lamberts SWJ (2003). Serum insulin-like growth factor binding protein-2 levels as an indicator of functional ability in elderly men. *Eur J Endocrinol* **148**, 627–634.
- Benjamin M & Hillen B (2003). Mechanical Influences on Cells , Tissues and Organs – ‘ Mechanical Morphogenesis .’ *Eur J Morphol* **41**, 3–7.
- Bladt F, Riethmacher D, Isenmann S, Aguzzi A & Birchmeier C (1995). Essential role for the c-met receptor in the migration of myogenic precursor cells into the limb bud. **376**, 768–771.
- Blau HM, Pavlath GK, Hardeman EC, Chiu CP, Silberstein L, Webster SG, Miller SC & Webster C (1985). Plasticity of the differentiated state. *Science (80-)* **230**, 758–766.
- Bodine SC & Baehr LM (2014). Skeletal muscle atrophy and the E3 ubiquitin ligases MuRF1 and MAFbx/atrogen-1. *Am J Physiol - Endocrinol Metab* **307**, E469–E484.
- Bodine SC, Latres E, Baumhueter S, Lai VKM, Nunez L, Clarke BA, Poueymirou WT, Panaro FJ, Erqian Na, Dharmarajan K, Pan ZQ, Valenzuela DM, Dechiara TM, Stitt TN, Yancopoulos GD & Glass DJ (2001a). Identification of ubiquitin ligases required for skeletal muscle atrophy. *Science (80-)* **294**, 1704–1708.

- Bodine SC, Stitt TN, Gonzalez M, Kline WO, Stover GL, Bauerlein R, Zlotchenko E, Scrimgeour A, Lawrence JC, Glass DJ & Yancopoulos GD (2001b). Akt/mTOR pathway is a crucial regulator of skeletal muscle hypertrophy and can prevent muscle atrophy in vivo. *Nat Cell Biol* **3**, 1014–1019.
- Bogdanović O & Veenstra GJC (2009). DNA methylation and methyl-CpG binding proteins: Developmental requirements and function. *Chromosoma* **118**, 549–565.
- Brack AS & Rando TA (2012). Tissue-specific stem cells: Lessons from the skeletal muscle satellite cell. *Cell Stem Cell* **10**, 504–514.
- Bradey M., Lewis M. & Mudera VC (2008). Synergy between myogenic and non-myogenic cells in a 3D tissue-engineered craniofacial skeletal muscle construct. *J Tissue Eng Regen Med* **2**, 408–417.
- Brevet A, Elaine P, Peacock J & Stockdale FE (1976). Myosin Synthesis Increased by Electrical Stimulation of Skeletal Muscle Cell Cultures. *Science (80-)* **193**, 1152–1154.
- Bryan K, McGivney BA, Farries G, McGettigan PA, McGivney CL, Gough KF, MacHugh DE, Katz LM & Hill EW (2017). Equine skeletal muscle adaptations to exercise and training: Evidence of differential regulation of autophagosomal and mitochondrial components. *BMC Genomics* **18**, 1–26.
- Buckingham M, Bajard L, Chang T, Daubas P, Hadchouel J, Meilhac S, Montarras D, Rocancourt D & Relaix F (2003). The formation of skeletal muscle: From somite to limb. *J Anat* **202**, 59–68.
- Campbell PG, Durham SK, Hayes JD, Suwanichkul A & Powell DR (1999). Insulin-like Growth Factor-binding Protein-3 Binds Fibrinogen and Fibrin *. *J Biol Chem* **274**, 30215–30221.
- Capel AJ, Rimington RP, Fleming JW, Player DJ, Baker LA, Turner MC, Jones JM, Martin NRW, Ferguson RA, Mudera VC & Lewis MP (2019). Scalable 3D printed molds for human tissue engineered skeletal muscle. *Front Bioeng Biotechnol* **7**, 1–13.
- Cardamone M, Darras BT & Ryan MM (2008). Inherited myopathies and muscular dystrophies.

- Semin Neurol* **28**, 250–259.
- Carmeli E, Moas M, Reznick AZ & Coleman R (2004). Matrix metalloproteinases and skeletal muscle: A brief review. *Muscle and Nerve* **29**, 191–197.
- Caron M, Charette SJ, Maltais F & Debigaré R (2011). Variability of protein level and phosphorylation status caused by biopsy protocol design in human skeletal muscle analyses. *BMC Res Notes* **4**, 1–9.
- Carroll CC, Carrithers JA & Trappe TA (2004). Contractile protein concentrations in human single muscle fibres. *J Muscle Res Cell Motil* **25**, 55–59.
- Chal J & Pourquié O (2017). Making muscle: skeletal myogenesis *in vivo* and *in vitro*. *Development* **144**, 2104–2122.
- Cheema U, Brown R, Mudera V, Shi YY, Mcgrouter G & Goldspink G (2005). Mechanical signals and IGF-I gene splicing *in vitro* in relation to development of skeletal muscle. *J Cell Physiol* **202**, 67–75.
- Chen HH, Lu J, Guan YF, Li SJ, Hu TT, Xie ZS, Wang F, Peng XH, Liu X, Xu X, Zhao FP, Yu BL & Li XP (2016). Estrogen/ERR- α signalling axis is associated with fibre-type conversion of upper airway muscles in patients with obstructive sleep apnea hypopnea syndrome. *Sci Rep* **6**, 1–11.
- Chen R, Hong Q, Jiang J, Chen X, Jiang Z, Wang J, Liu S, Duan S & Shi S (2017). AGTR1 promoter hypermethylation in lung squamous cell carcinoma but not in lung adenocarcinoma. *Oncol Lett* **14**, 4989–4994.
- Chen YW, Nader GA, Baar KR, Fedele MJ, Hoffman EP & Esser KA (2002). Response of rat muscle to acute resistance exercise defined by transcriptional and translational profiling. *J Physiol* **545**, 27–41.
- Chinni C, De Niese MR, Deborah J T, Jenkins AL, Bottomley SP & Mackie EJ (1999). Thrombin, a survival factor for cultured myoblasts. *J Biol Chem* **274**, 9169–9174.
- Chiron S, Tomczak C, Duperray A, Lainé J, Bonne G, Eder A, Hansen A, Eschenhagen T, Verdier C & Coirault C (2012). Complex interactions between human myoblasts and the

- surrounding 3D fibrin-based matrix. *PLoS One* **7**, 2–9.
- Cho JH, Kim SA, Seo YS, Park SG, Park BC, Kim JH & Kim S (2017). The p90 ribosomal S6 kinase–UBR5 pathway controls Toll-like receptor signalling via miRNA-induced translational inhibition of tumour necrosis factor receptor–associated factor 3. *J Biol Chem* **292**, 11804–11814.
- Close RI (1972). Dynamic properties of skeletal muscles. *Physiol Rev* **52**, 129–197.
- Collins BC, Mader TL, Cabelka CA, Iñigo MR, Spangenburg EE & Lowe DA (2018). Deletion of estrogen receptor α in skeletal muscle results in impaired contractility in female mice. *J Appl Physiol* **124**, 980–992.
- Collins CA, Olsen I, Zammit PS, Heslop L, Petrie A, Partridge TA & Morgan JE (2005). Stem cell function, self-renewal, and behavioral heterogeneity of cells from the adult muscle satellite cell niche. *Cell* **122**, 289–301.
- Cong H, Sun L, Liu C & Tien P (2011). Inhibition of atrogen-1/MAFbx expression by adenovirus-delivered small hairpin RNAs attenuates muscle atrophy in fasting mice. *Hum Gene Ther* **22**, 313–324.
- Coolican SA, Samuel DS, Ewton DZ, McWade FJ & Florini JR (1997). The mitogenic and myogenic actions of insulin-like growth factors utilize distinct signalling pathways. *J Biol Chem* **272**, 6653–6662.
- Coons AH, Creech HJ, Jones RN & Berliner E (1942). The demonstration of pneumococcal antigen in tissues by the use of fluorescent antibody. *J Immunol* **45**, 159–170.
- Crown A, He X, Holly J, Lightman S & Stewart C (2000). Characterisation of the IGF system in a primary adult human skeletal muscle cell model, and comparison of the effects of insulin and IGF-I on protein metabolism. *J Endocrinol* **167**, 403–415.
- Dahiya S, Bhatnagar S, Hindi SM, Jiang C, Paul PK, Kuang S & Kumar A (2011). Elevated levels of active matrix metalloproteinase-9 cause hypertrophy in skeletal muscle of normal and dystrophin-deficient mdx mice. *Hum Mol Genet* **20**, 4345–4359.
- Danoviz M. & Yablonka-Reuveni Z (2012). Skeletal muscle satellite cells: background and

- methods for isolation and analysis in a primary culture system. In *Methods Mol Biol*, pp. 21–52.
- Davis RL, Weintraub H & Lassar AB (1987). Expression of a single transfected cDNA converts fibroblasts to myoblasts. *Cell* **51**, 987–1000.
- Deichmann U (2016). Epigenetics: The origins and evolution of a fashionable topic. *Dev Biol* **416**, 249–254.
- Delatte B, Deplus R & Fuks F (2014). Playing TET risk with DNA modifications. *EMBO J* **33**, 1198–1211.
- Denham J, Marques FZ, Bruns EL, O'Brien BJ & Charchar FJ (2016). Epigenetic changes in leukocytes after 8 weeks of resistance exercise training. *Eur J Appl Physiol* **116**, 1245–1253.
- Dennis RG, Kosnik PE, Gilbert ME & Faulkner JA (2001). Excitability and contractility of skeletal muscle engineered from primary cultures and cell lines. *Am J Physiol Physiol* **280**, C288–C295.
- Dieffenbach CW, Lowe TMJ & Dveksler GS (1993). General concepts for PCR primer design. *Genome Res*; DOI: 10.1101/gr.3.3.S30.
- Dimauro I, Scalabrin M, Fantini C, Grazioli E, Beltran Valls MR, Mercatelli N, Parisi A, Sabatini S, Di Luigi L & Caporossi D (2016). Resistance training and redox homeostasis: Correlation with age-associated genomic changes. *Redox Biol* **10**, 34–44.
- Ding Q, Gros R, Gray ID, Taussig R, Ferguson SSG & Feldman RD (2004). Raf kinase activation of adenylyl cyclases: Isoform-selective regulation. *Mol Pharmacol* **66**, 921–928.
- Dirks ML, Wall BT, Valk B Van De & Holloway TM (2016). One Week of Bed Rest Leads to Substantial Muscle Atrophy and Induces Whole-Body Insulin Resistance in the Absence of Skeletal Muscle Lipid Accumulation. *Diabetes* **65**, 2862–2875.
- Drummond MJ, Fry CS, Glynn EL, Dreyer HC, Dhanani S, Timmerman KL, Volpi E & Rasmussen BB (2009). Rapamycin administration in humans blocks the contraction-

- induced increase in skeletal muscle protein synthesis. *J Physiol* **587**, 1535–1546.
- Dyrvig M, Hansen HH, Christiansen SH, Woldbye DPD, Mikkelsen JD & Lichota J (2012). Epigenetic regulation of Arc and c-Fos in the hippocampus after acute electroconvulsive stimulation in the rat. *Brain Res Bull* **88**, 507–513.
- Eastwood M, Mudera VC, McGrouther DA & Brown RA (1998a). Effect of precise mechanical loading on fibroblast populated collagen lattices: Morphological changes. *Cell Motil Cytoskeleton* **40**, 13–21.
- Eastwood M, Mudera VC, McGrouther DA & Brown RA (1998b). Effect of precise mechanical loading on fibroblast populated collagen lattices: Morphological changes. *Cell Motil Cytoskeleton* **40**, 13–21.
- Eastwood M, Porter R, Khan U, McGrouther G & Brown R (1996). Quantitative analysis of collagen gel contractile forces generated by dermal fibroblasts and the relationship to cell morphology. *J Cell Physiol* **166**, 33–42.
- Eblen ST, Kumar NV, Shah K, Henderson MJ, Watts CKW, Shokat KM & Weber MJ (2003). Identification of novel ERK2 substrates through use of an engineered kinase and ATP analogs. *J Biol Chem* **278**, 14926–14935.
- Edgerton VR, Zhou M, Ohira Y, Klitgaard H, Jiang B, Bell G, Harris B, Saltin B, Gollnick PD, Roy RR, Day M. & Greenisen M (1995). Human fibre size and enzymatic properties after 5 and 11 days of spaceflight. *J Appl Physiol* **78**, 1733–1739.
- Egan B & Zierath JR (2012). Review Exercise Metabolism and the Molecular Regulation of Skeletal Muscle Adaptation. *Cell Metab* **17**, 162–184.
- Egner IM, Bruusgaard JC & Gundersen K (2016). Satellite cell depletion prevents fibre hypertrophy in skeletal muscle. *Dev* **143**, 2898–2906.
- Elia D, Madhala D, Ardon E, Reshef R & Halevy O (2007). Sonic hedgehog promotes proliferation and differentiation of adult muscle cells: Involvement of MAPK/ERK and PI3K/Akt pathways. *Biochim Biophys Acta - Mol Cell Res* **1773**, 1438–1446.
- Engler AJ, Griffin MA, Sen S, Bönnemann CG, Sweeney HL & Discher DE (2004). Myotubes

- differentiate optimally on substrates with tissue-like stiffness: Pathological implications for soft or stiff microenvironments. *J Cell Biol* **166**, 877–887.
- Eom GH, Kim KB, Kim JH, Kim JY, Kim JR, Kee HJ, Kim DW, Choe N, Park HJ, Son HJ, Choi SY, Kook H & Seo SB (2011). Histone methyltransferase SETD3 regulates muscle differentiation. *J Biol Chem* **286**, 34733–34742.
- Erskine RM, Jones DA, Williams AG, Stewart CE & Degens H (2010). Inter-individual variability in the adaptation of human muscle specific tension to progressive resistance training. *Eur J Appl Physiol* **110**, 1117–1125.
- Esser KA & White TP (1995). Mechanical load affects growth and maturation of skeletal muscle grafts. *J Appl Physiol* **78**, 30–37.
- Fasehee H, Fakhraee M, Davoudi S, Vali H & Faghihi S (2019). Cancer biomarkers in atherosclerotic plaque: Evidenced from structural and proteomic analyses. *Biochem Biophys Res Commun* **509**, 687–693.
- Ferrari G, Cusella-De Angelis G, Coletta M, Paolucci E, Stornaiuolo A, Cossu G & Mavilio F (1998). Muscle regeneration by bone marrow-derived myogenic progenitors. *Science (80-)* **279**, 1528–1530.
- Figeac N & Zammit PS (2015). Coordinated action of Axin1 and Axin2 suppresses β -catenin to regulate muscle stem cell function. *Cell Signal* **27**, 1652–1665.
- Fiorotto ML, Sosa HAJ & Davis TA (2012). In vivo measurement of muscle protein synthesis rate using the flooding dose technique. *Methods Mol Biol* **798**, 245–264.
- Van Der Flier A, Kuikman I, Kramer D, Geerts D, Kreft M, Takafuta T, Shapiro SS & Sonnenberg A (2002). Different splice variants of filamin-B affect myogenesis, subcellular distribution, and determine binding to integrin β subunits. *J Cell Biol* **156**, 361–376.
- Florini JR, Ewton DZ & Coolican SA (1996). Growth Hormone and the Insulin-Like Growth Factor System in Myogenesis. *Endocr Rev* **17**, 481–517.
- Foster RF, Thompson JM & Kaufman SJ (1987). A laminin substrate promotes myogenesis in

- rat skeletal muscle cultures: Analysis of replication and development using antidesmin and anti-BrdUrd monoclonal antibodies. *Dev Biol* **122**, 11–20.
- Foulstone EJ, Huser C, Crown AL, Holly JMP & Stewart CEH (2004). Differential signalling mechanisms predisposing primary human skeletal muscle cells to altered proliferation and differentiation: Roles of IGF-I and TNF α . *Exp Cell Res* **294**, 223–235.
- Franchi M V., Longo S, Mallinson J, Quinlan JI, Taylor T, Greenhaff PL & Narici M V. (2018). Muscle thickness correlates to muscle cross-sectional area in the assessment of strength training-induced hypertrophy. *Scand J Med Sci Sport* **28**, 846–853.
- Franchi M V, Reeves ND, Narici M V & Huey K (2017). Skeletal Muscle Remodeling in Response to Eccentric vs . Concentric Loading : Morphological , Molecular , and Metabolic Adaptations. *Front Physiol* **8**, 1–16.
- Friedmann-bette B, Schwartz FR, Eckhardt H, Billeter R, Bonaterra G & Kinscherf R (2012). Similar changes of gene expression in human skeletal muscle after resistance exercise and multiple fine needle biopsies. *Journal* **112**, 289–295.
- Frommer M, McDonald LE, Millar DS, Collis CM, Watt F, Grigg GW, Molloy PL & Paul CL (1992). A genomic sequencing protocol that yields a positive display of 5- methylcytosine residues in individual DNA strands. *Proc Natl Acad Sci U S A* **89**, 1827–1831.
- Fry CS, Lee JD, Jackson JR, Kirby TJ, Stasko SA, Liu H, Dupont-Versteegden EE, McCarthy JJ & Peterson CA (2014). Regulation of the muscle fibre microenvironment by activated satellite cells during hypertrophy. *FASEB J* **28**, 1654–1665.
- Fujita H, Fukuhara S, Sakurai A, Yamagishi A, Kamioka Y, Nakaoka Y, Masuda M & Mochizuki N (2005). Local activation of Rap1 contributes to directional vascular endothelial cell migration accompanied by extension of microtubules on which RAPL, a Rap1-associating molecule, localizes. *J Biol Chem* **280**, 5022–5031.
- Gilbert PM, Havenstrite KL, Magnusson KEG, Sacco A, Leonardi NA, Kraft P, Nguyen NK, Thrun S, Lutolf MP & Blau HM (2010). Substrate elasticity regulates skeletal muscle stem cell self-renewal in culture. *Science (80-)* **329**, 1078–1081.

- Gillies A. & Lieber R. (2011). Structure and Function of the Skeletal Muscle Extracellular Matrix. *Muscle Nerve* **44**, 318–331.
- Girven M, Dugdale HF, Owens DJ, Hughes DC, Stewart CE & Sharples AP (2016). l-glutamine Improves Skeletal Muscle Cell Differentiation and Prevents Myotube Atrophy After Cytokine (TNF- α) Stress Via Reduced p38 MAPK Signal Transduction. *J Cell Physiol* **231**, 2720–2732.
- Glass DJ (2003). Signalling pathways that mediate skeletal muscle hypertrophy and atrophy. *Nat Cell Biol* **5**, 87–90.
- Goel HL & Dey CS (2002). PKC-regulated myogenesis is associated with increased tyrosine phosphorylation of FAK, Cas, and paxillin, formation of Cas-CRK complex, and JNK activation. *Differentiation* **70**, 257–271.
- Goldberg A. (1968). PROTEIN SYNTHESIS DURING WORK-INDUCED GROWTH OF SKELETAL MUSCLE. *J Cell Biol* **36**, 653–658.
- Goldberg A., Etlinger J., Goldspink D. & Jablecki C (1975). Mechanism of work-induced hypertrophy of skeletal muscle. *Med Sci Sports* **7**, 185–198.
- Goldberg A. & Goodman HM (1969). Amino acid transport during work-induced growth of skeletal muscle. *Am J Physiol* **216**, 1111–1115.
- Goldberg A (1967). Work-induced growth of skeletal muscle in normal and hypophysectomized rats. *Am J Physiol* **213**, 1193–1198.
- Goldspink DF (1977). The influence of immobilization and stretch on protein turnover of rat skeletal muscle. *J Physiol* **264**, 267–282.
- Goldspink G (1999). Changes in muscle mass and phenotype and the expression of autocrine and systemic growth factors by muscle in response to stretch and overload. *J Anat* **194**, 323–334.
- Gomes AR, Soares AG, Peviani S, Nascimento RB, Moriscot AS & Salvini TF (2006). The effect of 30 minutes of passive stretch of the rat soleus muscle on the myogenic differentiation, myostatin, and atrogen-1 gene expressions. *Arch Phys Med Rehabil* **87**,

241–246.

- González-Pardo H & Marino P-Á (2013). Epigenetic and its implications for Psychology. *Psicothema* **25**, 3–12.
- Goodman CA, Frey JW, Mabrey DM, Jacobs BL, Lincoln HC, You JS & Hornberger TA (2011). The role of skeletal muscle mTOR in the regulation of mechanical load-induced growth. *J Physiol* **589**, 5485–5501.
- Goodman CA & Hornberger TA (2013). Measuring protein synthesis with SUNSET: a valid alternative to traditional techniques? *Exerc Sport Sci Rev* **41**, 107–115.
- Gravendeel LAM, De Rooi JJ, Eilers PHC, Van Den Bent MJ, Sillevius Smitt PAE & French PJ (2012). Gene expression profiles of gliomas in formalin-fixed paraffin-embedded material. *Br J Cancer* **106**, 538–545.
- Guadagnin E, Mázala D & Chen YW (2018). STAT3 in skeletal muscle function and disorders. *Int J Mol Sci* **19**, 1–16.
- El Haddad M, Notarnicola C, Evano B, El Khatib N, Blaquièrre M, Bonniieu A, Tajbakhsh S, Hugon G, Vernus B, Mercier J & Carnac G (2017). Retinoic acid maintains human skeletal muscle progenitor cells in an immature state. *Cell Mol Life Sci* **74**, 1923–1936.
- Haig D (2012). Commentary: The epidemiology of epigenetics. *Int J Epidemiol* **41**, 13–16.
- Hameed M, Orrell RW, Cubbold M, Goldspink G & Harridge SDR (2003). Expression of IGF-I splice variants in young and old human skeletal muscle after high resistance exercise. *J Physiol* **547**, 247–254.
- Han Y, Wang C, Park JS & Niu L (2010). Channel-opening kinetic mechanism for human wild-type GluK2 and the M867I mutant kainate receptor. *Biochemistry* **49**, 9207–9216.
- Hawke TJ, Atkinson DJ, Kanatous SB, Van Der Ven PFM, Goetsch SC & Garry DJ (2007). Xin, an actin binding protein, is expressed within muscle satellite cells and newly regenerated skeletal muscle fibres. *Am J Physiol - Cell Physiol* **293**, 1636–1644.
- Heher P, Maleiner B, Prüller J, Teuschl AH, Kollmitzer J, Monforte X, Wolbank S, Redl H, Rünzler D & Fuchs C (2015). A novel bioreactor for the generation of highly aligned 3D

- skeletal muscle-like constructs through orientation of fibrin via application of static strain. *Acta Biomater* **24**, 251–265.
- Heron MI & Richmond FJR (1993). In-series fibre architecture in long human muscles. *J Morphol* **216**, 35–45.
- Hjorth M, Norheim F, Meen AJ, Pourteymour S, Lee S, Holen T, Jensen J, Birkeland KI, Martinov VN, Langleite TM, Eckardt K, Drevon CA & Kolset SO (2015). The effect of acute and long-term physical activity on extracellular matrix and serglycin in human skeletal muscle. *Physiol Rep* **3**, 1–19.
- Van Horn R & Crow MT (1989). Fast myosin heavy chain expression during the early and late embryonic stages of chicken skeletal muscle development. *Dev Biol* **134**, 279–288.
- Hornberger TA, Armstrong DD, Koh TJ, Burkholder TJ & Esser KA (2005). Intracellular signalling specificity in response to uniaxial vs . multiaxial stretch: implications for mechanotransduction. *Am J Physiol Physiol* **288**, C185–C194.
- Huang Y, Dennis RG & Baar K (2006). Cultured slow vs . fast skeletal muscle cells differ in physiology and. *Am J Physiol* 1–34.
- Hughes VA, Frontera WR, Wood M, Evans WJ, Dallal GE, Roubenoff R & Fiatarone Singh MA (2001). Longitudinal muscle strength changes in older adults: Influence of muscle mass, physical activity, and health. *Journals Gerontol - Ser A Biol Sci Med Sci*; DOI: 10.1093/gerona/56.5.B209.
- Huraskin D, Eiber N, Reichel M, Zidek LM, Kravic B, Bernkopf D, von Maltzahn J, Behrens J & Hashemolhosseini S (2016). Wnt/ β -catenin signalling via Axin2 is required for myogenesis and, together with YAP/Taz and tead1, active in IIa/IIx muscle fibres. *Dev* **143**, 3128–3142.
- Huxley H. (1953). Electron microscope studies of the organisation of the filaments in striated muscle. *Biochim Biophys Acta* **12**, 387–394.
- Hyldahl RD, Nelson B, Xin L, Welling T, Groscost L, Hubal MJ, Chipkin S, Clarkson PM & Parcell AC (2015). Extracellular matrix remodeling and its contribution to protective

- adaptation following lengthening contractions in human muscle. *FASEB J* **29**, 2894–2904.
- Inoue M, Jiang Y, Barnes RH, Tokunaga M, Martinez-Santibañez G, Geletka L, Lumeng CN, Buchner DA & Chun TH (2013). Thrombospondin 1 mediates high-fat diet-induced muscle fibrosis and insulin resistance in male mice. *Endocrinology* **154**, 4548–4559.
- Ito S, Dalessio AC, Taranova O V., Hong K, Sowers LC & Zhang Y (2010). Role of tet proteins in 5mC to 5hmC conversion, ES-cell self-renewal and inner cell mass specification. *Nature* **466**, 1129–1133.
- Ivaska J, Reunanen H, Westermarck J, Koivisto L, Kahari V-M & Heino J (1999). Integrin $\alpha 2\beta 1$ Mediates Isoform-specific Activation of p38 and Upregulation of Collagen Gene Transcription by a Mechanism Involving the $\alpha 2$ Cytoplasmic Tail. *J Cell Biol* **147**, 401–415.
- Janssen IAN, Heymsfield SB, Wang ZIM, Ross R, Heymsfield SB & Wang Z (2000). Skeletal muscle mass and distribution in 468 men and women aged 18 – 88 yr. 81–88.
- Jones D, Round J & de Haan A (2004). *Skeletal Muscle from Molecules to Movement*. Churchill Livingstone. Available at: <http://www.lavoisier.fr/notice/fr283071.html>.
- Jones P., Veenstra GJ., Wade P., Vermaak D, Kass S., Landsberger N, Strouboulis J & Wolffe A. (1998). Methylated DNA and MeCP2 recruit histone deacetylase to repress transcription. *Nat Genet* **19**, 187–191.
- Jung KK, Liu XW, Chirco R, Fridman R & Kim HRC (2006). Identification of CD63 as a tissue inhibitor of metalloproteinase-1 interacting cell surface protein. *EMBO J* **25**, 3934–3942.
- Kalyani RR, Corriere M & Ferrucci L (2014). Age-related and disease-related muscle loss: the effect of diabetes, obesity, and other diseases. *Lancet Diabetes Endocrinol* **2**, 819–829.
- Kanazawa Y, Ikegami K, Sujino M, Koinuma S, Nagano M, Oi Y, Onishi T, Sugiyo S, Takeda I, Kaji H & Shigeyoshi Y (2017). Effects of aging on basement membrane of the soleus muscle during recovery following disuse atrophy in rats. *Exp Gerontol* **98**, 153–161.
- Kanehisa M (1997). A database for post-genome analysis. *Trends Genet* **13**, 375–376.
- Kanehisa M, Furumichi M, Tanabe M, Sato Y & Morishima K (2017). KEGG: New

- perspectives on genomes, pathways, diseases and drugs. *Nucleic Acids Res* **45**, D353–D361.
- Kanehisa M, Sato Y, Kawashima M, Furumichi M & Tanabe M (2016). KEGG as a reference resource for gene and protein annotation. *Nucleic Acids Res* **44**, D457–D462.
- Kang L, Ayala JE, Lee-Young RS, Zhang Z, James FD, Neuffer PD, Pozzi A, Zutter MM & Wasserman DH (2011). Diet-induced muscle insulin resistance is associated with extracellular matrix remodeling and interaction with integrin $\alpha 2\beta 1$ in mice. *Diabetes* **60**, 416–426.
- Kasper AM, Turner DC, Martin NRW & Sharples AP (2018). Mimicking exercise in three-dimensional bioengineered skeletal muscle to investigate cellular and molecular mechanisms of physiological adaptation. *J Cell Physiol* **233**, 1985–1998.
- Khodabukus A & Baar K (2009). Regulating fibrinolysis to engineer skeletal muscle from the C2C12 cell line. *Tissue Eng C, Methods* **15**, 501–511.
- Khodabukus A & Baar K (2012). Defined Electrical Stimulation Emphasizing Excitability for the Development and Testing of Engineered Skeletal Muscle. *Tissue Eng Part C Methods* **18**, 349–357.
- Khodabukus A & Baar K (2015). Glucose Concentration and Streptomycin Alter In Vitro Muscle Function and Metabolism. *J Cell Physiol* **230**, 1226–1234.
- Khodabukus A & Baar K (2016). Factors that affect tissue-engineered skeletal muscle function and physiology. *Cells Tissues Organs*; DOI: 10.1159/000446067.
- Khodabukus A, Baehr LM, Bodine SC & Baar K (2015). Role of contraction duration in inducing fast-to-slow contractile and metabolic protein and functional changes in engineered muscle. *J Cell Physiol* **230**, 2489–2497.
- Khodabukus A, Madden L, Prabhu NK, Koves TR, Jackman CP, Muoio DM & Bursac N (2018a). Electrical stimulation increases hypertrophy and metabolic flux in tissue-engineered human skeletal muscle. *Biomaterials*0–1.
- Khodabukus A, Paxton JZ, Donnelly K & Baar K (2007). Engineered muscle: A tool for

- studying muscle physiology and function. *Exerc Sport Sci Rev* **35**, 186–191.
- Khodabukus A, Prabhu N, Wang J & Bursac N (2018b). In Vitro Tissue-Engineered Skeletal Muscle Models for Studying Muscle Physiology and Disease. *Adv Healthc Mater* **7**, 1–20.
- Kim H, Kim M & Asada H. (2019). Extracellular matrix remodelling induced by alternating electrical and mechanical stimulations increases the contraction of engineered skeletal muscle tissues. *Sci Rep* **9**, 1–11.
- Köhler G & Milstein C (1976). Derivation of specific antibody-producing tissue culture and tumour lines by cell fusion. *Eur J Immunol* **6**, 511–519.
- Kong X, Ball AR, Pham HX, Zeng W, Chen H-Y, Schmiesing JA, Kim J-S, Berns M & Yokomori K (2014). Distinct Functions of Human Cohesin-SA1 and Cohesin-SA2 in Double-Strand Break Repair. *Mol Cell Biol* **34**, 685–698.
- Krüger M & Linke WA (2011). The giant protein titin: A regulatory node that integrates myocyte signalling pathways. *J Biol Chem* **286**, 9905–9912.
- Kurmasheva RT, Peterson CA, Parham DM, Chen B, McDonald RE & Cooney CA (2005). Upstream CpG island methylation of the PAX3 gene in human rhabdomyosarcomas. *Pediatr Blood Cancer* **44**, 328–337.
- Laker RC, Garde C, Camera DM, Smiles WJ, Zierath JR & Hawley JA (2017). Transcriptomic and epigenetic responses to short-term nutrient- exercise stress in humans. 1–12.
- Lakhdar R, Drost EM, MacNee W, Bastos R & Rabinovich RA (2017). 2D-DIGE proteomic analysis of vastus lateralis from COPD patients with low and normal fat free mass index and healthy controls. *Respir Res* **18**, 1–10.
- Langholz O, Röckel D, Mauch C, Kozłowska E, Bank I, Krieg T & Eckes B (1995). Collagen and collagenase gene expression in three-dimensional collagen lattices are differentially regulated by $\alpha 1\beta 1$ and $\alpha 2\beta 1$ integrins. *J Cell Biol* **131**, 1903–1915.
- Laukkanen PIA, Heikkinen E & Kauppinen M (1995). Muscle Strength and Mobility as Predictors of Survival in 75-84-Year-old People. *Age Ageing* **24**, 468–473.
- Lee SJ (2007). Quadrupling muscle mass in mice by targeting TGF- β signalling pathways.

- Lee Y, Ahn C, Han J, Choi H, Kim J, Yim J, Lee J, Provost P, Rådmark O, Kim S & Kim VN (2003). The nuclear RNase III Droscha initiates microRNA processing. *Nature* **425**, 415–419.
- Léger B, Cartoni R, Praz M, Lamon S, Dériaz O, Crettenand A, Gobelet C, Rohmer P, Konzelmann M, Luthi F & Russell AP (2006). Akt signalling through GSK-3 β , mTOR and Foxo1 is involved in human skeletal muscle hypertrophy and atrophy. *J Physiol* **576**, 923–933.
- Lessard SJ, MacDonald TL, Pathak P, Han MS, Coffey VG, Edge J, Rivas DA, Hirshman MF, Davis RJ & Goodyear LJ (2018). JNK regulates muscle remodeling via myostatin/SMAD inhibition. *Nat Commun* **9**, 1–14.
- Lewis M., Tippett H., Sinanan A., Morgan M. & Hunt N. (2000). Gelatinase-B (matrix metalloproteinase-9; MMP-9) secretion is involved in the migratory phase of human and murine muscle cell cultures. *J Muscle Res Cell Motil* **21**, 223–233.
- Lewis MP, Machell JRA, Hunt NP, Sinanan ACM & Tippett HL (2001). The extracellular matrix of muscle - Implications for manipulation of the craniofacial musculature. *Eur J Oral Sci* **109**, 209–221.
- Li Q, Birkbak NJ, Györfy B, Szallasi Z & Eklund AC (2011). Jetset: Selecting the optimal microarray probe set to represent a gene. *BMC Bioinformatics* **12**, 1–7.
- Li W, Tang R, Ma F, Ouyang S, Liu Z & Wu J (2018). Folic acid supplementation alters the DNA methylation profile and improves insulin resistance in high-fat-diet-fed mice. *J Nutr Biochem* **59**, 76–83.
- Li Y, Jiang BH, Ensign WY, Vogt PK & Han J (2000). Myogenic differentiation requires signalling through both phosphatidylinositol 3-kinase and p38 MAP kinase. *Cell Signal* **12**, 751–757.
- Li YP, Chen Y, John J, Moylan J, Jin B, Mann DL & Reid MB (2005). TNF- α acts via p38 MAPK to stimulate expression of the ubiquitin ligase atrogin1/MAFbx in skeletal muscle.

FASEB J **19**, 362–370.

- Litwiniuk A, Pijet B, Pijet-Kucicka M, Gajewska M, Pająk B & Orzechowski A (2016). FOXO1 and GSK-3 β are main targets of insulin-mediated myogenesis in C2C12 muscle cells. *PLoS One* **11**, 1–25.
- Liu D, Sartor MA, Nader GA, Gutmann L, Treutelaar MK, Pistilli EE, IglayReger HB, Burant CF, Hoffman EP & Gordon PM (2010a). Skeletal muscle gene expression in response to resistance exercise: Sex specific regulation. *BMC Genomics*; DOI: 10.1186/1471-2164-11-659.
- Liu H, Chen SE, Jin B, Carson JA, Niu A, Durham W, Lai JY & Li YP (2010b). TIMP3: A physiological regulator of adult myogenesis. *J Cell Sci* **123**, 2914–2921.
- Loughna PT & Brownson C (1996). Two myogenic regulatory factor transcripts exhibit muscle-specific responses to disuse and passive stretch in adult rats. *FEBS Lett* **390**, 304–306.
- Lovelock J & Bishop M (1959). Prevention of freezing damage to living cells by dimethyl sulphoxide. *Nature* **183**, 1394–1395.
- Lundberg TR, Fernandez-gonzalo R, Tesch PA, Rullman XE & Gustafsson T (2016). Aerobic exercise augments muscle transcriptome profile of resistance exercise. *Am J Physiol* **310**, 1279–1287.
- Machida S, Spangenburg EE & Booth FW (2004). Primary rat muscle progenitor cells have decreased proliferation and myotube formation during passages. *Cell Prolif* **37**, 267–277.
- Mackey AL, Kjaer M, Dandanell S, Mikkelsen KH, Holm L, Døssing S, Kadi F, Koskinen SO, Jensen CH, Schrøder HD & Langberg H (2007). The influence of anti-inflammatory medication on exercise-induced myogenic precursor cell responses in humans. *J Appl Physiol* **103**, 425–431.
- MacLaren D & Morton J (2011). *Biochemistry for Sport and Exercise Metabolism*. Wiley; 1 edition.
- MacNeil LG, Melov S, Hubbard AE, Baker SK & Tarnopolsky MA (2010). Eccentric Exercise

- Activates Novel Transcriptional Regulation of Hypertrophic Signalling Pathways Not Affected by Hormone Changes. *PLoS One* **5**, 1–11.
- Maksimovic J, Gordon L & Oshlack A (2012). SWAN: Subset-quantile within array normalization for illumina infinium HumanMethylation450 BeadChips. *Genome Biol* **13**, 1–12.
- Mamchaoui K et al. (2011). Immortalized pathological human myoblasts: Towards a universal tool for the study of neuromuscular disorders. *Skelet Muscle*; DOI: 10.1186/2044-5040-1-34.
- Martin NRW, Passey SL, Player DJ, Khodabukus A, Ferguson RA, Sharples AP, Mudera V, Baar K & Lewis MP (2013). Factors affecting the structure and maturation of human tissue engineered skeletal muscle. *Biomaterials* **34**, 5759–5765.
- Matheny RW & Nindl BC (2011). Loss of IGF-IEa or IGF-IEb impairs myogenic differentiation. *Endocrinology* **152**, 1923–1934.
- Matheny W, Merritt E, Zannikos S V., Farrar RP & Adamo ML (2009). Serum IGF-I-deficiency does not prevent compensatory skeletal muscle hypertrophy in resistance exercise. *Exp Biol Med* **234**, 164–170.
- Mauro A (1961). Satellite Cell of Skeletal Muscle Fibres. *J Cell Biol* **9**, 493–495.
- Mccarthy JJ, Mula J, Miyazaki M, Erfani R, Garrison K, Farooqui AB, Srikuea R, Lawson BA, Grimes B, Keller C, Van Zant G, Campbell KS, Esser KA, Dupont-Versteegden EE & Peterson CA (2011). Effective fibre hypertrophy in satellite cell-depleted skeletal muscle. *Development* **138**, 3657–3666.
- McKay BR, O'Reilly CE, Phillips SM, Tarnopolsky MA & Parise G (2008). Co-expression of IGF-1 family members with myogenic regulatory factors following acute damaging muscle-lengthening contractions in humans. *J Physiol* **586**, 5549–5560.
- McPherron AC & Lee SJ (1997). Double muscling in cattle due to mutations in the myostatin gene. *Proc Natl Acad Sci U S A* **94**, 12457–12461.
- Mehan RS, Greybeck BJ, Emmons K, Byrnes WC & Allen DL (2011). Matrix

- metalloproteinase-9 deficiency results in decreased fibre cross-sectional area and alters fibre type distribution in mouse hindlimb skeletal muscle. *Cells Tissues Organs* **194**, 510–520.
- Mendias CL, Marcin JE, Calerdon DR & Faulkner JA (2006). Contractile properties of EDL and soleus muscles of myostatin-deficient mice. *J Appl Physiol* **101**, 898–905.
- Mitin BN, Ramocki MB, Koneczny SF & Taparowsky EJ (2001). Ras Regulation of Skeletal Muscle Differentiation and Gene Expression. *Methods* **333**, 232–247.
- Miyazaki M, Mccarthy JJ, Fedele MJ & Esser KA (2011). Early activation of mTORC1 signalling in response to mechanical overload is independent of phosphoinositide 3-kinase/Akt signalling. *J Physiol* **589**, 1831–1846.
- Morse CI, Thom JM, Reeves ND, Birch KM & Narici M V. (2005). In vivo physiological cross-sectional area and specific force are reduced in the gastrocnemius of elderly men. *J Appl Physiol* **99**, 1050–1055.
- Mudera V, Smith AST, Brady MA & Lewis MP (2010). The effect of cell density on the maturation and contractile ability of muscle derived cells in a 3D tissue-engineered skeletal muscle model and determination of the cellular and mechanical stimuli required for the synthesis of a postural phenotype. *J Cell Physiol* **225**, 646–653.
- Mudera VC, Pleass R, Eastwood M, Tarnuzzer R, Schultz G, Khaw P, McGrouther DA & Brown RA (2000). Molecular responses of human dermal fibroblasts to dual cues: Contact guidance and mechanical load. *Cell Motil Cytoskeleton* **45**, 1–9.
- Mullis K & Faloona F (1987). Specific Synthesis of DNA in Vitro via a Polymerase-Catalyzed Chain Reaction. *Methods Enzymol* **155**, 335–350.
- Muráni E, Murániová M, Ponsuksili S, Schellander K & Wimmers K (2007). Identification of genes differentially expressed during prenatal development of skeletal muscle in two pig breeds differing in muscularity. *BMC Dev Biol* **7**, 1–16.
- Murton AJ, Billeter R, Stephens FB, Des Etages SG, Graber F, Hill RJ, Marimuthu K & Greenhaff PL (2014). Transient transcriptional events in human skeletal muscle at the

- outset of concentric resistance exercise training. *J Appl Physiol* **116**, 113–125.
- Nazari H, Khaleghian A, Takahashi A, Harada N, Webster NJG, Nakano M, Kishi K, Ebina Y & Nakaya Y (2011). Cortactin, an actin binding protein, regulates GLUT4 translocation via actin filament remodeling. *Biochem* **76**, 1262–1269.
- Nettersheim D, Biermann K, Gillis AJM, Steger K, Looijenga LHJ & Schorle H (2011). NANOG promoter methylation and expression correlation during normal and malignant human germ cell development. *Epigenetics* **6**, 114–122.
- Nguyen AT, Xiao B, Neppl RL, Kallin EM, Li J, Chen T, Wang DZ, Xiao X & Zhang Y (2011). DOT1L regulates dystrophin expression and is critical for cardiac function. *Genes Dev* **25**, 263–274.
- Nilsson MI, Nissar AA, Al-Sajee D, Tarnopolsky MA, Parise G, Lach B, Fürst DO, Van Der Ven PFM, Kley RA & Hawke TJ (2013). Xin is a marker of skeletal muscle damage severity in myopathies. *Am J Pathol* **183**, 1703–1709.
- Nishisho T, Yukata K, Matsui Y, Matsuura T, Higashino K, Suganuma K, Nikawa T & Yasui N (2012). Angiogenesis and myogenesis in mouse tibialis anterior muscles during distraction osteogenesis: VEGF, its receptors, and myogenin genes expression. *J Orthop Res* **30**, 1767–1773.
- Nissar AA, Zemanek B, Labatia R, Atkinson DJ, van der Ven PFM, Fürst DO & Hawke TJ (2012). Skeletal muscle regeneration is delayed by reduction in Xin expression: Consequence of impaired satellite cell activation? *Am J Physiol - Cell Physiol* **302**, 220–227.
- Nygaard V, Rødland EA & Hovig E (2016). Methods that remove batch effects while retaining group differences may lead to exaggerated confidence in downstream analyses. *Biostatistics* **17**, 29–39.
- Oliveira GP, Porto WF, Palu CC, Pereira LM, Petriz B, Almeida JA, Viana J, Filho NNA, Franco OL & Pereira RW (2018). Effects of acute aerobic exercise on rats serum extracellular vesicles diameter, concentration and small RNAs content. *Front Physiol* **9**,

1–11.

Oliveira S, Storm G & Schiffelers R (2006). Targeted delivery of siRNA. *J Biomed Biotechnol* **2006**, 1–9.

Osman AA, Hancock J, Hunt DG, Ivy JL & Mandarino LJ (2001). Exercise training increases ERK2 activity in skeletal muscle of obese Zucker rats. *J Appl Physiol* **90**, 454–460.

Owens DJ, Sharples AP, Polydorou I, Alwan N, Donovan T, Tang J, Fraser WD, Cooper RG, Morton JP, Stewart C & Close GL (2015). A systems-based investigation into vitamin D and skeletal muscle repair, regeneration, and hypertrophy. *Am J Physiol - Endocrinol Metab* **309**, E1019–E1031.

Pansters NAM, Schols AMWJ, Verhees KJP, de Theije CC, Snepvangers FJ, Kelders MCJM, Ubags NDJ, Haegens A & Langen RCJ (2015). Muscle-specific GSK-3 β ablation accelerates regeneration of disuse-atrophied skeletal muscle. *Biochim Biophys Acta - Mol Basis Dis* **1852**, 490–506.

Patton BL, Connolly AM, Martin PT, Cunningham JM, Mehta S, Pestronk A, Miner JH & Sanes JR (1999). Distribution of ten laminin chains in dystrophic and regenerating muscles. *Neuromuscul Disord* **9**, 423–433.

Pérez-schindler J, Esparza MC, Mckendry J, Breen L & Philp A (2017). Overload-mediated skeletal muscle hypertrophy is not impaired by loss of myofibre STAT3. *Am J Physiol Cell Physiol* **313**, 257–261.

Periasamy M & Kalyanasundaram A (2007). SERCA pump isoforms: Their role in calcium transport and disease. *Muscle and Nerve* **35**, 430–442.

Peters LL, John KM, Lu FM, Eicher EM, Higgins A, Yialamas M, Turtzo LC, Otsuka AJ & Lux SE (1995). Ank3 (epithelial ankyrin), a widely distributed new member of the ankyrin gene family and the major ankyrin in kidney, is expressed in alternatively spliced forms, including forms that lack the repeat domain. *J Cell Biol* **130**, 313–330.

Peviani SM, Gomes ARS, Moreira RFC, Moriscot AS & Salvini TF (2007). Short bouts of stretching increase myo-D, myostatin and atrogen-1 in rat soleus muscle. *Muscle and*

- Nerve* **35**, 363–370.
- Phillips BE, Williams JP, Gustafsson T, Bouchard C, Rankinen T, Knudsen S, Smith K, Timmons JA & Atherton PJ (2013). Molecular Networks of Human Muscle Adaptation to Exercise and Age. *PLoS Genet*; DOI: 10.1371/journal.pgen.1003389.
- Phillips SM, Tipton KD, Aarsland A, Wolf SE & Wolfe RR (1997). Mixed muscle protein synthesis and breakdown after resistance exercise in humans. *Am J Physiol* **E99**–E107.
- Philp A, Hamilton DL & Baar K (2011). Highlighted topic signals mediating skeletal muscle remodeling by activity signals mediating skeletal muscle remodeling by resistance exercise: PI3-kinase independent activation of mTORC1. *J Appl Physiol* **110**, 561–568.
- Pierron M, Pinan-Lucarré B & Bessereau JL (2016). Preventing illegitimate extrasynaptic acetylcholine receptor clustering requires the RSU-1 protein. *J Neurosci* **36**, 6525–6537.
- Pines M, Levi O, Genin O, Lavy A, Angelini C, Allamand V & Halevy O (2017). Elevated Expression of Moesin in Muscular Dystrophies. *Am J Pathol* **187**, 654–664.
- Player DJ, Martin NRW, Passey SL, Sharples AP, Mudera V & Lewis MP (2014). Acute mechanical overload increases IGF-I and MMP-9 mRNA in 3D tissue-engineered skeletal muscle. *Biotechnol Lett* **36**, 1113–1124.
- Pletz N, Medack A, Rieß EM, Yang K, Kazerouni ZB, Hüber D & Hoyer-Fender S (2013). Transcriptional activation of Odf2/Cenexin by cell cycle arrest and the stress activated signalling pathway (JNK pathway). *Biochim Biophys Acta - Mol Cell Res* **1833**, 1338–1346.
- Pomerantz JL (1999). NF-kappa B activation by a signalling complex containing TRAF2, TANK and TBK1, a novel IKK-related kinase. *EMBO J* **18**, 6694–6704.
- Powell CA, Smiley BL, Mills J & Vandeburgh HH (2002). Mechanical stimulation improves tissue-engineered human skeletal muscle. *AJP Cell Physiol* **283**, C1557–C1565.
- Powell JA, Molgó J, Adams DS, Colasante C, Williams A, Bohlen M & Jaimovich E (2003). I_{p3} receptors and associated Ca²⁺ signals localize to satellite cells and to components of the neuromuscular junction in skeletal muscle. *J Neurosci* **23**, 8185–8192.

- Prescott MJ & Lidster K (2017). Improving quality of science through better animal welfare: The NC3Rs strategy. *Lab Anim (NY)* **46**, 152–156.
- Puntschart A, Wey K, Jostarndt K, Vogt M, Wittwer M, Widmer H., Hoppeler H & Billeter R (1999). Expression of fos and jun genes in human skeletal muscle after exercise. *Am J Physiol - Cell Physiol* **274**, 129–137.
- Ramakrishnan V (1997). Histone structure and the organization of the nucleosome. *Annu Rev Biophys Biomol Struct* **26**, 83–112.
- Rao L, Qian Y, Khodabukus A, Ribar T & Bursac N (2018). Engineering human pluripotent stem cells into a functional skeletal muscle tissue. *Nat Commun* **9**, 1–12.
- Raue U, Trappe TA, Estrem ST, Qian H, Helvering LM, Smith RC & Trappe S (2012). Transcriptome signature of resistance exercise adaptations : mixed muscle and fibre type specific profiles in young and old adults. *J Appl Physiol* **112**, 1625–1636.
- Rayagiri SS, Ranaldi D, Raven A, Mohamad Azhar NIF, Lefebvre O, Zammit PS & Borycki AG (2018). Basal lamina remodeling at the skeletal muscle stem cell niche mediates stem cell self-renewal. *Nat Commun* **9**, 1–12.
- Rehfeldt C, Renne U, Sawitzky M, Binder G & Hoeflich A (2010). Increased fat mass, decreased myofibre size, and a shift to glycolytic muscle metabolism in adolescent male transgenic mice overexpressing IGFBP-2. *Am J Physiol - Endocrinol Metab* **299**, 287–298.
- Relaix F, Montarras D, Zaffran S, Gayraud-Morel B, Rocancourt D, Tajbakhsh S, Mansouri A, Cumano A & Buckingham M (2006). Pax3 and Pax7 have distinct and overlapping functions in adult muscle progenitor cells. *J Cell Biol* **172**, 91–102.
- Relaix F, Rocancourt D, Mansouri A & Buckingham M (2005). A Pax3/Pax7-dependent population of skeletal muscle progenitor cells. *Nature* **435**, 948–953.
- Rigamonti E, Touvier T, Clementi E, Manfredi AA, Brunelli S & Rovere-Querini P (2013). Requirement of Inducible Nitric Oxide Synthase for Skeletal Muscle Regeneration after Acute Damage. *J Immunol* **190**, 1767–1777.

- Robinson MM, Dasari S, Konopka AR, Johnson ML, Manjunatha S, Esponda RR, Carter RE, Lanza IR & Nair KS (2017). Enhanced Protein Translation Underlies Improved Metabolic and Physical Adaptations to Different Exercise Training Modes in Young and Old Humans. *Cell Metab* **25**, 581–592.
- Romanazzo S, Forte G, Ebara M, Uto K, Pagliari S, Aoyagi T, Traversa E & Taniguchi A (2012). Substrate stiffness affects skeletal myoblast differentiation in vitro. *Sci Technol Adv Mater* **13**, 1–9.
- Rosenblatt JD & Parry DJ (1992). Gamma irradiation prevents compensatory hypertrophy of overloaded mouse extensor digitorum longus muscle. *J Appl Physiol* **73**, 2538–2543.
- Rothberg JM et al. (2011). An integrated semiconductor device enabling non-optical genome sequencing. *Nature* **475**, 348–352.
- Rowlands DS et al. (2014). Multi-omic integrated networks connect DNA methylation and miRNA with skeletal muscle plasticity to chronic exercise in Type 2 diabetic obesity. *Physiol Genomics Exerc Heal Dis Multi-omic* **7**, 47–765.
- Ruiz JR, Sui X, Lobelo F, Morrow Jr JR, Jackson AW, Sjostrom M & Blair SN (2008). men : prospective cohort study. *BMJ* **337**, 1–9.
- Russell AP, Lamon S, Boon H, Wada S, Güller I, Brown EL, Chibalin A V., Zierath JR, Snow RJ, Stepto N, Wadley GD & Akimoto T (2013). Regulation of miRNAs in human skeletal muscle following acute endurance exercise and short-term endurance training. *J Physiol* **591**, 4637–4653.
- Ryan NA, Zwetsloot KA, Westerkamp LM, Hickner RC, Pofahl WE & Gavin TP (2006). Lower skeletal muscle capillarization and VEGF expression in aged vs. young men. *J Appl Physiol* **100**, 178–185.
- Sachs M, Brohmann H, Zechner D, Müller T, Hülsken J, Walther I, Schaeper U, Birchmeier C & Birchmeier W (2000). Essential role of Gab1 for signalling by the c-Met receptor in vivo. *J Cell Biol* **150**, 1375–1384.
- Sahni A, Artland OD & Francis CW (2003). FGF-2 but not FGF-1 binds fibrin and supports

- prolonged endothelial cell growth. *J Thromb Haemost* **1**, 1304–1310.
- Sahni A & Francis CW (2000). Vascular endothelial growth factor binds to fibrinogen and fibrin and stimulates endothelial cell proliferation. *Blood* **12**, 3772–3778.
- Sailani MR, Halling JF, Møller HD, Lee H, Plomgaard P, Pilegaard H, Snyder MP & Regenberg B (2019). Lifelong physical activity is associated with promoter hypomethylation of genes involved in metabolism, myogenesis, contractile properties and oxidative stress resistance in aged human skeletal muscle. *Sci Rep* **9**, 1–11.
- Sale DG (1988).  Neural Adaptation to Resistance Exercise. *Med Sci Sport Exerc* **20**, S135–S145.
- Salmon N., Reijo Pera R. & Yujun Xu E (2006). A Gene Trap Knockout of the Abundant Sperm Tail Protein, Outer Dense Fibre 2, Results in Preimplantation Lethality. *Genesis* **44**, 515–522.
- Schiaffino S, Pierobon Bormioli S & Aloisi M (1972). Cell proliferation in rat skeletal muscle during early stages of compensatory hypertrophy. *Virchows Arch B Cell Pathol Zell-pathologie* **11**, 268–273.
- Schiaffino S, Pierobon Bormioli S & Aloisi M (1976). The fate of newly formed satellite cells during compensatory muscle hypertrophy. *Virchows Arch B Cell Pathol* **21**, 113–118.
- Schiaffino S & Reggiani C (2011). FIBRE TYPES IN MAMMALIAN SKELETAL MUSCLES. *Physiol Rev* **91**, 1447–1531.
- Schmidt EK, Clavarino G, Ceppi M & Pierre P (2009). SUnSET, a nonradioactive method to monitor protein synthesis. *Nat Methods* **6**, 275–277.
- Schmittgen TD & Livak KJ (2008). Analyzing real-time PCR data by the comparative CT method. *Nat Protoc* **3**, 1101–1108.
- Schmoll M, Unger E, Sutherland H, Haller M, Bijak M, Lanmuller H & Jarvis JC (2018). SpillOver stimulation : A novel hypertrophy model using co-contraction of the plantar-flexors to load the tibial anterior muscle in rats. *PLoS One* **13**, 1–19.
- Seaborne R., Hughes DC, Turner DC, Owens DJ, Baehr LM, Gorski P, Semenova EA, Borisov

- O V., Larin AK, Popov D V., Generozov E V., Sutherland H, Ahmetov II, Jarvis JC, Bodine SC & Sharples AP (2019). UBR5 is a novel E3 ubiquitin ligase involved in skeletal muscle hypertrophy and recovery from atrophy. *J Physiol* **597**, 3727–3749.
- Seaborne R., Strauss J, Cocks M, Shepherd S, Brien TDO & Someren KA Van (2018a). Data Descriptor : Methylome of human skeletal muscle after acute & chronic resistance exercise training , detraining & retraining. *Nat Publ Gr* **5**, 1–9.
- Seaborne R., Strauss J, Cocks M, Shepherd S, O'Brien T., Van Someren K., Bell P., Murgatroyd C, Morton J., Stewart C. & Sharples A. (2018b). Human Skeletal Muscle Possesses an Epigenetic Memory of Hypertrophy. *Sci Rep* **8**, 1–17.
- Seward DJ, Haney JC, Rudnicki MA, Swoap SJ, David J, Haney JC, Rudnicki MA & Swoap SJ (2001). bHLH transcription factor MyoD affects myosin heavy chain expression pattern in a muscle-specific fashion. *Am J Physiol Cell Physiol* **85**, 408–413.
- Shahini A, Choudhury D, Asmani M, Zhao R, Lei P & Andreadis ST (2018). NANOG restores the impaired myogenic differentiation potential of skeletal myoblasts after multiple population doublings. *Stem Cell Res* **26**, 55–66.
- Sharples AP, Al-Shanti N, Hughes DC, Lewis MP & Stewart CE (2013). The role of insulin-like-growth factor binding protein 2 (IGFBP2) and phosphatase and tensin homologue (PTEN) in the regulation of myoblast differentiation and hypertrophy Adam. *Growth Horm IGF Res* **23**, 53–61.
- Sharples AP, Hughes DC, Deane CS, Saini A, Selman C & Stewart CE (2015). Longevity and skeletal muscle mass: The role of IGF signalling, the sirtuins, dietary restriction and protein intake. *Aging Cell* **14**, 511–523.
- Sharples AP, Player DJ, Martin NRW, Mudera V, Stewart CE & Lewis MP (2012). Modelling in vivo skeletal muscle ageing in vitro using three-dimensional bioengineered constructs. *Aging Cell* **11**, 986–995.
- Sharples AP, Polydorou I, Hughes DC, Owens DJ, Hughes TM & Stewart CE (2016a). Skeletal muscle cells possess a ‘memory’ of acute early life TNF- α exposure: role of epigenetic

- adaptation. *Biogerontology* **17**, 603–617.
- Sharples AP & Seaborne RA (2019). Exercise and DNA methylation in skeletal muscle. In *Sports, Exercise, and Nutritional Genomics*, ed. Barh D & Ahmetov II, pp. 211–229. Elsevier.
- Sharples AP & Stewart CE (2011). Myoblast models of skeletal muscle hypertrophy and atrophy. *Curr Opin Clin Nutr Metab Care* **14**, 230–236.
- Sharples AP, Stewart CE & Seaborne RA (2016b). Does skeletal muscle have an ‘epi’-memory? The role of epigenetics in nutritional programming, metabolic disease, aging and exercise. *Aging Cell* **15**, 603–616.
- Sinanan ACM, Machell JRA, Wynne-hughes GT, Hunt NP & Lewis MP (2008). $\alpha\beta3$ and $\alpha\beta5$ integrins and their role in muscle precursor cell adhesion. *J Oral Sci* **100**, 465–477.
- Smith AST, Passey S, Greensmith L, Mudera V & Lewis MP (2012). Characterization and optimization of a simple, repeatable system for the long term in vitro culture of aligned myotubes in 3D. *J Cell Biochem* **113**, 1044–1053.
- Smith P, Krohn R, Hermanson G, Mallia A, Gartner F, Provenzano M, Fujimoto E, Goeke N, Olson B & Klenk D (1985). Measurement of protein using bicinchoninic acid. *Anal Biochem* **150**, 76–85.
- Song W, Kwak HB, Kim JH & Lawler JM (2009). Exercise training modulates the nitric oxide synthase profile in skeletal muscle from old rats. *Journals Gerontol - Ser A Biol Sci Med Sci* **64**, 540–549.
- Sugiura T, Mlyata H, Kawai Y, Matoba H & Murakami N (1993). Changes in myosin heavy chain isoform expression of overloaded rat skeletal muscles. *Int J Biochem* **25**, 1609–1613.
- Sutrave P, Kelly AM & Hughes SH (1990). Ski can cause selective growth of skeletal muscle in transgenic mice. *Genes Dev* **4**, 1462–1472.
- Tajbakhsh S, Rocancourt D & Buckingham M (1996). Muscle progenitor cells failing to respond to positional cues adopt non-myogenic fates in myf-5 null mice. *Nature* **384**, 266–269.

- Tajbakhsh S, Rocancourt D, Cossu G & Buckingham M (1997). Redefining the genetic hierarchies controlling skeletal myogenesis: Pax-3 and Myf-5 act upstream of MyoD. *Cell* **89**, 127–138.
- Tando T et al. (2016). Smad2/3 proteins are required for immobilization-induced skeletal muscle atrophy. *J Biol Chem* **291**, 12184–12194.
- Taylor L., Wilborn C., Kreider R. & Willoughby DS (2012). Effects of Resistance Exercise Intensity on Extracellular Signal-Regulated Kinase 1/2 Mitogen-Activated Protein Kinase Activation in Men. *J Strength Cond Res* **26**, 599–607.
- Tee JM & Peppelenbosch MP (2010). Anchoring skeletal muscle development and disease: The role of ankyrin repeat domain containing proteins in muscle physiology. *Crit Rev Biochem Mol Biol* **45**, 318–330.
- Thalacker-Mercer A, Stec M, Cui X, Cross J, Windham S & Bamman M (2013). Cluster analysis reveals differential transcript profiles associated with resistance training-induced human skeletal muscle hypertrophy. *Physiol Genomics* **45**, 499–507.
- Tortora G. & Derrickson B (2012). *Principles of Anatomy & Physiology*. John Wiley & Sons, Inc.
- Tost J & Gut IG (2007). DNA methylation analysis by pyrosequencing. *Nat Protoc* **2**, 2265–2275.
- Trasler J, Deng L, Melnyk S, Pogribny I, Hiou-Tim F, Sibani S, Oakes C, Li E, James SJ & Rozen R (2003). Impact of Dnmt1 deficiency, with and without low folate diets, on tumour numbers and DNA methylation in min mice. *Carcinogenesis* **24**, 39–45.
- Trendelenburg AU, Meyer A, Rohner D, Boyle J, Hatakeyama S & Glass DJ (2009). Myostatin reduces Akt/TORC1/p70S6K signalling, inhibiting myoblast differentiation and myotube size. *Am J Physiol - Cell Physiol* **296**, 1258–1270.
- Trenerry MK, Carey KA, Ward AC & Cameron-Smith D (2007). STAT3 signalling is activated in human skeletal muscle following acute resistance exercise. *J Appl Physiol* **102**, 1483–1489.

- Troy A, Cadwallader AB, Fedorov Y, Tyner K, Tanaka KK & Olwin BB (2012). Coordination of satellite cell activation and self-renewal by par-complex-dependent asymmetric activation of p38 α / β MAPK. *Cell Stem Cell* **11**, 541–553.
- Tseng BS, Kasper CE & Edgerton VR (1994). Cytoplasm-to-myonucleus ratios and succinate dehydrogenase activities in adult rat slow and fast muscle fibres. *Cell Tissue Res* **275**, 39–49.
- Tsumagari K, Baribault C, Terragni J, Varley KE, Gertz J, Pradhan S, Badoo M, Crain CM, Song L, Crawford GE, Myers RM, Lacey M & Ehrlich M (2013). Early de novo DNA methylation and prolonged demethylation in the muscle lineage. *Epigenetics* **8**, 317–332.
- Turner DC, Kasper AM, Seaborne RA, Brown AD, Close GL, Murphy M, Stewart CE, Martin NRW & Sharples AP (2019a). Exercising Bioengineered Skeletal Muscle In Vitro: Biopsy to Bioreactor. In *Methods in Molecular Biology*, Myogenesis., ed. Rønning S., pp. 55–79. Springer International Publishing, New York, NY.
- Turner DC, Seaborne RA & Sharples AP (2019b). Comparative Transcriptome and Methylome Analysis in Human Skeletal Muscle Anabolism , Hypertrophy and Epigenetic Memory. *Sci Rep* **9**, 1–12.
- Tuzmen S, Kiefer J & Mousses S (2007). Validation of Short Interfering RNA Knockdowns by Quantitative Real-Time PCR. In *Protocols for Nucleic Acid Analysis by Nonradioactive Probes*, Methods in., ed. Hilario E & Mackay J, pp. 177–203. Humana Press.
- Vandenburgh H, Karlisch P & Farr L (1988). Maintenance of Highly Contractile Tissue-Cultured Avian Skeletal Myotubes in Collagen Gel Author (s): Herman H . Vandenburgh , Patricia Karlisch , Lynne Farr Published by : Society for In Vitro Biology Stable URL : <http://www.jstor.org/stable/4296193> MA. *Vitr Cell Dev Biol* **24**, 166–174.
- Vandenburgh H & Kaufman S (1979). In vitro model for stretch-induced hypertrophy of skeletal muscle. *Science (80-)* **203**, 265–268.
- Vandenburgh H, Shansky J, Benesch-Lee F, Barbata V, Reid J, Thorrez L, Valentini R & Crawford G (2008). Drug-screening platform based on the contractility of tissue-

- engineered muscle. *Muscle and Nerve* **37**, 438–447.
- Vandenburgh HH (1988). A Computerized Mechanical Cell Stimulator for Tissue Culture : Effects on Skeletal Muscle Organogenesis. *Vitr Cell Dev Biol* **24**, 609–619.
- Vandenburgh HH, Hatfaludy S, Karlisch P & Shansky J (1989). Skeletal muscle growth is stimulated in tissue culture by intermittent. *Am J Physiol Physiol* **256**, C674–C682.
- Vandenburgh HH & Karlisch P (1989). Longitudinal Growth of Skeletal Myotubes In Vitro in a New Horizontal Mechanical Cell Stimulator. **25**, 607–616.
- Vissing K & Schjerling P (2014). Simplified data access on human skeletal muscle transcriptome responses to differentiated exercise. *Sci Data* 1–9.
- Van De Vyver M & Myburgh KH (2012). Cytokine and satellite cell responses to muscle damage: Interpretation and possible confounding factors in human studies. *J Muscle Res Cell Motil* **33**, 177–185.
- Wackerhage H (2014). *Molecular Exercise Physiology*.
- Waddington CH (1942). The epigenotype. *Endeavor* **1**, 18–20.
- Wehrle U, Düsterhöft S & Pette D (1994). Effects of chronic electrical stimulation on myosin heavy chain expression in satellite cell cultures derived from rat muscles of different fibre-type composition. *Differentiation* **58**, 37–46.
- Wessner B, Liebensteiner M, Nachbauer W & Csapo R (2019). Age-specific response of skeletal muscle extracellular matrix to acute resistance exercise: A pilot study. *Eur J Sport Sci* **19**, 354–364.
- Widmann M, Nieß AM & Munz B (2019). Physical Exercise and Epigenetic Modifications in Skeletal Muscle. *Sport Med* **49**, 509–523.
- Willoughby DS & Nelson MJ (2002). Myosin heavy-chain mRNA expression after a single session of heavy-resistance exercise. *Med Sci Sports Exerc* **34**, 1262–1269.
- Wright WE, Sassoon DA & Lin VK (1989). Myogenin, a factor regulating myogenesis, has a domain homologous to MyoD. *Cell* **56**, 607–617.
- Xin X, Wang T, Liu X, Sui G, Jin C, Yue Y, Yang S & Guo H (2017). A yeast two-hybrid

- assay reveals CMYA1 interacting proteins. *Comptes Rendus - Biol* **340**, 314–323.
- Xu Q, Wu N, Cui L, Wu Z & Qiu G (2017). Filamin B: The next hotspot in skeletal research? *J Genet Genomics* **44**, 335–342.
- Yabumoto C, Akazawa H, Yamamoto R, Yano M, Kudo-Sakamoto Y, Sumida T, Kamo T, Yagi H, Shimizu Y, Saga-Kamo A, Naito AT, Oka T, Lee JK, Suzuki JI, Sakata Y, Uejima E & Komuro I (2015). Angiotensin II receptor blockade promotes repair of skeletal muscle through down-regulation of aging-promoting C1q expression. *Sci Rep* **5**, 1–15.
- Yaffe D & Saxel O (1977). Serial passaging and differentiation of myogenic cells isolated from dystrophic mouse muscle. *Nature* **270**, 725–727.
- Yang J, Huang J, Dasgupta M, Sears N, Miyagi M, Wang B, Chance MR, Chen X, Du Y, Wang Y, An L, Wang Q, Lu T, Zhang X, Wang Z & Stark GR (2010). Reversible methylation of promoter-bound STAT3 by histone-modifying enzymes. *Proc Natl Acad Sci U S A* **107**, 21499–21504.
- Yang S, Alnaqeeb M, Simpson H & Goldspink G (1996). Cloning and characterization of an IGF-1 isoform expressed in skeletal muscle subjected to stretch. *J Muscle Res Cell Motil* **17**, 487–495.
- Yang SY & Goldspink G (2002). Different roles of the IGF-I Ec peptide (MGF) and mature IGF-I in myoblast proliferation and differentiation. *FEBS Lett* **522**, 156–160.
- Yasuda N, Miura SI, Akazawa H, Tanaka T, Qin Y, Kiya Y, Imaizumi S, Fujino M, Ito K, Zou Y, Fukuhara S, Kunimoto S, Fukuzaki K, Sato T, Ge J, Mochizuki N, Nakaya H, Saku K & Komuro I (2008). Conformational switch of angiotensin II type 1 receptor underlying mechanical stress-induced activation. *EMBO Rep* **9**, 179–186.
- Yen-Chih Huang, Robert G. Dennis, Lisa Larkin and KB (2005). Rapid formation of functional muscle in vitro using fibrin gels Yen-Chih. **98**, 706–713.
- You J-S, McNally RM, Jacobs BL, Privett RE, Gundermann DM, Lin K-H, Steinert ND, Goodman CA & Hornberger TA (2019). The role of raptor in the mechanical load-induced regulation of mTOR signalling, protein synthesis, and skeletal muscle hypertrophy.

- FASEB J* **33**, 4021–4034.
- Zammit PS (2017). Function of the myogenic regulatory factors Myf5, MyoD, Myogenin and MRF4 in skeletal muscle, satellite cells and regenerative myogenesis. *Semin Cell Dev Biol* **72**, 19–32.
- Zammit PS, Golding JP, Nagata Y, Hudon V, Partridge TA & Beauchamp JR (2004). Muscle satellite cells adopt divergent fates: A mechanism for self-renewal? *J Cell Biol* **166**, 347–357.
- Zammit PS, Heslop L, Hudon V, Rosenblatt JD, Tajbakhsh S, Buckingham ME, Beauchamp JR & Partridge TA (2002). Kinetics of myoblast proliferation show that resident satellite cells are competent to fully regenerate skeletal muscle fibres. *Exp Cell Res* **281**, 39–49.
- Zhang Q, Joshi SK, Lovett DH, Zhang B, Bodine S, Kim H & Liu X (2014). Matrix metalloproteinase-2 plays a critical role in overload induced skeletal muscle hypertrophy. *Muscles Ligaments Tendons J* **4**, 362–370.
- Zhang SX, Garcia-Gras E, Wycuff DR, Marriot SJ, Kadeer N, Yu W, Olson EN, Garry DJ, Parmacek MS & Schwartz RJ (2005). Identification of direct serum-response factor gene targets during Me 2SO-induced P19 cardiac cell differentiation. *J Biol Chem* **280**, 19115–19126.
- Zhang W, Xu Y, Zhang L, Wang S, Yin B, Zhao S & Li X (2018). Synergistic effects of TGF β 2, WNT9a, and FGFR4 signals attenuate satellite cell differentiation during skeletal muscle development. *Aging Cell* **17**, 1–13.
- Zhang W, Zhang S, Xu Y, Ma Y, Zhang D, Li X & Zhao S (2019a). The DNA methylation status of wnt and Tgff β signals is a key factor on functional regulation of skeletal muscle satellite cell development. *Front Genet* **10**, 1–11.
- Zhang X, Wang L, Qiu K, Xu D & Yin J (2019b). Dynamic membrane proteome of adipogenic and myogenic precursors in skeletal muscle highlights EPHA2 may promote myogenic differentiation through ERK signalling. *FASEB J* **33**, 5495–5509.
- Zhao MJ, Xie J, Shu WJ, Wang HY, Bi J, Jiang W & Du HN (2019). MiR-15b and miR-322

inhibit SETD3 expression to repress muscle cell differentiation. *Cell Death Dis*; DOI: 10.1038/s41419-019-1432-5.

Zhou Y, Song N, Li X, Han Y, Ren Z, Xu J xian, Han Y chen, Li F & Jia X (2017). Changes in the methylation status of the Oct 3/4, Nanog, and Sox2 promoters in stem cells during regeneration of rat tracheal epithelium after injury. *Oncotarget* **8**, 2984–2994.

Zhu Y, James RM, Peter A, Lomas C, Cheung F, Harrison DJ & Bader SA (2004). Functional Smoothed is required for expression of GLI3 in colorectal carcinoma cells. *Cancer Lett* **207**, 205–214.

Zou Y, Akazawa H, Qin Y, Sano M, Takano H, Minamino T, Makita N, Iwanaga K, Zhu W, Kudoh S, Toko H, Tamura K, Kihara M, Nagai T, Fukamizu A, Umemura S, Iiri T, Fujita T & Komuro I (2004). Mechanical stress activates angiotensin II type 1 receptor without the involvement of angiotensin II. *Nat Cell Biol* **6**, 499–506.

CHAPTER 9

Thesis Appendices

Table 5.1. Mouse primer sequences for genes that are significantly regulated across the human transcriptome and methylome after acute RE in humans

Target Gene	Primer Sequence (5'-3')	Product Length (bp)	Reference Seq. Number
MSN	F: GGATGCCTTGGGTCTCAACA	75	NM_010833.2
	R: ATTTCACTCCACGGGAAGCC		
TIMP3	F: CAAGGGCCTCAATTACCGCT	107	NM_011595.2
	R: TGTCGGTCCAGAGACACTCA		
WNT9a	F: CTGGCCTCCTCAACCCTTTT	75	NM_139298.2
	R: GCATTACTGCAACGCTCTCG		
CTTN	F: AGCATGCCTCCCAGAAAGAC	70	NM_001357116.1
	R: TCTACACGGTCAGCTTGAC		
GSK3B	F: GAAGACTTGCCTTTGGCGTG	100	NM_019827.7
	R: TAGTGACCTCCCTGGGCTAC		
PAX3	F: TCAACCAGCTCGGAGGAGTA	105	NM_008781.4
	R: AAATGACGCAAGGCCGAATG		
AGTR1	F: TCGCACTCAAGCCTGTCTAC	98	XM_011244264.2
	R: ACCTCAGAACAAGACGCAGG		
FOS	F: TACTACCATTCCCCAGCCGA	113	NM_010234.3
	R: GCTGTCACCGTGGGGATAAA		
THBS1	F: TGTAAGCCTGAGACCTGCC	71	NM_001313914.1
	R: TTCGTAAAGGCCGAGTGCT		
ITPR3	F: TGTCTGACCAGAAGAACGCC	85	XM_006523712.3
	R: TTGCGGTAGTCCTCCTGAGA		

RARA	F: ATCTGTGGAGACCGACAGGA	96	NM_001361954.1
	R: CCGTTTCCGGACGTAGACTT		XM_006532592.3
			XM_006532597.2
			XM_006532593.2
			XM_006532593.2
			NM_001177302.1
			NM_001176528.1
			NM_009024.2
FLNB	F: AGTGCGATGCCCCGAGTTTTA	104	NM_001081427.1
	R: AGGGGCAGGAGGTACGTATT		XM_006518050.1
			NM_134080.1
LAMA5	F: CGGGTATCAACTGTGAGCGT	71	XM_017315832.1
	R: ATGAGGTGAGTCGAGAGGCT		XM_017315831.1
			XM_006500575.2
			NM_001081171.2
RASSF5	F: TCCATACCCTTTTCCTCGGGT	73	NM_001311094.2
	R: CTGGGCTGGTAGGGAAC TTT		NM_018750.4
			NM_001313731.1
CRK	F: GCGTCTCCCACTACATCATCA	106	XM_006532125.2
	R: TCTCCTATTCGGAGCCTGGA		XM_006532124.2
			NM_133656.5
			NM_001277219.1
SMAD3	F: CGTGGAGTATGTGTCCTGGG	80	XM_006510821.3
	R: TACATCAGGGTTGTGGTGCC		XM_006510819.2
			NM_016769.4
STAT3	F: CACATGCCACGTTGGTGTTT	73	XM_017314401.1
	R: GACTCTTGCAGGAATCGGCT		XM_011248846.2
			NM_011486.5
			NM_213660.3

			NM_213659.3
COL4A1	F: GGCTCTCCGGGTTCAATAGG	84	XM_017312555.1
	R: GCCGATGTCTCCACGACTAC		NM_009931.2
ITGB3	F: CTGCCGGAAGAACTGTCACT	93	XM_006532312.2
	R: TCCAATCTTGAGGCCACAC		NM_016780.2
KDR	F: TTTCACCTGGCACTCTCCAC	93	NM_001363216.1
	R: AACATCTTCGCCACAGTCCC		NM_010612.3
			XM_011240817.2
ADCY3	F: TTTATGCGGCTGACCTTCGT	70	XM_006514935.3
	R: GGCCTGCCTTTTGAAGTAG		XM_006514934.3
			XM_006514933.2
			XM_006514932.2
			NM_001159537.1
			NM_001159536.1
			NM_138305.3
CD63	F: TTGAAGCAGGCCATTACCCA	71	NM_001282966.1
	R: GCACCCACTGCAATGATGAC		NM_001042580.1
			NM_007653.3
DOT1L	F: AAGGGAGAAAGATGGCTGGC	76	NM_199322.2
	R: TTAGACTTGCGTTCGGCACT		XM_006513432.3
			XM_011243391.2
			XM_006513429.3
			XM_011243390.2
			XM_006513431.1
			XM_006513430.1
			XM_006504845.2
			NM_001291248.1
			NM_001291249.1
			NM_178576.3

F2RL3	F: ACGCCTCACTACTGGACTCT	100	NM_007975.4
	R: GGAGCCAGCTAATCGGAAGG		XM_006530660.3
ESR1	F: GGTGCCCTACTACCTGGAGA	77	XM_017313797.1
	R: TAGACCTGTAGAAGGCGGGA		XM_006512434.3
			XM_011243068.2
			XM_006512435.2
			XM_006512433.3
			XM_011243067.2
			XM_011243066.2
			NM_001302533.1
			NM_001302532.1
			NM_001302531.1
			NM_007956.5
LAMA3	F: AAGCCCAGCTCTTACTGCAC	70	NM_001347461.1
	R: AGCAGTCCGTTGTTCTCCAC		XM_006525689.3
			XM_017317841.1
			XM_006525687.3
			XM_006525686.3
			XM_006525685.3
			NM_010680.1
NANOG	F: CTCCGCTCCATAACTTCGGG	119	XM_011241473.1
	R: AAAATGCGCATGGCTTTCCC		XM_006506651.2
			NM_028016.3
			NM_001289831.1
			NM_001289828.1
			NM_001289830.1
GADD45G	F: GAGCTGGACTTAGCCGACTG	89	NM_011817.2
	R: AAGCTTCCACGATAGCGTCC		
DROSHA	F: GAAGACCTGAGAGCCGCTAC	78	XM_006520021.3

	R: TCCTTTCATAGCTGCGGTGG		NM_001130149.1
			NM_026799.3
NOS2	F: AGAGCCACAGTCCTCTTTGC	111	XM_006532446.3
	R: CTGGTCCATGCAGACAACCT		NM_001313922.1
			NM_001313921.1
			NM_010927.4
SMO	F: GGATGTGTCCGTTACCCCTG	117	NM_176996.4
	R: TTTTCTTCCGGCCCAAACG		XM_006505106.4
APAF1	F: CAGCGGAGGCTCACAGTATT	109	NM_001282947.1
	R: CTGAGGTAGTATGCCAGCG		NM_009684.2
			NM_001042558.1
ANK3	F: GTCCAATGGGTACAAGGGGG	114	XM_017313780.1
	R: AACGTCAGAGGGGTTGTTCC		XM_006513139.3
			XM_017313779.1
			XM_017313778.1
			XM_017313777.1
			XM_017313776.1
			XM_017313775.1
			XM_017313774.1
			XM_017313773.1
			XM_017313772.1
			XM_017313771.1
			XM_017313770.1
			XM_017313769.1
			XM_006513138.2
			XM_006513137.2
			XM_006513136.2
			XM_006513135.2
			XM_006513134.2

[XM_006513133.2](#)

[XM_011243310.1](#)

[XM_011243309.1](#)

[XM_011243308.1](#)

[XM_006513130.2](#)

[XM_011243307.1](#)

[XM_006513129.2](#)

[XM_006513128.2](#)

[XM_006513127.2](#)

[XM_006513126.2](#)

[XM_011243305.1](#)

[XM_006513125.2](#)

[XM_011243304.1](#)

[XM_011243303.1](#)

[XM_011243301.1](#)

[XM_011243300.1](#)

[XM_006513124.2](#)

[XM_011243299.1](#)

[XM_011243297.1](#)

[XM_011243296.1](#)

[XM_011243295.1](#)

[XM_011243294.1](#)

[XM_011243293.1](#)

[XM_011243292.1](#)

[XM_006513122.2](#)

[XM_011243291.1](#)

[XM_011243290.1](#)

[NM_170729.2](#)

[NM_170690.2](#)

[NM_170687.3](#)

[NM_170730.2](#)

[NM_146005.3](#)

[NM_009670.4](#)

[NM_170688.2](#)

[NM_170689.2](#)

[NM_170728.2](#)

[NM_153798.2](#)

RP-IIβ F: GGTCAGAAGGGAACTTGTGGTAT 197

R: GCATCATTAAATGGAGTAGCGTC

Table 5.2. Rat primer sequences for genes that are significantly regulated across the human transcriptome and methylome after acute RE in humans

Target Gene	Primer Sequence (5'-3')	Product Length (bp)	Reference Seq. Number
MSN	F: TTCTATGCTCCTCGGCTTCG	96	NM_030863.1
	R: AATGGTGTCAGGCTTTCGCC		
TIMP3	F: GGCAAGATGTACACAGGGCT	96	NM_012886.2
	R: ACCCAGGTGGTAGCGGTAAT		XM_006241162.3
WNT9a	F: TCCTAGAGCCCACCGATGAA	100	NM_001105783.1
	R: GGCATCTGAAGAGTACGGGG		XM_006246448.3
CTTN	F: TGTGCAAGGGCAGATATGGG	109	NM_021868.2
	R: ACGCGATGTAGTGTGAACCC		XM_006230889.3
			XM_017590270.1
			XM_006230891.3
GSK3 β	F: TGGTGCTGGACTATGTTCCG	70	NM_032080.1
	R: AGTGTCTGCTTGGCTCGAC		XM_006248373.3
			XM_006248374.3
			XM_006248375.3
PAX3	F: CAACCATCTCATTCGGGGG	99	NM_053710.1
	R: TGTGGAATAGACGTGGGCTG		XM_006245131.3
			XM_008767181.2
AGTR1a	F: CCCACTCAAGCCTGTCTACG	96	NM_030985.4
	R: CCTCAAAACAAGACGCAGGC		XM_008771594.2
			XM_008771593.2
			XM_006253882.3
AGTR1b	F: GGCTGTATGGATTTGGGGTT	71	NM_031009.2
	R: ATTGAGAGGGGACTGGAGACA		XM_008760879.2
			XM_006232187.2

FOS	F: TACTACCATTCCCCAGCCGA R: GCTGTCACCGTGGGGATAAA	113	NM_022197.2
THBS1	F: TAGCTGGAAATGTGGTGCCT R: AGCAAGCATCAGGCACTTCT	95	NM_001013062.1 -
ITPR3	F: GCCGGCGAGAAGATCAAGTA R: GTCCAGCTCGAAGAGAGACG	75	NM_013138.1 XM_008772710.2
RARA	F: GTGCGAAACGACCGAAACAA R: CTTTGCACCTTCTCGATG	109	NM_031528.2 XM_017597010.1 XM_017597009.1 XM_017597011.1 XM_008767945.2 XM_017597008.1
FLNB	F: GAACTGGCAAGACGGCAAAG R: GCATTATCCACCGGCTTTCG	105	NM_001107288.1 XM_006251780.3 XM_006251781.3 -
LAMA5	F: CTTTCCCAGCTGCATCCCTT R: AACGAAGTCCTGTCACTCGG	110	NM_001191609.1 -
RASSF5	F: ACTGCCCTCTCTACCTTCGT R: AGGCATCCCACTCTACGTCT	99	NM_019365.3 XM_006249796.3 XM_008769494.2
CRK	F: AGTTTCCAGATCAAGGCAGGG R: AAAGAGGGCCCGCACATAC	73	NM_019302.1 XM_006246913.1
SMAD3	F: CTTACAAGGCGGCACATTGG R: TTGCAGTTGGGAGACTGGAC	110	NM_013095.3 XM_008766216.2
STAT3	F: CTTGCCAGTCGTGGTGATCT R: TTGGTCCCAGGTTCCAATCG	136	NM_012747.2 XM_006247257.3 XM_006247258.3 XM_006247259.3

COL4A1	F: TACCCGGCCCTAAAGGTCTC	77	NM_001135009.1
	R: GAGCCCTGGTTCTCCTTTGAT		-
ITGB3	F: TGACCCGCTTCAATGACGAA	87	NM_153720.1
	R: CCTGCATGATGGCGTCAAAG		-
KDR	F: TGCAAGACACTCACAGTTCCC	74	NM_013062.1
	R: TCGGTGTCCCGATAGAAGCA		-
ADCY3	F: GTCGGTCTGGTGTGGACAT	117	NM_130779.2
	R: GATCTGGGCTGTGATGAGCA		XM_006239849.3
			XM_006239850.3
			XM_006239847.3
			XM_006239848.3
CD63	F: GTATGGCCAAGGACAGGGTC	113	NM_017125.3
	R: CGCTATAGTTTCCACGCAGC		XM_008765024.2
			XM_008765025.2
DOT1L	F: GCAGTGCCCGAATTGAGAGA	91	NM_001108733.1
	R: CCCACTAAGCCACCACCATT		XM_006240961.3
			XM_006240960.3
			XM_006240959.3
			XM_017594910.1
F2RL3	F: ACCTTCCTATTGGCTGGCTC	78	NM_053808.1
	R: TCTCCAATGGGAGGTCTGCT		NM_012689.1
ESR1	F: AGGCGGGATACGAAAAGACC	116	XM_017588795.1
	R: GGTGGCAGCTCTCATGTCT		XM_006227832.3
			XM_008758704.2
			XM_017588797.1
			XM_017588796.1
LAMA3	F: CGCAGTGTACGAATCGAAGG	109	XM_017601153.1
	R: CTTGGAAAGCAGGCGTTGAG		XM_008774089.2
			XM_003753026.4

NANOG	F: AAGACTAGCAACGGCCTGAC	90	NM_001100781.1
	R: CGCGTTCATCAGATAGCCCT		XM_006237310.2
GADD45G	F: CTACGAGTCCGCCAAAGTCC	91	NM_001077640.1
	R: GGCTATGTCGCCCTCATCTT		
DROSHA	F: TGGATCCGATGCACACACTC	89	NM_001107655.2
	R: AGCCTGCTTGTTCCCTACGAC		XM_006232050.3
			XM_006232049.3
NOS2	F: AACGTGTTACCCATGAGGCT	93	NM_012611.3
	R: GCCCTCGAAGGTGAGTTGAA		-
ANK3	F: AGCAGAAGTGGTGCGGTATT	93	NM_001033984.1
	R: AGTCGGGCTGAAATGTGGAG		NM_031805.1
ITGA2	F: AGCTTCGTTCACTCCAGACA	114	XM_001075558.5
	R: ATGGCCACTTGGTGGTTTTG		
GAB1	F: GCAACACTTACCAGGTCCCA	172	NM_001108444.1
	R: CTGTCAGTGTCTGATGCCGT		
ATM	F: ACTGCTACCGAGGTCTACGA	102	NM_001106821.1
	R: CAGCTCCACCACGATCTCTG		XM_006243068.1
			XM_008766222.2
POLR2a	F: GCTGGACCTACTGGCATGTT	102	XM_001079162.5
	R: ACCATAGGCTGGAGTTGCAC		-

Table 5.3. Human primer sequences for regulated genes across the human methylome after acute and chronic RE in humans

Target Gene	Primer Sequence (5'-3')	Product Length (bp)	Reference Seq. Number
UBR5	F: AGGCAACACCTTAGGAAGC	81	NM_015902.6
			XM_024447179.1
	XM_024447178.1		
	XM_011517106.3		
	XM_017013534.2		
	XM_017013533.2		
	XM_011517105.3		
	XM_011517104.3		
	NM_001282873.1		
	NM_001282873.1		
AFF3	F: AACGGGAGCTGAGAGCTGAT	70	NM_002285.3
	R: GGGTGTCGACTTCAAACCTTGC		-
ODF2	F: TTGTGGCGCACCCAGTGTA	71	NM_001242353.2
			NM_001351588.2
	NM_001351586.2		
	NM_001351584.2		
	NM_001351580.2		
	NM_153433.2		
	NM_001351587.2		
	NM_001351579.2		
	NM_002540.5		
	NM_001351582.2		
NM_001351583.2			
NM_001351585.2			
NM_001351581.1			
NM_001351578.1			

			NM_001351577.1
			NM_001242352.1
			NM_001242354.1
			NM_153437.2
			NM_153440.1
			NM_153432.1
			NM_153439.1
			NM_153436.1
			NM_153435.1
AXIN1	F: AAGGTCCCGAGGCTACTCAG R: GCATTTCTTTTGCACGCCAC	99	NM_003502.4 NM_181050.3 XM_017023745.2 XM_017023746.1 XM_011522684.2 XM_011522683.2 XM_011522682.2 XM_011522686.1
RSU1	F: TGCCGCCAGATATTGGGAAG R: CCTTAGGCAGCGAGATCAGG	78	NM_012425.4 XM_005252552.4 NM_152724.2
HEG1	F: AACGTTCGATCGCTGGGATT R: TGGTCGCTGGAAGTCCTTTG	73	NM_020733.2 -
TRAF1	F: GGAAGCTGCGTGTGTTTGAG R: AGCTGGCTCTGGTGGATAGA	97	NM_005658.5 NM_001190947.1 NM_001190945.1
SETD3	F: GACCCATCCTCATGCCAACA R: CAGAAGAGACTGCCACCTG	77	NM_199123.2 NM_032233.3 XM_011537232.3 XM_005268127.3

			XM_017021700.1
			XM_017021699.1
			XM_011537231.2
			XM_011537235.1
			XM_011537234.1
GRIK2	F: CACATACAGACCCGCTGGAA	103	XM_017010782.2
	R: GGTCTAAAATGGCACGGCTG		XM_017010781.2
			XM_005266946.4
			XM_024446411.1
			XM_011535777.3
			XM_024446410.1
			XM_005266945.2
			NM_001166247.1
			NM_175768.3
			NM_021956.4
PLA2G16	F: GATGACAAGTACTCGCCGCT	81	NM_001128203.1
	R: CTTGTAGAGCACCTCCTGCC		NM_007069.3
			XM_006718426.1
			XM_011544741.1
RPL35a	F: TAACTCGGGCCCATGGAAAC	76	NM_001316311.2
	R: TGTCCAATGGCCTTAGCAGG		NM_000996.4
ZFP2	F: TTCCACAGCCAGCATCTCAC	99	NM_030613.4
	R: TCAGTAATACCCGGCTTCGG		-
BICC1	F: GGCCATGTTACAAGCTGCTG	97	NM_001080512.3
	R: TGGCCAAGCAATCTGCGTAT		-
STAG1	F: GCATTTTTAGCAACTTCTACCAGC	115	NM_005862.3
	R: AACTTGAATTTGGCAGGGCA		XM_017005525.1
KLHDC1	F: TGGTGGGAGCAAAGATGACT	102	NM_172193.3
	R: TCAAGGCATGACCTGAGTAGTG		-

RPL13a

F: GGCTAAACAGGTACTGCTGGG

104

[NM_012423.4](#)

R: GGAAAGCCAGGTACTTCAACTT

-

Table 5.4. Mouse primer sequences for regulated genes across the human methylome after acute and chronic RE in humans

Target Gene	Primer Sequence (5'-3')	Product Length (bp)	Reference Seq. Number
UBR5	F: GTCTGCTGGAGCTCGTGATT	106	XM_006520182.3
	R: TGCTGGAATAACTGGCTGGG		XM_006520181.3
			XM_006520180.3
			XM_006520179.3
			NM_001081359.3
			NM_001112721.2
AFF3	F: TCGCCGCCTCCACTAATAAC	196	XM_011238447.2
	R: GAAGTCAACAACCCGTTGCC		XM_006495737.3
			XM_011238446.2
			XM_011238444.2
			XM_011238443.2
			NM_001290814.1
ODF2	F: TTGCACCGACATCAACACCT	114	NM_001355137.1
	R: TTGCAGTGCTGTTCCCTCAA		NM_001355136.1
			NM_001355138.1
			XM_017316304.1
			XM_017316300.1
			XM_017316299.1
			XM_017316295.1
			XM_017316294.1
			XM_017316293.1
			XM_017316292.1
			XM_017316291.1
	XM_017316290.1		
	XM_017316288.1		

			XM_017316286.1
			XM_017316285.1
			XM_017316284.1
			XM_017316283.1
			XM_017316281.1
			XM_017316280.1
			XM_017316279.1
			XM_017316276.1
			XM_017316275.1
			XM_017316273.1
			XM_017316272.1
			NM_001177661.1
			NM_001177659.1
			NM_001113214.1
			NM_001113213.1
			NM_013615.3
AXIN1	F: ACAGGATCCGTAAGCAGCAC	111	XM_006523516.2
	R: CCCGGATCTCCTTTGGCATT		XM_006523515.3
			NM_001159598.1
			NM_009733.2
RSU1	F: AACCCCTAGCAGCCAAGAAC	118	XM_006497405.3
	R: GAAAAGTAGGCACCAGCACG		NM_009105.4
HEG1	F: GAACGTAGAACGGGATGCCT	189	XM_017317159.1
	R: GCTTGAAATGAGCACGGAC		XM_006522718.2
			XM_006522715.3
			XM_006522716.1
			NM_175256.5
TRAF1	F: AGCATGCTGGTTATGGCTGA	193	XM_011239054.2
	R: GGCTCAATGTCCAAGCCTCA		XM_011239053.2

			XM_011239052.2
			XM_017317129.1
			XM_011239051.2
			XM_011239050.2
			NM_009421.4
			NM_001326601.1
SETD3	F: GGGTGACCTTGGCTCTGATT	91	NM_001364267.1
	R: CAGCGGTCATCTTCCAGGTT		NM_001364269.1
			NM_001364266.1
			XM_006516078.3
			NM_028262.3
			XM_011245945.1
			NM_001081217.1
GRIK2	F: CAGCACTGGTCTCATTCGCT	84	NM_001358866.1
	R: GCTGGCAGCTGACGAATTTT		NM_010349.3
			NM_001111268.2
			XM_011243127.2
			XM_006512545.3
			XM_011243125.2
			XM_011243124.2
			XM_011243123.2
			XM_011243122.2
			XM_011243121.2
			XM_011243120.2
			NM_001093749.3
PLA2G16	F: GAATGACTGCCAGTTTTTGGG	196	NM_001362425.1
	R: TGTTATCCAGAACAGAGCCCC		NM_139269.2
RPL35a	F: TATGCCCGAGATGAAACGGAG	171	NM_001130485.1
	R: GCTTCGGAATTTGGCACGAA		NM_001130484.1

			NM_021338.3
ZFP2	F: TGTGGGAAAACCTTCAGGCA	115	XM_017314508.1
	R: GGGAGGAGCGTTCGATGAAA		XM_017314507.1
			XM_017314506.1
			NM_178447.3
			NM_001044700.2
			NM_001044698.2
			NM_001044697.2
			NM_001294323.1
BICC1	F: TGGTAGCGGTACCTTCTGGA	75	NM_001347189.1
	R: TGCAGTGAAGACTGTCCACG		NM_031397.3
STAG1	F: GGGTACTGGCAAGAGAGTG	198	NM_001357265.1
	R: TTTCCATCCGACCTGTGCTG		NM_001357264.1
			NM_009282.4
			XM_011242692.2
			XM_006510925.2
			XM_006510924.2
			XM_006510923.2
			NM_008636.4
KLHDC1	F: CACACAGAGACGGGTTTGGA	173	XM_011244121.2
	R: TGGCTTCTGATCAACGGAGG		XM_011244119.2
RP-IIβ	F: GGTCAGAAGGGAAGTTGTGGTAT	197	NM_153798.2
	R: GCATCATTAATGGAGTAGCGTC		-

Table 5.5. Rat primer sequences for regulated genes across the human methylome after acute and chronic RE in humans

Target Gene	Primer Sequence (5'-3')	Product Length (bp)	Reference Seq. Number
UBR5	F: GCACCAATCCTGACGACTCT R: AATGTGTTCTGCTCCGGTCC	83	XM_017595225.1
			XM_006241570.3
			XM_008765469.2
			XM_008765468.2
			XM_008776462.2
			XM_006226059.3
AFF3	F: ATGTCCACTCTAGGCCGTGT R: TCTGGATCCGGTTGGAGAGT	175	NM_001191887.2
ODF2	F: AACATCGAGCGCATCAAGGA R: CCATTCAGCCTCCACCAGT	106	NM_017213.2
			NM_001145005.1
			XM_017591519.1
			XM_017591520.1
			XM_017591521.1
			XM_017591522.1
			XM_017591523.1
			XM_017591524.1
			XM_017591525.1
			XM_017591526.1
XM_017591527.1			
XM_017591528.1			
XM_017591529.1			

			XM_017591530.1
			XM_017591531.1
			XM_017591532.1
			XM_017591533.1
			XM_017591534.1
			XM_017591535.1
			XM_017591536.1
			XM_017591537.1
			XM_017591538.1
AXIN1	F: GGACCTCGGAGCAAGTTTCA R: GGTTGACAGGCCTCGAATCA	95	NM_024405.1
RSU1	F: TCGGCAACTTGGACCTAACC R: AAGCTGGAAGTGGTCAGCAA	89	NM_001109404.1
HEG1	F: CACTGCAAGGAACCATTGGC R: AGTCTGAGCTGTCACTCCCT	118	XM_017604360.1 XM_006221159.3
TRAF1	F: CCACAGGGCTGGTCTCTACT R: ACTCGTTTTTCATCAGGGGCT	90	NM_001271240.1
SETD3	F: GCAGCCATGAACCGAGAGTA R: CCCAGGTCCTCTCCTCGTA	80	NM_001346470.1 XM_017603284.1 XM_002726774.2
GRIK2	F: AACCTAGCCGCCTTTCTGAC R: CGTCCTCCACTGCTCCATAC	103	NM_019309.2
PLA2G16	F: TAAACAAAGGCATCCACGGC R: CTTGGGTTCTGGTATGGGCA	84	NM_017060.2
RPL35a	F: CTCCGGAACCAAAGAGAGCA R: ACTCAGTTTTTCATCTCGGGCA	70	NM_021264.3 XM_017604255.1 XM_003752497.4 XM_003752496.4 XM_017604361.1

ZFP2	F: AGGCAATGGCTGTTGGA R: TAGCTGCATCACTCCTCCCA	97	NM_001127558.1 -
BICC1	F: GAAGATCGGGGCAAATCCA R: TGACCCGGTTGCTTTTCGT	119	NM_001108531.1
STAG1	F: CCTGCCAAAAGTCACGTTA R: ATTAGCGGGTTGAGGGGGT	138	NM_001108179.1 XM_006243631.2 XM_008766528.2 XM_006243632.3
KLHDC1	F: ACAGCAATCGCGGACGATAA R: TACTTTGGGCCTTACCTGGG	152	NM_001108027.1
POLR2a	F: GCTGGACCTACTGGCATGTT R: ACCATAGGCTGGAGTTGCAC	102	XM_001079162.5
